STABLE UNBONDED FIBER REINFORCED ELASTOMERIC ISOLATORS

THE PERFORMANCE OF SU-FREIs

(STABLE UNBONDED – FIBER REINFORCED ELASTOMERIC ISOLATORS)

By

Hamid Toopchinezhad
B. Sc., M. Sc.

Faculty of Engineering

Department of Civil Engineering

A Thesis

Submitted to the School of Graduate Studies

in Partial Fulfillment of the Requirements

for the Degree of

Doctor of Philosophy

McMaster University

Doctor of Philosophy (2008)
(Civil Engineering)

McMaster University
Hamilton, Ontario

TITLE:	The Performance of SU-FREIs (Stable Unbonded – Fiber Reinforced Elastomeric Isolators)
AUTHOR:	Hamid Toopchinezhad
SUPERVISORS:	Dr. Robert G. Drysdale Dr. Michael J. Tait
NUMBER OF PAGES:	198 pages (i-xvi, 1-182)

Abstract

Steel-reinforced elastomeric isolator (SREI) bearings are currently the most commonly used type of seismic isolators. However, high manufacturing and associated installation costs prohibit their application in ordinary residential and commercial buildings. Fiber-reinforced elastomeric isolator (FREI) bearings are comprised of alternating layers of elastomer bonded to fiber-reinforcement layers. Research studies have shown that FREI bearings can be used as an alternative to SREI-bearings with comparable performance.

FREIs are much lighter in weight than traditional SREIs. In addition, their manufacturing cost can be lower, if individual FREI bearings, with the required size, are cut from a large sheet or a long strip, fabricated through mass production manufacturing techniques. An appealing application which simplifies the installation of FREI bearings is when they are placed between the substructure and superstructure with no bonding at their contact surfaces. This specific application is denoted as "unbonded application".

When an unbonded FREI bearing is deformed laterally, it shows "rollover deformation" due to lack of flexural rigidity in the fiber-reinforcement sheets. The rollover deformation, as a beneficial feature, reduces the lateral stiffness of the bearing and enhances its seismic isolation efficiency, compared to the same bearing employed with bonded contact surfaces. However, it is important that the bearing is properly sized to maintain its lateral stability, and hence exhibit "stable rollover" (SR) deformation. Such a bearing is termed in this thesis as "stable unbonded" (SU)-FREI bearing.

The main objectives of this research were to investigate the influence of geometry on the lateral response behavior of unbonded FREI bearings, and to evaluate the feasibility of employing SU-FREI bearings for seismic mitigation of low-rise buildings. The first objective was accomplished by conducting an experimental study on full-scale square FREI bearings. To achieve the latter objective a shake table study was performed on a ¼ scale 2-storey steel frame which was seismically isolated with ¼ scale SU-FREI bearings. The mechanical properties, including vertical and lateral stiffnesses and effective damping, of prototype samples of the ¼ scale SU-FREI bearings were evaluated by vertical compression testing

and cyclic lateral shear (under constant compression) testing. In addition, the influence of parameters such as lateral displacement amplitude and rate, amplitude history, and variations in the vertical pressure on the lateral response of the ¼ scale SU-FREI bearings, were investigated.

It was found that for FREI bearings having identical material properties and shape factor (the plan area of the bearing divided by the perimeter area of a single elastomer layer) the aspect ratio (length to total height of the bearing, also called second shape factor) plays an important role in achieving stable lateral response. All tested prototype ¼ scale SU-FREI bearings exhibited SR-deformation with sufficient lateral flexibility and damping. Lateral response was found to be nonlinear and dependent on the amplitude and history of lateral displacement. However, due to the application of a relatively low design vertical pressure of 1.6 MPa, the influence of ±50% variation in the design vertical pressure on the lateral response was found to be insignificant. Lateral displacement capacity of the SU-FREI bearings was attained when their originally vertical faces fully contacted the upper and lower horizontal supports. This was accompanied with a significant increase in the lateral stiffness of the bearings which maintains the overall stability of the bearing to unexpectedly large ground motions. Shake table tests clearly demonstrated that SU-FREI bearings were efficient in seismic mitigation of the test-structure.

The final component of this thesis involves investigating the applicability of two simplified analytical models in seismic response prediction of a base isolated structure. The two models use different techniques to simulate the lateral load-displacement hysteresis loops of prototype SU-FREI bearings which are obtained from cyclic shear tests (under constant compression). Model 1 includes the rate and the amplitude of bearings' lateral displacements to simulate the hysteresis loops through a multi-parameter curve fitting function. Model 2 uses bilinear idealization to simulate the hysteresis loops. Due to the highly nonlinear lateral response of SU-FREI bearings, these models utilize an iterative time history analysis approach to improve their accuracy. Comparisons with shake table results of a ¼ scale structure show that both models can be used in response prediction of ordinary structures which are seismically isolated with SU-FREI bearings.

Acknowledgement

I would like to express my deepest appreciation and sincere gratitude to my research supervisors, Dr. Michael J. Tait and Dr. Robert G. Drysdale for their interest, support, invaluable guidance and encouragement throughout this research. I am also extremely grateful to the members of my supervisory committee, Dr. Samir E. Chidiac, and Dr. Mukesh Jain for their valuable comments and advice throughout the course of this research work.

I would like to thank all of the technical staff working at the Applied Dynamic Laboratory (ADL), in particular Mr. David Perrett, for their assistance and advice during the experimental phases of this research. I also appreciate the help received from Mr. Peter Koudys.

This research was carried out as part of the mandate of the McMaster University Centre for Effective Design of Structures funded through the Ontario Research and Development Challenge Fund. The research was also funded by the discovery grants from Natural Sciences and Engineering Research Council of Canada (NSERC). The author also would like to gratefully acknowledge the financial support provided by the Ministry of Science, Research, and Technology (MSRT) of Iran.

Finally, and most importantly, I would like to thank my parents and my parents-in-law for their patience and support during my PhD study. This thesis is dedicated to my wife, *Soodeh* for her understanding, love, and encouragement, and to my sons, *Mostafa* and *Parsa*.

Publication List

This thesis consists of the following five papers:

Paper I

Toopchinezhad H., Tait M. J., and Drysdale R. G. (2007). "Testing and Modeling of Square Carbon Fiber-Reinforced Elastomeric Seismic Isolators." *Structural Control and Health Monitoring*, Vol. 15, No. 6, Pages 876–900, DOI: 10.1002/stc.225.

Paper II

Toopchinezhad H., Tait M. J., and Drysdale R. G. (2008). "Lateral Response Evaluation of Fiber-Reinforced Neoprene Seismic Isolators Utilized in an Unbonded Application." *Journal of Structural Engineering,* ASCE, Vol. 134, No. 10, Pages 1627-1638.

Paper III

Toopchinezhad H., Drysdale R. G., and Tait M. J., "Parametric Study on the Response of Stable Unbonded Fiber-Reinforced Elastomeric Isolators (SU-FREIs)." *Submitted on October 2008.*

Paper IV

Toopchinezhad H., Tait M. J., and Drysdale R. G., "Shake Table Study on an Ordinary Low-Rise Building Seismically Isolated with SU-FREIs (Stable Unbonded Fiber-Reinforced Elastomeric Isolators)." *Submitted on October 2008.*

Paper V

Toopchinezhad H., Tait M. J., and Drysdale R. G., "Simplified Analysis of a Low-Rise Building Seismically Isolated with SU-FREIs (Stable Unbonded Fiber-Reinforced Elastomeric Isolators)." *Submitted on October 2008.*

Co-Authorship

This thesis has been prepared in accordance with regulations for a "Sandwich" thesis format or as a compilation of papers stipulated by the Faculty of Graduate Studies at McMaster University and has been co-authored as:

Chapter 2: Testing and Modeling of Square Carbon Fiber-Reinforced Elastomeric Seismic Isolators
By: H. Toopchinezhad, M. J. Tait, and R. G. Drysdale
Fabrication of the full scale bearings, setup preparation, testing and data analysis was conducted by H. Toopchinezhad under the supervision of Dr. M.J. Tait and R.G. Drysdale. Paper was written by H. Toopchinezhad and modifications were done in consultation with Dr. M.J. Tait and R.G. Drysdale.

Chapter 3: Lateral Response Evaluation of Fiber-Reinforced Neoprene Seismic Isolators Utilized in an Unbonded Application
By: H. Toopchinezhad, M. J. Tait, and R. G. Drysdale
Fabrication of the model scale bearings, setup preparation, testing and data analysis was conducted by H. Toopchinezhad under the supervision of Dr. M. J. Tait and Dr. R. G. Drysdale. Paper was written by H. Toopchinezhad and modifications were done in consultation with Dr. M. J. Tait and Dr. R. G. Drysdale.

Chapter 4: Parametric Study on the Response of Stable Unbonded Fiber-Reinforced Elastomeric Isolators (SU-FREIs)
By: H. Toopchinezhad, R. G. Drysdale, and M. J. Tait
The testing and data analysis was conducted by H. Toopchinezhad under the supervision of Dr. M. J. Tait and Dr. R. G. Drysdale. Paper was written by H. Toopchinezhad and modifications were done in consultation with Dr. R. G. Drysdale and Dr. M. J. Tait.

Chapter 5: Shake Table Study on an Ordinary Low-Rise Building Seismically Isolated with SU-FREIs (Stable Unbonded Fiber-Reinforced Elastomeric Isolators)
By: H. Toopchinezhad, M. J. Tait, and R. G. Drysdale
Setup preparation was conducted by H. Toopchinezhad under the supervision of Dr. M. J. Tait and Dr. R. G. Drysdale. Testing and data analysis was conducted by H. Toopchinezhad under the supervision of Dr. M. J. Tait and Dr. R. G. Drysdale. Paper was written by H. Toopchinezhad and modifications were done in consultation with Dr. M. J. Tait and Dr. R. G. Drysdale.

Chapter 6: Simplified Analysis of a Low-Rise Building Seismically Isolated with SU-FREIs (Stable Unbonded Fiber-Reinforced Elastomeric Isolators)
By: H. Toopchinezhad, M. J. Tait, and R. G. Drysdale
The numerical analysis was conducted by H. Toopchinezhad under the supervision of Dr. M. J. Tait and Dr. R. G. Drysdale. Paper was written by H. Toopchinezhad and modifications were done in consultation with Dr. M. J. Tait and Dr. R. G. Drysdale.

Table of Contents

Abstract iii
Acknowledgement v
Publication List vi
Co-Authorship vii
Table of Contents viii
List of Tables xi
List of Figures xii

1. Outline of Study 1
1.1. Introduction 1
1.2. Fundamentals of Seismic Isolation 1
1.3. The Most Commonly Used Seismic Isolators 2
1.4. Fiber-Reinforced Elastomeric Isolators 4
1.5. Impetus for this Research 5
1.6. Creep and Longevity of Elastomeric Bearings 5
1.7. Research Objectives 7
1.8. Structure of Thesis 8
1.9. References 9

2. Testing and Modeling of Square Carbon Fiber-Reinforced Elastomeric Seismic Isolators 14
2.1. Summary 14
2.2. Introduction 14
2.3. Literature Review 17
2.4. Research Objectives 19
2.5. Test Specimens 19
2.6. Test Setup and Instrumentation 20
2.7. Vertical Compression Test 21
2.8. Horizontal Cyclic Displacement Tests 22
2.8.1. Test Procedure and Calculations 22
2.8.2. Rate Sensitivity Tests 23
2.8.3. Cyclic Test on Bearings B1 and B2 24
2.8.4. Cyclic Test on Bearing NB1 (R_{NB1} = 2.5) 25
2.8.5. Cyclic Test on Bearing NB2 (R_{NB2} = 2.9) 27
2.9. Observations of Performance 28
2.9.1. Stable Rollover (SR) Deformation 28
2.9.2. Influence of Aspect Ratio (R) 29
2.9.3. Influence of Compression Load 29
2.9.4. Influence of Rate and Amplitude of Displacement 30
2.9.5. Performance of Bearing NB1 30
2.9.6. Performance of Bearing NB2 32
2.10. Modeling 34
2.11. Conclusions 37
2.12. References 39

3. Lateral Response Evaluation of Fiber-Reinforced Neoprene Seismic Isolators Utilized in an Unbonded Application 54
3.1. Abstract 54
3.2. Introduction 54
3.3. Target Response Characteristics 55
3.4. Bearing Isolators 56
3.5. Test Program 58
3.6. Cyclic Lateral Tests 59
3.6.1. Objectives and Methodology 59
3.6.2. Overall Verification of the Lateral Response 59
3.6.3. Rate Sensitivity Tests 62
3.6.4. Cyclic Lateral Testing 63
3.7. Code Evaluation 66
3.8. Conclusions 68
3.9. References 70

4. Parametric Study on the Response of Stable Unbonded Fiber Reinforced Elastomeric Isolators (SU-FREIs) 81
4.1. Abstract 81
4.2. Introduction 81
4.3. The SU-FREI Bearings 82
4.4. Organization of the Test Program 83
4.5. Test Setup 83
4.6. Cyclic Lateral Testing 84
4.6.1. Mechanical Properties of Interest 84
4.6.2. Influence of Lateral Displacement Amplitude History 84
4.6.3. Influence of Vertical Pressure 86
4.7. Vertical Compression Testing 88
4.8. Robustness of the Lateral Response 90
4.9. Lateral Response under Extreme Lateral Displacement 91
4.10. Concluding Remarks 93
4.11. References 96

5. Shake Table Study on an Ordinary Low-Rise Building Seismically Isolated with SU-FREIs (Stable Unbonded Fiber-Reinforced Elastomeric Isolators) 107
5.1. Abstract 107
5.2. Introduction 107
5.2.1. Motivation for the Research 107
5.2.2. FREI versus SREI 108
5.2.3. Unbonded versus Bonded Application 109
5.2.4. Scope of this Study 110
5.3. Model Scale Base Isolated (BI) Structure 111
5.3.1. Test-Structure 111
5.3.2. Base Isolation System and Bearing Isolators 111
5.4. Test Program 112

5.5. Instrumentation 113
5.6. Input Earthquakes 113
5.7. Free Vibration Tests 115
5.8. Results of Shake Table Tests 116
5.8.1. Data Processing 116
5.8.2. Peak Response Values 116
5.8.3. Response Pattern along Height of the Test-Structures 119
5.8.4. Response History 121
5.8.5. Observed Dynamic Characteristics 121
5.8.6. Damage Status in the Bearings 123
5.9. Concluding Remarks 124
5.10. References 125

6. Simplified Analysis of a Low-Rise Building Seismically Isolated with SU-FREIs (Stable Unbonded Fiber-Reinforced Elastomeric Isolators) 142
6.1. Abstract 142
6.2. Introduction 142
6.3. Base Isolated System 144
6.4. Lateral Response Properties of the SU-FREI Bearings 145
6.5. Modeling of the Base Isolated System 146
6.5.1. Governing Equations 146
6.5.2. Superstructure 147
6.5.3. SU-FREI Bearings 149
6.5.4. Model 1: Rate and Amplitude Dependent Stiffness and Damping 150
6.5.5. Model 2: Bilinear Idealization 151
6.6. Input Earthquakes 154
6.7. Analytical Results and Discussion 155
6.8. Summary and Conclusions 157
6.9. References 159

7. Conclusions and Recommendations 174
7.1. Overview of the Research 174
7.2. Conclusions 175
7.3. Recommendations for Future Studies 179
7.3.1. Experimental Studies 179
7.3.2. Analytical Studies 180
7.3.3. References 181

List of Tables

Table 2.1. Effective damping ratio and horizontal stiffness of Bearings B1 and B2 resulting from sinusoidal cyclic tests having displacement amplitude of 47 mm with different frequencies 40
Table 2.2. Effective scragged horizontal stiffnesses and damping ratios of Bearing NB1 ($t_{r,NB1}$ = 70.5 mm) at different displacement amplitudes 41
Table 2.3. Effective scragged horizontal stiffnesses and damping ratios of Bearing NB2 ($t_{r,NB2}$ = 61.1 mm) at different displacement amplitudes 41
Table 2.4. *b*-parameters for Bearings NB1 and NB2 and for the finalized bearing 42

Table 3.1. Test sequence carried out on each bearing isolator 72
Table 3.2. Effective lateral stiffness values and damping ratios corresponding to various lateral displacement amplitudes in Bearings B1-1 and B2-1 73
Table 3.3. Parallel and perpendicular responses of Bearings B1-3, B2-1, and Bearing B2-3 74
Table 3.4. Diagonal response of Bearings B1-3 and B2-1 75

Table 4.1. Sequence of tests conducted on each SU-FREI bearing 97
Table 4.2. Maximum and minimum bearing lateral responses for loading in the parallel (0°)/perpendicular (90°) and diagonal (45°) directions 98
Table 4.3. Results of initial vertical test on Bearings B1-3 and B2-3 99
Table 4.4. Results of vertical test on Bearings B1-1, B1-3, B2-1, and B2-3 99

Table 5.1. Tests carried out on the base isolated test structure 127
Table 5.2. Ground motion specifications 128
Table 5.3. Measured response maxima and fundamental frequency of the base isolated (BI) structure and estimated response maxima of the corresponding 5%-damped fixed base (FB) structure 129

Table 6.1. Mechanical properties of the SU-FREI bearings including the effective lateral stiffness (k) and damping ratio (ξ) attributed to different amplitudes of lateral displacements 161
Table 6.2. Parameters to be used in Model 2 (bilinear idealization) 161
Table 6.3. Peak response values; comparison between the measured (shake table test results) and the normalized predicted responses 162

List of Figures

Figure 1.1. Decreased seismic acceleration due to increasing period and damping (Skinner et al. 1993) 11
Figure 1.2. Increasing displacement response with increasing period as offset by increasing damping (Skinner et al. 1993) 11
Figure 1.3. Typical laminated rubber bearing; top mounting plate not shown (Taylor and Igussa 2004) 12
Figure 1.4. Typical lead-plug rubber bearing; top mounting plate not shown (Taylor and Igussa 2004) 12
Figure 1.5. Typical hysteresis loops of a low-damped rubber bearing at 100% shear strain (Higashino and Okamoto 2006) 13
Figure 1.6. Typical hysteresis loops of a lead-plug bearing at 100% shear strain (Higashino and Okamoto 2006) 13
Figure 1.7. Typical hysteresis loops of a high-damped rubber bearing (Fuller et al. 1997) 13

Figure 2.1. Carbon–FREI bearings 43
Figure 2.2. An overview of the test setup 43
Figure 2.3. Test setup and instrumentation arrangement 44
Figure 2.4. Vertical load-deflection relationships under 64 kN vertical compression load 45
Figure 2.5. Variation of equivalent viscous damping ratio and horizontal stiffness of Bearings B1 and B2, at 50% t_r lateral displacement, with respect to frequency of the imposed sinusoidal horizontal displacement 45
Figure 2.6. Lateral load-displacement behavior for Bearings B1 and B2 (aspect ratio R = 1.9, and t_r = 94 mm), in a series of parallel loading (0° orientation) cyclic tests having amplitudes of 25, 50, 75, 100, 125, and 150% t_r, under constant 1.6 MPa vertical compression 46
Figure 2.7. Lateral load-displacement behavior for Bearings B1 and B2 (aspect ratio R = 1.9, and t_r = 94 mm), in a series of parallel loading (0° orientation) cyclic tests having amplitudes of 25, 50, 75, 100, and 125% t_r, under 3.2 MPa constant vertical compression 46
Figure 2.8. Parallel lateral load displacement behavior of Bearing NB1 under constant 1.6 MPa vertical compression, in a series of parallel loading (0° orientation) cyclic tests with different lateral displacement amplitudes ranging from 25% to 200% $t_{r,NB1}$ 47
Figure 2.9. Bearing NB1 under constant 1.6 MPa vertical compression, subjected to different amplitudes of lateral displacements parallel to the sides of the bearing (0° orientation) 48
Figure 2.10. Lateral load displacement behavior of Bearing NB1 under constant 1.6 MPa vertical compression when lateral displacements were imposed along the diagonal of the bearing (45°), in a series of cyclic tests with different amplitudes ranging from 25% to 200% $t_{r,B1}$ 49

Figure 2.11. Bearing NB1 under constant 1.6 MPa vertical compression, subjected to diagonal (45°) lateral displacements with different amplitudes 50
Figure 2.12. Bearing NB1 after completion of cyclic testing program; as indicated a significant delamination occurred in the bonding of one layer 51
Figure 2.13. Time history plots of sinusoidal input motion imposed to Bearing NB2 corresponding to two different lateral displacement amplitudes 51
Figure 2.14. Lateral load displacement behavior for Bearing NB2 under constant 1.6 MPa compression, in a series of cyclic tests having amplitudes 25, 50, 75, 100, 125, 150, and 200% $t_{r, NB2}$ ($t_{r, NB2}$ = 61.1 mm) when lateral displacements imposed on (a) parallel direction, and (b) diagonal direction of the bearing 52
Figure 2.15. Experimental vs. mathematical hysteresis loops for the tested bearings (Only half cycles is shown) 52
Figure 2.16. Mathematical hysteresis loops for the final bearing with an aspect ratio of R = 2.6, evaluated based on b-parameters indicated in the last column of Table 2.4 53

Figure 3.1. Seismic isolators 76
Figure 3.2. An overview of the test setup 76
Figure 3.3. Hysteresis loops corresponding to the final cycle of lateral displacement at each displacement amplitude (lateral displacement ranges: 25%, 50%, 75%, 100%, 150%, and 200% t_r; displ. rate = 30 mm/s) 77
Figure 3.4. Influence of displacement rates lower than 114 mm/s on lateral response at 100% t_r (19 mm) displacement amplitude (Values represent the average reduction in all 3 displacement cycles. 77
Figure 3.5. Parallel lateral response (0°) of Bearing B1-3 (lateral displ. ranges: 25%, 50%, 75%, 100%, 150%, and 200% t_r, displacement rate = 76 mm/s) 78
Figure 3.6. Photographs taken from parallel (0°) response of Bearing B1-3 at different amplitudes of lateral displacement 78
Figure 3.7. Lateral response values for Bearings B1-3 (at 0°), B2-1 (at 90°), and B2-3 (at 90°); (Response values represent the average of all 3 cycles at each displacement amplitude.) 79
Figure 3.8. Lateral response of Bearing B1-3 (at 0°) *versus* Bearing B2-3 (at 90°) 79
Figure 3.9. Photographs taken of diagonal (45°) response of Bearing B1-3 at different amplitudes of lateral displacement 80
Figure 3.10. Lateral response characteristics of Bearings B1-3 at 45° orientation; (Response values in Fig. (b) represent the average values at each displacement amplitude) 80

Figure 4.1. An overview of the test setup 100
Figure 4.2. Time histories of the input sinusoidal lateral displacements 100
Figure 4.3. Lateral load-displacement hysteresis loops for the virgin bearings at 0° 101

Figure 4.4. Photographs of B2-3 taken at different amplitudes of cyclic lateral displacement 101
Figure 4.5. Lateral load-displacement hysteresis loops for bearings at 45° 101
Figure 4.6. Lateral response properties of the SU-FREI bearings under cyclic lateral tests (values are the average of all cycles at each displacement) 102
Figure 4.7. Influence of variation in vertical design pressure on lateral response of Bearings B1-3, B2-1, and B2-3; (lateral displacement amplitude = 100% t_r or 19 mm, average displacement rate = 76 mm/s) 102
Figure 4.8. Time history of the input signals utilized for vertical tests on the bearings 103
Figure 4.9. Vertical compressive stress-strain behavior of Bearing B2-3 under 0.8, 1.6, and 2.4 MPa vertical pressure 103
Figure 4.10. Lateral response characteristics of all SU-FREI bearings during the repeated cyclic testing (values are the average of all cycles at each displacement) 104
Figure 4.11. Hysteresis loops for repeated cyclic testing of Bearing B1-3 104
Figure 4.12. Lateral response of virgin B1-3 versus retest B1-3 under an AA-pattern of cyclic lateral displacements at 0° 105
Figure 4.13. Longitudinal lateral response of the virgin Bearing TB1 to an AA-pattern of lateral displacement 105
Figure 4.14. Longitudinal lateral response for Bearing TB1 (ave. displ. rate = 76 mm/s) 106
Figure 4.15. Photographs of Bearing TB1 taken during cyclic lateral testing 106

Figure 5.1. An overview of the BI-structure and a close-up view of one of the SU-FREI bearings located between the test-structure and shake table with no bonding at the contact surfaces of the bearing 130
Figure 5.2. An overview of the FREI bearings used as seismic isolators 131
Figure 5.3. Lateral load-displacement hysteresis loops of the SU-FREI bearings under a set of cyclic lateral tests having an ascending pattern of displacement amplitudes ranging from 25% t_r to 200% t_r (where, t_r = 19 mm); Only half cycles are shown 131
Figure 5.4. Maximum (M) level of the input earthquakes; (a) table acceleration time history; (b) comparison between 5%-damped spectral acceleration of the input earthquake and the maximum considered earthquake response spectrum for Vancouver, BC, Canada 132
Figure 5.5. Photographs taken from one of the bearing isolators during shake table testing at the time instant of peak lateral displacement in the base isolation system 133
Figure 5.6. Lateral load-displacement hysteresis loops of the SU-FREI bearings corresponding to the design and maximum level of different input earthquakes 134
Figure 5.7. Lateral diagonal response of SU-FREI bearings at the maximum level of El Centro-s earthquake 135

Figure 5.8. Comparison between peak response values of the BI-structure and the corresponding 2% and 5% damped linear FB-structures to service, design, and maximum level of El Centro-s earthquake 136
Figure 5.9. Comparison between peak response values of the BI-structure and the corresponding 2% and 5% damped linear FB-structures to service, design, and maximum level of Saguenay-s 136
Figure 5.10. Comparison between peak response values of the BI-structure and the corresponding 2% and 5% damped linear FB-structures with 2% and 5% damping to service, design, and maximum level of Tabas-s 137
Figure 5.11. Amplification envelopes in BI and the corresponding 5%-damped FB structures for different levels of the input earthquakes 137
Figure 5.12. Comparison between response profiles of the BI-test-structure and the corresponding 5%-damped FB-structure under maximum (M) level of different input earthquakes. Response profiles are associated with the time instant of maximum drift 138
Figure 5.13. Accelerations for the BI-structure versus the 5%-damped FB-structure; Evolution of the floor accelerations Profile within maximum amplitude half-cycle of response at four different time instants 139
Figure 5.14. Time history of base shear and the roof lateral displacements relative to the base (total drift) in BI and corresponding 5%-damped FB structures during the maximum (M) level of different input earthquakes 140
Figure 5.15. Fourier amplitude spectra of the BI-structure subjected to maximum level of different input earthquakes; comparison between Fourier amplitudes of the roof horizontal accelerations and the vertical accelerations at the front of base floor (all accelerations in terms of cm/s^2 141

Figure 6.1. Sketch of the base isolated structure 163
Figure 6.2. Time History of Input Lateral Displacements 164
Figure 6.3. Lateral response of the SU-FREI bearings (under 1.6 MPa constant vertical pressure) 164
Figure 6.4. Mass-spring-dashpot idealization of the base isolated structure shown in Fig. 6.1 164
Figure 6.5. Translational (dynamic) and rotational (static) degrees of freedom in the superstructure 165
Figure 5.6. Comparison between the measured and predicted cyclic behavior of the SU-FREI bearings using Model 1 165
Figure 6.7. Comparison between the measured and Model 1 predicted cyclic behavior of the SU-FREI bearings, with the peak amplitude of bearing lateral displacement equal to or less than 50% t_r 166
Figure 6.8. Bilinear idealization (Model 2) of the SU-FREI Bearing lateral load-displacement hysteresis response 166
Figure 6.9. Ground acceleration time histories of the input earthquakes 167

Figure 6.10. Measured versus predicted (Model 1) lateral bearing displacement (v_b) and superstructure base shear (V_s) for El Centro-s 168
Figure 6.11. Measured versus predicted (Model 2) lateral bearing displacement (v_b) and superstructure base shear (V_s) for El Centro-s 168
Figure 6.12. Measured versus predicted lateral load-displacement hysteresis loops for SU-FREI bearings subjected to El Centro-s earthquake 169
Figure 6.13. Measured versus predicted (Model 1) bearings' lateral displacement (v_b) and superstructure base shear (V_s) for Saguenay-s earthquake 170
Figure 6.14. Measured versus predicted (Model 2) bearings' lateral displacement (v_b) and superstructure base shear (V_s) for Saguenay-s earthquake 170
Figure 6.15. Measured versus predicted lateral load-displacement hysteresis loops for SU-FREI bearings subjected to Saguenay-s earthquake 171
Figure 6.16. Measured versus predicted (Model 1) lateral bearing displacement (v_b) and superstructure base shear (V_s) to Tabas-s 172
Figure 6.17. Measured versus predicted (Model 2) lateral bearing displacement (v_b) and superstructure base shear (V_s) to Tabas-s 172
Figure 6.18. Measured versus predicted lateral load-displacement hysteresis loops for SU-FREI bearings subjected to Tabas-s earthquake 173

Chapter 1: Outline of Study

1.1. Introduction

Despite substantial improvements in the conventional seismic-resistant design of structures over the last few decades, the collapse of poorly constructed buildings remains a significant cause of major loss of life during strong earthquakes. In many countries, the engineering services including design, construction, and inspection allocated to small and low-rise private buildings may not be sufficiently comprehensive to provide an adequate level of structural safety against strong or sometimes moderate earthquakes. Seismic isolation is aimed at decreasing the seismic demand as opposed to increasing the earthquake resistant capacity of structures. Accordingly, if a simple, cost-effective, and reliable base isolation system was to be incorporated in ordinary buildings, a subsequent reduction in building failures and loss of life would occur.

1.2. Fundamentals of Seismic Isolation

The damage potential of an earthquake is basically due to unfortunate harmony between the fundamental periods of vibration of the majority of structures and the frequency content of the ground motions (Priestley et al. 1996). During an earthquake, these structures act as vibration amplifiers, magnifying the induced-accelerations. This amplification may result in significant damage to both the nonstructural and structural elements, and in the most severe cases, collapse. However, due to the insertion of a flexible layer to seismically isolate superstructure from the substructure, the fundamental period of the isolated system increases to a value beyond the critical period-range of the input earthquake. This leads to a large decrease in the accelerations induced in the isolated system (see Fig. 1.1). Further reduction of the induced accelerations may be achieved if increased damping, compared to the fixed base system, is provided by the isolation system (see Fig. 1.1).

During an earthquake, a fixed base structure experiences large interstory drifts. However, the first mode of vibration in the base isolated structure involves lateral deformation at the isolation level, whereas the superstructure remains nearly rigid. The lateral deformation of the isolators can be limited to a practical design magnitude by additional damping in the isolation system (see Fig. 1.2). In addition, a certain level of damping is necessary to restrain possible resonance at the isolation frequency (Naiem and Kelly 1999). However, the additional damping may increase floor accelerations and interstory drifts in the superstructure (Kelly 1999a). Seismic isolators are typically required to have sufficient stiffness under service lateral loads including minor earthquakes or wind to limit the lateral response of the isolated structure. In summary, the three basic requirements for seismic isolators are, flexibility, damping, and resistance to lateral service loads.

1.3. The Most Commonly Used Seismic Isolators

Although many types of seismic isolation systems have been developed, elastomeric isolators, sliding systems and hybrid systems are the most common generic types of isolators (Taylor and Igussa 2004).

Steel-reinforced elastomeric isolators (SREIs, also called laminated rubber bearings) consist of thin layers of natural or synthetic rubber bonded between steel plates in a vulcanization process (Fig. 1.3). The steel plates increase the vertical stiffness of the isolator by restricting the outward bulging of the rubber layers. As a result of low shear modulus of the rubber, the bearing is flexible under lateral loads. The steel plates have little influence on the lateral response as the lateral stiffness is typically several hundred times lower than the vertical stiffness (Naiem and Kelly 1999). Two thick steel plates (also called mounting plates) are typically bonded to the upper and lower surfaces of elastomeric isolators. In a bonded application, these thick plates are bolted to the substructure below and superstructure above. Alternatively, a dowelled shear connection can be used to transfer lateral loads to the contact surfaces of the bearing through shear keys. In the latter case, no vertical tension is transferred to the bearings (Kelly 1997). SREIs are available as three different types, namely: low-damped rubber bearings, lead-plug rubber bearings, and high-damped rubber bearings (Naiem and Kelly 1999).

Low-damped rubber bearings utilize pure (also called unfilled) rubber as the elastomeric material. Although the required flexibility with linear behavior up to shear strains above 100% is provided by this type of elastomeric bearings, the equivalent viscous damping ratio remains within the range of 2% to 5% which is not sufficient (Naiem and Kelly 1999, Priestley et al. 1996). Also, the bearing may sustain relatively large displacements under service lateral loads. Methods used to overcome these deficits include the use of supplementary damping devices such as lead cores in the bearings.

The lead-plug rubber bearing was developed in New Zealand in 1975 and has since become the most commonly used isolator (Naiem and Kelly 1999). Lead-plug bearings are similar to low-damped rubber bearings except, as shown in Fig. 1.4, they contain a lead-plug that is inserted into a central hole. The lead plug is forced to deform in shear by the reinforcing steel plates. The lead in these isolators respond in an elastic-perfectly plastic manner with a large initial shear modulus of nearly 130 MPa and a shear yield strength of approximately 10 MPa (Priestley et al. 1996). When the lead yields, the lateral stiffness of the bearing is proportional to the lateral stiffness of the rubber. Therefore, lead-plug rubber bearings exhibit a bilinear lateral response. Additionally, depending on the diameter of the lead core, damping values of up to 30% can be achieved (Taylor and Igussa 2004). During the Northridge (1994) and Kobe (1995) earthquakes, buildings isolated with lead-plug rubber bearings performed satisfactorily (Naiem and Kelly 1999). Lateral load-displacement hysteresis loops, up to 100% shear strain, for a typical low-damped rubber bearing and a lead-plug rubber bearing are shown in Figs. 1.5 and 1.6, respectively.

Another alternative to achieve the required level of damping and initial lateral stiffness in a laminated rubber bearing is the use of a high-damping rubber compound as the elastomer layers. In a high-damping natural rubber, first developed in 1982, 10% to 20% inherent damping is achieved by adding extra fine fillers to the rubber compound (Naiem and Kelly 1999). The material is characterized by higher damping and shear modulus at low shear strains. This can limit the lateral deformations under service loads. Within the intermediate range of shear strains where the bearing sustains design level of input earthquake, the shear modulus decreases which results in increased seismic isolation efficiency. At large shear strains, the shear modulus increases as a result of the strain crystallization process in

the rubber. This can limit lateral displacements under unexpectedly large levels of input earthquakes (Naiem and Kelly 1999). Figure 1.7 shows shear stress-strain hysteresis loops (up to 300% strain) for a typical high-damped rubber bearing.

The concept of sliding isolator systems is simple. An interface layer with a defined coefficient of friction between foundation and superstructure will limit the force which can be transferred to the superstructure by the coefficient of friction times the weight. For service lateral loads the coefficient of friction should be high enough to prevent any relative motion between contact surfaces at the interface layer. However, under design lateral loads sliding provides the required flexibility needed in an isolation system. If the system does not provide a restoring force, the isolated structure will end up in a displaced position after the earthquake. The two most common types of sliding isolators are, the friction pendulum system (FPS) with restoring force capability, and flat sliding systems with/without restoring force capability (Taylor and Igussa 2004). The most frequently used materials for the sliding surfaces are unfilled or filled polytetrafluoroethylene (PTFE, or Teflon) on stainless steel. It should be noted that the friction factor at the contact surface of the sliding systems are influenced by "temperature, velocity of interface motion, degree of wear, and cleanliness of the surface" (Naiem and Kelly 1999). Hybrid isolation systems employ different isolator types. The most common type for this generic category is a mixture of elastomeric isolators and flat sliding isolators (Taylor and Igussa 2004).

1.4. Fiber-Reinforced Elastomeric Isolators

Applications of SREI bearings are almost entirely limited to seismic isolation of buildings and structures which are typically large, expensive and of high importance (Tsai and Kelly 2001). The SREI bearings used in these applications are expensive, large, and heavy. The high cost of SREIs is primarily due to the labor intensive manufacturing process involved in fabrication of these bearings, and the vulcanization process which is conducted under high pressure and temperature for several hours (Kelly and Takhirov 2001). In addition, the need for an isolator mold may significantly increase the total cost of SREI bearings (Naiem and Kelly 1999). The heavy weight is due to the use of steel-reinforcing plates. This may in turn increase the lifting, handling, and transportation costs. As such, in spite of their effective performance, SREIs are not considered as a cost-effective earthquake-resistant

strategy for low-rise buildings of ordinary importance; a significant reduction in the weight and total cost, including manufacturing and installation costs, is required.

Fiber-reinforced elastomeric isolator (FREI) bearings can be used as an alternative to conventional SREIs (Kelly 1999b). Similar to SREIs, FREIs are generically elastomeric bearings in which elastomer layers are bonded to the fiber fabric reinforcement layers instead of steel-reinforcement plates. This change of the reinforcement layers may lead to significant cost savings as FREIs become much lighter in weight compared to SREIs. Additionally, labor expenses can be reduced if FREIs are produced in long rectangular strips through a mass production manufacturing technique and then cut to the required size (Kelly 2002).

1.5. Impetus for this Research

An appealing application for FREIs is when their contact surfaces are not bonded or fastened to the superstructure above and the substructure below. Limited experimental studies on unbonded FREI bearings can be found in the literature (Kelly and Takhirov 2001 and 2002, Summers et al. 2004, Mordini and Strauss 2008). To the best of the author's knowledge, no experimental data is available in the literature on the lateral displacement capacity of unbonded FREI bearings and their sensitivity to the rate and history of lateral loading and to the variations in the vertical pressure. Additionally, no experimental work such as a shake table study is found to verify the in-place performance of the FREI bearings to earthquake events.

1.6. Creep and Longevity of Elastomeric Bearings

Natural rubber and neoprene are the most commonly used elastomers in SREIs (Taylor et al. 1992). Elastomeric materials exhibit creep when subjected to a permanent load. Creep in rubber is typically more rapid in the first few weeks of loading and slows with time (Mullins 1984, Roberts 1988). The ratio of creep deflection to the instantaneous elastic deflection depends on the duration of load and the hardness of elastomer. Creep deflections in harder elastomers are more than in softer elastomers. Similarly, filled compounds of rubber exhibit larger creep than unfilled rubbers (Roberts 1988). The geometry of a bearing can influence the level of creep deformation. Bearings with low shape factor (defined as the area of the

bearing in plan divided by perimeter area of a single elastomer layer) usually creep more than bearings with high shape factor (Taylor et al. 1992).

The allowable limit for the maximum compressive creep primarily depends on the importance of the superstructure. For instance, for buildings, creep deformation up to 100% of the instantaneous elastic deformation has been permitted. For bridge structures the limit is 20% to 40% of the instantaneous elastic deformation to maintaining the vertical alignment of these structures (Taylor et al. 1992). These limits of creep, which can easily be satisfied by common formulation of natural rubber and neoprene used in elastomeric bearings (Taylor et al. 1992), would have generally negligible influence on lateral performance of the bearings (Takayama and Morita 1988, Yakut and Yura 2002). Nonetheless, for each design, the influence of elastomer creep on overall performance of the bearing should be evaluated separately. It is possible to estimate the creep deflections of elastomeric bearings over the useful life of the structure based on the short-term creep response data gathered from laboratory tests (Stevenson 1985).

Determining the long-term creep deflection of FREI bearings could be important. However, FREI bearings which are used in seismic isolation of small low-rise buildings are typically subjected to relatively light vertical pressure. In addition, to achieve the target base isolation period, the bearings should employ soft and perhaps unfilled elastomers. Due to high vertical stiffness of the bearings and the relatively light level of applied vertical pressure, the instantaneous elastic deflections would be very small (in the range of 1% to 4% of total thickness of rubber layers in the bearing as demonstrated in Chapters 2 and 4 of this thesis). The use of soft elastomeric compounds in the bearings with reasonable shape factor implies the limited ratios of creep deflection to the instantaneous elastic deflection. As such, the influence of creep on the overall lateral performance of these bearings is not expected to be of any significant concern. Nevertheless, this expectation deserves to be evaluated in a separate research study. Investigation of the creep behavior of FREI bearings is beyond the scope of this thesis.

The normal causes of deterioration in elastomers, such as oxidation and ozone attack, produce only surface effects in a component as large as an elastomeric bearing (Mullins

1984, Stevenson 1985, Roberts 1988). Rubber layers in a vertically compressed bearing are subjected to compression. Ozone attack, which may occur in a rubber in tension, does not occur in a rubber in compression (Mullins 1984). Also, resistance to oxidation and ozone attack can be raised significantly by adding suitable antioxidants and antiozonants ingredients to the rubber compound (Roberts 1988). The most reasonable method for assessing the long-term performance of elastomeric bearings would be inspection and testing of bearings which have been removed from service after many years. However, in view of the lack of such data, results obtained from field inspection and laboratory testing such as accelerated thermal oxidation on the new bearings may be used to evaluate the long-term behavior of the elastomeric bearings (Taylor et al. 1992). In general, elastomeric bearings, which have been in use for over 45 years, have a good record in structural engineering application due to their durability and maintenance-free life (Mullins 1984, Roberts 1988). This fact, to a large extent, provides confidence regarding the expected long-term performance of FREI bearings. Study on the long-term performance of FREI bearings is beyond the scope of this research.

1.7. Research Objectives

The main objectives of this research are as follows:

- Conduct an experimental study on full-scale FREI bearings to evaluate the feasibility of unbonded application, and the role of bearing's geometry in achieving stable lateral response (Unbonded FREI bearings with stable lateral response and capability to provide restoring force are named in this thesis as stable unbonded (SU)-FREIs.).
- Evaluate and verify the mechanical properties of prototype ¼ scale SU-FREI bearings through vertical compression testing as well as cyclic lateral testing under a prescribed constant vertical pressure.
- Investigate the lateral displacement capacity of the ¼-scale SU-FREI bearings, and sensitivity of their lateral response to parameters such as lateral displacement amplitude, amplitude history, displacement rate, and variations in the vertical pressure applied on the bearings.

- Investigate the feasibility of a novel base isolation system that employs SU-FREI bearings in seismic mitigation of a ¼ scale low-rise test-structure through shake table testing.
- Examine the performance of two different analytical models in dynamic response prediction of a low-rise structure seismically isolated with SU-FREI bearings.

1.8. Structure of Thesis

This thesis consists of previously published/prepared material (the sandwich thesis). Therefore, each chapter includes its own bibliography. Although the chapters are related they are discrete with overlaps mainly occurring in their introduction, allowing the chapters to become stand-alone documents. The terms bearing, isolator, and isolator bearing are used interchangeably in this thesis.

Chapter 2 (Paper I) includes a brief literature review of experiments carried out on FREI bearings, and presents the results of an experimental program conducted on full scale square FREIs, with different aspect ratios, to determine the mechanical properties of the bearings. The concept of stable rollover (SR) deformation for properly designed unbonded FREI bearings is introduced. Subsequently, a model to simulate the lateral load-displacement hysteresis loops of the bearings is briefly discussed.

Chapter 3 (Paper II) contains the experimentally-evaluated lateral response of ¼ scale FREIs which were designed to serve as seismic isolators for a ¼ scale base isolated low-rise building. The target response characteristics, design of the bearings, the influence of displacement rate on lateral response, and verification of the lateral response based on provisions of ASCE (2005) have been discussed in this chapter.

Chapter 4 (Paper III) contains the results of an investigation of the influence of parameters such as lateral displacement amplitude, amplitude history, and variations in the vertical pressure on the lateral response of ¼ scale stable unbonded (SU)-FREI bearings. In addition, results of vertical compression tests before and after cyclic lateral testing are presented and discussed. The robustness of the bearings and their lateral displacement capacity are also addressed in this chapter.

Chapter 5 (Paper IV) contains the findings of a shake table study conducted on a ¼ scale test-structure that was mounted on four SU-FREI bearings. Detailed quantitative dynamic response measurements of the tested base isolated structure (BI-structure), when subjected to three different input earthquakes, are compared to the response of a corresponding linear fixed base structure (FB-structure).

Chapter 6 (Paper V) investigates the performance of two analytical models in simulation of lateral response of the SU-FREI bearings, obtained from cyclic lateral testing. Due to the highly nonlinear lateral response of the bearings, the analytical models are employed in an iterative time history analysis approach. Iterations are carried out in order to select model variables that match the experimentally-evaluated hysteresis loops corresponding to the calculated peak lateral displacement of the bearings. The accuracy of these analytical models is verified by comparing the results of the implemented time history analyses with the shake table tests.

In Chapter 7 the important conclusions drawn from this research study and recommendations for future work which would be valuable in this area are reviewed.

1.9. References

ASCE. (2005). "Minimum Design Loads for Buildings and other Structures." *ASCE/SEI 7-05,* American Society of Civil Engineers, New York.

Fuller K. N. G., Gough J., Pond T. J., and Ahmadi H. R. (1997). "High Damping Natural Rubber Isolators" *Journal of Structural Control,* Vol. 4, No. 2. Pages 19-40.

Higashino M., Okamoto S. (2006). *Response Control and Seismic Isolation of Buildings,* Taylor & Francis Group, London.

Kelly, J. M. (1997). *Earthquake-Resistant Design with Rubber,* 2nd edition, Springer-Verlag, London.

Kelly J. M. (1999a). "The Role of Damping in Seismic Isolation" *Earthquake Engineering & Structural Dynamics,* Vol. 28, No. 1, Pages 3-20.

Kelly J. M. (1999b). "Analysis of Fiber-Reinforced Elastomeric Isolators." *Journal of Seismology and Earthquake Engineering (JSEE),* Vol. 2, No. 1, Pages 19-34.

Kelly J. M. (2002). "Seismic Isolation Systems for Developing Countries." *Earthquake Spectra,* Vol. 18, No. 3, Pages 385–406.

Kelly J. M., and Takhirov S. M. (2001). "Analytical and Experimental Study of Fiber-Reinforced Elastomeric Isolators." *PEER Report 2001/11,* Pacific Earthquake Engineering Research Center, University of California, Berkeley.

Kelly J. M., and Takhirov S. M. (2002). "Analytical and Experimental Study of Fiber-Reinforced Strip Isolators." *PEER Report 2002/11*, Pacific Earthquake Engineering Research Center, University of California, Berkeley.

Mullins L. (1984). "Rubber Bearings for the Protection of Buildings from Earthquakes." *Physics in Technology*, Vol. 15, No. 4, Pages 177-183.

Mordini A., and Strauss A. (2008). "An Innovative Earthquake Isolation System using Fiber-Reinforced Rubber Bearings." *Engineering Structures*, (In Press) DOI:10.1016/j.engstruct.2008.03.010.

Naiem F., and Kelly J. M. (1999). *Design of Seismic Isolated Structures*, Wiely, New York.

Priestley M. J. N., Seible F., and Calvi G. M. (1996). *Seismic Design and Retrofit of Bridges*, John Wiley & Sons, Inc., New York.

Robert A. D. (1988). *Natural Rubber Science and Technology*, Oxford University Press, Oxford.

Skinner R. I., Robinson W. H., and McVerry G. H. (1993). *An Introduction to Seismic Isolation*, Wiley, England.

Stevenson A. (1985). "Longevity of Natural Rubber in Structural Bearings." *Plastics and Rubber Processing and Applications*, Vol. 5, No. 3, Pages 253-258.

Summers P., Jacob P., Marti J., Bergamo G., Dorfmann L., Castellano G., Poggianti A., Karabalis D., Silbe H., and Triantafillou S. (2004) "Development of New Base Isolation Devices for Application at Refineries and Petrochemical Facilities." *Proceedings, 13th World Conference on Earthquake Engineering, Vancouver, BC, Canada*, Paper No. 1036.

Takayama M. and Morita K. (1988). "Creep Tests of Full-Scaled Laminated Rubber Bearings." *Proceedings, The ASME/JSME Joint Pressure Vessels and Piping Conference, San Diego, CA*, Pages 95-102.

Taylor A. W., Lin A. N., and Martin J. W. (1992). "Performance of Elastomers in Isolation Bearings: A Literature Review." *Earthquake Spectra*, Vol. 8, No. 2, Pages 279-303.

Taylor A. W., and Igussa T. (2004). *Primer on Seismic Isolation*, American Society of Civil Engineers, ASCE, Reston, Virginia.

Tsai H. C., and Kelly J. M. (2001). "Stiffness Analysis of Fiber-Reinforced Elastomeric Isolators." *PEER Report 2001/05*, Pacific Earthquake Engineering Research Center, University of California, Berkeley.

Yakut A., and Yura J. A. (2002). "Evaluation of Elastomeric Bearing Performance at Low Temperatures." *Journal of Structural Engineering, ASCE*, Vol. 128, No. 8, Pages 995-1002.

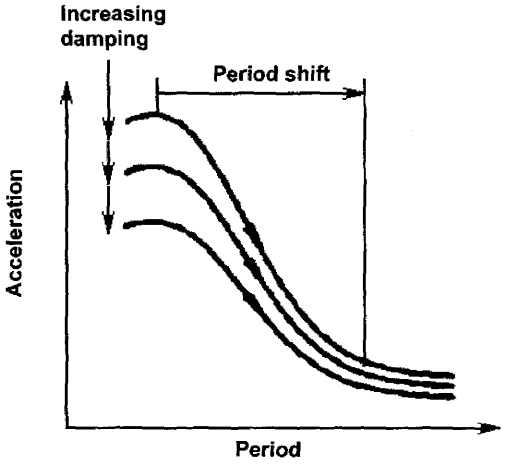

Figure 1.1. Decreased seismic acceleration due to increasing period and damping (Skinner et al. 1993)

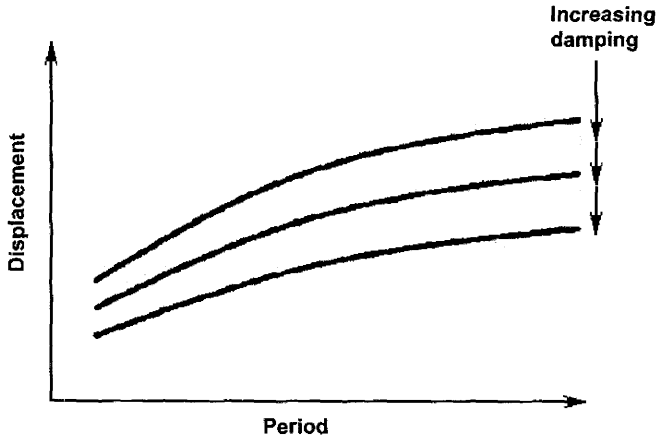

Figure 1.2. Increasing displacement response with increasing period as offset by increasing damping (Skinner et al. 1993)

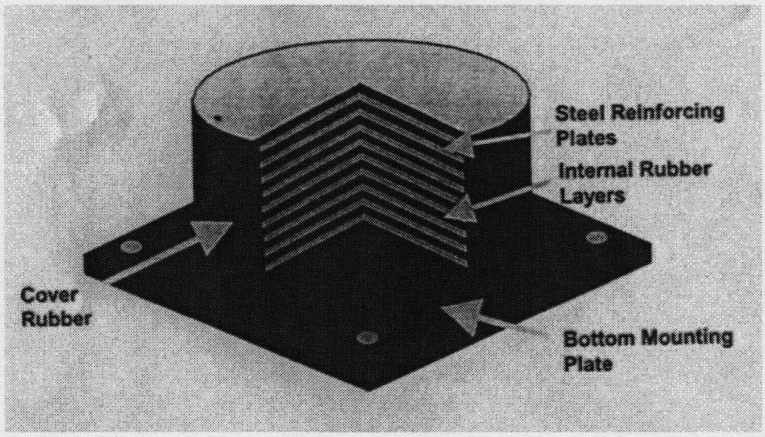

Figure 1.3. Typical laminated rubber bearing; top mounting plate not shown (Taylor and Igussa 2004)

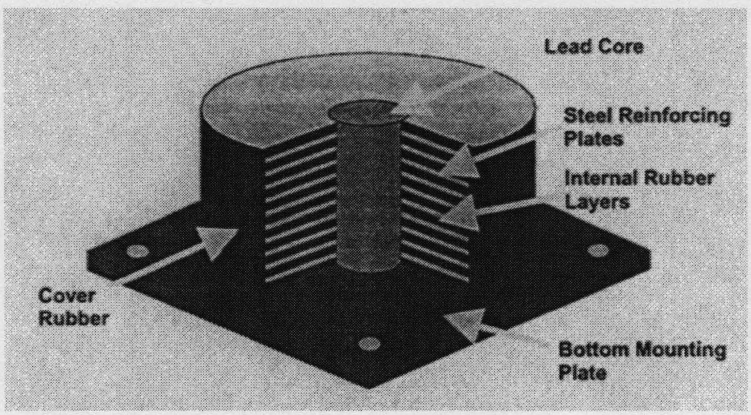

Figure 1.4. Typical lead-plug rubber bearing; top mounting plate not shown (Taylor and Igussa 2004)

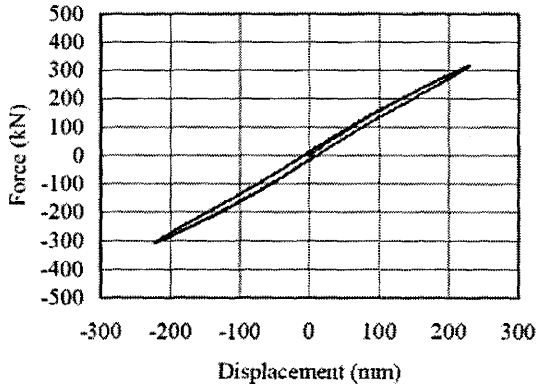

Figure 1.5. Typical hysteresis loops of a low-damped rubber bearing at 100% shear strain (Higashino and Okamoto 2006)

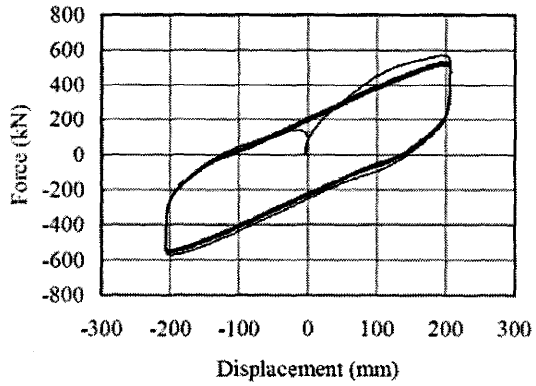

Figure 1.6. Typical hysteresis loops of a lead-plug bearing at 100% shear strain (Higashino and Okamoto 2006)

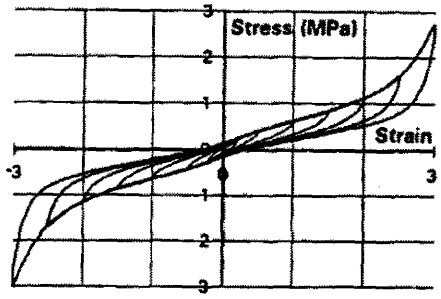

Figure 1.7. Typical hysteresis loops of a high-damped rubber bearing (Fuller et al. 1997)

Chapter 2: Testing and Modeling of Square Carbon Fiber-Reinforced Elastomeric Seismic Isolators

2.1. Summary

Steel-reinforced elastomeric isolators (SREIs), as an effective seismic isolation device, are the most common isolators in use. However, SREIs are typically heavy and expensive and, as a result, application of these devices is often limited to large and expensive structures. A reduction in the cost and weight of elastomeric isolators would permit a significant increase in their application to many ordinary residential and commercial buildings. Fiber-reinforced elastomeric isolators (FREIs) are a new type of elastomeric bearing that employs fiber as the reinforcement material rather than steel. FREIs have several advantages over traditional SREIs including superior damping properties, lower manufacturing cost, light weight, and the possibility of being produced in long rectangular strips with individual isolators cut to the required size. This paper presents a brief literature review on experiments with FREIs, and reports on an experimental study conducted on carbon FREIs from which the mechanical properties of the bearings, including displacement characteristics and damping values are evaluated. A brief description of an analytical approach to model the cyclic response of the bearings is another component of this paper. As a special application, the bearings considered in this study were not bonded to the test platens. For bearings having suitable aspect ratio values, this particular type of application resulted in a stable rollover deformation, which reduced the horizontal stiffness and increased the efficiency of the bearing as a seismic isolator device. Test results suggest that for many high seismic risk regions worldwide, the application considered in this study can be viable for the base isolation of ordinary low-rise buildings.

2.2. Introduction

The philosophy of conventional seismic design is that structural collapse must be prevented during severe earthquake events and structural damage should be avoided or minimized in moderate seismic events. To satisfy these criteria, a structure must have sufficient strength

to resist seismic forces, enough ductility to absorb earthquake energy, and adequate stiffness to maintain structural integrity and serviceability. In many countries, the engineering design, construction, and inspection services allocated to small and low-cost private buildings may not be sufficiently comprehensive to provide an adequate level of structural safety against strong or even moderate ground motions. Past earthquakes, especially in developing countries, have indicated that major loss of life often occurs due to the collapse of poorly constructed buildings. If the level of seismic demand on these buildings were reduced through a simple but reliable engineering solution, this would result in fewer building failures and less loss of life.

Base isolation, which is aimed at reducing the seismic demand instead of increasing the earthquake-resistant capacity of the structure, is an attractive alternative to conventional earthquake-resistant design methods. The idea is particularly effective for low to medium-rise (i.e. stiff) buildings where the fundamental period of vibration is in the range where earthquake energy content is concentrated. During an earthquake, these buildings act as vibration amplifiers, increasing the induced accelerations and inter-story drifts at top floors. This amplification may result in damage to structural elements of the building. In an isolated structure however, due to the insertion of a flexible layer between the foundation and the superstructure, the fundamental period of the system increases to a value longer than the predominant energy containing time periods of earthquake ground motions. The first mode of vibration in an isolated structure involves deformation only at the isolation level, whereas the superstructure remains nearly rigid. In this way, seismic isolation, if economically and practically justified, becomes an attractive technique to mitigate seismic demands on many ordinary buildings. In general, a seismically isolated structure designed in conformance with current code provisions should be able to: (1) withstand minor and moderate levels of earthquake ground motion without damage to structural elements, nonstructural components, or building contents; and (2) resist severe earthquakes without failure of the isolation system, without significant damage to structural elements and nonstructural components, and without major interruption to facility function (ASCE 2005). Such a rewarding design philosophy seeks the survival of life as well as the building asset against a strong ground motion.

Steel-reinforced elastomeric isolator (SREI) bearings are the most common type of isolators in use. SREIs are typically large, heavy, and expensive; their application as a superior earthquake-resistant strategy is primarily justified for large and expensive buildings. However, this justification cannot be easily extended to ordinary housing and commercial buildings. As a common practice, the manufacture of a SREI requires steel plates to be cut, sand blasted, acid cleaned, and coated with bonding compound. Next, the assembly of compounded sheets of rubber and interleaved steel plates are pressed in a mold, and heated for several hours. The heavy weight is due to the reinforcing steel plates, and the high cost is primarily due to the highly labor-intensive manufacturing tasks, as well as the vulcanization process, which occurs under high pressure and temperature (Kelly 2002). Therefore, potential cost savings exist if the steel plates are replaced with other materials having approximately the same order of elastic stiffness as steel, so that the construction process of the bearing becomes easier and less labor-intensive, perhaps by eliminating the vulcanization and automating the manufacturing technique.

Fiber-reinforced elastomeric isolators (FREIs), which utilize fibers as the reinforcing material instead of steel, are a relatively new type of laminated bearing. In contrast to the steel-reinforcement in a SREI, which remains relatively rigid in both extension and flexure, the thin layers of fiber-reinforcement used in a FREI are more flexible in extension and have no flexural rigidity. Fiber-reinforcement comprises a large number of individual fibers which are grouped into strands, woven into a fabric, and embedded into a thin polymer matrix. Since in-plane tension in the fabric tends to straighten out the fiber strands and stretch the fabric, the fiber-reinforcement is more flexible in extension than the individual fibers. This stretching action also results in an increasing effective tensile modulus with increased stretching of the fiber-reinforcement. Initial studies (Kelly 1999, 2002) indicate that it is possible to achieve adequate vertical and horizontal stiffnesses in FREIs. Moreover, FREIs have a number of advantages over SREIs including superior energy dissipation capability, potentially low manufacturing cost, light weight, and the possibility of being produced in long rectangular strips or large sheets and being modified to the required size locally.

The use of seismic isolation in new low-rise buildings cannot be extended unless an alternative strategy is adopted. Clearly, an alternative seismic isolation strategy should employ cost effective isolators in a simple application. Square carbon FREIs, as an example of alternative bearing isolators, were studied in this research program. To reduce the manufacturing cost, bearings were constructed in a square shape without any bonded thick end plates so that in practice they can be easily cut to size from a strip FREI. Additionally, being square, identical mechanical properties in the two perpendicular directions of movement can be achieved.

As a novel application, square FREI bearings can be placed easily between the superstructure and the foundation with no bonding at the contact surfaces. As a result, installation of the bearings is significantly simplified and is well suited where no detachment, due to overturning, occurs between the superstructure and bearings. An additional advantage is that, compared with traditional application for SREI bearings, the FREI bearings can be placed close together. Therefore, reinforced concrete support beams, which are constructed above the bearings to support the superstructure between bearings, are not required to be heavily reinforced. Therefore, no major additional cost is imposed on construction of the base isolated building.

This paper includes a brief literature review of experiments with FREIs, and presents the results of an experimental program conducted on square carbon FREIs constructed at McMaster University. Stable rollover (SR) deformation of bearings is introduced as a unique characteristic of using FREIs with unbonded boundary conditions at its contact surfaces. Subsequently, an analytical approach to model the bearings is briefly discussed.

2.3. Literature Review

Kelly (1999) conducted an experimental study on cylindrical handmade bearings consisting of high damped rubber with 8% effective damping and 0.69 MPa nominal shear modulus, reinforced with Kevlar fibers. From the test results, it was revealed that fiber-reinforcement can provide acceptable compressive stiffness. Additionally, lack of flexural rigidity of this reinforcement was shown to have only a small effect on the horizontal stiffness of the bearing. The generated hysteresis loops under combined compression (6.90 MPa) and shear

showed the same general characteristics as traditional SREI bearings with a stable behavior up to a peak shear strain of 150%. Furthermore, the obtained damping ratio of 15% at 100% shear strain was higher than anticipated and revealed a new source of energy dissipation in the bearing. This was an unexpected advantage of using fiber as the reinforcement in elastomeric bearings.

Seven rectangular carbon FREIs that used rubber compound sheets with nominal shear modulus of 0.69 MPa were tested (Kelly 2002, Moon et al. 2003) under both a compression load (to measure the compressive stiffness) and a combination of compression and shear loading (to measure the horizontal stiffness and effective damping). For the latter case, under different values of vertical compression, namely 1.73, 3.45, and 6.90 MPa, the tests were conducted under displacement control (up to 150% shear strain) and repeated for orientations of 0°; 90°; and 45°; respectively, with respect to the longitudinal direction of the strip. It was observed that loading along 0° produced stiffening in the hysteresis loops, whereas along 90° (i.e. the cross direction) a softening behavior tended to occur. Loading at 45° produced neither softening nor stiffening. Experimental results confirmed that it is possible to produce a strip FREI that matches the behavior of a SREI. The measured horizontal stiffnesses and the maximum accommodated displacement indicated that the concept of carbon strip FREI is viable.

Moon et al. (2002) compared the performance of a cylindrical carbon FREI with that of the same size SREI. The difference between the steel plate and the fiber thickness was adjusted by using more layers of fiber and rubber in the FREI. Accordingly, bulging of the FREI was smaller than that of the SREI due to the thinner layers of rubber in the FREI. Unlike previous studies (Kelly 2002, Moon et al. 2003), where the bearings were built without end plates and were not bonded to the test machine during the test, both types of bearings were bonded to thick end plates. The researchers concluded that the performance of the FREI was superior to that of the SREI. However, additional comparative studies between FREIs and SREIs in a bonded application still need to be carried out.

Summers et al. (2004) conducted an experimental study on prototype rectangular carbon FREIs as a potential seismic protection strategy for liquid storage tanks. The bearings consisted of high damped rubber compound (11% effective damping) with 0.4 MPa nominal shear modulus. They were subjected to a 100% maximum shear deformation, with an average displacement rate of 100 mm/s, under constant vertical compression of 1.79 MPa. The recorded hysteresis loops showed stable behavior.

2.4. Research Objectives

The main objective of this study was to evaluate the design properties including displacement characteristics and damping properties of square carbon FREI bearings through vertical compression and horizontal cyclic tests. As mentioned earlier, the bearings were for the application of seismic isolation in ordinary low-rise residential or commercial buildings. To reduce both construction and labor costs, the bearings were intended to be placed between the superstructure and foundation with no bonding at the contact surfaces. To simulate this novel application, isolator bearings were not bonded to the test machine. The viability of this special application and the effectiveness of employing carbon FREIs as a seismic isolation device were examined through test results.

2.5. Test Specimens

Two carbon FREI bearings were built in the Applied Dynamic Laboratory (ADL) at McMaster University. Each bearing consisted of bonded layers of intermediate elastomer and reinforcement as well as two bonded thinner elastomeric covers at the top and bottom. The total thickness of rubber layers was t_r = 94 mm: The width was b = 200 mm and the total height was approximately h = 105 mm: The shape factor (defined as the ratio of loaded area to load free area of the elastomer layer) was S = 10.6 and the aspect ratio (i.e. width to total height ratio, sometimes called the second shape factor) of the bearings was approximately R = 1.9.

The elastomer was a soft compound of natural gum rubber with a hardness of 40±5 Durometer (Shore A (ASTM 2005)). Bi-directional (orientations 0/90°) carbon fiber fabric was utilized as the reinforcement. The matrix volume fraction in the fiber-reinforcement

was approximately 56%. The bearings were made without the use of a mold, and as indicated in Fig. 2.1a, all lateral faces were trimmed with a standard band saw. Next, a finishing coat of bonding compound was applied to the lateral faces of each bearing to prevent any premature delamination (see Fig. 2.1b).

2.6. Test Setup and Instrumentation

An overview of the test setup and its sketch can be seen in Figs. 2.2 and 2.3, respectively. The test setup was designed to perform both the vertical and horizontal (cyclic) testing on the prototype bearings. The bearing was located between two 100 mm thick steel platens. Horizontal displacements were imposed via a horizontal hydraulic actuator attached to the lower platen. The lower platen was mounted on four linear bearings that permitted ±150mm displacement with respect to the upper platen. The upper platen was braced to the body of the horizontal actuator at its lateral sides through two arms providing a self-equilibrating system. The bearing was subjected to near pure shear as the horizontal action and the reaction forces passed through its midheight.

A function generator was used to generate the desired amplitude and frequency of sinusoidal signals. A linear variable differential transducer (LVDT#1 in Fig. 2.3a) was attached to the setup to measure the relative horizontal displacements between the upper and lower platens and acted as the feedback signal for the closed-loop system. The vertical actuator was operated in load control in order to maintain the magnitude of the vertical load, while the cyclic (horizontal) test was in progress.

Figures 2.3b and 2.3c illustrate the instrumentation used for the test setup. Load cell #1 was used to measure the horizontal loads corresponding to different horizontal deflections imposed on the bearing. The relative horizontal movement between the lower and upper platens was monitored through a string pot (SP #1). Four laser displacement transducers (LDT #1 to #4) were used to measure the vertical deflection of the bearing at its four sides during the vertical testing. The vertical deflection was calculated by taking the average value of the LDTs readings. To achieve a symmetrical setup, four identical load cells (i.e. cells #2 to #5) were used to measure the vertical load. Steel bearings were placed between

the upper platen and these four load cells to ensure no horizontal load was transferred to the load cells measuring the vertical load.

2.7. Vertical Compression Test

The vertical compression modulus as well as the maximum vertical deflection of the bearings was evaluated through vertical compression testing, which was conducted under load control. Each bearing was monotonically loaded up to 1.6 MPa design vertical pressure (64 kN). Next, three fully reversed cycles with ±0.35 MPa variation with respect to the design vertical pressure were performed, and subsequently the bearing was monotonically unloaded. Figures 2.4a and 2.4b present the results of the vertical test on Bearings B1 and B2, respectively. The photo in each figure shows the corresponding test in progress. The slope of the dashed straight line represents the average stiffness of each bearing at design load during the cyclic reversals of loading.

From the test results, the tangent vertical stiffness values, described above, were calculated as $(K_v)_{B1}$ = 76.13 kN/mm; and $(K_v)_{B2}$= 72.87 kN/mm; respectively, for Bearings B1 and B2. These correspond to effective compression modulus values of $(E_c)_{B1}$ = 178.9 MPa and $(E_c)_{B2}$ = 171.2 MPa. The corresponding calculated effective vertical frequency values of $(f_v)_{B1}$ = 17.2 Hz and $(f_v)_{B2}$ = 16.8 Hz; respectively, are considered satisfactory values for isolation applications (Kelly 2002). Accordingly, these bearings provide sufficient vertical stiffness for vertical pressures around the design value of 1.6 MPa. The total vertical deformation of the Bearings B1 and B2 at the design vertical compression was 3.9 and 3.1 mm, respectively. Since the relaxation rate of a natural gum rubber is generally as low as approximately 1.5% per decade (Robert 1988), no significant long-term increase in the vertical deformation of the bearings is expected.

As illustrated in Figs. 2.4a and 2.4b, both bearings showed a significant run-in before developing any vertical stiffness. The results of tensile tests conducted on coupon specimens, made from the carbon-reinforcement sheets, showed a similar pattern for tensile load versus elongation. This indicates that carbon fibers in the constructed bearings were not initially sufficiently taut to develop stress under initial vertical and corresponding

horizontal deformations. However, since the required compression modulus was developed at design vertical pressure, this is not considered a significant shortcoming.

2.8. Horizontal Cyclic Displacement Tests

2.8.1. Test Procedure and Calculations

Cyclic tests on prototype isolators provide one of the most reliable methods to identify the deformation characteristics and damping values of any isolation system. Cyclic tests are performed under horizontal displacement control and vertical load control. All tests were conducted at room temperature (21 ± 2 °C) and data were sampled at a rate of 200 Hz. The testing procedure was as follows: while the bearing was subjected to a constant vertical pressure, four fully reversed sinusoidal cycles of horizontal displacement at amplitudes of 25% t_r; 50% t_r; 75% t_r; 100% t_r; 125% t_r; 150% t_r; and 200% t_r (where t_r is the total thickness of rubber layers in each bearing) were applied. The bearing was vertically unloaded after cyclic loading at each amplitude.

The bearing's effective horizontal stiffness, corresponding to each load cycle of the test, can be calculated based on the peak lateral load and peak displacement as follows (ASCE 2005):

$$K_{h,eff} = (F_{\max} - F_{\min})/(\Delta_{\max} - \Delta_{\min}) \tag{2.1}$$

where F_{max}; F_{min}; Δ_{max}; and Δ_{min} are the peak values of horizontal load and horizontal displacement, respectively, at the extremes of the cyclic displacement range. The calculation of the ratio of equivalent viscous damping of the bearing at each cycle is given below (Clough and Penzien 1975)

$$\xi = W_d /(4\pi W_s) \tag{2.2}$$

where W_d represents the dissipated energy (area within the hysteresis loop) and W_s is the restored (elastic) energy calculated as

$$W_s = \tfrac{1}{2} K_{h,eff} \Delta^2_{\max,ave} \tag{2.3}$$

In which $\Delta_{\max,ave} = (\Delta_{\max} + |\Delta_{\min}|)/2$

2.8.2. Rate Sensitivity Tests

For a rate-sensitive base isolator, the most reliable results will be achieved when the sinusoidal cyclic test is performed dynamically at a frequency equal to the inverse of the target period of the isolator device (ASCE 2005). However, due to the cost of real-time dynamic experiments, a compromise can be made by selecting a lower frequency (or rate) at which experimental results remain sufficiently accurate from an engineering application point of view.

To identify a suitable lateral displacement rate, Bearings B1 and B2 were subjected to a set of sinusoidal cyclic tests having identical displacement amplitudes of 47 mm (i.e. 50% t_r) at different frequencies ranging from 0.16 to 0.66 Hz. Under a constant vertical pressure of 1.6 MPa each bearing was subjected to three fully reversed cycles. The maximum frequency of 0.66 Hz at 47 mm horizontal displacement was the highest rate achievable by the horizontal actuator used in the test setup. The effective damping and horizontal stiffnesses are listed in Tables 2.1a and 2.1b. Figure 2.5 contains plots of these values corresponding to different frequencies. These results reflect the average values of horizontal stiffnesses and damping ratios of the bearings after three reversed displacement cycles based on Eqs. (2.1) and (2.2).

From the test results, the rate variation had negligible influence on the effective horizontal stiffness and, at frequencies larger than 0.48 Hz, also had negligible influence on damping ratios of the bearings. To work within the equipment's capabilities, an average displacement rate of approximately 90 mm/s (corresponding to the frequency of 0.48 Hz at 50% t_r) was selected for the cyclic testing program. This rate was consistent with the values used in previous experimental studies (Kelly 2002, Moon et al. 2003).

2.8.3. Cyclic Test on Bearings B1 and B2

Bearings B1 and B2 were tested under constant 1.6 MPa vertical compression with the following sequence of peak cyclic lateral displacements: 25; 50; 75; 100; 125; and 150% t_r (where t_r = 94 mm). Figures 2.6a and 2.6b show the horizontal load–displacement curves associated with all cycles of testing for Bearings B1 and B2, respectively. As illustrated, the horizontal load–displacement behavior of Bearings B1 and B2 was found to be very consistent for all amplitudes tested. Both bearings behaved almost linearly up to approximately 75% t_r horizontal displacement (70.5 mm) with an effective horizontal stiffness of 0.13 kN/mm and a 2.1% effective damping ratio calculated using Eqs. (2.1) and (2.2), respectively. At larger lateral displacements, a nonlinear softening behavior was observed. This softening is associated with the rollover deformation of the bearing, which resulted from the unattached boundary conditions at its contact surfaces. It also implies that no strain crystallization occurred in the elastomer to provide stress hardening.

To study the influence of higher vertical pressure on improving the horizontal response of the bearing, cyclic tests were duplicated under an increased constant vertical pressure of 3.2 MPa (Fig. 2.7). Analogous to the previous case, a linear response of up to 75% t_r horizontal displacement was observed but the effective horizontal stiffness of the bearing decreased to 0.12 kN/mm and the effective damping ratio increased to 5.2%. A significant increase in the damping values of FREIs due to higher vertical pressure is a unique feature not found in SREIs. This fact reveals one of the advantages of using fibers as the reinforcement (Kelly 1999). At lateral displacements larger than 75% t_r; as indicated in Figs. 2.7a and 2.7b, both bearings performed nonlinearly and again tended to show a softening-type behavior.

No damage was visible after the cyclic tests were completed. Furthermore, the repeatable pattern of the load hysteresis loops, even up to the maximum lateral displacements, implied that negligible damage occurred in the bearings. As a result of the softening behavior at high displacements, the performance of bearings B1 and B2 with an aspect ratio of R = 1.9 was deemed unacceptable. In an attempt to improve the lateral load–displacement response of the bearings, it was decided to increase the aspect ratio by reducing the bearing thickness. In order to study the influence of different aspect ratios on improving the lateral response,

new Bearings NB1 and NB2 were cut from B1 and B2 to achieve aspect ratios of R_{NB1} = 2.5 and R_{NB2} = 2.9, respectively.

2.8.4. Cyclic Test on Bearing NB1 (R_{NB1} = 2.5)

Figures 2.8a to 2.8d show the hysteresis loops of Bearing NB1, when subjected to horizontal cyclic displacements parallel to the sides of the bearing (0° orientation) with different amplitudes ranging from 17.5 to 140 mm which correspond to 25–200% $t_{r,NB1}$, respectively (where total thickness of rubber layers $t_{r,NB1}$ = 70.5 mm). Such a response is denoted here as parallel response. Figures 2.9a to 2.9d show photographs taken during cyclic testing on Bearing NB1 at different extreme lateral displacements.

As illustrated in Fig. 2.8a, the bearing performs almost linearly up to 75% $t_{r,NB1}$ (53mm lateral displacement) with an effective stiffness of 0.21 kN/mm and effective damping ratio of 1.5%. However, at larger lateral displacements, due to the rollover deformation of the bearing, the tangent horizontal stiffness dramatically drops to its minimum-yet-positive value. At extreme lateral displacements (larger than 150% $t_{r,NB1}$ as illustrated in Fig. 2.8c), a hardening behavior is observed when the vertical faces of the bearing contact the upper and lower platens (see Fig. 2.9d). This hardening is considered to be an advantage as it limits the maximum lateral displacement of the bearing and ensures the overall stability of the device against the maximum considered earthquake (MCE). After the completion of these second series cyclic tests, no delamination or any other damage was observed in the bearing.

Figures 2.10a to 2.10d show the lateral load–displacement data from Bearing NB1 when horizontal displacements were imposed along the diagonal (45° orientation) of the bearing. Figures 2.11a to 2.11d show photographs taken from cyclic testing at different amplitudes of horizontal displacements. Such a response is denoted here as diagonal response. As indicated in Figs. 2.10b to 2.10d, due to rollover deformation of the bearing, the tangent horizontal stiffness dramatically decreases to a minimum positive value at high displacements. This will result in increased efficiency of the seismic isolation device. In fact, the diagonal response of the bearing is the same as the response in the 0 and 90° directions, except that the hardening behavior occurs at lateral displacements larger than 200% $t_{r,NB1}$.

Since no zero or negative tangent horizontal stiffness was observed, the diagonal performance of the bearing is considered to be acceptable.

As indicated in Figs. 2.8d, 2.10b, and 2.10c, during the first cycle of displacement, the tested bearings exhibited higher stiffness and damping than in the following cycles. In general, for given amplitude of lateral displacement, the hysteresis loops stabilized after the first cycle of the test, resulting in stable horizontal stiffness and damping values. Such stable properties are usually denoted as "scragged" properties (Taylor and Igusa 2004). This effect, which is associated with internal changes in the rubber, is prominent in low modulus elastomer bearings especially at larger lateral displacements. Depending on the compound of the elastomer, all or some of the unscragged properties are usually recovered after a period of time. Table 2.2 summarizes the scragged values of effective horizontal stiffnesses and damping ratios of Bearing NB1 associated with parallel and diagonal response of the bearing, respectively. These values were calculated based on Eqs. (2.1) and (2.2). According to Table 2.2, while the scragged values of parallel and diagonal horizontal stiffnesses corresponding to different displacement amplitudes are comparable, damping ratios in the diagonal performance, due to more distorted pattern of deformation in the bearing, are higher than the response in the parallel direction.

After completion of the diagonal cyclic test with the extreme amplitude of 200% $t_{r,NB1}$; as indicated in Fig. 2.12, significant delamination in one of the laminated layers of the bearing was observed. However, according to Fig. 2.10c, the resulting hysteresis loops remained stable with no significant stiffness degradation. Therefore, the bearing did not experience a failure but the interfacial friction at opposite faces of the debonded layer did dissipate more energy. Even in the case of complete debonding along one laminate interface of the bearing, the shear force will be transmitted between the adjacent two delaminated parts through friction. Therefore, no significant degradation in the horizontal response is expected. Previous experimental studies have revealed that, in fiber-reinforced bearings, it is possible to effectively employ two bearings in a stacked pattern of application in which one simply sits on the top of the other (Kelly 2002).

2.8.5. Cyclic Test on Bearing NB2 (R_{NB2} = 2.9)

Bearing NB2, with a total thickness of 69 mm, was cut through the thickness of Bearing B2 so that an aspect ratio of R_{NB2} = 2.9 was achieved. The total thickness of rubber layers of the bearing was reduced to $t_{r,NB2}$ = 61.1 mm: Similar to the previous bearings, under constant 1.6 MPa vertical compression, this bearing was subjected to sinusoidal cyclic lateral displacements with different displacement amplitudes ranging from 25 to 200% of the total thickness of the rubber layers in the bearing. Figures 2.13a and 2.13b are typical examples of the time history plots of the imposed lateral displacements having amplitudes of 91.6 and 122 mm corresponding to 150% $t_{r,NB2}$ and 200% $t_{r,NB2}$, respectively.

Figure 2.14a shows the hysteresis loops from a set of parallel cyclic tests conducted on Bearing NB2. This bearing showed a linear behavior up to approximately 75% $t_{r,NB2}$ (≈ 46 mm) lateral displacement with an effective stiffness of 0.25 kN/mm and an effective damping ratio of 1.3%. However, due to rollover deformation, the tangent horizontal stiffness of the bearing gradually decreases to its minimum value at larger lateral displacements (see Table 2.3). Similar to the parallel loading behavior of Bearing NB1, at extreme lateral displacements when the vertical faces of the bearing contacted the upper and lower platens, a hardening behavior was observed. In the diagonal test direction, the bearing showed a bilinear behavior with positive tangent stiffness throughout (Fig. 2.14b). As listed in Table 2.3, for given amplitudes of displacement, effective scragged horizontal stiffnesses of the bearing along the diagonal direction are close to the corresponding values for loading in the parallel direction. This is not the case for damping ratios as, due to the increased distorted pattern of deformation, the diagonal response produces more energy dissipation than the response for loading in the parallel direction.

After completion of the cyclic tests, no damage was visible in Bearing NB2. Additionally, the stable pattern and repeatability of hysteresis loops at different displacement amplitudes including 122 mm (200% $t_{r,NB2}$) indicated that no noticeable damage had occurred inside the bearing. As a result, the bearing can be safely subjected to the maximum 122 mm lateral displacement.

2.9. Observations of Performance

2.9.1. Stable Rollover (SR) Deformation

In this study, all bearings exhibited a rollover type of deformation when subjected to lateral loads. This rollover deformation results from the unbonded boundary condition of the bearing at its contact surfaces as well as the lack of flexural rigidity in the fiber-reinforcement layers. This deformation and the resulting significant reduction in the horizontal stiffness of the bearing are considered acceptable if the resulting tangent horizontal stiffness of the bearing remains positive. In such a case, when the vertical faces of the bearing touch the upper and lower platens at very large lateral displacements, a hardening behavior is observed. This hardening limits the maximum lateral displacement of the bearing and ensures its overall stability. As such it is considered to be an advantage. Such an admissible deformation is denoted hereafter as a stable rollover (SR) deformation. A SR deformation neither results in a softening behavior nor does it compromise the overall stability of the bearing. Furthermore, being a seismic isolation device, it adds to the efficiency of the bearing as the horizontal stiffness is reduced during early stages of rollover. As a result, this unique performance is considered advantageous for the application of FREIs with unbonded contact surfaces.

Considering the SR deformation of bearings at large lateral displacements, a transverse tension, especially at the extreme edges of the bearing, is likely to develop between the elastomer and fiber-reinforcement layers. According to the experimental observations, even at extreme lateral displacements, this tension was resisted by the polymer matrix rather than the fiber fabric so that the bearing maintained its integrity and remained functional.

The SR deformation cannot be expected in a fiber-reinforced bearing with bonded contact surfaces. Additionally, traditional SREI bearings even with an unbonded boundary condition at contact surfaces cannot exhibit such behavior because of the flexural rigidity in the steel-reinforcement plates. Test results suggest that a FREI bearing having an appropriate aspect ratio, which exhibits a SR deformation in an unbonded application, will sustain larger lateral displacements, and have lower horizontal stiffnesses than the same bearing in a bonded application. Therefore, in an unbonded application, it will perform more efficiently. In order

to achieve the same level of seismic mitigation efficiency, the effective horizontal stiffness of a bearing (SREI or FREI) employed in a bonded application could be reduced through an increase in the total height of the bearing. This will usually be accompanied by an extension in plan dimensions of the bearing to prevent any instability at extreme lateral displacements. As a result, to achieve identical efficiency, the bearings engaged in a bonded application will have larger physical dimensions than the FREI bearings in an unbonded application. This implies that an unbonded application of a FREI is more cost effective than the traditional bonded application. The idea seems to be an appealing seismic isolation strategy which is well suited for ordinary low-cost residential and commercial buildings.

2.9.2. Influence of Aspect Ratio (R)

The lateral load–displacement performances of Bearings B1 and B2 were found to be unacceptable as they exhibited negative tangent horizontal stiffness due to unstable rollover deformation (Fig. 2.6). The same unacceptable behavior was observed when the vertical compression was doubled (Fig. 2.7). Tests of Bearings NB1 and NB2 revealed that, for a FREI with given material properties and shape factor (S), the aspect ratio (R) of the bearing plays a crucial role in achieving a SR deformation (Figs. 2.8, 2.10, and 2.14).

2.9.3. Influence of Compression Load

According to the test observations, a 100% increase in the vertical compression of Bearings B1 and B2 resulted in only a small reduction in the effective horizontal stiffness of these bearings. This implies that the vertical load was sufficiently below the buckling load of the bearing so that its influence on the horizontal stiffness of the bearing was negligible. On the other hand, a doubled vertical pressure resulted in a significant increase in the energy dissipated by the FREI bearings (see Figs. 2.6 and 2.7). This is attributed to an increase in the parallel tension in the fibers. Carbon fiber fabric consists of strands of fibers woven together. When a FREI bearing is deformed laterally, the reinforcement layers become curved due to the lack of flexural rigidity. Accordingly, it is reasoned that the in-plane tension in the curved fibers forces the strands to slip against each other, which dissipates energy through friction (Kelly 1999).

2.9.4. Influence of Rate and Amplitude of Displacement

In an unfilled (or pure) natural rubber, shear modulus and inherent damping are almost rate independent (Robert 1988). Since the horizontal stiffness of the bearing is primarily governed by mechanical properties including the shear modulus of the rubber, the rate of lateral displacement should not significantly influence the horizontal stiffness of the bearing. Test results confirmed this expectation (see Tables 2.1a and 2.1b).

As long as no damage occurs in the bearing components, it is postulated that there are two sources providing energy dissipation in the bearings tested in this study. These are the inherent damping of the natural rubber, which is almost rate independent in the case of an unfilled compound of elastomer, and that of the carbon fiber-reinforcement. More experimental studies are required to explore the influence of rate on energy dissipation of the fiber-reinforcement in FREI bearings that exhibit SR deformation.

Test results showed that, as the horizontal stiffness decreased with increasing lateral displacement amplitude, the damping ratio increased. This is independent for the orientation of the horizontal displacement of the bearing. The decrease in horizontal stiffness is due to the decrease in the shear modulus of the rubber at higher strain amplitudes as well as the rollover deformation of the bearing. It is postulated that an increase in the damping properties with increased amplitude of displacement can be attributed to larger energy dissipation in the fiber-reinforcement as the pattern of deflection becomes more distorted. A comparison of the parallel loading versus diagonal responses of the bearings (see Tables 2.2 and 2.3) implies that, in the diagonal response, higher energy dissipation is achieved as strands of fibers are involved in a more distorted pattern of deformation providing greater interfacial slippage.

2.9.5. Performance of Bearing NB1

As illustrated in Fig. 2.8d, for displacements parallel to the sides of the bearing, the nonlinear behavior of Bearing NB1, due to a SR deformation, has three distinct response components that can be modeled with a simple trilinear idealization. A bilinear idealization can be used to model the horizontal response of the bearing for displacements in the diagonal direction. The bearing behaved almost linearly up to a lateral displacement of

53mm (≈ 75% $t_{r,NB1}$). For minor earthquakes, which may occur several times during the service life of a structure, this bearing can be designed to remain within its initial stage of lateral load–displacement response with an effective horizontal stiffness ranging from 0.21 to 0.27 kN/mm (see Table 2.2).

Overall, the tangent horizontal stiffness values of the bearing for loading in the diagonal direction are larger than in the parallel direction. Thus, diagonal loading raises fewer concerns regarding the stability of the device and load recovery. Despite this fact, according to Table 2.2, the values of effective horizontal stiffnesses of the bearing for loading in the diagonal direction are in close agreement with the parallel loading direction values indicating that similar seismic mitigation benefits can be achieved in the two orientations. However, at extreme lateral displacement, the bearing showed lower effective stiffness for loading in the diagonal direction; accordingly, the extreme performance in this direction may be more effective than the parallel loading direction response. An examination of Figs. 2.8d and 2.10d reveals that the shear force transmitted to the superstructure under diagonal displacement is smaller than under parallel displacement.

According to provisions of most seismic design codes (e.g. ASCE, 2005), two levels of seismic excitation (design basis earthquake (DBE) and maximum considered earthquake (MCE)) must be taken into account in the design of any base isolated building. At DBE, the design lateral displacement of Bearing NB1, can vary between 70 and 105 mm (i.e. around 100–150% $t_{r,NB1}$). Test results showed that NB1 can sustain large cyclic lateral displacements up to a maximum value of 140 mm (≈ 200% $t_{r,NB1}$) in both the parallel and diagonal directions of movement, with no significant stiffness degradation. Accordingly, at MCE, with 2% probability of exceedance within 50 years (2500 year return period), an upper limit of 140 mm can be accepted for design purposes as the maximum admissible lateral displacement of this bearing. To achieve the maximum efficiency against DBE, the effective parallel horizontal stiffness can be reduced to the minimum value of 0.13 kN/mm. The corresponding value for the diagonal response will be 0.14 kN/mm. At MCE, the bearing is allowed to undergo larger lateral displacements and, in the case of parallel loading it exhibits a hardening behavior with an effective horizontal stiffness of 0.15 kN/mm, which is still significantly lower than the initial stiffness. In the diagonal loading

direction, the effective horizontal stiffness at extreme lateral displacement will decrease to a minimum value of 0.11 kN/mm, implying even more seismic protection than for the parallel direction of loading.

Typical earthquake accelerations have dominant periods of between 0.1 and 1.0 s with maximum severity often in the range of 0.2–0.6 s (Skinner et al. 1993). Owing to this, a base isolation device with an isolated period longer than 1 s can effectively mitigate the hazard level for many typical low-rise structures. An initial horizontal stiffness of 0.21 kN/mm, in Bearing NB1 under a constant vertical load of 64 kN, results in a minimum isolated period of 1.1 s. However, depending on the magnitude of earthquake energy, the effective horizontal stiffness can drop as low as 0.13 kN/mm and the instantaneous isolated period can reach a value of 1.4 s, which results in increased seismic mitigation. The effective horizontal stiffness values of 0.22 and 0.11 kN/mm related to lateral displacements of 75% $t_{r,NB1}$ and 200% $t_{r,NB1}$, respectively, imply that the instantaneous isolated period of the bearing along its diagonal direction, in a moderate (DBE) to severe (MCE) seismic event, will fluctuate between 1.1 and 1.5 s, respectively. As a result, this bearing provides sufficiently long isolated periods (at least 10 times longer than the fixed base period of a typical low-rise structure) to provide protection for, including but not limited to, masonry shear wall buildings.

Due to the smaller total volume of carbon fiber-reinforcement utilized in Bearing NB1, this bearing exhibited lower damping ratios than Bearing B1. Depending on the amplitude of lateral displacement, effective damping of Bearing NB1 varies roughly from 1% to 3% which is not sufficient for an effective seismic isolation device.

2.9.6. Performance of Bearing NB2

Comparing Fig. 2.8d with Fig. 2.14a, the nonlinearity of the parallel loading response of Bearing NB2 is not as significant as for Bearing NB1. Nevertheless, it can also be modeled with a simple trilinear idealization. The effective horizontal stiffnesses of Bearing NB2 corresponding to 75, 125, 150, and 200% $t_{r,NB2}$ lateral displacements were calculated to be 0.25, 0.20, 0.18, and 0.18 kN/mm, respectively. Therefore, the isolated period of Bearing NB2 under parallel displacement will fluctuate between 1 and 1.2 s. In contrast to Bearing

NB1, the effective horizontal stiffness of NB2 gradually decreased with an increase in the amplitude of lateral displacement.

As was the case for Bearing NB1, in the diagonal loading direction, NB2 showed a bilinear response with an almost linear behavior up to 46mm (≈ 75% $t_{r,NB2}$) lateral displacement. Considering the effective horizontal stiffnesses of NB2 under 1.6MPa constant vertical compression, corresponding to 75 and 200% $t_{r,NB2}$, the instantaneous isolated period in the diagonal direction will fluctuate between 1.0 and 1.3 s. Comparing Fig. 2.14a with Fig. 2.14b, at the extreme lateral displacement in the diagonal direction, a lower shear force will be transmitted to the superstructure than in the parallel direction. Accordingly, similar to Bearing NB1, the diagonal performance of this bearing is more effective than its behavior for loading in the parallel direction.

The smaller volume of material (including carbon fiber-reinforcement) in Bearing NB2, compared with that of Bearing NB1, implies lower damping ratios of Bearing NB2. The test results confirmed this expectation. Depending on the amplitude of lateral displacement, the effective damping of Bearings NB2 varied from 0.8% to 2.3%. It is evident that these values are insufficient for effective base isolation application.

The ratio of base isolated period to the fixed base period of a given superstructure is a measure of the efficiency of the base isolation system (Naiem and Kelly 1999). The higher this ratio is, the more efficient the base isolation system is for earthquake mitigation. For a bearing with nonlinear lateral load–displacement behavior, the ratio of maximum instantaneous isolated period to the minimum isolated period reflects the efficiency of the base isolation system. The ratios for parallel loading response of Bearings NB1 and NB2 are 1.27 and 1.20, respectively. For diagonal response these are 1.41 and 1.32, respectively. Therefore, Bearing NB1 provides better seismic mitigation than NB2. As a result, for a FREI bearing with the given width, shape factor, vertical load, and elastomer modulus, by providing a higher efficiency, an aspect ratio of 2.5 is close to the optimum value for the application considered in this study. Furthermore, Bearing NB2 would transmit larger shear force to the superstructure than Bearing NB1.

2.10. Modeling

In contrast to the steel-reinforcement in a SREI, which is rigid in both extension and flexure, the fiber-reinforcement used in a FREI is relatively flexible in extension and has no flexural rigidity. The flexibility of the fiber significantly influences the mechanical properties of the bearing such as vertical and horizontal stiffnesses as well as its effective damping, and therefore, cannot be ignored in modeling. The compression modulus of a rectangular FREI bearing can be analytically predicted (Tsai and Kelly 2002) based on mechanical properties and physical dimensions of the elastomer and fiber-reinforcement wherein the flexibility of the reinforcement in extension is incorporated into the theoretical solution.

The rigorous analytical modeling and prediction of horizontal response of an elastomeric bearing is a challenging task. It should include large displacements, highly nonlinear elastic strain of the elastomer, elastomer incompressibility and damping characteristics, and the effects of displacement rate and amplitude on the lateral response of the device. For a FREI bearing, the influence of reinforcement flexibility also needs to be incorporated into the analysis, and, in the case of an unbonded application, the highly distorted pattern of deformation due to cross-sectional warping increases the complexity of the model. Even though the mechanics of the commonly employed traditional SREI bearings are well understood and the design process for a building at a specific site is a routine task (Naiem and Kelly 1999), currently no analytical solution exists to predict the horizontal stiffness of a FREI bearing in an unbonded application based on properties of its components including the elastomer and fiber-reinforcement. Although sophisticated finite element modeling utilizing a hyperelastic material model for the elastomer can be investigated, expensive and time consuming experiments typically would be needed to define the constitutive law for a hyperelastic elastomer material (Wang and Lue 2003). The reliability of the analysis would depend heavily on the accuracy of experimentally evaluated material parameters incorporated into the model.

Difficulties and uncertainties associated with analytical response prediction of unbonded FREI bearings suggest that, currently, conducting cyclic testing on prototype samples of the bearing provides the most reliable data on displacement characteristics and damping values to be used in the final analysis and design of the base isolated structure. The lateral

response of the device can be mathematically modeled based on the experimental results. In terms of bearings tested in this study, as a simple approach, the parallel and diagonal lateral load displacement behavior of both Bearings NB1 and NB2 can be modeled with a trilinear and bilinear idealization, respectively. However, in a more advanced approach, the shear force experienced by the bearing in a time history analysis can be attributed to the sum of the restoring force and the damping force which are functions of relative displacement and relative velocity of the bearing (Pan and Yang 1996) as follows:

$$F(x(t),\dot{x}(t)) = K(x(t),\dot{x}(t))x(t) + C(x(t),\dot{x}(t))\dot{x}(t) \tag{2.4}$$

$$K(x(t),\dot{x}(t)) = \frac{b_1 + b_2 x^2(t) + b_3 x^4(t)}{b_4 + b_5 x^2(t) + b_6 x^4(t)} + \frac{b_7}{\cosh^2(b_8 \dot{x}(t))} \tag{2.5}$$

$$C(x(t),\dot{x}(t)) = \frac{b_9 + b_{10} x^2(t)}{\sqrt{b_{11} + \dot{x}^2(t)}} \tag{2.6}$$

The 11 parameters b_1 - b_{11} are constants to be determined by applying the least-squares fitting technique on the results of cyclic tests conducted on the bearing. Table 2.4 presents the b-values and Figs. 2.15a and 2.15b show plots of the mathematical hysteresis curves for Bearings NB1 and NB2. An excellent correlation factor in each case represents a good fit.

The hysteresis loops of Bearing NB1 (Fig. 2.8b) indicate that the tangent horizontal stiffness drops to a minimum value which is close to zero. Although NB1 maintained a positive stiffness value, in order to obtain a larger safety margin from a zero stiffness value, an aspect ratio of R = 2.6 could be selected in the final design of the bearing. Table 2.4 presents the corresponding b-parameters for this bearing, which are evaluated through linear interpolation between b-parameters of Bearings NB1 and NB2. The mathematical hysteresis curve for the final bearing with an aspect ratio of R = 2.6 is shown in Fig. 2.16. The merit of this approach is that decisions can be made on the appropriate aspect ratio of the final design based on available experimental data of two bearings with identical material properties and shape factors but different aspect ratios that bracket the aspect ratio of the final design.

Following is a discussion on an approach that can be used for the preliminary design of the bearing. Eq. (2.7) provides a good estimate on the horizontal stiffness of a SREI bearing with rigid steel-reinforcement plates in a bonded application when the influence of vertical compression on the horizontal stiffness is negligible (Robert 1988).

$$K_{h,eff} = \frac{GA}{t_r} \tag{2.7}$$

where G is the actual shear modulus of rubber, A is the cross-section area of the bearing in plan, and t_r represents the total thickness of rubber layers in the bearing. In general, the shear modulus of an elastomer is a function of shear strain amplitude and rate, magnitude of vertical compression, and temperature. Depending on the compound of the elastomer, the degree of sensitivity to these parameters can be varied. In a traditional SREI bearing with bonded application, lateral displacement of the bearing is primarily governed by shear deformation of individual rubber layers. Accordingly, the experimentally evaluated horizontal stiffnesses of the bearing at different shear strains directly reflect the corresponding shear modulus of the elastomer. However, in general, due to the lack of flexural rigidity in fiber-reinforcements, this is not the case in a FREI bearing especially in the case of an unbonded application when a rollover deformation occurs. Despite these facts, Eq. (2.7) still can be used as an initial estimate of the horizontal stiffness of the bearing at least at the preliminary design stage.

As provided by the supplier, the rubber had a nominal tensile modulus at 100% elongation of approximately 1.04 MPa. Theoretically, for a soft gum rubber which is assumed incompressible with a Poisson's ratio of 0.5, the nominal shear modulus is estimated to be 0.35 MPa. As described previously, the actual shear modulus of the rubber in a FREI bearing with an unbonded application cannot be evaluated from the horizontal cyclic test results because of rollover deformation of the bearing. Nevertheless, by inserting the nominal value of shear modulus in Eq. (2.7) the horizontal stiffnesses of Bearings NB1 and NB2 are calculated as 0.199 and 0.229 kN/mm, respectively. According to Tables 2.2 and 2.3, the horizontal stiffnesses of Bearings NB1 and NB2 corresponding to 75% t_r and 100% t_r lateral

displacement in each case bracket the value of horizontal stiffnesses calculated above. As mentioned earlier, the design and maximum lateral displacements in both Bearings NB1 and NB2, corresponding to DBE and MCE excitations, are 150% t_r and 200% t_r. The horizontal stiffnesses evaluated through Eq. (2.7) overestimate the real horizontal stiffness of the bearing against DBE and MCE excitations. In fact, the real efficiency of the bearing against these seismic hazards is underestimated.

2.11. Conclusions

The results from an experimental study conducted on square carbon FREI bearings employing soft compound low damped natural rubber as the elastomer are presented in this paper. The bearings are meant to be used for base isolation of ordinary low-rise residential and commercial buildings in a special application in which the bearings are not bonded to the superstructure or foundation. To simulate this in the experimental study, the bearings were not bonded to the test platens. As described in this paper, the experimental outcomes provide a reliable basis for analytical modeling of the bearings in time history analysis of a base isolated structure.

Vertical compression testing revealed that carbon fiber-reinforcement in the FREI bearings tested provides an acceptable vertical stiffness. A vertical frequency of around 17 Hz was achieved in Bearings B1 and B2 which is considered to be an acceptable value for seismic isolation application. Bearings NB1 and NB2 showed accepted cyclic performance and exhibited even larger vertical stiffness and higher vertical frequency values than Bearings B1 and B2 due to their shorter height.

Horizontal cyclic tests showed that, for bearings having suitable aspect ratio values (i.e. Bearings NB1 and NB2), the unbonded application can result in a stable rollover (SR) lateral deformation, which reduces the horizontal stiffness and increases the efficiency of the bearing as a seismic isolation device. For fiber-reinforced bearings with identical physical and material properties, the unbonded application results in superior performance compared with the traditional bonded application. The isolated period of Bearings NB1 and NB2 under parallel loading, depending on the severity of earthquake, will vary between 1.1-1.4 s and 1.0-1.2 s, respectively. Furthermore, in the diagonal direction of loading, the

instantaneous isolated periods of these bearings will fluctuate between 1.1-1.5 s and 1.0-1.3 s, respectively. Bearing NB1 was tested up to 140mm lateral displacement and Bearing NB2 up to 120 mm. These values correspond to 200% of the thickness of the total rubber layers in each bearing and are considered to be sufficient (ASCE 2005) for many high seismic risk regions worldwide, provided that at least 5% effective damping can be achieved in the base isolation system. In such a case, application of these bearings can significantly reduce the earthquake-induced force and interstory drift in a typical low-rise building such as a masonry shear wall structure with a fixed base period in the range of 0.1 s.

A low damping ratio and lack of sufficient horizontal stiffness against service lateral loads are two shortcomings of the bearings tested in this study. The low damping ratios of all tested bearings indicated the inherent low damping in soft compounds of natural rubber. Even the additional source of energy dissipation due to the use of fiber-reinforcement in the bearings, under light vertical compression, cannot provide the required amount of damping for a seismic isolation device. The low initial horizontal stiffness of the bearing implies that lateral displacements due to service lateral loads such as wind loads may exceed admissible limits. These issues can be easily resolved by utilizing a high damped rubber with high initial shear modulus and higher damping properties, or using supplementary devices to provide higher initial stiffness and higher damping ratios.

Lower weight, the possibility of being manufactured in a long strip or a large sheet and subsequently cut to the required size, adequate vertical stiffness, and superior damping properties are some of the advantages of fiber-reinforced elastomeric isolator (FREI) bearings. The smaller physical dimensions including shorter operational height of an unbonded FREI bearing compared with the traditional bonded application implies that there is a significant potential for FREI bearings to be cost effective, and they would provide a potential engineering solution for seismic isolation of many structures including the low-rise small residential and commercial buildings. Extensive use of the bearings in ordinary small buildings is not feasible unless the bearings are made through a mass production manufacturing process and supplied as a catalogue product. Development of a suitable finite element model would be beneficial as it would permit the study of the influences of various design variables on the response of a FREI bearing with unbonded boundary

conditions. Nonetheless, more experimental studies, including shake table testing on prototype buildings mounted on these bearings should be carried out to verify the in-place performance of this base isolation system.

2.12. References

ASCE. (2005). "Minimum Design Loads for Buildings and other Structures." *ASCE/SEI 7-05*, American Society of Civil Engineers, New York.

ASTM (2005). "Standard Test Method for Rubber Property-Durometer Hardness." *ASTM D2240*, American Society for Testing and Materials, Philadelphia.

Clough R., and Penzien J. (1975). *Dynamics of Structures*, McGraw-Hill, New York.

Kelly J. M. (1999). "Analysis of Fiber-Reinforced Elastomeric Isolators." *Journal of Seismology and Earthquake Engineering (JSEE)*, Vol. 2, No. 1, Pages 19-34.

Kelly J. M. (2002). "Seismic Isolation Systems for Developing Countries." *Earthquake Spectra*, Vol. 18, No. 3, Pages 385–406.

Moon B. Y., Kang G. J., Kang B. S., and Kelly J. M. (2002). "Design and Manufacturing of Fiber-Reinforced Elastomeric Isolator for Seismic Isolation." *Journal of Materials Processing Technology*, Vol. 130-131, Pages 145–150.

Moon B. Y., Kang B. S., and Kim H. S. (2003). "Mechanical Property Analysis and Design of Shock Absorber System using Fiber Bearing by Experimental Method." *JSME International Journal, Series C: Mechanical Systems, Machine Elements and Manufacturing*, Vol. 46, No. 1, Pages 289–296.

Naiem F., and Kelly J. M. (1999). *Design of Seismic Isolated Structures*, Wiely, New York.

Pan T. C., and Yang G. (1996). "Nonlinear analysis of base-isolated MDOF structures." *Proceedings, The 11th World Conference on Earthquake Engineering, Mexico*, Paper No. 1534.

Robert A. D. (1988). *Natural Rubber Science and Technology*, Oxford University Press, Oxford.

Skinner R. I., Robinson W. H., and McVerry G. H. (1993). *An Introduction to Seismic Isolation*, Wiley, England.

Summers P., Jacob P., Marti J., Bergamo G., Dorfmann L., Castellano G., Poggianti A., Karabalis D., Silbe H., and Triantafillou S. (2004). "Development of New Base Isolation Devices for Application at Refineries and Petrochemical Facilities." *Proceedings, 13th World Conference on Earthquake Engineering, Vancouver, BC, Canada*, Paper No. 1036.

Taylor A. W., and Igussa T. (2004). *Primer on Seismic Isolation*, American Society of Civil Engineers, ASCE, Reston, Virginia.

Tsai, H. C., and Kelly, J. M. (2002). "Stiffness Analysis of Fiber-Reinforced Rectangular Seismic Isolators." *Journal of Engineering Mechanics*, Vol. 128, No. 4, Pages 462- 470.

Wang L. R., and Lue Z. H. (2003). "Modeling Methods of Constitutive Law of Rubber Hyperelasticity based on Finite Element Simulations." *Rubber Chemistry and Technology*, Vol. 76, No. 1, Pages 271–285

Table 2.1. Effective damping ratio and horizontal stiffness of Bearings B1 and B2 resulting from sinusoidal cyclic tests having displacement amplitude of 47 mm with different frequencies

(a) Bearing B1

Frequency f (Hz)	Average Damping ξ_{ave}^{f} (%)	Average Stiffness $K_{h,ave}^{f}$ (kN/mm)
0.16	2.90	0.160
0.32	2.50	0.159
0.48	2.17	0.157
0.53	2.10	0.157
0.66	2.07	0.154

(b) Bearing B2

Frequency f (Hz)	Average Damping ξ_{ave}^{f} (%)	Average Stiffness $K_{h,ave}^{f}$ (kN/mm)
0.16	2.83	0.1603
0.32	2.47	0.1589
0.48	2.13	0.1586
0.53	2.10	0.1582
0.66	2.00	0.1559

Table 2.2. Effective scragged horizontal stiffnesses and damping ratios of Bearing NB1 ($t_{r,NB1}$ = 70.5 mm) at different displacement amplitudes

	Parallel Response		Diagonal Response	
Displ. Amplitude (% $t_{r,NB1}$)	Average Stiffness (kN/mm)	Average Damping (%)	Average Stiffness (kN/mm)	Average Damping (%)
25	0.27	1.3	0.25	1.5
50	0.24	1.5	0.24	1.5
75	0.21	1.5	0.22	1.8
100	0.18	1.8	0.19	2.2
125	0.16	2.1	0.17	2.8
150	0.13	2.4	0.14	3.6
200	0.15	3.1	0.11	6.4

Note: Values indicated for horizontal stiffness and damping are an average of corresponding values in cycles 2 to 4 of horizontal displacements when the elastomer shows its scragged properties.

Table 2.3. Effective scragged horizontal stiffnesses and damping ratios of Bearing NB2 ($t_{r,NB2}$ = 61.1 mm) at different displacement amplitudes

	Parallel Response		Diagonal Response	
Displ. Amplitude (% $t_{r,NB1}$)	Average Stiffness (kN/mm)	Average Damping (%)	Average Stiffness (kN/mm)	Average Damping (%)
25	0.31	1.0	0.28	1.3
50	0.29	1.0	0.28	1.3
75	0.25	1.3	0.26	1.6
100	0.23	1.5	0.23	1.9
125	0.20	1.7	0.21	2.2
150	0.18	1.9	0.18	2.8
200	0.18	2.2	0.15	4.3

Note: Values indicated for horizontal stiffness and damping are an average of corresponding values in cycles 2 to 4 of horizontal displacements when the elastomer shows its scragged properties.

Table 2.4. b-parameters for Bearings NB1 and NB2 and for the finalized bearing

b-Values	NB1 (R=2.5)	NB2 (R=2.9)	Finalized Bearing (R=2.6)
b_1	178.0486	192.9246	181.7676
b_2	0.054266	0.103088	0.066472
b_3	-7.2E-07	-1.9E-06	-1E-06
b_4	-1976.34	-3873.63	-2450.67
b_5	-0.05086	-0.05366	-0.05156
b_6	-4.2E-06	-1.4E-05	-6.7E-06
b_7	0.358687	0.350695	0.356689
b_8	0.001175	0.001258	0.001196
b_9	0.815267	7.041431	2.371808
b_{10}	0.000223	0.002475	0.000786
b_{11}	62562.41	6649634	1709330
R^2 *Value*	0.9972671	0.998089	N/A

Note: For the finalized bearing (R=2.6), b-values were evaluated based on linear interpolation between the corresponding b-values of Bearings NB1 (R=2.5) and NB2 (R=2.9). This is based on the assumption that the same material properties, including a low damped rubber, are used in the manufacturing of the finalized bearing.

(a) Trimming the edges with an appropriate band saw

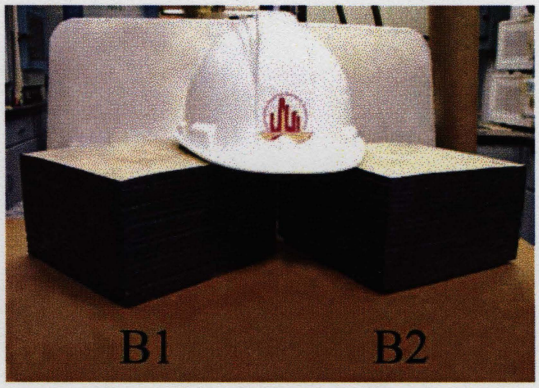

(b) An overview of the completed bearings

Figure 2.1. Carbon–FREI bearings

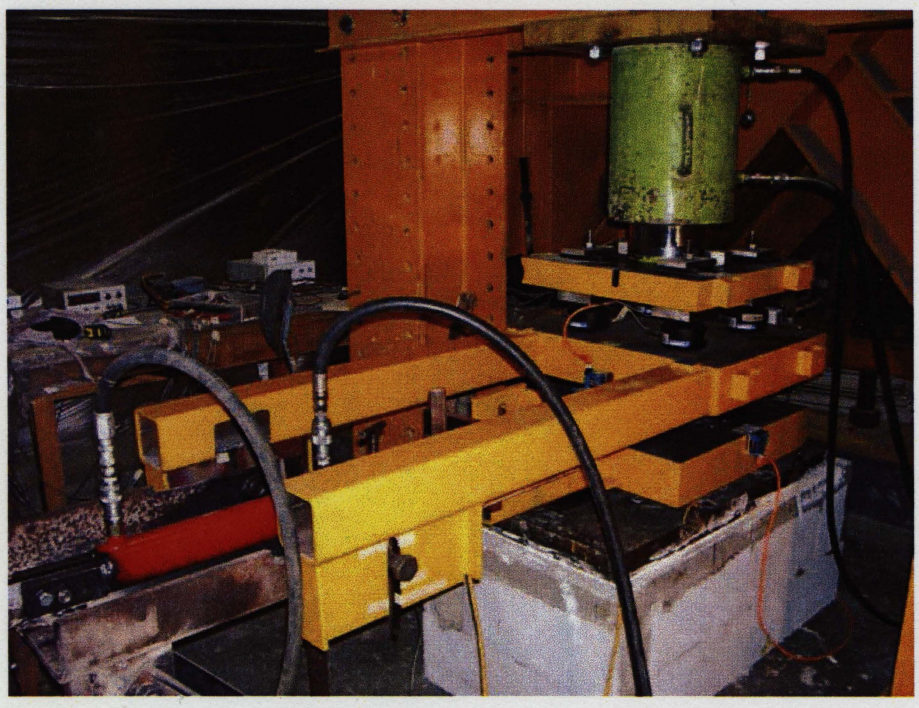

Figure 2.2. An overview of the test setup

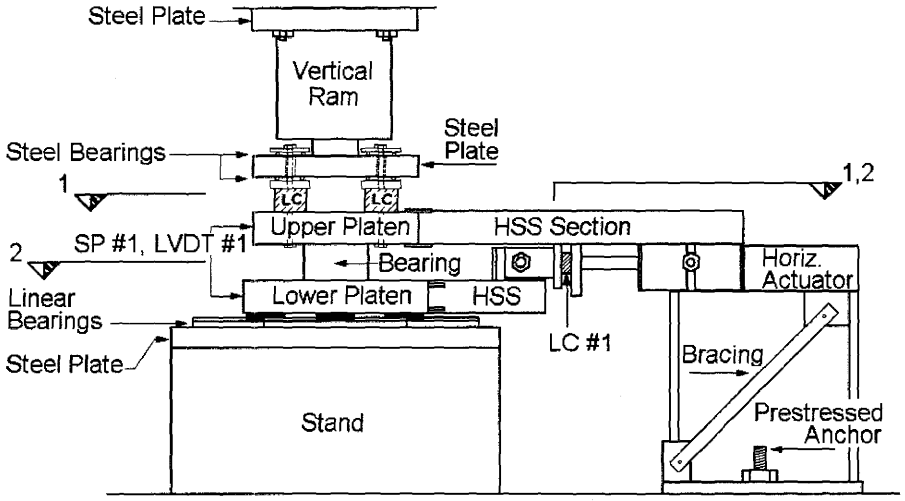

(a) Side view

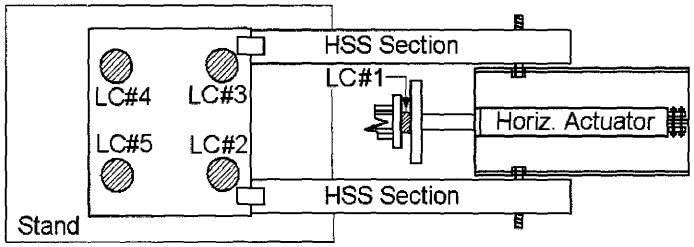

(b) Section 1-1

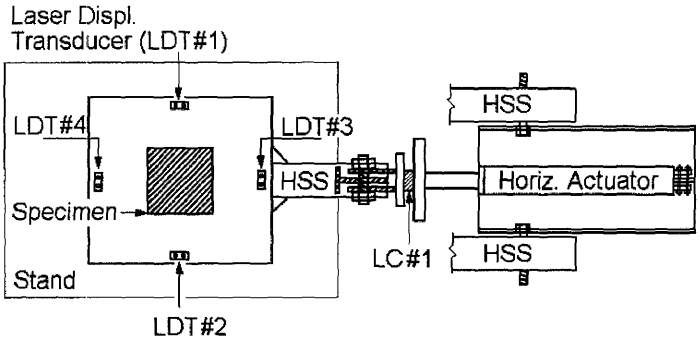

(c) Section 2-2

Figure 2.3. Test setup and instrumentation arrangement

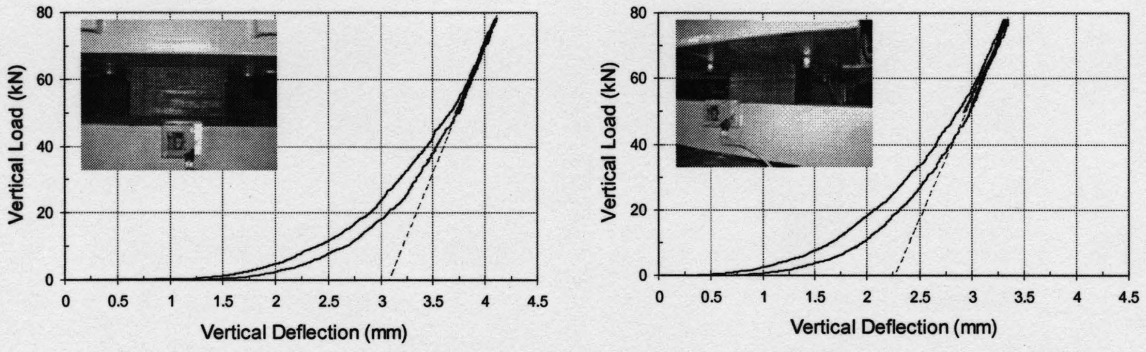

(a) Bearing B1 (b) Bearing B2

Figure 2.4. Vertical load-deflection relationships under 64 kN vertical compression load

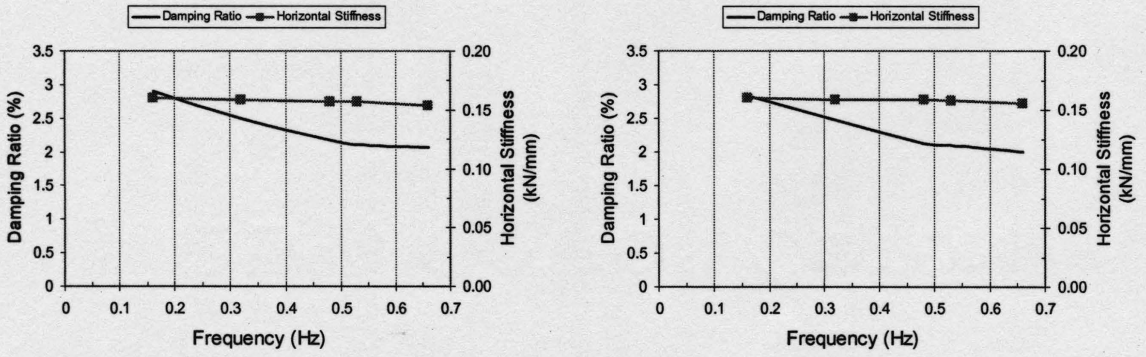

(a) Bearing B1 (b) Bearing B2

Figure 2.5. Variation of equivalent viscous damping ratio and horizontal stiffness of Bearings B1 and B2, at 50% t_r lateral displacement, with respect to frequency of the imposed sinusoidal horizontal displacement

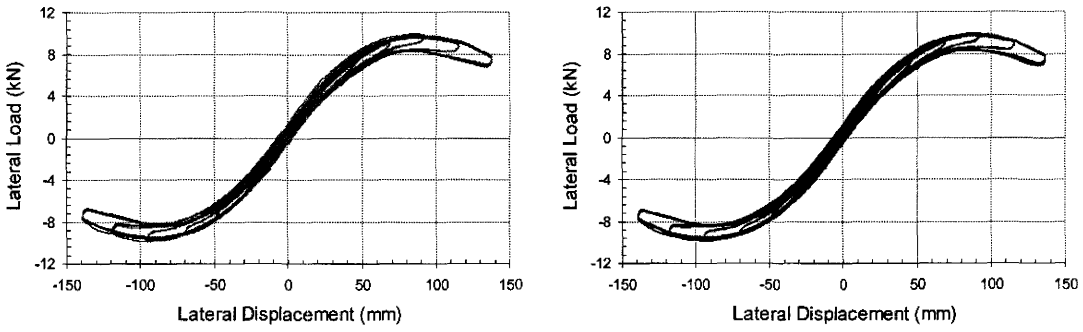

(a) Bearing B1 (b) Bearing B2

Figure 2.6. Lateral load-displacement behavior for Bearings B1 and B2 (aspect ratio R = 1.9, and t_r = 94 mm), in a series of parallel loading (0° orientation) cyclic tests having amplitudes of 25, 50, 75, 100, 125, and 150% t_r, under constant 1.6 MPa vertical compression

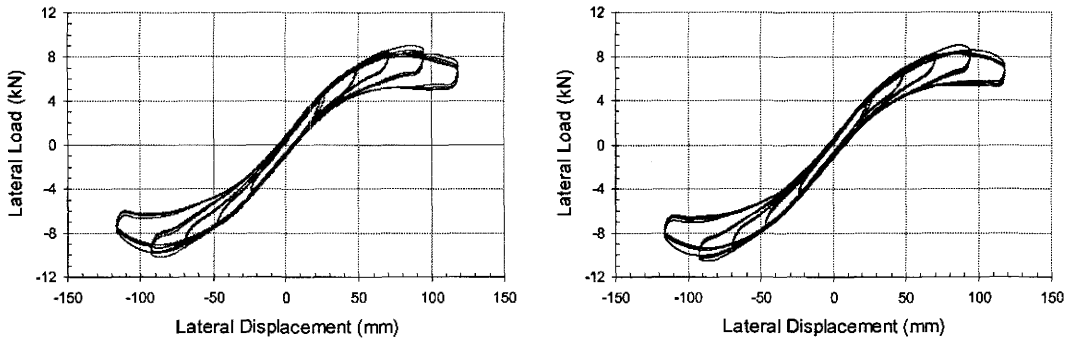

(a) Bearing B1 (b) Bearing B2

Figure 2.7. Lateral load-displacement behavior for Bearings B1 and B2 (aspect ratio R = 1.9, and t_r = 94 mm), in a series of parallel loading (0° orientation) cyclic tests having amplitudes of 25, 50, 75, 100, and 125% t_r, under 3.2 MPa constant vertical compression

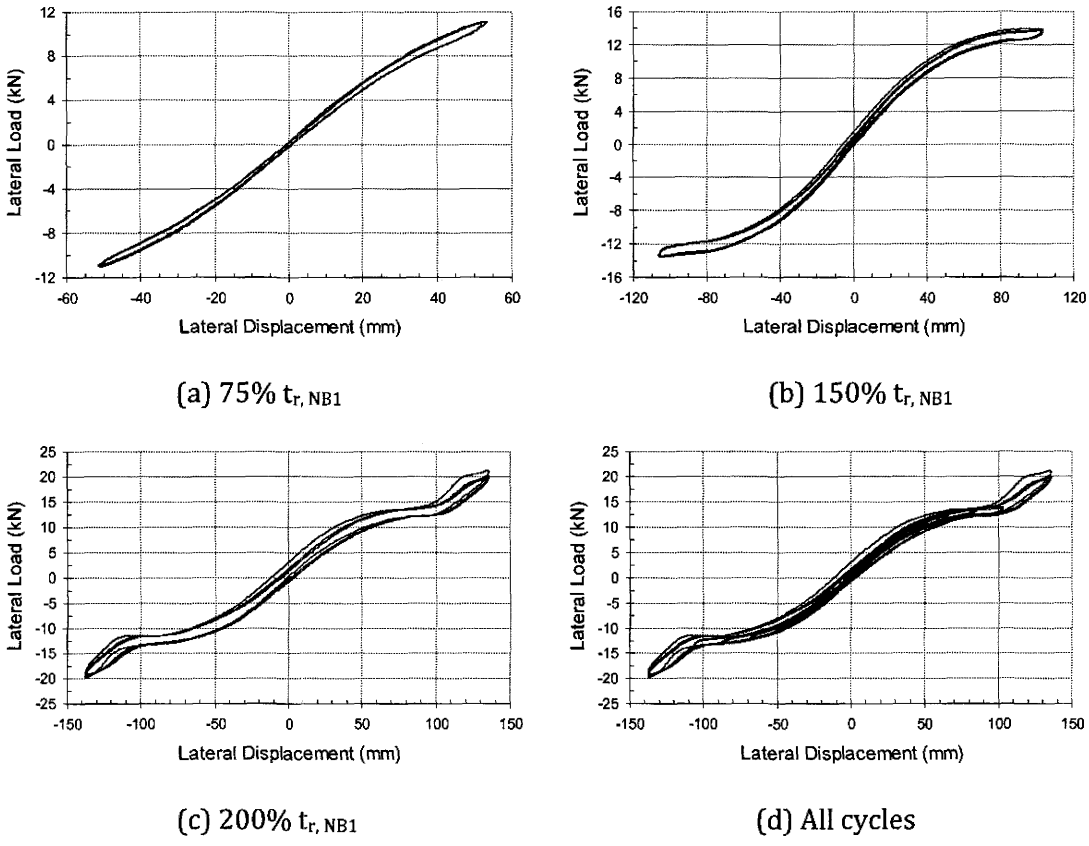

Figure 2.8. Parallel lateral load displacement behavior of Bearing NB1 under constant 1.6 MPa vertical compression, in a series of parallel loading (0° orientation) cyclic tests with different lateral displacement amplitudes ranging from 25% to 200% $t_{r, NB1}$

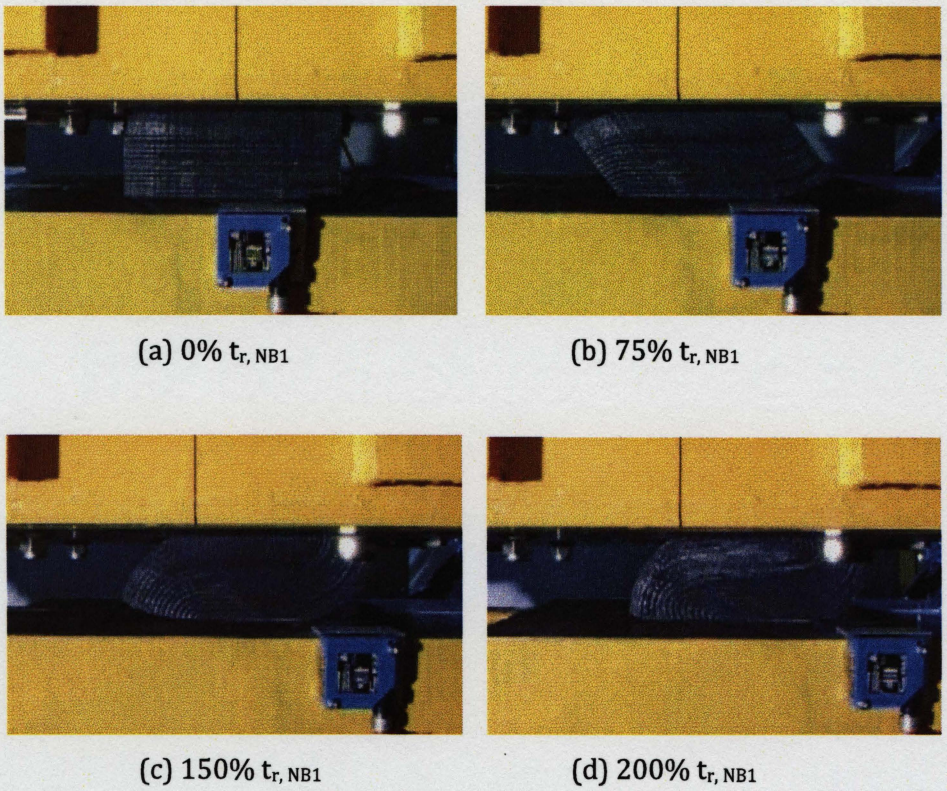

(a) 0% $t_{r,\,NB1}$ (b) 75% $t_{r,\,NB1}$

(c) 150% $t_{r,\,NB1}$ (d) 200% $t_{r,\,NB1}$

Figure 2.9. Bearing NB1 under constant 1.6 MPa vertical compression, subjected to different amplitudes of lateral displacements parallel to the sides of the bearing (0° orientation)

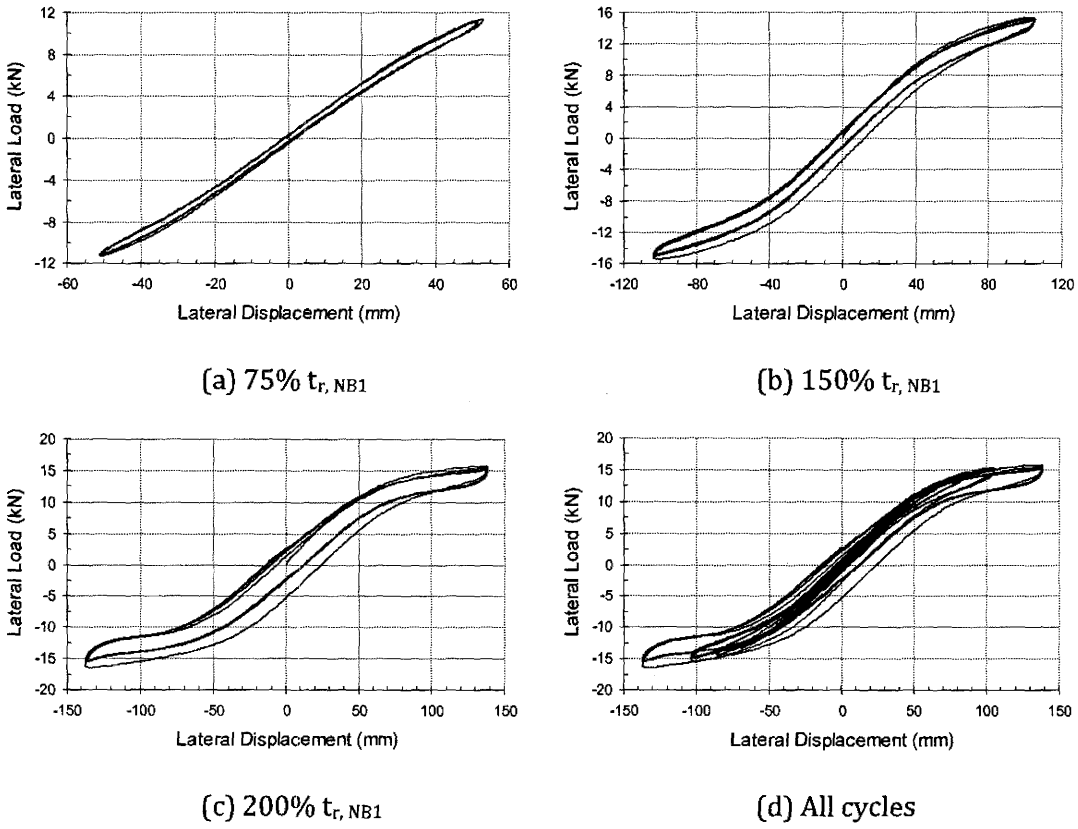

Figure 2.10. Lateral load displacement behavior of Bearing NB1 under constant 1.6 MPa vertical compression when lateral displacements were imposed along the diagonal of the bearing (45°), in a series of cyclic tests with different amplitudes ranging from 25% to 200% $t_{r,B1}$

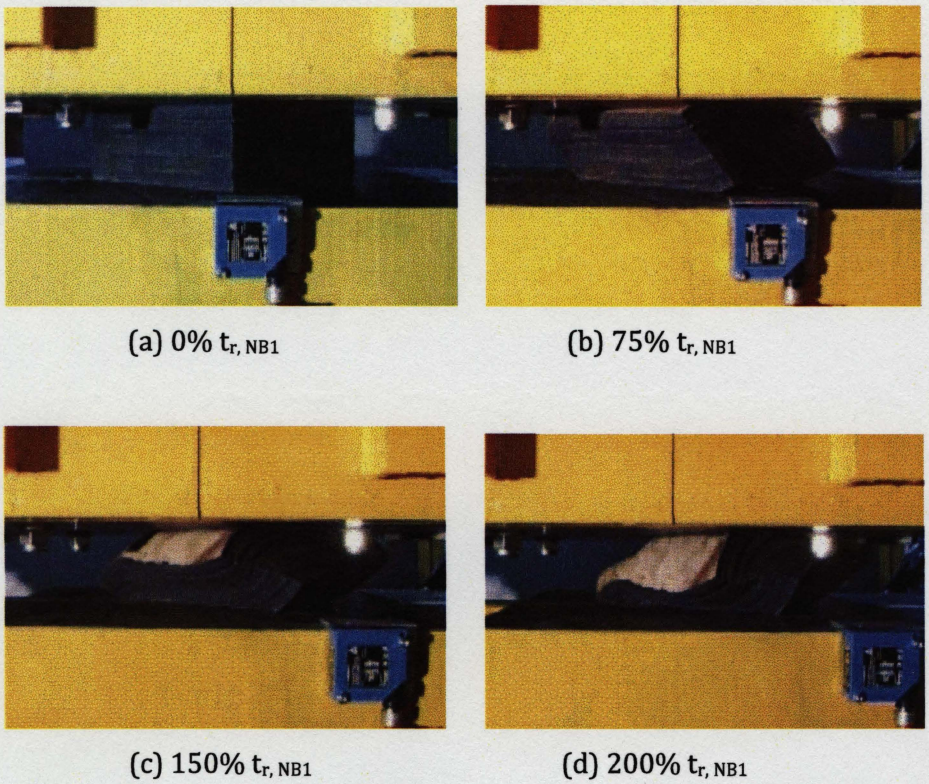

(a) 0% $t_{r, NB1}$ (b) 75% $t_{r, NB1}$

(c) 150% $t_{r, NB1}$ (d) 200% $t_{r, NB1}$

Figure 2.11. Bearing NB1 under constant 1.6 MPa vertical compression, subjected to diagonal (45°) lateral displacements with different amplitudes

Figure 2.12. Bearing NB1 after completion of cyclic testing program; as indicated a significant delamination occurred in the bonding of one layer

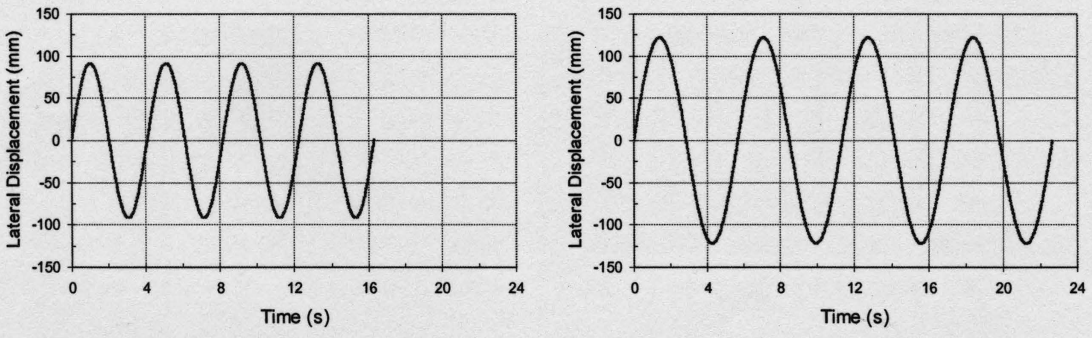

(a) 150% $t_{r,\,NB2}$ (b) 200% $t_{r,\,NB2}$

Figure 2.13. Time history plots of sinusoidal input motion imposed to Bearing NB2 corresponding to two different lateral displacement amplitudes

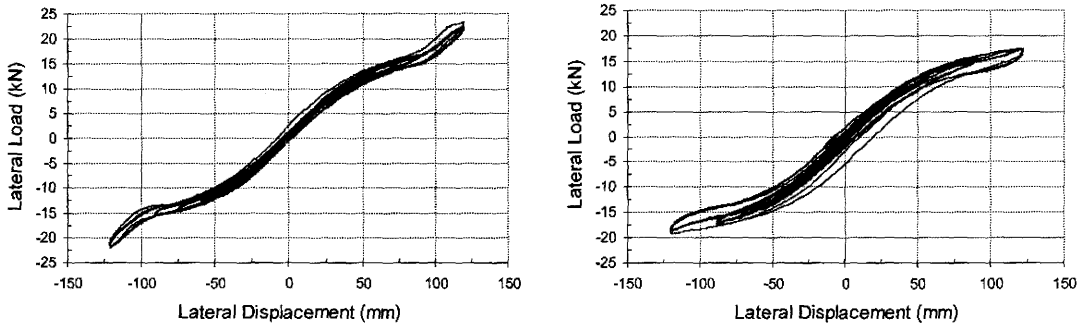

(a) Parallel cyclic response (b) Diagonal cyclic response

Figure 2.14. Lateral load displacement behavior for Bearing NB2 under constant 1.6 MPa compression, in a series of cyclic tests having amplitudes 25, 50, 75, 100, 125, 150, and 200% $t_{r,\,NB2}$ ($t_{r,\,NB2}$ = 61.1 mm) when lateral displacements imposed on (a) parallel direction, and (b) diagonal direction of the bearing

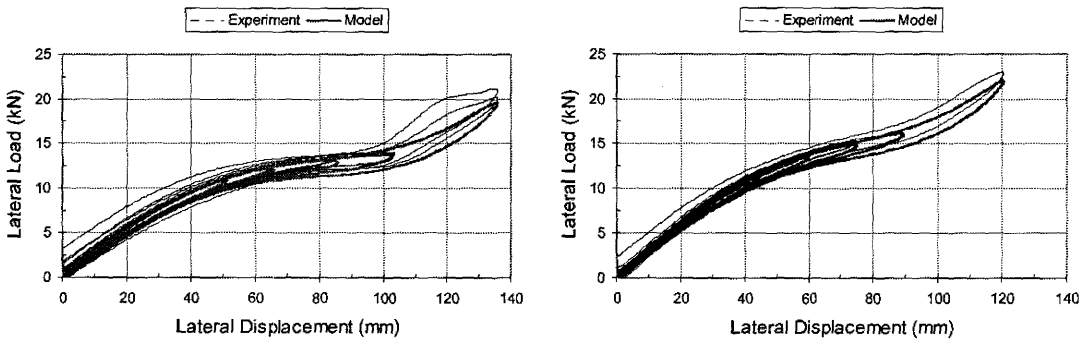

(a) Bearing NB1 (b) Bearing NB2

Figure 2.15. Experimental vs. mathematical hysteresis loops for the tested bearings (Only half cycles is shown)

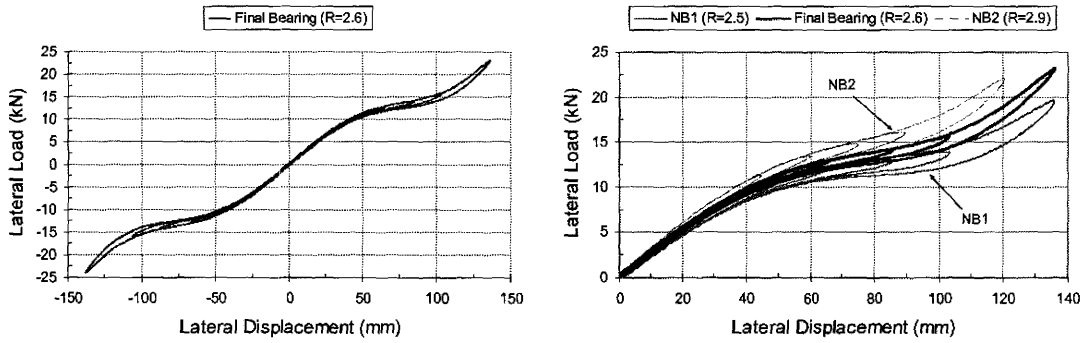

(a) Final bearing (b) NB1, NB2, and the final bearing

Figure 2.16. Mathematical hysteresis loops for the final bearing with an aspect ratio of R = 2.6, evaluated based on b-parameters indicated in the last column of Table 2.4

Chapter 3: Lateral Response Evaluation of Fiber-Reinforced Neoprene Seismic Isolators Utilized in an Unbonded Application

3.1. Abstract

This study examines the experimentally obtained lateral response characteristics of model scale square fiber-reinforced elastomeric isolator (FREI) bearings, which are intended to mitigate seismic induced forces on ordinary low-rise buildings. The bearings consist of an unfilled soft neoprene compound as the elastomer material and bidirectional carbon fiber fabric as the reinforcement. The bearings have been employed in an unbonded application, which means they are not attached to the upper and lower platens of the test machine. This unbonded application results in a stable rollover deformation, which decreases the effective lateral stiffness of the bearings and maximizes their efficiency as a seismic isolator device. Lateral load-displacement hysteresis loops of the FREI bearings with unbonded application are generally found to be comparable to that of conventional high damped steel-reinforced bearings. The adequacy of the bearings has been verified in conformance with provisions of ASCE in 2005.

3.2. Introduction

Research studies have shown that seismic isolators can be designed using layers of rubber interspersed and bonded with thin layers of bidirectional fiber fabric, which are flexible in extension and have no flexural rigidity, in place of steel-reinforcement plates (Kelly 1999, 2002, Moon et al. 2002, Toopchinezhad et al. 2007b). It has been shown that the lateral response characteristics of fiber-reinforced elastomeric isolator (FREI) bearings, which are indicators of a isolator's performance, are equal, if not superior, to conventional steel-reinforced elastomeric isolator (SREI) bearings (Kelly 1999, Moon et al. 2002). Additionally, a significant savings in manufacturing costs may be achievable as a result of less labor-intensive fabrication process requirements (Kelly 2002). The fact that the bearing isolator can be made as a long strip or as a wide sheet, and then easily cut to the required size,

implies that the manufacturing cost can be reduced to a level suitable for application in ordinary low-rise housing. Further, the use of these bearing isolators in an unbonded application will result in additional cost savings. As the bearing is unbonded (not attached to the foundation or the superstructure) this leads to construction savings and introduces significant technical advantages through changes in the bearing's mechanical properties (Toopchinezhad et al. 2007b).

In an unbonded application, as the base is displaced laterally, separation will occur along the trailing edge of the bearing and the base support and between the loading edge of the bearing and the superstructure. This phenomenon is defined as "rollover" and results in a significant decrease in effective lateral stiffness, which increases the efficiency of the bearing as a seismic isolator device. The full contact vertical face lateral displacement, denoted by δ_{fc}, is reached when the originally vertical faces of the bearing completely contact the horizontal faces of the lower support (base) and the upper support (superstructure), which results in a stiffening behavior of the bearing. The bearing can be sized so that it maintains a positive incremental lateral load-resisting capacity throughout the hysteresis loops. As such, it remains stable and the resulting rollover is called "stable rollover" (SR) deformation (Toopchinezhad et al. 2007b). As an advantage, a properly designed unbonded FREI bearing exhibits larger lateral displacement capacity compared to the same bearing in a bonded application (Toopchinezhad et al. 2007b).

This paper examines the overall lateral response of four model scale carbon FREIs and evaluates their adequacy as seismic isolators in conformance with the design provisions of ASCE (2005). In this paper, bearing, isolator, and bearing isolator are used interchangeably.

3.3. Target Response Characteristics

The ratio of the base isolated period to the fixed base period of a structure reflects the efficiency of the utilized base isolation system (Naiem and Kelly 1999). In the constant velocity region of an earthquake design spectrum, the base shear of the building, when seismically isolated, is decreased by an increase in this ratio. Typical earthquakes have significant energy at periods of between 0.1 and 1.0 s with maximum energy often occurring in the range of 0.2–0.6 s (Skinner et al. 1993). Therefore, a base isolation system with an

isolated period of longer than 1 s can be effectively used for seismic mitigation purposes in many typical low-rise buildings with a fixed base period in the range of 0.1–0.2 s. Isolators in small low-rise buildings are likely to a be subjected to relatively low level of vertical pressure. Based on results of an analytical study conducted on a base isolated model of a typical low-rise masonry building (Toopchinezhad et al. 2007), the design vertical pressure in the current study was set to p = 1.6 MPa, and a target value of 5% effective damping was selected for the bearings. The low level of vertical pressure and the relatively low level of the required damping permitted the use of a soft unfilled (low-damped) elastomer compound in the bearings.

3.4. Bearing Isolators

Two laminated fiber-reinforced elastomeric sheets, denoted as Sheets B1 and B2, having physical dimensions of 200×200×25 mm were constructed. Each sheet consisted of 12 layers of soft unfilled neoprene rubber (hardness: 37±5 Durometer, shore A (ASTM 2005)) that were interlaminated with 11 layers of bidirectional (0/90 orientation) carbon fiber fabric as the reinforcement. A cold vulcanizing chemical compound (a rubber cement) was utilized to bond the elastomer and reinforcement layers together. The matrix volume fraction, defined as the relative volume of matrix to the fibers in each fiber-reinforcement layer, was approximately 54%. Sheets B1 and B2 were subsequently cut to produce eight bearings in total. Bearings B1-1 and B1-3, which were originally located along the diagonals of Sheet B1, were selected for the prototype testing (see Fig. 3.1a). Bearings B2-1 and B2-3 were similarly chosen from Sheet B2. The four remaining bearings were preserved for future studies. These ¼ scale model bearings of the prototype full size bearings had 70×70 mm dimensions in plan. The total bearing thickness was approximately 25 mm of which the total thickness of the twelve 1.58 mm thick rubber layers was t_r = 19 mm combined with eleven 0.54 mm thick reinforcing layers. For a 54% matrix volume fraction, the implied thickness of the carbon fiber fabric was (1-0.54)(0.54 mm) = 0.25 mm. To prevent any unexpected premature delamination, two coats of the bonding compound were applied to the perimeter surfaces of the bearings. The four model bearings studied in this paper are shown in Fig. 3.1b.

The supplier-provided nominal tensile modulus of the elastomer elastomer at 100% elongation was 1.2 MPa. This implied a nominal shear modulus of G = 0.4 MPa for an incompressible elastomer with a Poisson's ratio of 0.5. Owing to this, the nominal effective lateral stiffness of a bearing with cross-section area of A (in plan) was estimated by $GA/\ t_r$ to be 103 N/mm. This equation suggests a uniform distribution of shear stress. It can be used to approximate the shear stiffness of conventional SREI bearings within the practical shear strain range (typically up to 100%), where experimental observations imply a nearly linear lateral load-displacement relationship (Mori et al. 1999). It is realized that this equation overestimates the value of effective lateral stiffness for a FREI bearing in an unbonded application due to the additional degree of freedom at the contact surfaces compared to traditional bearing in a bonded application (Toopchinezhad et al. 2008). For a vertical pressure of p = 1.6 MPa, the estimated effective lateral stiffness results in an isolated period of 0.55 s for the ¼ scale bearing. According to similitude law in a true replica model (Harris and Sabnis 1999), displacement, period, and stiffness of the full scale model are, respectively, four, two, and four times larger than the corresponding values of the ¼ scale model. Using the scaling factor, the corresponding estimated period is 1.1 s for the full scale bearing. From the above-presented estimated period, the initial design of the bearings meet the desired target isolated period provided that the bearings exhibited SR deformation under large lateral displacements.

The aspect ratio (R) and shape factor (S) are two crucial physical properties of an elastomeric bearing that significantly influence its mechanical characteristics. By definition, the shape factor is the ratio of vertically loaded area on one face of the elastomer layer to its perimeter load-free area, and aspect ratio reflects the ratio of length to total thickness of the bearing. The shape factor of the bearings studied was approximately S = 11, and the aspect ratio was R = 2.8. Aspect ratio plays an important role in achieving SR deformation in an unbonded FREI bearing. A smaller aspect ratio makes the FREI bearing more susceptible to rollout instability (Toopchinezhad et al. 2008). In this regard, a block-type FREI bearing with an appropriate aspect ratio should be employed in an unbonded application. SR deformation in a block type FREI bearing with unbonded contact surfaces results in a significantly decreased effective lateral stiffness. Accordingly, sufficient flexibility can be achieved in the lateral response of the base isolation system.

3.5. Test Program

As a result of being square in plan view, the bearings were expected to exhibit similar mechanical properties in the two perpendicular directions of movement. One of the vertical faces of each bearing was marked with the bearing's name and deemed as the reference face. The response of the bearing for loading parallel and perpendicular to the reference face was denoted as 0 and 90° response, respectively. A 45° response corresponds to the case where the lateral displacement was along the diagonal of the bearing. Overall, a bearing's response to lateral displacement was categorized as either parallel (i.e., at 0°), perpendicular (i.e., at 90°), and diagonal response (i.e., at 45°).

All of the bearings were tested under vertical compression (vertical test). Additionally, under a prescribed constant level of vertical pressure, the bearings were subjected to sinusoidal cycles of lateral displacement (cyclic test). An overview of the test setup is shown in Fig. 3.2. The bearing was located between two 100 mm thick steel platens. Lateral displacements were imposed to the lower platen, which was mounted on four linear bearings. The upper platen was braced to the body of the horizontal actuator by two arms, providing a self-equilibrating system. The FREI bearing was subjected to pure shear as the horizontal action and the reaction forces passed through its midheight. A vertical actuator was used to apply a constant vertical load during cyclic testing. The relative horizontal movement between the platens was monitored using a string pot and four laser displacement transducers were used to measure the vertical deflection of the bearing at its four sides. A load cell measured horizontal loads. To achieve a symmetrical setup, four identical load cells were used to measure the vertical load. Steel bearings were placed between the upper platen and these four load cells to ensure no horizontal load was transferred to them.

The time history pattern of lateral displacement in the cyclic testing portion of the study was varied in terms of displacement rate (*rate*) and pattern of variation in the amplitude of cyclic lateral displacements. The lateral displacement time history pattern had either an increasing amplitude pattern (*ascending amplitude*) or a decreasing amplitude pattern (*descending amplitude*). All tests were conducted at room temperature. Table 3.1 lists the

test sequence and details for each bearing of which only those tests relevant to this paper (i.e., cyclic tests with ascending displacement amplitude pattern and rate sensitivity tests) are discussed.

3.6. Cyclic Lateral Tests

3.6.1. Objectives and Methodology

The effective lateral stiffness and the equivalent viscous damping ratio are the two mechanical properties of interest that can be evaluated through lateral displacement cyclic testing. The effective stiffness resembles the secant stiffness, which is computed from the peak to peak response in each cycle of lateral load-displacement. The equivalent viscous damping is computed from the area within the hysteresis loops at each cycle. ASCE (2005) provides a set of expressions for evaluating the mechanical properties of any desired seismic isolation device based on results obtained from cyclic testing. These expressions were used in this study.

Cyclic lateral tests were conducted under displacement control with vertical load controlled to maintain a constant vertical compressive force. Each bearing was subjected to fully reversed sinusoidal cycles of lateral displacement having amplitudes of 25%, 50%, 75%, 100%, 150%, and 200% t_r. Considering the total thickness of rubber layers in each bearing (t_r = 19 mm), these correspond to lateral displacement amplitudes of 4.8, 9.5, 14.3, 19.0, 28.5, and 38.0 mm, respectively.

3.6.2. Overall Verification of the Lateral Response

When displaced under pure shearing action, a FREI bearing in an unbonded application exhibits rollover deformation. This deformation occurs due to the absence of flexural rigidity in the reinforcement layers as well as the unbonded boundary condition at the contact surfaces of the bearing. A previous study (Toopchinezhad et al. 2008) revealed that for a FREI bearing employed in an unbonded application, given the material properties and shape factor (S), the aspect ratio (R) plays an important role in achieving SR deformation in the bearing. Currently, no closed form solution exists to evaluate the proper aspect ratio that leads to SR deformation, based on the physical geometry and material properties of the

FREI bearing. However, results from cyclic lateral tests on prototype bearings having identical characteristics but different aspect ratios can be used to determine a suitable aspect ratio in the final design of the bearing (Toopchinezhad et al. 2008).

As a primary study only ¼ scale Bearing B1-1, with an aspect ratio of R = 2.8, was cut from Sheet B1 (see Fig. 3.1a). The objective was to verify the suitability of the selected aspect ratio in achieving SR deformation in the bearing. Further, there was a need to verify the adequacy of the resulting effective lateral stiffness and damping values at different amplitudes of lateral displacement, through examining the cyclic test results.

Bearing B1-1, at its virgin state, was initially subjected to a set of cyclic tests, at 0° orientation, with different amplitudes of lateral displacement. For each amplitude of displacement, the bearing was loaded to p = 1.6 MPa vertical pressure. It was subjected to four fully reversed sinusoidal displacements with identical amplitudes and then vertically unloaded. The average rate of cyclic displacements was approximately 30 mm/s. This bearing remained stable and showed acceptable behavior over the entire test range of lateral displacement amplitudes. Next, Bearing B2-1 with the same physical dimensions as B1-1 was cut from Sheet B2 and was subjected to cyclic lateral displacements at 0° orientation under constant 1.6 MPa vertical pressure. As before, the selected displacement rate was 30 mm/s. However, unlike the case of Bearing B1-1, only three cycles of lateral displacement were performed at the six displacement amplitudes ranging from 25 to 200% t_r and the constant vertical pressure was maintained on the bearing without unloading between the various displacement amplitudes. For the sake of clarity, only the hysteresis loops for Bearing B2-1 (at 0°), corresponding to the final cycle of lateral displacements at each displacement amplitude, are shown in Fig. 3.3a where, similar to B1-1, acceptable performance was observed.

The diagonal response of Bearing B1-1 was also investigated through a test sequence similar to the 0° orientation test for Bearing B1-1. Fig. 3.3b shows the resulting hysteresis loops corresponding to the final cycle for each displacement amplitude. The diagonal cyclic test usually resulted in the most distorted pattern of deformation in the bearing. After completion of the diagonal test, partial debonding in one of the laminates near midheight of

Bearing B1-1 was observed. The delamination existed over a length of approximately 1 mm on one face of the bearing and was difficult to see. As shown in Fig. 3.3b, the bearing remained stable and showed an acceptable lateral response even during the last cycle of displacement.

From Figs. 3.3a and 3.3b, it was observed that, due to rollover deformation in the bearing, the effective lateral stiffness decreased with increased amplitude of lateral displacement. However, positive values of the tangent lateral stiffness throughout the hysteresis loops implied that the bearings showed an acceptable SR deformation. Table 3.2 contains the test results, discussed earlier, for Bearings B1-1 (at 0 and 45°) and B2-1 (at 0°).

In general, the lateral response of Bearings B1-1 and B2-1 appeared to be consistent. Considering the resulting effective lateral stiffness values, the corresponding isolated periods of the tested ¼ scale bearings would range between 0.5 and 0.8 s depending on the lateral displacement amplitude. Therefore, the bearing isolated periods of the corresponding full scale bearing are expected to range from 1.0 to 1.6 s, which is either equal to or beneficially longer than the target isolated period.

At 100% elongation, the rubber supplier specified a nominal damping of the elastomer of approximately 5%, whereas significantly larger damping values ranging from 7 to 13% in both the parallel and diagonal response were achieved, depending to the displacement amplitude. This implies that the fiber-reinforcement is a new source of energy dissipation in an unbonded FREI bearing. It is postulated that significant curvature in the fiber-reinforcement sheets due to rollover deformation of the bearing forces the individual fibers, which are in tension, to slip against each other dissipating energy through friction (Kelly 1999). Additionally, Bearing B1-1 performed more effectively in the diagonal response (45°) than the parallel response (0°) due to the lower effective lateral stiffness and larger damping values achieved. Consequently, the selected aspect ratio of R=2.8 was deemed to be adequate and the preliminary design of the bearings was verified.

3.6.3. Rate Sensitivity Tests

For rate sensitive isolators, cyclic testing with sinusoidal lateral displacements should be conducted with an excitation frequency equal to the natural frequency of the isolator at the design displacement (ASCE 2005). According to the cyclic test results on Bearings B1-1 and B2-1 (see Table 3.2), at the design lateral displacement (i.e., around 100% t_r = 19 mm), an isolated period of approximately 0.67 s will be achieved. This implies a natural frequency of 1.5 Hz and an average displacement rate of 114 mm/s in the input sinusoidal cycles of lateral displacement. Although the lateral actuator used in the test setup was able to operate at this rate at ±19 mm (±100% t_r) lateral displacement, it was not able to operate at this rate at higher amplitudes. Therefore, a lower rate that would still provide results sufficiently accurate from an engineering prospective was required. This section discusses the procedure followed, leading to the selection of a suitable displacement rate.

All of the model bearings, under constant 1.6 MPa vertical pressure, were subjected to three fully reversed sinusoidal cycles of 100% t_r = 19 mm lateral displacement sequentially at average rates of 30, 45, 76, and 114 mm/s. A 1.6 MPa constant vertical pressure was maintained. As mentioned earlier, the average rate of 114 mm/s was associated with the natural frequency of the bearing at the design displacement and was chosen as the reference rate for comparison. The influence of displacement rate on effective lateral stiffness and damping ratio of the bearings can be seen in Figs. 3.4a and 3.4b, respectively.

Overall, both effective stiffness and damping increased with increased displacement rate. Bearing B2-1 showed the most sensitivity to the displacement rate with approximately a 9% reduction in the effective stiffness and more than 16% reduction in the damping of the bearing at the lowest rate (30 mm/s). Unlike Bearing B2-1, cyclic tests for all other bearings started with the lowest rate and ended at the highest rate. As a result, at displacement rates lower than 114 mm/s, these bearings showed less than 6 and 11% reduction in the effective stiffness and damping, respectively. A rate sensitivity test on Bearing B1-1 was also carried out at 150% t_r (28.5 mm) lateral displacement. Test results showed a similar trend of reduction in stiffness and damping at lower displacement rates.

In order to work within the range of equipment capability, an average displacement rate of 76 mm/s was selected. This rate resembled an excitation frequency of approximately 1 Hz at 100% t_r lateral displacement, which was sufficiently close to the bearings' natural frequency (i.e., approximately 1.5 Hz). At this rate, as the worst case scenario (results of Bearing B2-1 as shown in Fig. 3.4), the effective lateral stiffness and damping at each cycle were on average 6 and 10% lower than the corresponding values at the natural frequency of the bearings. These variations are considered minor and can be neglected for many practical applications (ASCE 2005).

3.6.4. Cyclic Lateral Testing

A time history plot of the input excitation, comprising six displacement amplitudes in an ascending pattern, with an average displacement rate of 76 mm/s can be seen in Fig. 3.5a. The displacement history contain three fully reversed cycles at amplitudes of 25, 50, 75, 100, 150, and 200% t_r (where t_r = 19 mm). Bearing B1-3, at its virgin state, was initially subjected to this displacement history, which was imposed at 0° orientation on the bearing. Fig. 3.5b shows the resulting hysteresis loops for all cycles of the test and Table 3.3 contains the corresponding properties of this bearing.

As seen in Fig. 3.5b, as with Bearings B1-1 and B2-1, the hysteresis loops showed acceptable response characteristics. However, the resulting mechanical properties are more accurate due to incorporating a more representative displacement rate in the cyclic testing. Figs. 3.6a to 3.6d contain photographs of Bearing B1-3 at various displacement amplitudes for cyclic testing in the parallel (0°) direction. Bearings B2-1 and B2-3 were subjected to the same displacement history presented in Fig. 3.5a along their perpendicular (90°) orientation. Table 3.3 contains the resulting mechanical characteristics of these bearings.

During the first cycle of lateral displacements with constant amplitude, all bearings tested in this study exhibited higher stiffness and damping than in the following cycles (see Fig. 3.5b and Table 3.3). When an elastomer in its virgin condition is subjected to any constant amplitude of cyclic tension, compression, or shear loading, reloading of the elastomer up to the maximum previously achieved displacement amplitude usually requires lower stress than the initial cycle. The maximum difference in the required reloading stresses exists

between the first and the second cycles and becomes negligible after 6 to 10 cycles depending on the elastomer compound (Dorfmann and Odgen 2004). This phenomenon, which is observed in both unfilled and particle-reinforced rubber, is known as the "Mullins effect" (Marckmann et al. 2002). In all bearings tested in this study, after the first cycle of a constant lateral displacement amplitude, the hysteresis loops stabilized so that stable effective lateral stiffness and damping values in the second and third cycles were achieved. Such stable properties are usually denoted as "scragged" properties. The untangling or breakage of weak cross-links in an unfilled rubber can be considered as a micromechanical interpretation of this phenomenon (Marckmann et al. 2002). Depending on the elastomer compound, partial recovery of unscragged properties with time is likely to occur (Whittaker et al. 2007).

Figs. 3.7a and 3.7b present the variations of lateral response with the amplitudes of cyclic lateral displacement for the bearings listed in Table 3.3. The values in Fig. 3.7 represent the average response of all cycles at each displacement amplitude of cyclic testing. As indicated in Fig. 3.7a, due to rollover deformation, the effective lateral stiffness significantly decreased with increased amplitude of lateral displacement. However, according to Fig. 3.7b, the reduction in damping at displacements larger than 100% t_r was approximately 10%, which is considered to be negligible (ASCE 2005). This indicates that the bearings would effectively reduce the shear force transmitted to the superstructure, and maintain a sufficient amount of damping to limit the bearing's lateral displacement against severe excitations.

Unlike Bearing B1-3, Bearings B2-1 and B2-3 had been subjected to a previous set of cyclic tests in the parallel (0°) direction (see Table 1). Accordingly, as indicated in Table 3.3, although damping values were comparable, Bearings B2-1 and B2-3 showed lower effective lateral stiffness than B1-3. Scragging in one direction had likely influenced the response behavior of the bearing in the orthogonal direction. A recent study on bidirectional response of conventional elastomeric bearings confirms this observation (Whittaker et al. 2007). Bearing B2-3 showed more response reduction in the perpendicular direction (90°) than Bearing B2-1. This bearing had been subjected to previous cyclic testing with a descending pattern of displacement amplitudes starting at 200% t_r and ending at 25% t_r. As

a result, it is postulated that such a lateral displacement history may had resulted in more damage to the elastomer cross-links.

Bearings B1-3 (at 0°) and B2-3 (at 90°) provided upper and lower bounds for the resulting effective lateral stiffness values against lateral displacements with an ascending amplitude pattern (see Fig. 3.7a). The scragged hysteresis loops associated with the second cycle at each constant displacement amplitude for these two bearings are shown in Fig. 3.8a. The response curves were relatively consistent everywhere except at the extreme end of each cycle where the virgin Bearing B1-3 showed greater stiffening. However, as shown in Fig. 3.8b, the maximum difference between the effective lateral stiffness and damping values of Bearings B1-3 and B2-3 (including the unscragged response), with respect to the average response value at each displacement amplitude was about 9 and 5%, respectively, which is deemed acceptable for practical applications (ASCE 2005). At the design and maximum lateral displacements (i.e., over the range of 100-200% t_r), which are of more interest to designers, the variations in effective lateral stiffness and damping values between the bearings were found to be lower (see Fig. 3.8b). For Bearings B2-1 and B2-3 the individual cycle responses exhibited a maximum of 3% variation from the average response values for each displacement amplitude tested (see Table 3.3).

Bearings B1-3 and B2-1 were also subjected to diagonal cyclic testing, where the displacement history, shown in Fig. 3.5a, was applied along the diagonal of the bearings (45° orientation). The test results are listed in Table 3.4 and Fig. 3.9 contains photographs of Bearing B1-3 at various displacement amplitudes.

Similar to the parallel and perpendicular responses (0 or 90°) of the bearings, the response characteristics at 45° orientation showed SR deformation and a similar pattern of variation with the displacement amplitude (see Fig. 3.10). However, being scragged, stable hysteresis loops at each displacement level were achieved. The elastomer showed minor unscragged properties at the first cycle of 200% t_r displacement. After completion of the test program no visible damage was observed in Bearings B1-3, B2-1, and B2-3.

3.7. Code Evaluation

The relevant design provisions of ASCE (2005), a commonly employed standard in the design of seismically isolated structures, are utilized here. As with many seismic design codes, two seismic hazard levels are adopted in ASCE (2005). These are design basis earthquake (DBE) and maximum considered earthquake (MCE). The spectral earthquake acceleration parameters for DBE are taken as 2/3 of MCE. According to ASCE (2005), MCE represents the level of ground motion with 2% probability of exceedence within 50 years (≈2,500 year return period). In this section, the adequacy of both the parallel/perpendicular and diagonal responses of the tested bearings against both 0.4 and 0.5 g levels of 5% damped spectral accelerations at 1 s period ($SM1$) (ASCE 2005) are verified. It is also assumed that the site class effects (soil properties) are accounted for in these spectral values.

The equivalent lateral-force procedure in ASCE (2005) can be used for the design of many seismically isolated low-rise buildings with regular configuration. This approach takes advantage of the fact that, in this particular type of base isolated building, the first mode of vibration involves lateral displacements almost entirely at the isolation level, whereas the superstructure remains nearly rigid. Owing to this, the verification procedure can be started by evaluating the design lateral displacement D_D and corresponding effective period T_D given by the following (ASCE 2005):

$$D_D = \frac{gS_{D1}T_D}{4\pi^2 B_D} \tag{3.1}$$

$$T_D = 2\pi\sqrt{\frac{W}{k_{D\min}g}} \tag{3.2}$$

where S_{D1} = 2/3 S_{M1}, B_D accounts for the effective damping of the isolator at D_D, W represents the effective seismic weight (vertical load) on the isolator; and $k_{D\min}$ = minimum effective lateral stiffness of the isolator at D_D, obtained from cyclic testing. At MCE, D_M and T_M are calculated based on a similar set of expressions, however, the subscript D is replaced with M so the variables involved represent the corresponding values at MCE.

Given S_{D1}, an iterative procedure using Eqs. (3.1) and (3.2) can be utilized in order to evaluate the D_D and T_D values of the base isolated system. First, an initial estimate of D_D is made. Next, the equivalent full scale value of k_{Dmin} is obtained from Table 3.3 or 3.4 through linear interpolation between the stiffness values corresponding to the lateral displacement levels that bracket the current value of D_D. Additionally, for D_D > 200% t_r, the test results at 200% t_r are utilized. Substituting W and k_{Dmin} in Eq. (3.2), T_D is evaluated and D_D is updated using Eq. (3.1). Iterations are carried out until D_D and T_D converge to their unique values. It is noted that the vertical pressure of p = 1.6 MPa implies W = 125.4 kN for the full scale bearing.

Parallel/Perpendicular Response Evaluation: Conservatively, the effective damping in the tested bearings at D_D and D_M are assumed to be 8 and 7%, respectively (see Table 3.3). This yields values of B_D = 1.12 for DBE and B_M = 1.08 corresponding to MCE (ASCE 2005). Additionally, to ensure a conservative design, the effective lateral stiffness values, corresponding to the third cycle of the test, for Bearing B2-3 tested at 90° are utilized (see Table 3.3). At a specific site with S_{M1} = 0.4 and S_{D1} = 0.27, the iterative procedure described in the previous paragraph at DBE leads to a base isolated period of T_D = 1.33 s and lateral displacement of D_D = 80 mm (≈ 105% t_r) at the center of rigidity of the base isolation system. At MCE this results in a base isolated period of T_M = 1.48 s and a lateral displacement of D_M = 136 mm (≈ 180% t_r). Similar calculations carried out for a region with S_{M1} = 0.5 and S_{D1} = 0.33 gave values of T_D = 1.43 s and D_D = 106 mm (≈ 140% t_r) at DBE and T_M = 1.50 s and D_M = 172 mm (≈ 226% t_r) at MCE.

Diagonal Response Evaluation: According to Table 3.4, for lateral displacements larger than 100% t_r, the damping in Bearings B1-3 and B2-1 ranges from 9 to 11%. Therefore, a conservative value of 9% effective damping, against both the DBE and MCE, is assumed. This leads to B_D = B_M = 1.16 (ASCE 2005). A similar iterative process, which accounts for the minimum effective lateral stiffness values (interpolated from Table 3.4), was carried out. For a spectral acceleration of S_{D1} = 0.27 at DBE, T_D = 1.34 s, and D_D = 76 mm (100% t_r),

and at MCE with S_{M1} = 0.4, T_M = 1.55 s, and D_M = 133 mm (175% t_r). Similarly, at a specific site with S_{M1} = 0.5 and S_{D1} = 0.33, at DBE, T_D = 1.44 s and D_D = 103 mm (≈ 136% t_r) and at MCE, T_M = 1.61 s and D_M = 173 mm (≈ 228% t_r).

A close examination of Fig. 3.6d revealed that at 200% t_r lateral displacement the originally vertical faces of the bearings had not fully contacted the upper and lower platens. Therefore, this lateral displacement was not the full contact lateral displacement (δ_{fc}) of the bearings. Results from cyclic tests conducted on a bearing with similar properties to the bearings tested in this research program showed that the bearing was able to safely accommodate lateral displacements greater than 250% t_r. Consequently, it is expected that the bearings studied in this research would be able to perform satisfactorily under the levels of seismic hazard specified in this study.

Significant seismic mitigation is expected in low-rise buildings (having fixed base periods of around 0.1–0.2 s), that are seismically isolated using the proposed bearings. If due to enormous torsional effects or higher earthquake hazards, a larger lateral displacement capacity in the bearings is needed, the bearing's design can be modified accordingly. Results of vertical testing showed that vertical frequency of the ¼ scale bearings exceeded 40 Hz. This is equivalent to 20 Hz for the full scale bearings, which is more than sufficient as it is significantly higher than the maximum resulting base isolated frequency (i.e., $1/T_{min}$ = 1/(1.33 s) = 0.75 Hz). As a result, the contribution of the rocking modes in the dynamic response of the base isolated structure becomes insignificant.

3.8. Conclusions

Cyclic lateral testing was conducted on ¼ scale carbon FREI bearings. The bearings were employed in an unbonded application as they were not attached to the upper and lower platens of the test machine. As the fiber-reinforcement had no appreciable flexural rigidity, the unbonded application resulted in a SR deformation in the bearings when they were laterally deformed. The full contact vertical face lateral displacement (δ_{fc}) of the bearings occurred when their originally vertical faces completely came in contact with the upper and lower platens. Rollout instability lateral displacement, which is denoted as δ_{max} (Naiem and

Kelly 1999), is expected to be significantly larger than δ_{fc}. All tested bearings exhibited a positive incremental load-resisting capacity throughout their lateral load-deflection response. The bearings showed damping ratios larger than the supplier-specified inherent damping of the utilized elastomer. It is postulated that interfacial friction between the fibers provides an additional source of energy dissipation in the laterally deformed unbonded FREI bearings. The effective lateral stiffness and damping increased with an increase in the rate of lateral displacements. However, the effective lateral stiffness was found to be less sensitive than the damping to variations in the lateral displacement rate.

Although a soft unfilled (low-damped) neoprene was used as the elastomer, the lateral response of the tested FREI bearings in an unbonded application was found to be, in general, comparable to that of conventional high-damped steel-reinforced elastomeric bearings. The response can be characterized by larger effective lateral stiffness and damping values at lower lateral displacement levels, which tend to minimize response under wind load and minor seismic excitations. Over the lateral displacement range of 100-200% t_r), the effective lateral stiffness is significantly decreased due to rollover deformation in the bearing. The decreased effective lateral stiffness increases the isolated period of the bearing, which improves its efficiency as a seismic isolator. At larger lateral displacements (larger than 200% t_r) when the originally vertical faces of bearing fully contact the upper and lower platens, a significant stiffening in the hysteresis loops is observed. This effectively places a limit on the lateral displacements that can occur under unanticipated seismic excitation levels. As such, efficient seismic mitigation can be achieved with the bearings proposed in this study.

For those bearings that were subjected to similar loading history, the variability of the observed response was relatively low. This can be observed by comparing test results for Bearings B1-1 and B2-1 in Table 3.2, Bearings B2-1 and B2-3 in Table 3.3, and bearings cited in Table 3.4. The predicted nominal effective lateral stiffness of the bearings (i.e., GA/t_r = 103 N/mm) was found to be in close agreement with experimental results at lateral displacements of approximately 50% t_r. Accordingly, in the preliminary design, it can be used as a conservative approximation for the lateral stiffness of the bearings at design lateral displacements (i.e., 100-150% t_r). Currently no closed form solution exists to predict

the lateral stiffness of a FREI bearing in an unbonded application. Therefore, as with other types of base isolation systems, cyclic tests on prototype isolator units are employed to verify the design (ASCE 2005).

The idea of exploiting square FREI bearings in an unbonded application is considered feasible. According to the design provisions in ASCE (2005), the tested bearings may be effectively used in seismic mitigation of many low-rise buildings with fixed base period of around 0.2 s that are constructed in seismic regions with a 5% damped spectral acceleration at 1 s period (S_{M1}) of up to 0.5 g. The design of the FREI bearings may be modified to permit their use in regions of higher seismic acceleration. Unique advantages, such as superior damping properties, possibility for mass production, simplicity of cutting, ease of unbonded installation, and eliminating the need for the thick steel end plates highlights the significant potential of this base isolation system to be applied as a cost effective method to mitigate the seismic response of many ordinary low-rise buildings worldwide.

3.9. References

ASCE. (2005). "Minimum Design Loads for Buildings and other Structures." *ASCE/SEI 7-05*, American Society of Civil Engineers, New York.

ASTM. (2005). "Standard Test Method for Rubber Property-Durometer Hardness." *ASTM D2240*, American Society for Testing and Materials, Philadelphia.

Dorfmann, A., and Ogden, R. W. (2004). "A Constitutive Model for the Mullins Effect with Permanent Set in Particle-Reinforced Rubber." *International Journal of Solids and Structures*, Vol. 41, No. 7, Pages 1855-1878.

Harris, H. G. and Sabnis, G. M. (1999). *Structural Modeling and Experimental Techniques*, CRC Press, New York.

Kelly, J. M. (1999). "Analysis of Fiber-Reinforced Elastomeric Isolators." *Journal of Seismology and Earthquake Engineering (JSEE)*, Vol. 2, No. 1, Pages 19-34.

Kelly, J. M. (2002). "Seismic Isolation Systems for Developing Countries." *Earthquake Spectra*, Vol. 18, No. 3, Pages 385–406.

Marckmann, G., et al. (2002). "A Theory of Network Alteration for the Mullins Effect." *Journal of the Mechanics and Physics of Solids*, Vol. 50, No. 9, Pages 2011-2028.

Moon, B. Y., Kang, G. J., Kang, B. S., and Kelly, J. M. (2002). "Design and Manufacturing of Fiber-Reinforced Elastomeric Isolator for Seismic Isolation." *Journal of Materials Processing Technology*, Vol. 130-131, Pages 145-150.

Mori, A., Moss, P. J., Cooke, N., and Carr, A. J. (1999). "The Behavior of Bearings Used for Seismic Isolation Under Shear and Axial Load." *Earthquake Spectra*, Vol. 15, No. 2, Pages 199-224.

Naeim, F., and Kelly, J. M. (1999). *Design of Seismic Isolated Structures*, Wiley, New York.

Skinner, R. I., Robinson, W. H., and McVerry, G. H. (1993). *An Introduction to Seismic Isolation*, Wiley, Chichester, U.K.

Toopchinezhad H., Tait M. J., and Drysdale R. G. (2007). "Base Isolation of Small Low-Rise Buildings using Fiber-Reinforced Elastomeric Bearings." *Proceedings, CSCE (Canadian Society for Civil Engineering) Annual General Meeting & Conference, Yellowknife, Northwest Territories, Canada*, Paper 192.

Toopchinezhad, H., Tait, M. J., and Drysdale, R. G. (2008). "Testing and Modeling of Square Carbon Fiber-reinforced Elastomeric Seismic Isolators." *Structural Control and Health Monitoring*, Vol. 15, No. 6, Pages 876-900, DOI: 10.1002/stc.225 (*Chapter 2 of this thesis*).

Whittaker, A., Thompson, A. C. T., Huang, W. H., and Fenves, G. L. (2007). "Bi-Directional Characterization of Seismic Isolation Bearings." *PEER Report* (in press), Pacific Earthquake Engineering Research Center, University of California, Berkeley.

Table 3.1. Test sequence carried out on each bearing isolator

Sequence	Model Scale Bearing			
	B1-1	B1-3	B2-1	B2-3
1	Cyclic test (0°) *ascending amp.,* *rate = 30 mm/s*	Vertical test *p = 0.8, 1.6, 2.4 MPa*	Cyclic test (0°) *ascending amp.,* *rate = 30 mm/s*	Vertical test *p = 0.8, 1.6, 2.4 MPa*
2	Rate sensitivity test *0° response,* *displ. amp. = 100% t_r,* *rate = 30, 45, 76, 114 mm/s*	Cyclic test (0°) *ascending amp.,* *rate = 76 mm/s*	Rate sensitivity test *0° response,* *displ. amp. = 100% t_r,* *rate = 114, 76, 45, 30 mm/s*	Cyclic test (0°) *descending amp.,* *rate = 76 mm/s*
3	Rate sensitivity test *90° response,* *displ. amp. = 150% t_r,* *rate = 30, 45, 76, 114 mm/s*	Cyclic test (90°) *descending amp.,* *rate = 76 mm/s*	Cyclic test (90°) *ascending amp.,* *rate = 76 mm/s*	Cyclic test (90°) *ascending amp.,* *rate = 76 mm/s*
4	Infl. of vert. pressure on horz. response *90° response,* *p = 1.1, 1.6, 2.4 MPa,* *displ. amp. = 100% t_r,* *rate = 30 mm/s*	Infl. of vert. pressure on horz. response *90° response,* *p = 0.8, 1.6, 2.4 MPa,* *displ. amp. = 100% t_r,* *rate = 76 mm/s*	Infl. of vert. pressure on horz. response *90° response,* *p = 0.8, 1.6, 2.4 MPa,* *displ. amp. = 100% t_r,* *rate = 76 mm/s*	Infl. of vert. pressure on horz. response *90° response,* *p = 0.8, 1.6, 2.4 MPa,* *displ. amp. = 100% t_r,* *rate = 76 mm/s*
5	Infl. of vert. pressure on horz. response *90° response,* *p = 1.1, 1.6, 2.4 MPa,* *displ. amp. = 150% t_r,* *rate = 30 mm/s*	Rate sensitivity test *0° response,* *displ. amp. = 100% t_r,* *rate = 30, 45, 76, 114 mm/s*	Cyclic test (45°) *ascending amp.* *rate = 76 mm/s*	Rate sensitivity test *0° response,* *displ. amp. = 100% t_r,* *rate = 30, 45, 76, 114 mm/s*
6	cyclic test (45°) *ascending amp.,* *rate = 30 mm/s*	Cyclic test (45°) *ascending amp.,* *rate = 76 mm/s*		

Note: Unless otherwise stated, cyclic tests were conducted under constant p = 1.6 MPa vertical pressure

Table 3.2. Effective lateral stiffness values and damping ratios corresponding to various lateral displacement amplitudes in Bearings B1-1 and B2-1

Displacement Amplitude		B1-1, 0° (virgin)		B2-1, 0° (virgin)		B1-1, 45°	
		Stiffness (N/mm)	Damping (%)	Stiffness (N/mm)	Stiffness (N/mm)	Stiffness (N/mm)	Damping (%)
25% t_r	1st cycle	115.5[a]	12.5[a]	135.7	12.7	105.9	13.2
	Last cycle	112.1[a]	11.1[a]	130.4	11.1	105.5	12.3
50% t_r	1st cycle	96.8	10.4	107.4	9.7	83.4	10.8
	Last cycle	91.6	8.7	102.6	8.5	82.4	9.8
75% t_r	1st cycle	82.3	9.3	90.7	8.5	71.2	10.0
	Last cycle	77.2	7.9	86.4	7.5	70.3	8.8
100% t_r	1st cycle	72.5	8.7	79.2	8.0	64.1	9.8
	Last cycle	68.3	7.4	76.0	7.1	63.1	8.5
150% t_r	1st cycle	59.2	9.7	65.2	8.7	54.6	10.9
	Last cycle	53.8	7.6	60.4	6.9	52.9	9.0
200% t_r	1st cycle	54.2	9.5	61.0	8.5	47.7	12.9
	Last cycle	47.0	8.6	54.2	7.1	43.9	11.4

Note: Average rate of lateral displacements for all bearings cited in this table = 30 mm/s
[a] These values belong to 27.5% t_r lateral displacement amplitude

Table 3.3. Parallel and perpendicular responses of Bearings B1-3, B2-1, and Bearing B2-3

Displacement Amplitude	Cycle	B1-3, 0° (virgin)		B2-1, 90°		B2-3, 90°	
		Stiffness (N/mm)	Damping (%)	Stiffness (N/mm)	Damping (%)	Stiffness (N/mm)	Damping (%)
25% t_r	1	164.0	13.7	142.7	12.4	136.5	12.5
	2	155.6	13.4	139.8	11.8	134.0	12.4
	3	154.1	13.3	138.8	12	133.2	12.8
50% t_r	1	123.3	11.9	109.1	11.2	105.3	11.2
	2	116.5	10.9	104.8	10.5	101.9	10.5
	3	114.6	10.8	103.8	10.4	100.8	10.7
75% t_r	1	103.3	10.2	89.9	9.8	86.3	9.8
	2	97.1	9.5	86.2	9.5	83.3	9.6
	3	95.3	9.4	85.2	9.4	82.4	9.5
100% t_r	1	89.3	9.4	78.6	9.1	75.0	9.1
	2	84.7	8.8	75.8	8.8	73.0	8.9
	3	83.6	8.7	75.2	8.7	72.3	8.7
150% t_r	1	72.9	9.9	65.7	9.2	61.8	9.3
	2	68.8	8.4	63.2	8.3	59.8	8.4
	3	67.1	8.3	62.2	8.1	58.9	8.2
200% t_r	1	68.5	9.4	65.6	8.7	61.2	8.7
	2	63.3	8.3	61.0	7.7	57.4	8.0
	3	61.6	8.1	60.0	7.4	56.4	7.8

Note: Average rate of lateral displacements for all bearings cited in this table = 76 mm/s

Table 3.4. Diagonal response of Bearings B1-3 and B2-1

Displacement Amplitude	Cycle	B1-3, 45°		B2-1, 45°	
		Stiffness (N/mm)	Damping (%)	Stiffness (N/mm)	Damping (%)
25% t_r	1	135.7	15.8	130.2	14.0
	2	131.5	16.1	130.5	14.2
	3	130.6	16.1	129.7	14.2
50% t_r	1	102.5	12.1	101.9	11.2
	2	101.0	11.5	99.8	10.3
	3	99.9	11.4	99.0	10.1
75% t_r	1	84.0	10.7	83.7	9.8
	2	82.3	10.4	81.7	9.4
	3	81.9	10.2	81.1	9.4
100% t_r	1	72.3	10.2	72.9	9.4
	2	71.3	9.7	71.6	8.8
	3	70.8	9.7	71.2	8.8
150% t_r	1	58.7	10.9	59.8	10.0
	2	57.7	10.0	59.1	8.9
	3	57.1	9.8	58.3	8.9
200% t_r	1	51.9	11.7	54.5	10.6
	2	49.4	11.0	51.8	9.4
	3	48.4	10.9	50.5	9.2

Note: Average rate of lateral displacements for all bearings cited in this table = 76 mm/s

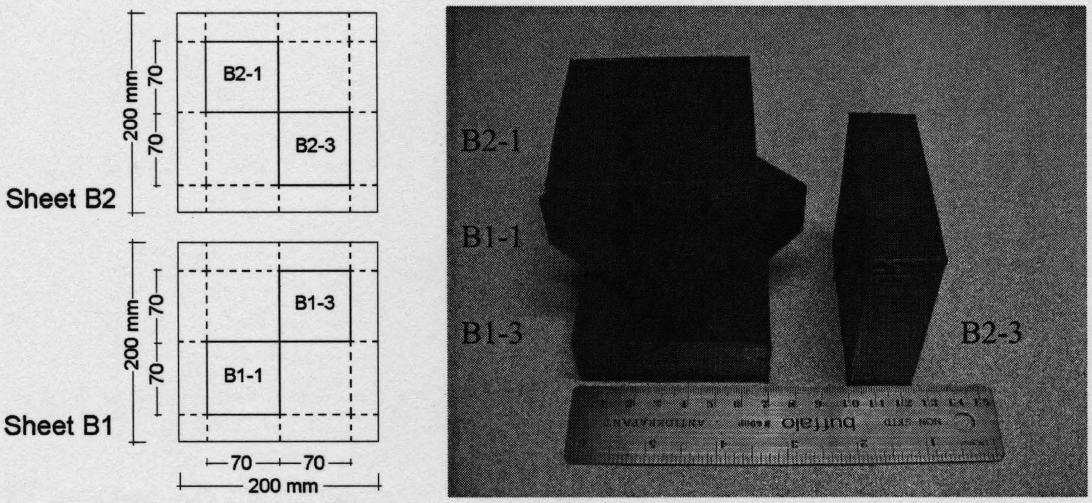

(a) Sketch of Sheets B1 & B2 (b) View of the model fiber-reinforced bearings

Figure 3.1. Seismic isolators

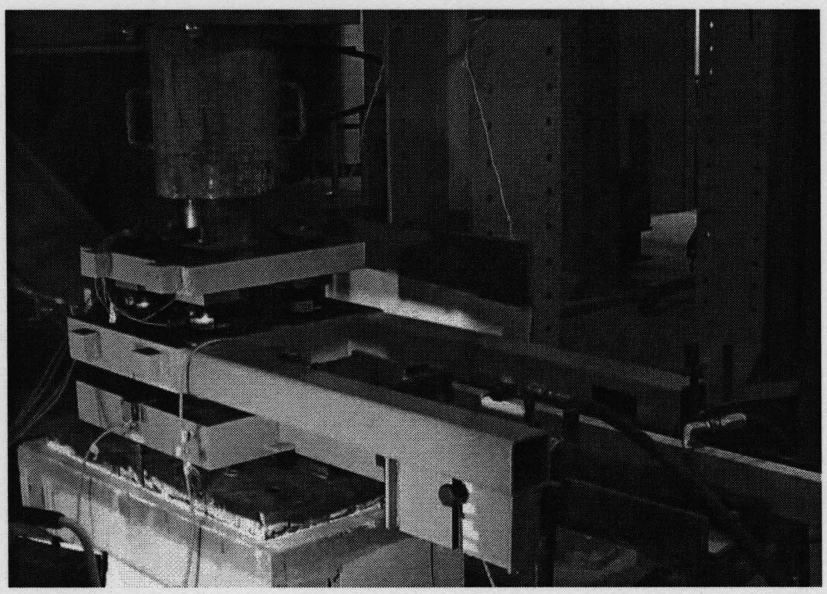

Figure 3.2. An overview of the test setup

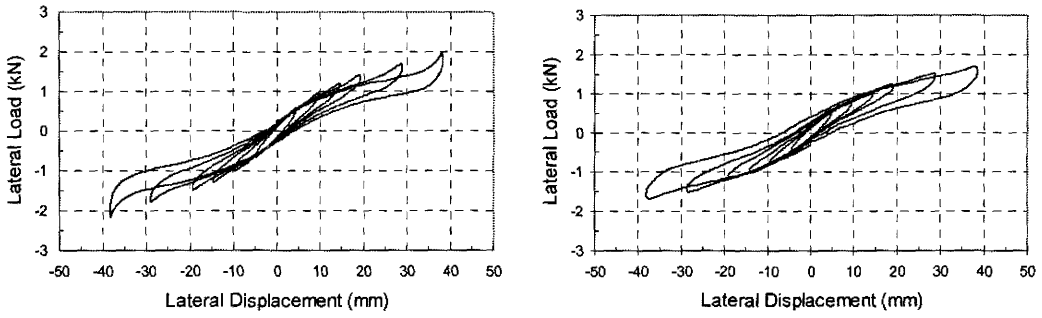

(a) Bearing B2-1 (Parallel Response) (b) Bearing B1-1 (Diagonal Response)

Figure 3.3. Hysteresis loops corresponding to the final cycle of lateral displacement at each displacement amplitude (lateral displacement ranges: 25%, 50%, 75%, 100%, 150%, and 200% t_r; displ. rate = 30 mm/s)

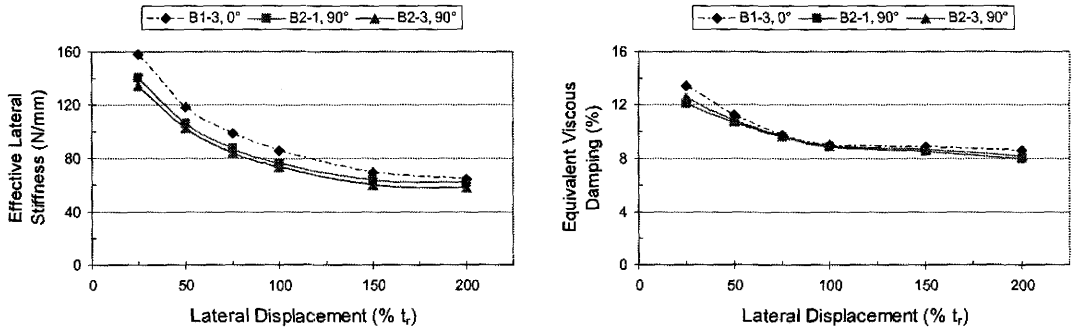

(a) Reduction in Effective Stiffness (b) Reduction in Effective Damping

Figure 3.4. Influence of displacement rates lower than 114 mm/s on lateral response at 100% t_r (19 mm) displacement amplitude (Values represent the average reduction in all 3 displacement cycles.

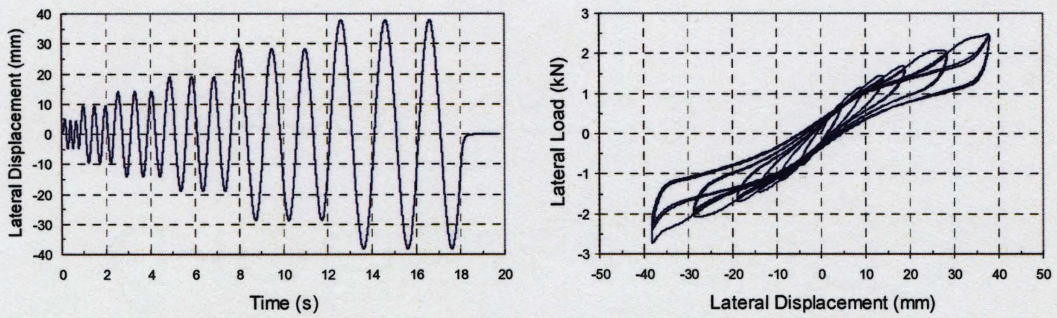

(a) Input signal at 6 displacement amplitudes (b) Hysteresis loops for all cycles

Figure 3.5. Parallel lateral response (0°) of Bearing B1-3 (lateral displ. ranges: 25%, 50%, 75%, 100%, 150%, and 200% t_r, displacement rate = 76 mm/s)

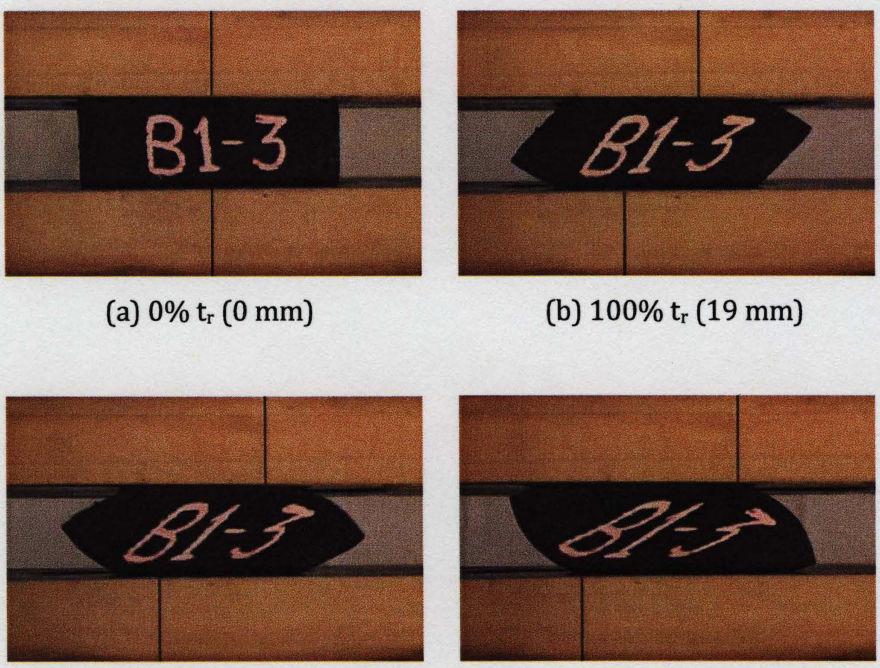

(a) 0% t_r (0 mm) (b) 100% t_r (19 mm)

(c) 150% t_r (28.5 mm) (d) 200% t_r (38 mm)

Figure 3.6. Photographs taken from parallel (0°) response of Bearing B1-3 at different amplitudes of lateral displacement

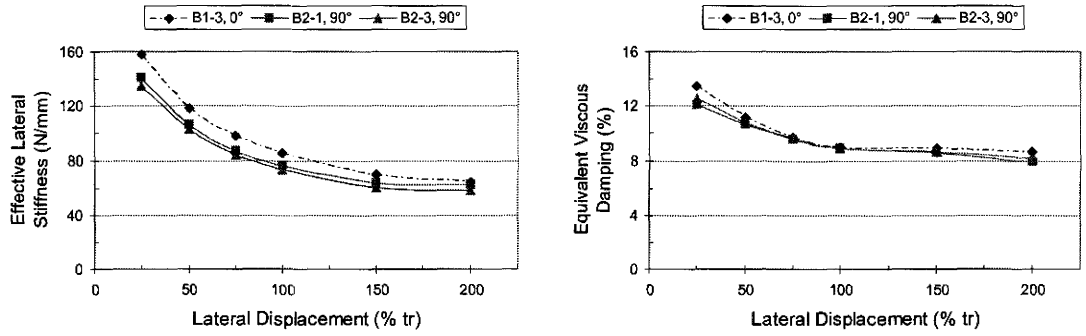

(a) Effective Stiffness (b) Effective Damping

Figure 3.7. Lateral response values for Bearings B1-3 (at 0°), B2-1 (at 90°), and B2-3 (at 90°); (Response values represent the average of all 3 cycles at each displacement amplitude.)

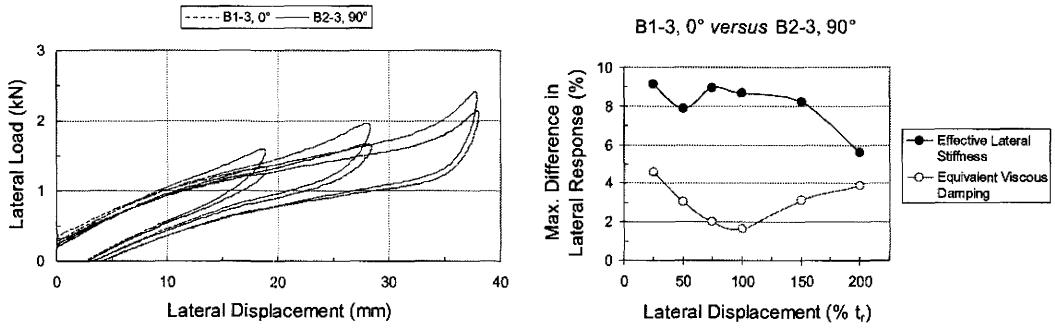

(a) Hysteresis loops at 100%, 150%, and 200% t_r lateral displacement (only half of the scragged cycles is shown)

(b) Maximum difference between response values of the bearings with respect to the average response value at each cycle

Figure 3.8. Lateral response of Bearing B1-3 (at 0°) *versus* Bearing B2-3 (at 90°)

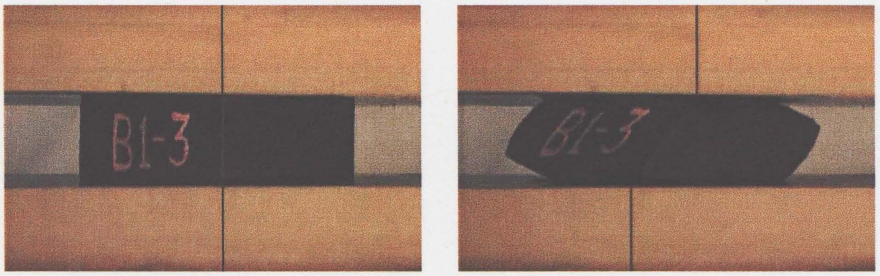

(a) 0% t_r (0 mm) (b) 100% t_r (19 mm)

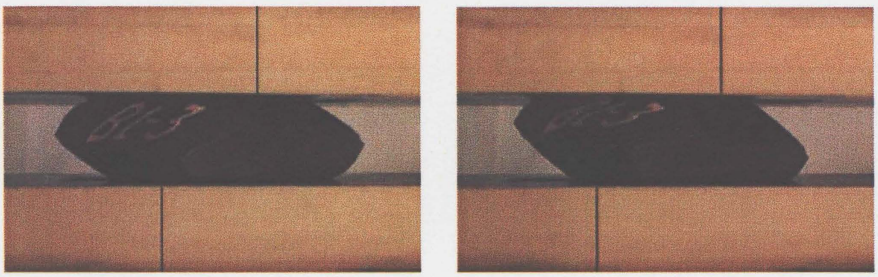

(c) 150% t_r (28.5 mm) (d) 200% t_r (38 mm)

Figure 3.9. Photographs taken of diagonal (45°) response of Bearing B1-3 at different amplitudes of lateral displacement

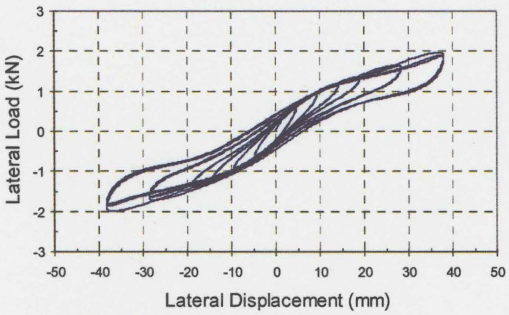

(a) Hysteresis loops for all cycles

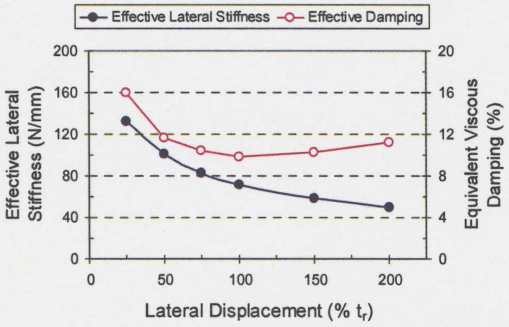

(b) Response variations with displacement amplitude

Figure 3.10. Lateral response characteristics of Bearings B1-3 at 45° orientation; (Response values in Fig. (b) represent the average values at each displacement amplitude)

Chapter 4: Parametric Study on the Response of Stable Unbonded Fiber Reinforced Elastomeric Isolators (SU-FREIs)

4.1. Abstract

Tests on stable unbonded (SU) square carbon fiber-reinforced elastomeric isolator (FREI) bearings were conducted to investigate their lateral and vertical response. The bearings are intended for seismic isolation of low-rise buildings including those of ordinary importance. To simulate the in-place application of SU-FREI bearings, the contact surfaces of the bearings were not bonded to the platens of the test machine. This unbonded application permitted stable rollover (SR) deformation to occur which enhances the bearing's isolation efficiency. The bearings were shown to safely sustain large lateral displacements. When subjected to large lateral displacements, their originally vertical faces completely contacted the horizontal surfaces of the upper and lower platens which created a stiffening response and ensured the stability of these very large displacements. The sensitivity of SU-FREI bearings to lateral displacement history and vertical pressure applied on the bearings were investigated. Regarding the latter parameter, it was found that the effect of variations in vertical pressure on the lateral response can be neglected when the SU-FREI bearings are subjected to relatively light vertical pressures such as considered for low-rise buildings.

4.2. Introduction

Seismic isolation may be used to decrease the cost of building designed for earthquake loading (Skinner et al. 1993). The basic objective in seismic isolation is to substantially reduce the transmission of the earthquake motion and energy into the structure. Base isolated buildings, which are designed in conformance with current seismic codes (e.g., ASCE (2005)), are expected to withstand severe earthquakes without failure of the isolation system and with no significant damage to the building's structural elements. However, currently available seismic isolation systems may not be cost effective for hazard mitigation of ordinary low-rise housing.

Fiber-reinforced elastomeric isolators (FREIs) are a relatively new type of laminated bearing in which fiber fabric, rather than conventional steel plates, serve as the reinforcement layers. Previous studies have indicated that this type of bearing would perform adequately as a seismic isolation device (Kelly 1999, Moon et al. 2002). Recently, it has been shown that employing an unbonded installation technique (i.e., the bearing is not bonded to the contact surfaces of the superstructure or foundation's support) results in a significant increase in efficiency due to the occurrence of "Stable Rollover" (SR) deformation for bearings constructed with carbon fiber reinforcing between layers of pure natural rubber (Toopchinezhad et al. 2008a). Due to their stable lateral response, such FREI bearings are hereafter referred to "stable unbonded (SU)" FREI bearings.

The cost-effective use of SU-FREIs in ordinary buildings can be achieved through mass production of large sheets of FREIs cut to catalogue bearing sizes without the need for subsequently expensive vulcanization technique or bonding of rigid steel mounting plates. Close spacing of SU-FREIs reduces the need for an expensive foundation and load distribution system in small masonry buildings (Toopchinezhad et al. 2007).

Four prototype SU-FREI bearings were tested to provide required data for subsequent use of similar bearings in shake table testing of a ¼ scale model low-rise building when the scale was constrained by shake table capacity. The preliminary design of the SU-FREI bearings, the influence of displacement rate on lateral response, and verification of the lateral response based on provisions of ASCE (2005) have been discussed previously (Toopchinezhad et al. 2008b). This paper reports on the influence of amplitude history of imposed lateral displacements and variations in the vertical pressure. In addition, results of vertical compression tests before and after cyclic lateral testing are presented and discussed. The robustness of the response and the extreme lateral displacement capacity of the bearings are also addressed in this paper.

4.3. The SU-FREI Bearings

The SU-FREI bearings consisted of 12 layers of an unfilled compound of soft neoprene (hardness: 37± 5 Durometer, shore A (ASTM 2005)) as the elastomer and 11 bi-directional

(0°/90°) carbon fiber fabric as the reinforcing material. The supplier-provided damping of the utilized neoprene at 100% elongation was 5%. The bearings were square in plan with an area of A = 4900 mm^2 and a total thickness of 25 mm, wherein the 12 rubber layers had the total thickness of t_r = 19 mm and the matrix volume fraction, defined as the relative volume of matrix to the fibers in each fiber-reinforcement layer, was approximately 54%. The shape factor, defined as the ratio of vertically loaded area on one face of the elastomer layer to its perimeter load-free area, was approximately S = 11 and the aspect ratio, equal to length divided by total thickness of the bearing, was R = 2.8. To avoid any premature delamination, two finishing coats of the bonding compound were applied to the sides of the bearing.

4.4. Organization of the Test Program

Table 4.1 lists the sequence of tests conducted on each bearing. A bearing's responses to lateral displacements in the two similar perpendicular principal directions were denoted as 0° and 90° responses. A 45° response indicated the bearing's response when loaded along one of its diagonals. The time history pattern of lateral displacement in the cyclic testing component of this study was varied in terms of average displacement rate (*rate*) and pattern of variation in the amplitude of sinusoidal lateral displacement. The lateral displacement time history had either an ascending amplitude (AA) pattern or a decreasing amplitude (DA) pattern. Lateral responses of the bearings to a total of 6 different displacement amplitudes namely, 25, 50, 75, 100, 150, and 200% t_r were investigated. For these full-range cyclic tests a 1.6 MPa constant vertical pressure was applied to the bearings. Sensitivity of the bearings' lateral response to the displacement rate and the vertical pressure were studied at a design displacement amplitude of 100% t_r. In addition, for Bearing B1-1 these were also investigated at 150% t_r. Documentation of the effect of testing sequence was a key objective of this research.

4.5. Test Setup

Figure 4.1 is a photograph of the test setup for both vertical and cyclic lateral testing of the prototype bearings. The test bearing was located between two 100 mm thick steel platens with no bonding or fastening at its contact surfaces. Lateral displacements were imposed

via a horizontal hydraulic actuator attached to the lower platen. The lower platen was mounted on four linear bearings permitting ±150 mm of lateral relative motion with respect to the upper platen. The upper platen was prevented from moving laterally using two axially rigid braces attached to the body of the horizontal actuator; this resulted in a self-equilibrating system. The bearing was subjected to near pure shear as the action and the reaction lateral forces were positioned to pass through its midheight. A load cell was used to measure the lateral loads corresponding to different lateral displacements imposed on the bearing. A string-pot potentiometer was used to measure the relative horizontal displacements between the lower and upper platens. Four laser displacement transducers (LDTs) were used to measure the vertical deflection of the bearing at its four sides during both the vertical and lateral cycling loading. Four identical symmetrically arranged load cells were used to measure the vertical load. Steel roller bearings were placed between the upper platen and the four load cells to prevent the transfer of horizontal loads to the load cells measuring the vertical load. All tests were conducted at room temperature and the data was sampled at 250 Hz.

4.6. Cyclic Lateral Testing

4.6.1. Mechanical Properties of Interest

The two mechanical properties of interest were the effective (secant) lateral stiffness and equivalent viscous damping ratio of the bearings at various amplitudes of lateral displacements. Effective lateral stiffness was calculated based on the peak to peak lateral response in each cycle of the test. Damping ratio of the bearing was calculated from the area within the hysteresis loops (ASCE 2005). Since the simplest definition of equivalent viscous damping is based on the measured response of the bearings to a harmonic excitation (Chopra 2007), the lateral displacements followed a sinusoidal pattern.

4.6.2. Influence of Lateral Displacement Amplitude History

The influence of displacement amplitude history on the lateral response was investigated using the ascending (AA) and descending (DA) input lateral displacement patterns, shown in Figs. 4.2a and 4.2b, respectively. The time histories had the same 76 mm/s average displacement rate with amplitudes ranging from 25% t_r (4.75 mm) to 200% t_r (28 mm) with

t_r = 19 mm. As indicated in Table 4.1 for full-range cyclic testing, Bearings B1-3 and B2-1 were subjected initially to an AA-pattern, and Bearings B2-3 was tested with a DA-pattern of displacements. In addition, Bearings B1-3 and B2-3 were retested perpendicular to the original directions using the DA and AA pattern of lateral displacements, respectively.

Figures 4.3a and 4.3b show the resulting lateral load-displacement hysteresis loops at 0° for the virgin B1-3 and B2-3 bearings. By definition, the term "virgin" in this paper applies to a bearing which has not been previously tested in any lateral direction. As seen in Fig. 4.3a, at each lateral displacement level, the larger load-resisting capacity and damping observed during the first cycle when the bearing was unscragged (Taylor and Igussa 2004). Once scragged at each level of displacement amplitude, the bearing exhibited stable hysteresis loops. The hysteresis loops for scragged behavior at each displacement amplitude, showed significant stiffening at the ends of the loops for AA-pattern testing. However, this response was not observed for DA-pattern testing. As shown in Fig. 4.3b, the initial cycle with displacement amplitude of 200% t_r scragged the virgin B2-3 bearing so that stable hysteresis loops resulted for all subsequent cycles with the same or smaller displacement amplitudes. Figure 4.4 shows lateral deformation of Bearing B2-3 at various displacement amplitudes.

Figure 4.5 contains the lateral load-displacement hysteresis loops for the diagonal (45°) responses of Bearings B1-3 and B2-3 under AA and DA lateral displacement patterns, respectively. As these bearings had been loaded previously in the two perpendicular lateral directions, they had already been scragged. Therefore, except for the first cycle of the largest displacement amplitude (200% t_r), no appreciable unscragged behavior was observed.

Regardless of the orientation and history of the imposed lateral displacements, all of the bearings maintained positive incremental load-resisting capacity throughout the lateral response and exhibited stable rollover (SR) deformation.

The variation of effective lateral stiffness and the damping ratio related to different lateral displacement amplitudes are shown in Fig. 4.6a and Fig. 4.6b for the AA and DA-patterns,

respectively. The bearings generally exhibited lower effective stiffness and higher damping ratio at 45°-orientation, compared to 0° or 90° orientations. Overall, when subjected to the DA-pattern of displacements, the bearings were found to have lower effective stiffness values and higher damping ratios for all orientations compared to the corresponding values for the AA-pattern of displacements.

Table 4.2 contains data from the bearings which showed the maximum and minimum responses for 0°, 90° and 45° loading orientations. Considering a vertical design pressure of p = 1.6 MPa, and the values of effective lateral stiffness (k) given in Table 4.2, the base isolation period ($T_i = 2\pi\sqrt{pA/(kg)}$) of the bearings for the ¼ scale building would range between 0.4 to 0.7 s for 0°/90° direction, depending on the amplitude of lateral displacement. In the 45° loading direction, the isolation periods would range between 0.5 to 0.8 s. Larger lateral displacements results in longer base isolation periods. It is noted that, according to dynamic similitude law (Harris and Sabnis 1999), the corresponding full-scale isolation periods would be approximately double (i.e., 0.8 to 1.4 s at 0°/90°, and 1.0 to 1.6 s at 45°).

As a result of the interaction between the fiber-reinforcement and the elastomer layers, damping ratios of the tested bearings were found to be significantly larger than the inherent damping of the elastomer (see Table 4.2). The relative volume of carbon fiber to elastomer in the bearings was approximately 14.5%. It is postulated that the supplementary damping attributed to the fiber-reinforcement is influenced by the relative volume of fiber to elastomer in a SU-FREI bearing. For example, in a previous study (Toopchinezhad et al. 2008a), where the lateral response of SU-FREI bearings with 5% relative volume of carbon fiber to elastomer (natural rubber) was investigated, negligible supplementary damping was found.

4.6.3. Influence of Vertical Pressure

Cyclic tests were conducted at three different vertical pressures to study the influence on lateral response. In the test procedure, the bearing was monotonically loaded to the target vertical pressure and three fully reversal cycles of sinusoidal lateral displacements at

frequency of 1 Hz (average displacement rate of 76 mm/s) and amplitude of 100% t_r (19 mm) were applied. The three prescribed vertical pressures were 0.8, 1.6, and 2.4 MPa where, the upper and lower values represent ±50% variation with respect to the design pressure of 1.6 MPa.

In Fig. 4.7, the test results showed that both effective lateral stiffness and damping ratio increased with the increased vertical pressure. However, under the investigated vertical pressure range, the damping ratio was found to be more sensitive to variation in the vertical pressure than the effective lateral stiffness. It is suggested that the differences in the lateral response values were primarily due to variation in the tension force introduced into the carbon fiber-reinforcement as it was stretched laterally due to lateral expansion of the elastomer under vertical load.

Fiber-reinforcement consists of individual fibers grouped into strands and woven into a fabric. The fabric is embedded into a thin polymer matrix to form the fiber-reinforcement sheet. The lateral expansion in the bearing and corresponding tension in the fabric tends to straighten the fabric. In this regard, the fiber fabric is less rigid in extension than the individual strands which, in turn have lower axial stiffness than the individual fibers. The extent of straightening of the fabric, the strands in the fabric and the fibers in the strand are affected by the level of vertical pressure on the bearing. The unbonded contact surfaces of a SU-FREI bearing leads to the flexible reinforcement sheets becoming curved under lateral loads. Therefore, it is postulated that the internal tension in the curved reinforcement sheet forces the fibers to slip relative to each other in the strands, and strands to slip relative to each other in the fabric. Both actions dissipate energy through friction (Kelly 1999). Thus, the additional damping at higher vertical pressure is attributed to increased internal tension in the fibers, and higher frictional forces during interfacial slippage. This phenomenon does not exist in steel-reinforced bearings and is most pronounced in unbonded fiber-reinforced bearings.

Any variations in the mechanical properties of the fiber-reinforcement will affect the lateral response of a SU-FREI bearing. In this regards, results of tensile tests on carbon-

reinforcement specimens showed that at low loads, the effective tensile modulus of fiber-reinforcement increased with increasing tensile load. Thus, it is postulated that the increase in the effective lateral stiffness of the bearings, with increased vertical pressure, may be related to the increased effective tensile modulus of the fiber-reinforcement. Increasing effective lateral stiffness with increased vertical pressure is not expected to continue at high levels of vertical pressure. At some limiting level of vertical pressure, additional straightening of the strands in the fabric and the fibers in the strands would become insignificant and increases in fiber modulus would be negligible. In such a case, a decrease in the effective lateral stiffness with increasing vertical pressure would be expected as the vertical pressure approaches the buckling pressure (Kelly 1997) of the bearing.

As seen in Fig. 4.7, for the range of vertical stresses tested, the variations in effective lateral stiffness and damping ratio were approximately 4% and 14%, respectively. Similar cyclic tests (not shown) at 100% t_r and 150% t_r lateral displacement amplitudes with a lower average displacement rate of 30 mm/s were conducted on Bearing B1-1. Under the prescribed vertical pressure levels of 1.1, 1.6, and 2.4 MPa, this bearing also showed a consistent increase in effective lateral stiffness and damping with increasing vertical pressure. The largest variations occurred at 150% t_r displacement amplitude, where, compared to tests at 1.6 MPa vertical pressure, the effective lateral stiffness decreased by 4% under 1.1 MPa vertical pressure, and increased by 10% under 2.4 MPa vertical pressure.

4.7. Vertical Compression Testing

The vertical frequency of an elastomeric bearing, as an important design parameter, is directly controlled by its vertical compressive stiffness. Vertical testing was carried out under load control where all of the bearings were initially loaded monotonically to the target vertical pressure p. Next, three fully reversed loading cycles with amplitudes of $\pm 20\%p$ were applied and followed by monotonic unloading (see Fig. 4.8). The influence of vertical pressure on vertical stiffness was evaluated using vertical pressures of 0.8, 1.6, and 2.4 MPa.

Results of vertical tests on the virgin Bearings B1-3 and B2-3 are listed in Table 4.3. As a representative example, the resulting compressive stress-strain curves for B2-3 at the three levels of vertical pressure are presented in Fig. 4.9a. The slope of a straight line fitted to the cyclic portion of the curve (as shown in Fig. 4.9b) reflects the effective compressive modulus of the bearing under the specified pressure. As was the case for all four bearings, this clearly shows the increasing effective compressive modulus with increasing vertical pressure.

As in the case with conventional steel-reinforced elastomeric bearings, the resulting vertical compressive stress-strain curves of the tested fiber-reinforced bearings were found to be highly nonlinear with significant run-in before the full vertical stiffness was developed. The nonlinear response is primarily due to the nonlinear behavior of the elastomer in compression (Robert 1988). The initial run-in response depends on issues related to workmanship, alignment of the reinforcing layers (Kelly 1997) and, in the case of fiber-reinforced bearings, flexibility of the reinforcement in extension (Kelly 1999). To reduce the initial run-in effect, a special device was designed to apply orthogonal in-plane tension to the bi-directional fabric prior to being bonded to the elastomer layers. While stretched in tension, to straighten and align fibers, strands, and the fabric, the carbon fiber fabric was bonded to one face of an elastomer layer. The tension was maintained in the fabric until curing of the bonding compound was complete. Comparing the vertical load-deflection test results in this study with a previous experimental study (Toopchinezhad et al. 2008a) indicates that increasing the initial tautness of the fiber-reinforcement significantly reduces the initial run-in in the load-deflection response. In general, this initial run-in is of little concern as long as the bearings develop adequate vertical stiffness under the expected minimum vertical loads.

After completion of cyclic lateral testing vertical tests were performed on Bearings B1-1 and B2-1 and repeated on B1-3 and B2-3 (see Table 4.1). The results of these vertical tests on bearings that had already been exposed to extreme lateral displacements are listed in Table 4.4. Compared to the results from tests on virgin bearings (see Table 4.3), maximum decreases of 10% and 12% in the vertical stiffness of the bearings at 1.6 MPa and 2.4 MPa

vertical pressure were observed. These small changes, occurring as a result of acceptably small invisible damage to the bearings, indicated that no serious serviceability issues would exist regarding the vertical performance of the bearings after a major earthquake. No debonding in the bearings was visible after completion of these vertical tests. However, more careful examination of Bearing B1-1 in a deformed state showed that its slightly lower stiffness may have been due to a small amount of debonding at one of the laminates during the 45° cyclic lateral test.

The vertical stiffness of elastomeric bearings is usually several hundred times larger than the effective lateral stiffness of the bearing. This ensures that rocking vibration modes are prevented from participating in the response of a base isolated building. Given the vertical stiffness (k_v) of a bearing under vertical pressure of p, the vertical frequency f_v is calculated as $f_v = \frac{1}{2\pi}\sqrt{k_v g/(pA)}$ where g is the acceleration of gravity and A is the plan area of the bearing. According to the results in Tables 3 and 4, the bearings exhibited vertical frequencies ranging from 42 Hz to 64 Hz, depending on the level of the vertical pressure. These values are significantly higher than the base isolated frequency range (i.e., 2 Hz or less) of the bearings. Accordingly, the vertical performance of the bearings is considered to be satisfactory.

4.8. Robustness of the Lateral Response

Since no significant damage was visible in the bearings, cyclic lateral testing using the displacement history shown in Fig. 4.2a was repeated on all of the previously tested bearings. The main objective was to evaluate the lateral response degradation of bearings previously subjected to large lateral displacements in the 0°, 90°, and 45° directions. All bearings were retested at 0° orientation and, additionally, B1-3 was tested at 90°. Figure 4.10 shows the consistent variations of average lateral response with amplitude of lateral displacements. As a typical data, hysteresis loops corresponding to all cycles of the repeated test on B1-3 (at 0° orientation) are shown in Fig. 4.11. As seen in this figure, stable loops were obtained for all three test-cycles at each level of lateral displacement. However, unlike the previous cyclic test at 0° (Fig. 4.3a), no appreciable unscragged response behavior was

observed. This is not surprising as the bearing had already been scragged during the previous large-amplitude lateral displacements.

The right half of the hysteresis loops of retested B1-3 for the second cycle at 100%, 150%, and 200% t_r displacements have been re-plotted in Fig. 4.12a over the corresponding half hysteresis loops of the virgin B1-3 (from Fig. 4.3a). Unlike the virgin B1-3, the retested B1-3 bearing did not show any significant stiffening at the extreme portion of 100% and 150% t_r cycles but significant stiffening was observed at the 200% t_r displacement. As shown in Fig. 4.12b, retested B1-3 showed lower effective lateral stiffness and higher damping ratios relative to virgin B1-3. The maximum decrease in average lateral stiffness was found to be 22% which occurred at 150% t_r displacement. At this displacement, a 13% increase in the damping ratio was found. Despite their reduced stiffnesses, all of the retested bearings showed SR-deformation (see Fig. 4.11) and would continue function effectively after a major earthquake.

A comparison of Figs. 4.6b and 4.10a shows that, except at the 200% t_r displacement, the bearings exhibited larger effective stiffness in the repeated cyclic lateral testing than in the cyclic testing with a DA-pattern. Since both Figs. 4.6b and 4.10a present the scragged properties of the bearings, the lower stiffness values in Fig. 4.6b highlight the importance of the lateral displacement history on lateral response of the bearings.

4.9. Lateral Response under Extreme Lateral Displacement

The tested bearings were intended for trial use in shake table testing of a ¼ scale building. Therefore, to avoid significantly damaging the bearings, their lateral response under extreme displacements was not investigated directly. Instead, Bearing TB1, which had the same characteristics of the tested bearings but a different width, was tested. This bearing had 70 × 41 mm physical dimensions in plan, a total thickness of approximately 25 mm, and a total thickness of the neoprene layers of t_r = 19 mm. Bearing TB1 had an aspect ratio of R = 2.8 in its longitudinal direction. The shape factor for the bearing was S = 8.2 due to its reduced width. No finishing coats of bonding compound were applied to the perimeter

surfaces of this bearing as there was an interest in studying the role of finishing coats on damage protection of the bearing at large lateral displacements.

The bearing was subjected to the ascending displacement history shown in Fig. 4.2a under a constant vertical pressure of 1.6 MPa. Figure 4.13 contains the lateral load-displacement hysteresis loops for all cycles of the test up to 200% t_r on the virgin TB1 in its longitudinal direction. As seen in Fig. 4.13, it exhibited SR-deformation and no delamination or any other damage was observed after completion of this cyclic testing. This observation implied that the other tested bearings would safely sustain lateral displacements up to 200% t_r even in the absence of a finishing coat. Since no platen restrained induced vertical tension is developed in a laterally-deformed SU-FREI bearing, the internal bonding between elastomer and reinforcing sheets are subjected to a much lower stress demand compared to the same bearing in a bonded application. Accordingly, the SU-FREI bearings were able to survive multiple cycles of large lateral displacements.

The full contact vertical face lateral displacement (δ_{fc}) occurs when the originally vertical faces of the bearings completely contact the upper and lower platens of the test machine. As can be seen in Fig. 4.4b, where the original vertical faces of the bearings did not completely contact the upper and lower platens, and from observation of all previous cyclic lateral tests, δ_{fc} was larger than 200% t_r. At lateral displacements significantly larger than δ_{fc}, it was anticipated that SU-FREI bearings could experience an unstable mode of behavior called "rollout" (Kelly 1997). The rollout instability would occur when the bearing's lateral load-displacement curve exhibits softening behavior with negative slope. In order to study the ultimate response of TB1, the displacement time history shown in Fig. 4.14a, was applied to the bearing under a constant vertical pressure of 1.6 MPa. Having been previously scragged, no significant unscragged properties were observed up to 200% t_r displacement. However, during the first cycles at 250% and 300% t_r, displacement, the bearing showed unscragged responses with larger effective lateral stiffness and damping than in the subsequent cycles.

Figure 4.14b shows the hysteresis loops corresponding to the last (third) test cycle for TB1 at 200%, 250%, and 300% t_r displacements. Figures 4.15a to 4.15f are photographs taken of

TB1 at these displacements. The hysteresis plots in Fig. 4.14b showed that TB1 maintained a positive incremental lateral load-resisting capacity for displacements of 200% and 250% t_r. The latter amplitude approximates δ_{fc} (see Fig. 4.15c). Bearing TB1 also exhibited SR-deformation during the first two cycles of 300% t_r (57 mm) displacement. However, the hysteresis loop for the third 300% t_r cycle of the test showed significant stiffness degradation as a result of a localized major delamination at one of the bearing's laminates (see Fig. 4.15f). As seen in Fig. 4.14b, the hysteresis loop at the third 300% t_r displacement exhibited nearly zero slope during the positive displacement and softening behavior during the negative displacement. This region of near constant resistance to lateral displacement was followed by a stiffening behavior as the lateral displacement increased from 250% to 300% t_r. The stiffened behavior at the extreme portion of the 300% t_r lateral displacement indicates that this level of lateral displacement did not result in rollout instability. Close examination of Fig. 4.15f shows that the SU-FREI bearing had moved left during the final left displacement at 300% t_r. Also a slip displacement at the location of a delamination is clearly visible. However, the delamination damage and subsequent 6 mm (32% t_r) slip in the SU-FREI bearing due to the large friction forces between the rubber material and the top and bottom contact surfaces are judged to continue bearing failure. Therefore, 250% t_r ($\approx \delta_{fc}$) is considered to be a reasonable limit for maximum allowed lateral displacement of Bearing TB1.

The tests of Bearing TB1 under extreme lateral displacement provide confidence that the other bearings, which were covered with 2 coats of the chemical compound used to bond the laminates, would safely sustain a 250% t_r (47.5 mm) lateral displacement.

4.10. Concluding Remarks

Four stable unbonded fiber-reinforced elastomeric isolator (SU-FREI) bearings designed for shake table testing of a ¼ scale building were tested under various loading sequences. All of these unbonded bearings showed stable rollover (SR) deformation when subjected to cyclic lateral testing in the 0°, 90°, and 45° directions. SR-deformation enhanced the seismic efficiency of the bearings as the effective lateral stiffness significantly decreased with increasing displacement amplitude. Even though an unfilled elastomer was utilized,

damping ratio values were found to be significantly larger than that of the utilized elastomer as a result of interaction between fiber-reinforcement and elastomer layers in the bearings. Owing to the lower stress demand on the internal bond between the elastomer and reinforcement layers of a laterally-deformed SU-FREI bearing, large displacements during cyclic testing did not result in any significant damage to the bearings. This indicated the robustness of the SU-FREI bearings.

Vertical compression testing revealed that the tested SU-FREI bearings had a vertical frequency which was at least 20 times larger than the maximum expected base isolated frequency of the bearings. Therefore, the contribution of rocking vibration modes in the base isolated response would be insignificant. After completing the cyclic lateral tests, subsequent vertical tests showed that vertical stiffness degradation of the bearings was negligible.

In general, the lateral response of the SU-FREI bearings was found to be highly nonlinear with sensitivity to both the amplitude and amplitude history of the cyclic lateral displacements imposed to the bearings. The response was also sensitive to the level of vertical pressure on the bearings. Additionally, the transition between virgin and scragged properties of the elastomer added to the complexity of the response. From the tests described in this paper, the following conclusions can be drawn.

Lateral displacement amplitude: The effective lateral stiffness of the bearings decreased significantly (approximately 60%) with increasing amplitude of lateral displacement. The equivalent viscous damping ratios of the bearings also decreased with increasing lateral displacement. However, at least 8% damping was achieved for the largest lateral displacement.

Lateral displacement amplitude history: The shape of the lateral load-displacement hysteresis loops was influenced by the history of the lateral displacements. The virgin bearings that were subjected to a displacement history with an ascending amplitude (AA) pattern exhibited unscragged response properties during the first cycle of each increased

displacement. The unscragged effective lateral stiffness and damping values were at most 10% and 19% larger, respectively, than the average response values of the scragged-loops. The minimum effective lateral stiffnesses and the maximum damping ratios were obtained when the bearings were subjected to a descending amplitude (DA) pattern of lateral displacements.

Variations in vertical pressure: The influence of a ±50% variation in the 1.6 MPa vertical pressure on the effective lateral stiffness was found to be negligible. This implies that the prescribed vertical pressure were significantly below the buckling pressure of the bearings. Compared to the effective lateral stiffness the damping ratio was found to be more influenced by variations in vertical pressure. A 50% increase in the vertical pressure resulted in a 10% increase in the damping ratio. For most practical cases, this variation can be neglected from an engineering design prospective (ASCE 2005).

Lateral displacement capacity: At $\delta_{fc} \approx 250\%\ t_r$ (47.5 mm), the originally vertical faces of the bearings completely contacted the upper and lower supports. This displacement was chosen as the maximum lateral displacement capacity for the bearings examined in this study. Rollout instability would be expected to occur at significantly larger lateral displacements. However, as shown in the extreme displacement tests the bearings would probably experience significant damage and change of behavior before rollout instability took place.

Considering the calculated base isolated periods of the bearing designed for the ¼ scale building, in conformance to dynamic similitude law (Harris and Sabnis 1999), the isolated periods for the corresponding full-scale bearings for the full-scale building would range from 0.8 to 1.4 s in the parallel/perpendicular direction, and from 1 to 1.6 s in the diagonal direction, depending on the amplitude of lateral displacement. Additionally, the lateral displacement capacity of the full-scale bearings would be 190 mm (250% t_r) in conjunction with an 8% or higher damping ratio. Therefore, the full-scale SU-FREI bearings can be used effectively for seismic hazard mitigation of many structures, including but not limited to, low-rise buildings with fixed base period of 0.1 to 0.2 s, located in moderate to high seismic

regions (ASCE 2005). In some practical cases, even if the lateral displacement capacity of the bearings is beyond the maximum demand, special protectors (Xi-Yuan et al. 2003) may be utilized to protect the superstructure when unexpectedly large displacements occur in the bearings. This would depend on the importance of the structure and is a precaution also employed in application of conventional base isolators.

4.11. References

ASCE. (2005). "Minimum Design Loads for Buildings and other Structures." *ASCE/SEI 7-05*, American Society of Civil Engineers, New York.

ASTM. (2005). "Standard Test Method for Rubber Property-Durometer Hardness." *ASTM D2240*, American Society for Testing and Materials, Philadelphia.

Chopra, A. K. (2007). *Dynamics of Structures; Theory and Applications to Earthquake Engineering*, 3rd edition, Prentice Hall, Upper Saddle River, New Jersey.

Harris, H. G. and Sabnis, G. M. (1999). *Structural Modeling and Experimental Techniques*, CRC Press, New York.

Kelly, J. M. (1997). *Earthquake-Resistant Design with Rubber*, 2nd edition, Springer-Verlag, London.

Kelly, J. M. (1999). "Analysis of Fiber-Reinforced Elastomeric Isolators." *Journal of Seismology and Earthquake Engineering (JSEE)*, Vol. 2, No. 1, Pages 19-34.

Moon, B. Y., Kang, G. J., Kang, B. S., and Kelly, J. M. (2002). "Design and Manufacturing of Fiber-reinforced Elastomeric Isolator for Seismic Isolation." *Journal of Materials Processing Technology*, Vol. 130-131, Pages 145-150.

Robert A. D. (1988). *Natural Rubber Science and Technology*, Oxford University Press, Oxford.

Skinner, R. I., Robinson, W. H., and McVerry, G. H. (1993). *An Introduction to Seismic Isolation*, Wiley, Chichester, U.K.

Taylor A. W., and Igussa T. (2004). *Primer on Seismic Isolation*, American Society of Civil Engineers, ASCE, Reston, Virginia.

Toopchinezhad H., Tait M. J., and Drysdale R. G. (2007). "Base Isolation of Small Low-Rise Buildings using Fiber-Reinforced Elastomeric Bearings." *Proceedings, CSCE (Canadian Society for Civil Engineering) Annual General Meeting & Conference, Yellowknife, Northwest Territories, Canada*, Paper 192.

Toopchinezhad, H., Tait, M. J., and Drysdale, R. G. (2008a). "Testing and Modeling of Square Carbon Fiber-Reinforced Elastomeric Seismic Isolators." *Structural Control and Health Monitoring*, Vol. 15, No. 6, Pages 876-900, DOI: 10.1002/stc.225 (*Chapter 2 of this thesis*).

Toopchinezhad H., Tait M. J., and Drysdale R. G. (2008b). "Lateral Response Evaluation of Fiber-Reinforced Neoprene Seismic Isolators Utilized in an Unbonded Application." *Journal of Structural Engineering, ASCE*, Vol. 134, No. 10, Pages 1627-1638 (*Chapter 3 of this thesis*).

Xi-Yuan Z., Han M., and Yang L. (2003). "Study on Protection Measures for Seismic Isolation Rubber Bearing." *SISET Journal of Earthquake Technology*, Vol. 40, No. 2-4, Pages 137-160.

Table 4.1. Sequence of tests conducted on each SU-FREI bearing

Sequence	Model Scale Bearing			
	B1-1	B1-3	B2-1	B2-3
1	Cyclic test (0°) *AA-pattern,* *rate = 30 mm/s*	Vertical test *p = 0.8, 1.6, 2.4 MPa*	Cyclic test (0°) *AA*-pattern, *rate = 30 mm/s*	Vertical test *p = 0.8, 1.6, 2.4 MPa*
2	Rate sensitivity test *0° response,* *displ. amp. = 100% t_r,* *rate = 30, 45, 76, 114 mm/s*	Cyclic test (0°) *AA-pattern,* *rate = 76 mm/s*	Rate sensitivity test *0° response,* *displ. amp. = 100% t_r,* *rate = 114, 76, 45, 30 mm/s*	Cyclic test (0°) *DA*-pattern, *rate = 76 mm/s*
3	Rate sensitivity test *90° response,* *displ. amp. = 150% t_r,* *rate = 30, 45, 76, 114 mm/s*	Cyclic test (90°) *DA*-pattern, *rate = 76 mm/s*	Cyclic test (90°) *AA*-pattern, *rate = 76 mm/s*	Cyclic test (90°) *AA*-pattern, *rate = 76 mm/s*
4	Infl. of vert. pressure on horz. response *90° response,* *p = 1.1, 1.6, 2.4 MPa,* *displ. amp. = 100% t_r,* *rate = 30 mm/s*	Infl. of vert. pressure on horz. response *90° response,* *p = 0.8, 1.6, 2.4 MPa,* *displ. amp. = 100% t_r,* *rate = 76 mm/s*	Infl. of vert. pressure on horz. response *90° response,* *p = 0.8, 1.6, 2.4 MPa,* *displ. amp. = 100% t_r,* *rate = 76 mm/s*	Infl. of vert. pressure on horz. response *90° response,* *p = 0.8, 1.6, 2.4 MPa,* *displ. amp. = 100% t_r,* *rate = 76 mm/s*
5	Infl. of vert. pressure on horz. response *90° response,* *p = 1.1, 1.6, 2.4 MPa,* *displ. amp. = 150% t_r,* *rate = 30 mm/s*	Rate sensitivity test *0° response,* *displ. amp. = 100% t_r,* *rate = 30, 45, 76, 114 mm/s*	Cyclic test (45°) *AA*-pattern, *rate = 76 mm/s*	Rate sensitivity test *0° response,* *displ. amp. = 100% t_r,* *rate = 30, 45, 76, 114 mm/s*
6	Cyclic test (45°) *AA*-pattern, *rate = 30 mm/s*	Cyclic test (45°) *AA*-pattern, *rate = 76 mm/s*	Vertical test *p = 0.8, 1.6, 2.4 MPa*	Cyclic test (45°) *DA*-pattern, *rate = 76 mm/s*
7	Vertical test *p = 0.8, 1.6, 2.4 MPa*	Vertical test *p = 0.8, 1.6, 2.4 MPa*	Cyclic test (0°) *AA*-pattern, *rate = 76 mm/s*	Vertical test *p = 0.8, 1.6, 2.4 MPa*
8	Cyclic test (0°) *AA*-pattern, *rate = 76 mm/s*	Cyclic test (90°) *AA*-pattern, *rate = 76 mm/s*		Cyclic test (0°) *AA*-pattern, *rate = 76 mm/s*
9		Cyclic test (0°) *AA*-pattern, *rate = 76 mm/s*		

Notes: AA-pattern: ascending amplitude pattern of lateral displacements
DA-pattern: descending amplitude pattern of lateral displacements
Unless otherwise stated, cyclic tests were conducted under a constant vertical pressure of p = 1.6 MPa

Table 4.2. Maximum and minimum bearing lateral responses for loading in the parallel (0°)/perpendicular (90°) and diagonal (45°) directions

Displacement Amplitude	Cycle	Displacement Orientation							
		Parallel/Perpendicular				Diagonal			
		Virgin B1-3, 0° (AA - Pattern)		B1-3, 90° (DA - Pattern)		B1-3, 45° (AA - Pattern)		B2-3, 45° (DA - Pattern)	
		K (N/mm)	ξ (%)	K (N/mm)	ξ (%)	K (N/mm)	ξ (%)	K (N/mm)	ξ (%)
25% t_r (4.75 mm)	1	164.0	13.7	108.5	11.2	135.7	15.8	97.9	11.0
	2	155.6	13.4	108.0	9.8	131.5	16.1	101.1	11.5
	3	154.1	13.3	108.4	10.1	130.6	16.1	101.9	10.9
50% t_r (9.50 mm)	1	123.3	11.9	86.5	11.8	102.5	12.1	81.7	11.7
	2	116.5	10.9	85.9	11.4	101.0	11.5	81.8	11.4
	3	114.6	10.8	86.2	11.1	99.9	11.4	82.0	11.3
75% t_r (14.25 mm)	1	103.3	10.2	72.1	10.7	84.0	10.7	68.7	10.7
	2	97.1	9.5	72.2	10.7	82.3	10.4	68.7	10.5
	3	95.3	9.4	72.4	10.7	81.9	10.2	68.8	10.6
100% t_r (19.00 mm)	1	89.3	9.4	62.5	10.6	72.3	10.2	59.8	10.2
	2	84.7	8.8	62.8	10.1	71.3	9.7	60.6	10.1
	3	83.6	8.7	63.0	10.0	70.8	9.7	60.7	10.1
150% t_r (28.50 mm)	1	72.9	9.9	50.8	10.4	58.7	10.9	49.1	9.9
	2	68.8	8.4	50.6	10.1	57.7	10.0	49.1	9.8
	3	67.1	8.3	50.9	10.1	57.1	9.8	49.4	9.6
200% t_r (38.00 mm)	1	68.5	9.4	64.7	10.8	51.9	11.7	52.5	12.4
	2	63.3	8.3	61.4	8.6	49.4	11.0	50.1	10.0
	3	61.6	8.1	60.2	8.4	48.4	10.9	48.8	9.5

Notes: AA - Pattern: Lateral displacements with an ascending amplitude pattern
DA - Pattern: Lateral displacements with a descending amplitude pattern
K: Effective (secant) lateral stiffness
ξ: Equivalent viscous damping ratio

Table 4.3. Results of initial vertical test on Bearings B1-3 and B2-3 (before cyclic lateral testing)

Bearing	Vertical Load (kN)	Vertical Pressure (MPa)	Vertical Stiffness (kN/mm)	Compressive Modulus (MPa)	Vertical Frequency (Hz)
B1-3	4	0.82	57.5	223.6	59.8
	8	1.63	88.1	342.4	52.3
	12	2.45	111.7	434.3	48.1
B2-3	4	0.82	59.9	232.8	61.0
	8	1.63	98.0	380.8	55.2
	12	2.45	115.0	447.1	48.8

Table 4.4. Results of vertical test on Bearings B1-1, B1-3, B2-1, and B2-3 (after cyclic lateral testing)

Bearing	Vertical Load (kN)	Vertical Pressure (MPa)	Vertical Stiffness (kN/mm)	Compressive Modulus (MPa)	Vertical Frequency (Hz)
B1-1	4	0.82	50.0	194.4	55.7
	8	1.63	72.2	280.7	47.4
	12	2.45	85.9	334.0	42.2
B1-3	4	0.82	56.2	218.5	59.1
	8	1.63	79.5	309.1	49.7
	12	2.45	98.2	381.8	45.1
B2-1	4	0.82	53.9	209.6	57.9
	8	1.63	81.7	317.6	50.4
	12	2.45	105.3	409.4	46.7
B2-3	4	0.82	58.0	225.5	60.0
	8	1.63	95.6	371.7	54.5
	12	2.45	112.3	436.6	48.2

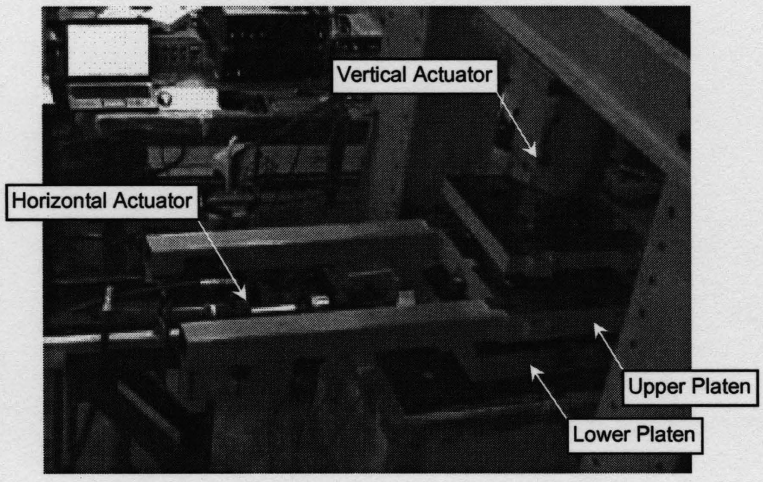

Figure 4.1. An overview of the test setup

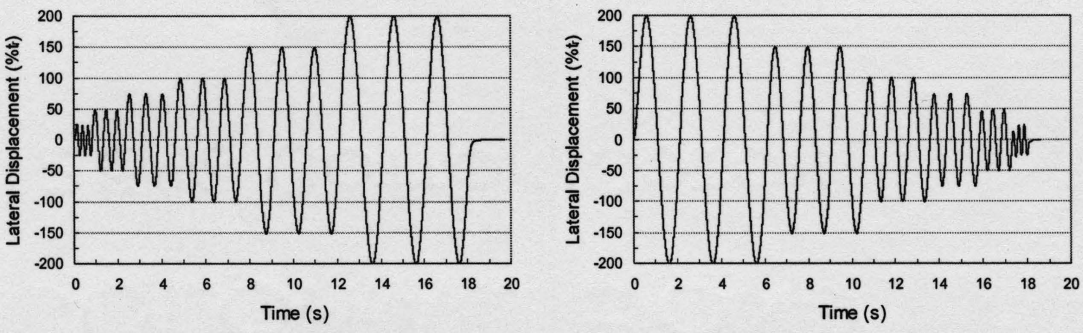

(a) Ascending Amplitude (AA) Pattern (b) Descending Amplitude (DA) Pattern

Figure 4.2. Time histories of the input sinusoidal lateral displacements

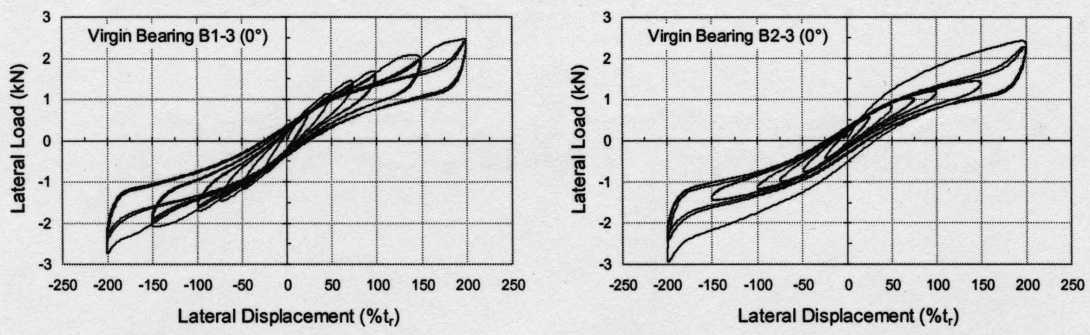

(a) Bearing B1-3 under AA-Pattern (b) Bearing B2-3 under DA-Pattern

Figure 4.3. Lateral load-displacement hysteresis loops for the virgin bearings at 0°

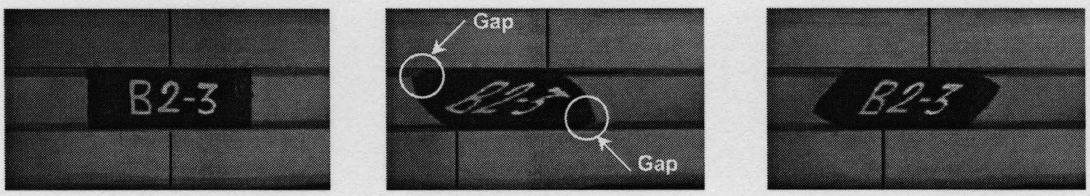

(a) Undeformed (b) 200% t_r (38 mm) (c) 100% t_r (19 mm)

Figure 4.4. Photographs of B2-3 taken at different amplitudes of cyclic lateral displacement (DA-pattern)

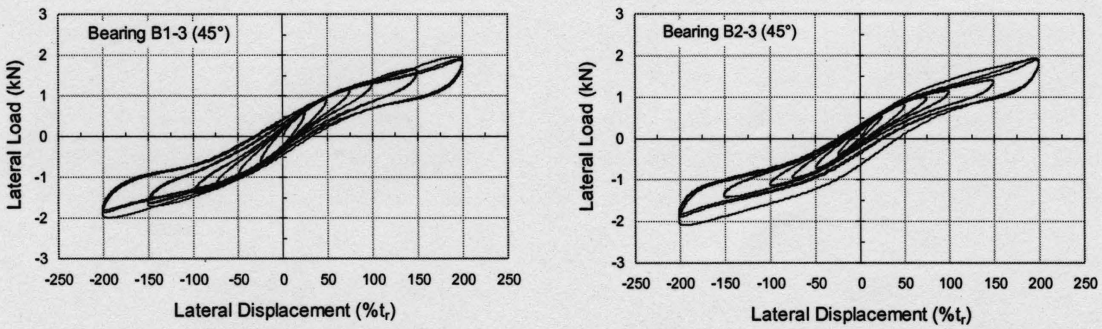

(a) Bearing B1-3 under AA-Pattern (b) Bearing B2-3 under DA-Pattern

Figure 4.5. Lateral load-displacement hysteresis loops for bearings at 45°

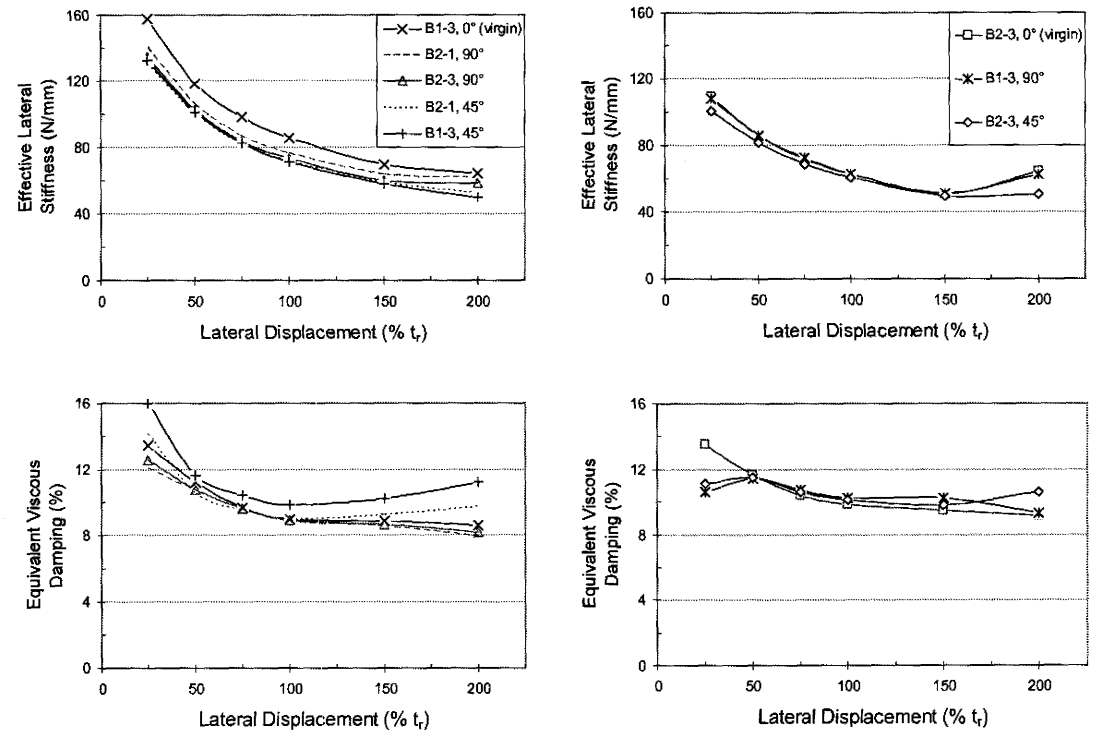

(a) AA-Pattern (b) DA-Pattern

Figure 4.6. Lateral response properties of the SU-FREI bearings under cyclic lateral tests (values are the average of all cycles at each displacement)

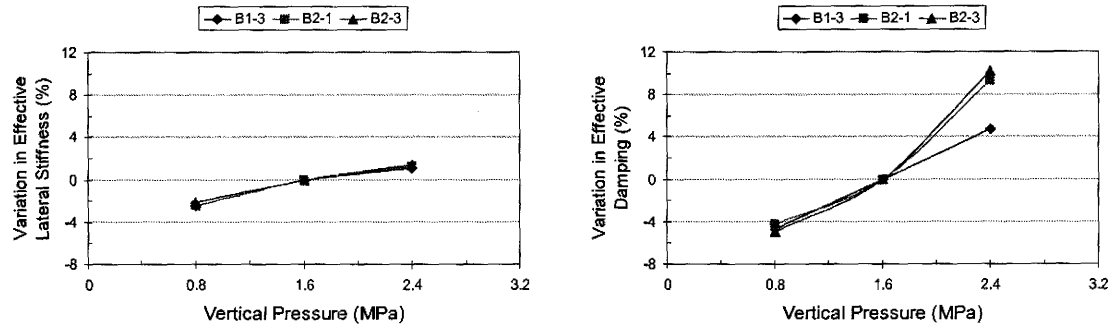

(a) Variation in Effective Lateral Stiffness (b) Variation in Effective Damping

Figure 4.7. Influence of variation in vertical design pressure on lateral response of Bearings B1-3, B2-1, and B2-3; (lateral displacement amplitude = 100% t_r or 19 mm, average displacement rate = 76 mm/s)

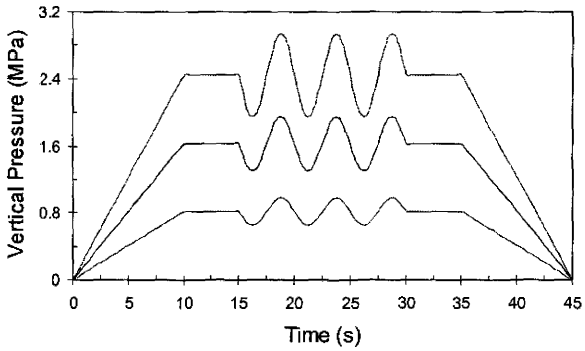

Figure 4.8. Time history of the input signals utilized for vertical tests on the bearings

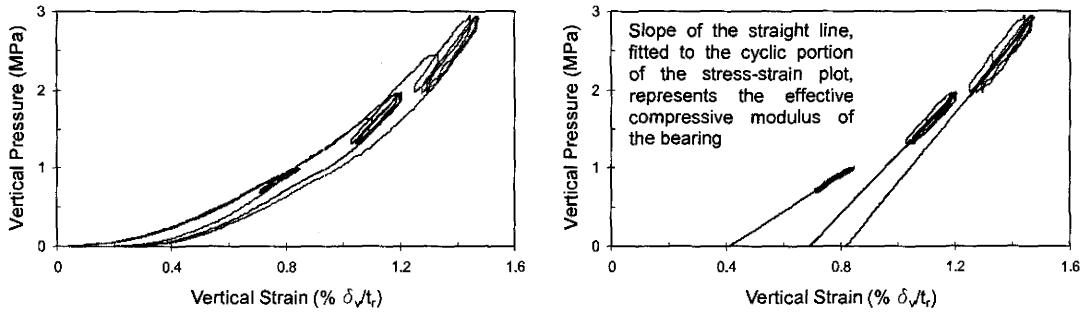

(a) Stress-Strain Plot (b) Effective Compressive Modulus

Figure 4.9. Vertical compressive stress-strain behavior of Bearing B2-3 under 0.8, 1.6, and 2.4 MPa vertical pressure

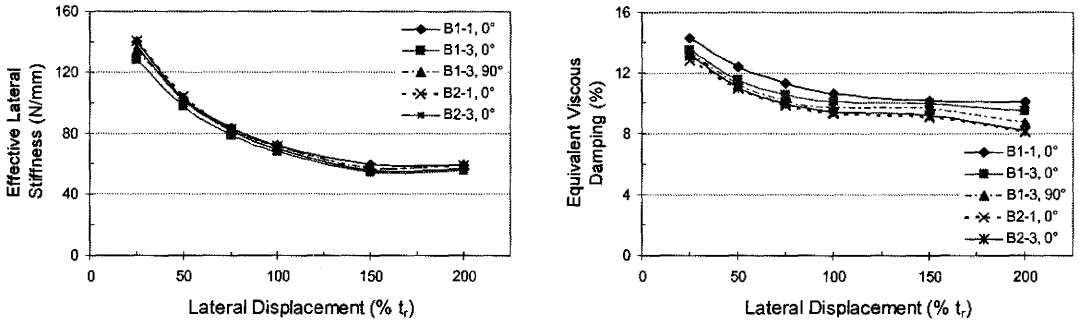

(a) Effective Lateral Stiffness (b) Effective Damping

Figure 4.10. Lateral response characteristics of all SU-FREI bearings during the repeated cyclic testing (values are the average of all cycles at each displacement)

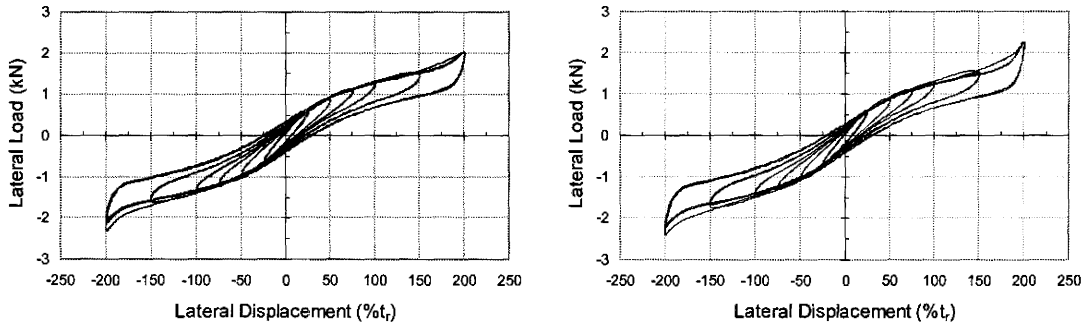

(a) 0° Response (b) 90° Response

Figure 4.11. Hysteresis loops for repeated cyclic testing of Bearing B1-3

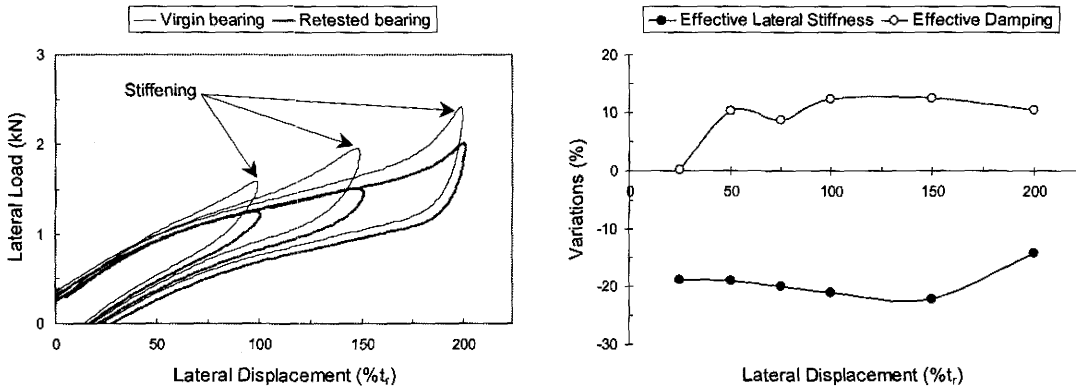

(a) Half hysteresis loops for 2nd test cycle

(b) Variation of average response of retested B1-3 versus virgin B1-3

Figure 4.12. Lateral response of virgin B1-3 versus retest B1-3 under an AA-pattern of cyclic lateral displacements at 0°

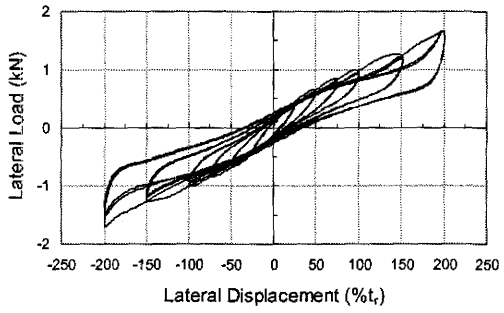

Figure 4.13. Longitudinal lateral response of the virgin Bearing TB1 to an AA-pattern of lateral displacement

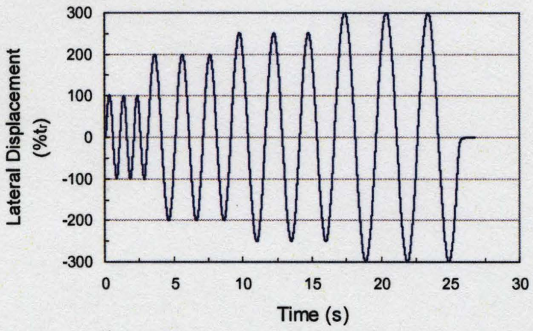

(a) Input lateral displacements

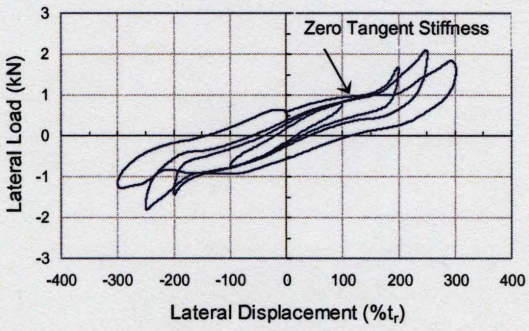

(b) Hysteresis loops for the 3rd cycle of each displacement

Figure 4.14. Longitudinal lateral response for Bearing TB1 (ave. displ. rate = 76 mm/s)

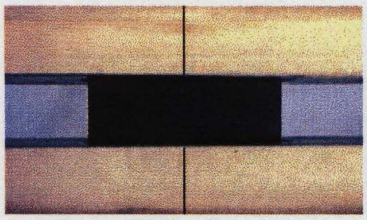

(a) Start (0% t_r)

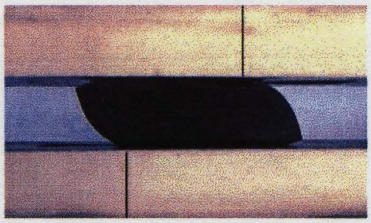

(b) 200% t_r (38 mm) - cycle 3

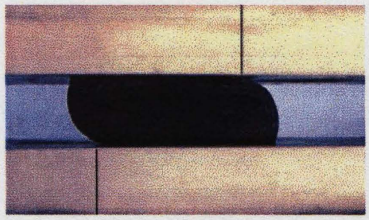

(c) 250% t_r (47.5 mm) - cycle 3

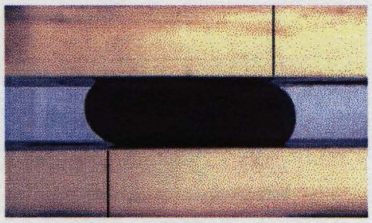

(d) 300% t_r (57 mm) - cycle 1

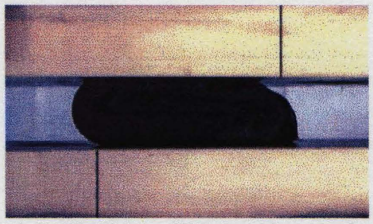

(e) 300% t_r (57 mm) - cycle 3

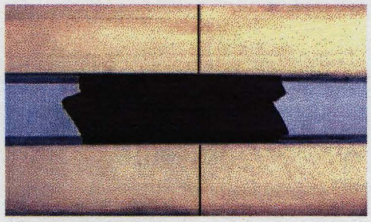

(f) End (0% t_r)

Figure 4.15. Photographs of Bearing TB1 taken during cyclic lateral testing

Chapter 5: Shake Table Study on an Ordinary Low-Rise Building Seismically Isolated with SU-FREIs (Stable Unbonded Fiber-Reinforced Elastomeric Isolators)

5.1. Abstract

Despite the widespread acceptance of conventional steel-reinforced elastomeric isolator (SREI) bearings as an effective means of seismic isolation, their application in ordinary low-rise buildings may not be economically justified. This paper reports on the investigation of a novel alternative low-cost fiber-reinforced elastomeric isolator (FREI) bearing, which does not have thick end plates, and is used in an unbonded application. Due to the stable lateral load-displacement response exhibited by the unbonded FREI bearings, the proposed bearings are referred to as stable unbonded (SU)-FREIs. A shake table test program was conducted on a 2-story test-structure having well defined elastic response characteristics. Compared to the results for the corresponding fixed base (FB) structure, the peak response values, distribution of lateral response throughout the height of the structure, and response time histories of the tested base isolated structure indicate that significantly improved response can be achieved. This study clearly indicates that SU-FREI bearings can provide an effective seismic isolation system.

5.2. Introduction

5.2.1. Motivation for the Research

Base isolation is aimed at decreasing the seismic demand placed on a structure. Seismic base isolation systems utilize a flexible interface system to isolate the structure from ground motion and a damping mechanism to dissipate earthquake energy. Despite its worldwide availability, application of seismic isolation is currently limited to a "small percentage of newly engineered or rehabilitated structures" (May 2002) which are usually of high importance. Lack of extensive use stems from a combination of concerns about the cost, and more time consuming and complicated design and construction processes.

Additionally, "the overly burdensome requirements" for design certification is a barrier to the adoption of this technology (May 2002). These factors have hindered the use of base isolation technology as a common alternative to conventional seismic design of ordinary low-rise buildings.

An innovative elastomeric base isolation system, developed to address some of the aforementioned concerns, is introduced and evaluated in this paper. The proposed base isolation system utilizes cost effective stable unbonded fiber-reinforced elastomeric isolator (SU-FREI) bearings.

5.2.2. FREI versus SREI

Steel-reinforced elastomeric isolator (SREI) bearings are the most commonly used isolator. However, SREIs are typically expensive due to the labor intensive manufacturing process, and the vulcanization (curing) process which requires high temperature and pressure (Kelly 2002). In addition, the need for an isolator mold may significantly increase the total cost of these bearings (Naiem and Kelly 1999). Another characteristic of SREIs is that they are usually heavy as a result of using steel-reinforcing plates. This can lead to large lifting, handling, and transportation costs. As such, in spite of their favorable performance, SREIs have not become a cost effective isolation solution for low-rise buildings of ordinary importance; a significant reduction in the manufacturing and associated installation costs is required.

Research studies have shown that fiber-reinforced elastomeric isolator (FREI) bearings can be used as an alternative to conventional SREIs (Kelly 1999, 2002, Moon et. al. 2002, Toopchinezhad et al. 2008a, b, c, Dehghani Ashkezari et. al. 2008). Similar to SREIs, FREIs utilize elastomeric layers, however, the steel-reinforcement plates are replaced with fiber fabrics. Experiments conducted on SREIs, which have been in use for nearly 45 years (Taylor et. al. 1992), provide a high level of confidence regarding the expected longevity and long-term performance of FREIs. The alternating layers of fiber-reinforcement and elastomers can be effectively bonded together using a cold-vulcanized bonding compound without the need for any mold. This technique has been employed to produce a large FREI sheet (Toopchinezhad et al. 2008b). Using a standard band saw the FREI sheet were easily

cut into individual FREI bearings without damaging the laminates (Toopchinezhad et al. 2008a, b). Labor expenses can be significantly reduced if large FREI sheets are constructed through an automated mass production manufacturing technique similar to that used to produce large conveyor belts. Significant cost savings in the design of a base isolated (BI) structure that employs FREI bearings can be achieved, if the bearings are supplied as catalogue products with supplier-provided design properties. It is evident that FREIs are significantly lighter in weight than SREIs. Further reduction in the isolator's weight can be achieved, if unlike a conventional SREI, no thick steel end-plates are bonded to the lower and upper faces of FREI. This feature facilitates the mass production and subsequent cutting of a large FREI sheet in order to produce individual isolator bearings. From the above discussion it is evident that significant potential exists to reduce the total cost of FREI bearings to a level that justifies their use in seismic mitigation of many structures including ordinary low-rise buildings.

5.2.3. Unbonded versus Bonded Application

To simplify the installation of FREI bearings, they can be simply placed between the foundation and structure with no bonding at the contact surfaces of the bearings. This simplified installation method, designated as "unbonded application", leads to construction savings compared to both conventional bolted (bonded) or dowelled shear connections which are commonly used for SREIs. Additionally, the unbonded application results in improved lateral load-displacement characteristics (Toopchinezhad et al. 2008a). As the base is displaced laterally, the top and bottom faces of a FREI bearing roll off the upper and lower contact supports, respectively. This unique lateral deformation is denoted as "rollover deformation". It occurs as a result of both the unbonded application and lack of flexural rigidity of the fiber-reinforcement sheets. Previous research studies (Toopchinezhad et al. 2008a, b, c) have shown that a properly designed FREI bearing can sustain large lateral displacements while remaining stable, by maintaining a positive incremental lateral load resisting-capacity throughout the hysteresis loops. As such, the resulting permissible deformation was called "stable rollover" (SR) deformation (Toopchinezhad et al. 2008a). An unbonded FREI bearing that exhibits SR-deformation is denoted hereafter as a "stable unbonded" (SU) FREI. In a SU-FREI bearing, the "full contact vertical face lateral displacement" (δ_{fc}) occurs when the originally vertical faces of the

bearing completely contact the horizontal upper and lower supports. The lateral displacement at rollout instability (Naiem and Kelly 1999), for this particular type of bearing is significantly larger than δ_{fc} (Toopchinezhad et al. 2008b).

Unlike the case of a bonded application, no tension normal to the reinforcing layer is introduced in a laterally deformed SU-FREI bearing. Therefore, the internal bond between the reinforcement and elastomer layers of an unbonded FREI bearing are subjected to significantly lower stress-demands compared to the same bearing installed in a traditional bonded application. This reduced stress-demand introduces another cost saving opportunity as the bonding requirements between elastomer and reinforcement layers are less than for traditional SREIs. Additionally, a SU-FREI bearing exhibits larger lateral displacement capacity than for a similar bearing with bonded contact surfaces (Toopchinezhad et al. 2008a). The additional rotational degrees of freedom introduced at the contact surfaces of a SU-FREI bearing, lead to a significant reduction in the lateral stiffness of the bearing resulting in superior seismic isolation efficiency. Also, interaction between the elastomer and fiber fabric reinforcement in a SU-FREI introduces another energy dissipating mechanism in addition to the inherent damping of the elastomer (Kelly 1999 and Toopchinezhad et al. 2008b). In SU-FREIs constructed with an unfilled (low-damped) soft neoprene, sufficient damping (8% to 14%) was obtained. As a result, their lateral load-displacement characteristics were found to be comparable to those of conventional high-damped SREIs (Toopchinezhad et al. 2008b, c).

5.2.4. Scope of this Study

Significant potential exists for base isolation utilizing SU-FREI bearings to be sufficiently cost-effective for application in low-rise buildings of ordinary importance. The feasibility of SU-FREIs has already been investigated through compression and cyclic shear tests on prototype bearing specimens (Toopchinezhad et al. 2008a, b, c). However, due to the novelty of this base isolation system, and lack of data in the literature, shake table tests were conducted in order to examine the in-place performance of SU-FREIs relative to dynamic loading of a representative building. To illustrate the effectiveness of the proposed base isolation system, a shake table study was conducted on a ¼ scale test-structure that was mounted on four square carbon-FREI bearings. Detailed quantitative dynamic response

measurements of the tested base isolated structure (BI-structure), when subjected to three different input earthquakes, were compared to the response of a corresponding fixed base structure (FB-structure).

5.3. Model Scale Base Isolated (BI) Structure

5.3.1. Test-Structure

The ¼ scale test-structure was a two-story, one-bay, moment resisting steel frame with physical dimensions of 1500 × 1400 mm in plan and total height of 1628 mm. A geometric scale factor of S_L = 4 was selected in order to remain within the dimension and payload capacity limits of the shake table. Figure 5.1 is a photograph of the two-story test-structure wherein the columns were square hollow sections (HSS 64×64×6.4 mm) and the beams, made of rectangular hollow sections (HSS 76×51×6.4 mm), were welded to the columns to create rigid joints. The clear height for each story was 700 mm. Each precast concrete two-way floor slab, used to provide rigid diaphragms, had four firmly attached thick steel plates to provide the additional mass required to satisfy dynamic similitude (Harris and Sabnis 1999). The total weight of the test-structure was 31.1 kN. Unidirectional motion of the shake table was parallel to the larger span of the test frame.

5.3.2. Base Isolation System and Bearing Isolators

As shown in Fig. 5.1, the base isolation system consisted of 4 SU-FREI bearings. A single bearing was located under each column-line below a flat steel plate, which was welded to the base of the column. It is important to note that the FREI bearings were simply placed between the shake table and test-structure with no bonding at their upper and lower contact surfaces.

Figure 5.2 is a photograph of the similar FREI bearings used in the tests. Consistent with the test-structure, the FREI bearings represented a ¼ scale model of the full scale prototype bearings with the same material properties. The bearings had 70 × 70 mm dimensions in plan and a total thickness of approximately 25 mm. Each bearing consisted of 12 layers of soft unfilled neoprene rubber (total rubber thickness of t_r = 19 mm) that were interlaminated with 11 bonded layers of bi-directional (0/90 orientation) carbon fiber

sheet. Considering the total weight of the test-structure (31.1 kN), each bearing was subjected to 1.59 MPa vertical pressure.

A set of four prototype SU-FREI bearings with the same properties as the bearings shown in Fig. 5.2 were previously tested individually under both vertical compression and cyclic shear (Toopchinezhad et al. 2008b, c). Figure 5.3 contains typical lateral load displacement hysteresis loops of the tested SU-FREI bearings. The imposed sinusoidal lateral displacements in the relevant cyclic tests had an ascending amplitude pattern ranging from 25% t_r to 200% t_r during which the bearings were subjected to constant 1.6 MPa vertical pressure. According to Fig. 5.3, the effective (secant) lateral stiffness decreased with increasing lateral displacement amplitude. Based on the cyclic test results (Toopchinezhad et al. 2008b), depending on the displacement amplitude, the anticipated base isolated frequency range of the tested bearings, was between 1.25 to 2.50 Hz (0.4 to 0.8 s), regardless the orientation of lateral displacements. Results of vertical compression testing showed that under a vertical pressure of 1.6 MPa, the vertical frequency ranged between 47 to 55 Hz (Toopchinezhad et al. 2008c). These values are deemed acceptable as they are significantly larger than the base isolation frequencies of the bearings for lateral motion.

5.4. Test Program

Table 5.1 contains a summary of the shake table tests conducted on the BI-test-structure (hereafter called BI-structure). Scaled versions of three different earthquake ground histories (El Centro, Saguenay and Tabas) were used as the three different input time histories to the BI-structure (See Table 5.2). Each of the input earthquakes was applied at three different levels of increasing intensity. The largest intensity level, Test Run 3, was selected so as to represent the maximum (M) expected level of the earthquake for Vancouver, Canada (with a return period of approximately 2500 years). Test Runs 1 and 2 were respectively attributed to the corresponding service (S) and design (D) levels of the input earthquake.

As the bearings were square, similar lateral responses in the two perpendicular directions of movement (0° and 90°) were expected. The bearing orientation during El Centro

earthquake test runs was denoted as 0° orientation. For both the Saguenay and Tabas input motions, the bearings were rotated 90°.

In addition to Tests 1 to 9 (see Table 5.1), 6 additional tests (Tests 10 to 15 in Table 5.1) were carried out on the BI-structure. Tests 10 to 12 were conducted to assess the lateral response repeatability of the base isolation system as well as its reliability to resist a subsequent intensive earthquake as large as the previous major earthquake. An additional objective for running Test 11 was to examine the response degradation of the base isolators, compared to Test 3, due to possible bearing damage or scragging. Finally, Tests 13 to 15 were aimed at assessing the feasibility of the proposed base isolation system for a ground motion parallel to the bearings' diagonal (45° orientation).

5.5. Instrumentation

A displacement transducer and an accelerometer were attached on the shake table as well as at each floor level of the test-structure in order to record the relevant absolute lateral displacement and acceleration. To monitor any significant motion in the test-structure in the horizontal and vertical directions perpendicular to the table movements, two bi-directional accelerometers were attached to the front and rear of the base floor. To verify that the test-structure remained elastic during testing, a total of 4 strain gages, one on each of the opposite faces of two diagonally opposite columns, were attached close to the connection between the column and the base floor beam. All measurements were recorded simultaneously at 200 Hz and filtered at 50 Hz.

5.6. Input Earthquakes

Ground motion specifications for both the original and scaled earthquakes (El Centro (Imperial Valley, 1940), Saguenay (Quebec, Canada, 1988), and Tabas (Tabas, Iran, 1978)) are summarized in Table 5.2. Given the geometry scale-factor of the test-structure (i.e., ¼), the ground motion records of the original earthquakes were compressed in time by a factor of 2 to satisfy dynamic similitude requirements. Furthermore, the accelerations of the original earthquakes were scaled so that their peak values met or exceeded the maximum expected PGA for Vancouver, BC as a typical region with high seismic risk in Canada (NBCC 2005). The scaled versions of the original El Centro, Saguenay, and Tabas earthquakes are

hereafter denoted by El Centro-s, Saguenay-s, and Tabas-s, respectively. Alternatively, since the scaled earthquakes are the input earthquakes to the BI-structure, they are called as the "input earthquakes".

Figure 5.4a contains the time histories of the M-level of input earthquakes and Fig. 5.4b shows the corresponding 5%-damped acceleration response spectrum. Also shown in Fig. 5.4b is the model scale site specific acceleration spectrum for Vancouver, BC, with soil properties consistent with the relevant seismograph station of the original earthquake (see Table 5.2). For Tabas-s earthquake, due to lack of information about the soil type, the reference soil specification (Soil C) of NBCC (2005) was selected. It is worth noting that the plotted site specific spectra are attributed to an earthquake with 2% probability of exceedence in 50 years (NBCC 2005). ASCE (2005) has specified this as the maximum considered earthquake (MCE) level in the design of a BI-structure.

The FB-period of the test-structure (i.e., 0.14 s as discussed in the following section) and the expected period range for the BI-structure (0.4 to 0.8 s as discussed in Section 2.2) are shown in Fig. 5.4b. A close examination of the plots in Fig. 5.4b indicates that over a wide range of periods, including FB and BI-periods, the scaled earthquakes reasonably simulate the expected level of seismic hazard. In the constant velocity region of the site specific spectra, amplification of the input earthquakes were either larger or close to the expected values for Vancouver, BC. According to Fig. 5.4b, the Tabas-s and Saguenay-s earthquakes showed larger amplifications at lower periods than El Centro-s. This revealed the significant damage potential of these two earthquakes for low-rise buildings with dominant fixed base periods in the range of 0.05 to 0.10 s (0.10 to 0.20 s for the corresponding full scale building). Table 5.2 contains the calculated Housner intensity (Clough and Penzein 2003) of the input earthquakes as a measure of their damage potential over a wider period range. As indicated in Table 5.2, El Centro-s had the largest and Saguenay-s had the lowest Housner intensity. Saguenay-s represented an earthquake with very limited peak ground displacement, having significant energy at higher frequencies. Peak ground accelerations for all of the input earthquakes were approximately the same and Tabas-s had the largest peak ground displacement.

5.7. Free Vibration Tests

For each of the different bearing orientations considered (0°, 90°, and 45°) a series of free vibration tests were conducted on the BI-structure prior to shake table testing. The objective was to evaluate the initial fundamental frequencies and equivalent viscous damping ratios of the bearings at minor lateral displacement levels. Fundamental frequencies were obtained by performing a Fourier transform on the roof acceleration time histories measured during free vibration tests. In addition, the equivalent viscous damping ratio was estimated using the logarithmic decrement method (Clough and Penzein 2003).

At 0° and 90° orientation of the bearings, the average value of the initial natural frequency of the BI-structure was found to be 4.00 Hz (0.25 s). Additionally, the equivalent viscous damping ratio was found to be 7%. At 45° orientation, the average values of natural frequency and damping ratio for the bearings were found to be 3.57 Hz (0.28 s) and 8%, respectively.

After completion of all shake table tests on the BI-structure listed in Table 5.1, the bearings were removed and the structure was directly mounted on the shake table. Additionally, to simulate the fixed base configuration, the translational and rotational degrees of freedom at the base of all columns of the model structure were physically restrained. Free vibration tests on the FB-structure were aimed at evaluating the fundamental frequency of the structure to validate the mass and stiffness matrices to be used in prediction of its analytical seismic response. Consistent to the superstructure of the BI-structure, the performance objective for the corresponding FB-structure was to remain within its linear elastic range. The FB-structure, assuming a minimum damping ratio of 2%, was designed to remain elastic under the maximum level of input earthquakes that were utilized in the tests. Although it was reasonable to assume a 2% damping ratio for a fixed base bare frame, a conservative value of 5% was utilized in the time history analysis, as this value is commonly used for the seismic design of ordinary buildings.

From the Fourier amplitude spectra of measured roof accelerations, during free vibration tests, the fundamental modal frequency of the FB-structure was found to be f_{FB} = 7.4 Hz (T_{FB} ≈ 0.14 s). The analytically-evaluated fundamental frequency of the FB-structure was

calculated to be 7.6 Hz (≈ 0.13 s) which was in good agreement with the experimentally-evaluated value. The damping ratio for the fundamental mode was calculated to be 0.6%. This damping ratio corresponded to horizontal displacements expected in the test-structure when seismically isolated. However, the response of the FB-structure is expected to undergo significantly larger horizontal displacements.

5.8. Results of Shake Table Tests

5.8.1. Data Processing

The dynamic response parameters of the BI-structure were evaluated using displacements and accelerations recorded at each floor level. The displacements of each floor relative to the base were calculated by subtracting the absolute lateral displacement recorded at each floor level from the corresponding lateral displacement of the table. Accelerometer readings at each floor level were multiplied by the floor mass to calculate the corresponding inertia force. Base shear, V_b, was obtained by summing the inertia forces at middle floor and at the roof of the structure. Base moment, M_b, was calculated by summing the product of story inertia forces multiplied by their corresponding height above the base isolation system. Summation of the base shear and inertia force at the base floor resulted in the total shear acting on the base isolation system.

5.8.2. Peak Response Values

Table 5.3 contains measured peak response values of the BI-structure at different levels of input earthquakes. It also includes estimated peak response values for a corresponding 5%-damped linear elastic FB-structure; for a consistent response comparison, the FB-structure was considered to be subjected to the same input motion as the BI-structure.

Results presented in Table 5.3 indicate that, regardless the earthquake level, the proposed base isolation system was capable of effectively attenuating the peak response values of the BI-structure relative to the corresponding 5%-damped FB-structure. For example, for the M-level of El Centro-s, the peak floor acceleration (a_2), base shear (V_b), and total drift (Δ)

decreased by 73%, 68%, and 61%, respectively. The response reduction values for the M-level of Saguenay-s were 71%, 69%, 67%, respectively, and for the M-level of Tabas-s the corresponding reduction in the peak response values were 80%, 76%, and 75%, respectively. The base isolation system significantly increased the minimum factor of safety against structure overturning (see Table 5.3).

Figures 5.5a and 5.5b show typical photographs of the FREI bearings taken at the peak lateral displacement in the base isolation system during the M-level of El Centro-s and Tabas-s earthquakes. For the Saguenay-s earthquake, the bearings' peak lateral displacement, even at the M-level of earthquake, was too small to be clearly illustrated in a photo (see X_0 in Table 5.3). The largest lateral displacement experienced by the bearings was 161% t_r (i.e., 30.5 mm) which occurred during the M-level of El Centro-s earthquake (Table 5.3). A previous study revealed that these bearings were able to safely experience lateral displacements up to 250% t_r (Toopchinezhad et al. 2008c). Therefore, the bearings were capable of resisting earthquakes with significantly greater intensity.

As shown in Fig. 5.5a at the peak lateral displacement, significant rollover occurred in the bearing. It can be observed that the original vertical faces of the bearing were close to coming into contact with the horizontal supports, namely, the shake table (lower support) and the column's base plate (upper support). Experimental observations showed that during all of the test runs, the bearings remained stable and the test-structure returned to its original position when the test was completed. Additionally, examination of the lateral load-displacement hysteresis loops corresponding to both the design and maximum levels of the input earthquakes indicated that the bearings showed "stable rollover" (SR) deformation as they maintained a positive incremental lateral load-resisting capacity throughout the hysteresis loops (see Figs. 5.6a and 5.6b).

A photo of one bearing prior to Test 15 (see Table 5.1) is shown in Fig. 5.7a. The SR-deformation of the same bearing at the instant of maximum lateral displacement in the base isolation system can be seen in Fig. 5.7b. Since the bearings in Tests 13 to 15 were laterally loaded along their 45° orientation, the corresponding response was denoted as diagonal response. The resulting lateral load-displacement hysteresis loops of the bearings,

presented in Fig. 5.7c, indicated that the diagonal response of the BI-system was equally as effective as at the 0° or 90° orientations. This can be verified by comparing the peak values of the recorded diagonal response (Tests 13 to 15) with corresponding 0° responses (Tests 1 to 3) at the 3 different levels of El Centro-s, where comparable response mitigation was observed.

Variation in the peak response parameters of the BI and FB structures with the service, design, and maximum peak ground acceleration (PGA) of all three input earthquakes are shown in Figures 5.8 to 5.10. These figures include results of all tests conducted on the BI-structure (see Table 5.1). Tests 11 and 12 were duplicated versions of Test 3 where the BI-structure was subjected to the M-level of El Centro-s earthquake. In general, inspection of Fig. 5.8 indicates that, due to the scragging, the peak BI-response values in Tests 11 and 12 were slightly lower than in Test 3 where the bearings were unscragged. The BI-responses shown for Tests 13 to 15 indicated that the bearings were equally effective in the diagonal (45°) orientation.

As seen in Figures 5.9 and 5.10 in the case of the Saguenay-s and Tabas-s earthquakes, the lateral responses of the 2% and 5% damped FB-structure linearly increased with increasing PGA. However, this linear relationship was not observed for the El Centro-s earthquake (see Fig. 5.8). There was a minor inconsistency between the service, design, and maximum El Centro-s earthquake time histories due to shake table performance limitations. However, these three earthquake levels were considered to be representative of service, design, and maximum earthquakes.

The results presented in Figs. 5.8 to 5.10 show that the proposed base isolation system effectively decreased the peak response values of the test-structure. Additionally, test results indicated that the seismic mitigation efficiency of the base isolators increased with increasing PGA of the earthquake. Therefore, the difference between peak response values of the BI and FB structures increased as the earthquake intensity (PGA) increased (see Fig. 5.8 to 5.10). The increased efficiency at higher PGA occurred as a result of SR-deformation in the SU-FREI bearings.

Figure 5.11 contains the amplification envelopes for both the BI and corresponding 5%-damped linear FB-structure. In this figure, the ratio of peak acceleration at each floor level to the peak ground acceleration (PGA) for all of the input service, design, and maximum earthquakes have been plotted. It should be noted that the peak floor accelerations generally did not occur at the same instant. As indicated in Fig. 5.11, while the FB-structure amplified the input base acceleration and this amplification dramatically increased with floor height, the peak floor accelerations in the BI-structure were generally less than the peak table accelerations for all of the design and maximum input earthquakes. Additionally, the relative response reduction increased with increasing earthquake intensity.

For all three M-level input earthquakes and the D-level El Centro-s earthquake, the resulting overturning moments in the FB-structure were significantly larger than the overturning-resisting moment. This resulted in overturning factors of safety of less than unity (see column 13 in Table 5.3). In contrast, for the BI-structure a minimum overturning factor of safety of 2.30 was achieved as a result of the significant reduction in the earthquake-induced overturning moment.

Strain gages readings confirmed that the test-structure remained within its linear elastic range with a significant margin of safety. A maximum recorded strain of 0.02%, which occurred during the M-level El Centro-s test run, was significantly lower than the 0.175% calculated yield strain of the steel material.

5.8.3. Response Pattern along Height of the Test-Structures

Figure 5.12 contains response profiles of BI and 5%-damped FB structures at the instant of peak total drift (Δ) during the M-level of input earthquakes. For the BI-structure, these profiles were plotted with respect to the base floor of the test-structure. In all cases, the effectiveness of the proposed base isolation system can be clearly seen. Significant differences are observed in deflected shapes, inertia forces, story shears, and story moments for the BI and its corresponding 5%-damped linear FB test-structures.

In addition to examining the instant of peak response, the variation of lateral response was also studied by presenting results of three sequential time instants leading up to the peak

response. Profiles of four sequential lateral accelerations related to one half-cycle of roof accelerations leading to the peak response are shown in Fig. 5.13. These acceleration profiles corresponded to the M-level of input earthquakes. Each profile was numbered based on its sequence of occurrence. Time Instant 1 corresponded to zero value of the roof acceleration. Instants 2 and 3 were attributed to the local extermum points in the roof acceleration time history of the BI-structure within the selected half-cycle and before the total peak acceleration (i.e., Instant 4) was reached. Time Instances 1 and 4 for the FB-structure had the same definition as for the BI-structure. Time Instances 2 and 3 in the FB-structure were selected so that their relative distances from Time Instances 1 and 4 were proportional to those of the BI-structure.

In addition to the roof level of the BI-structure, the local extermum points were also observed in acceleration records of the base floor. These local extermums were produced due to contribution of 2nd vibration mode of the BI-structure which had a relatively flexible superstructure. As discussed earlier in this paper, the FB-period of the test-structure was found to be approximately 0.14 s. This was equivalent to 0.28 s for the corresponding full-scale structure, which implied a fairly flexible 2-story building. It should be noted that the 2nd mode shape along the height of BI-structure was characterized with two nodes one at the table level (below the base isolation system) and the other near the middle floor together with an inflection point between these two nodes. The proximity of the second node to the middle floor suggested that no significant response amplification was expected to occur at this floor as a result of 2nd mode effects. This was verified by examining the acceleration record of middle floor where no local extermum points were found before the total peak acceleration at each half-cycle was reached.

Close examination of the acceleration profiles presented in Fig. 5.13 show that at each floor level of the 5%-damped FB-structure, variations in the sequential lateral accelerations were significantly larger than those of the BI-structure. Furthermore, unlike the BI-structure, variations of lateral accelerations along the height of the FB-structure were significant. It should be noted that the time interval between Instants 1 to 4 in the BI-structure were significantly longer than those of the FB-structure due to the increased period of vibration of the BI-structure.

5.8.4. Response History

Time histories of base shear and total drift, as two important design parameters, during the M-level of input earthquakes are shown in Figs. 5.14a to 5.14c. In these figures experimental results for the BI-structure were plotted over the time history analysis results of the corresponding linear FB-structure with 5% equivalent viscous damping. Compared to the FB-response, a longer period of vibration and significant response mitigation of the BI-structure can be clearly seen.

5.8.5. Observed Dynamic Characteristics

The ratio of the BI-period to the FB-period of a given structure indicates the efficiency of the seismic isolation system (Naiem and Kelly 1999). In the constant velocity region of the design spectrum, the spectral acceleration decreases with increased period of the base isolation system (For example, see the design spectrum for Vancouver, BC, in Fig. 5.4b.). Owing to the linear elastic behavior of the given FB-structure, its fundamental period remained unchanged. Therefore, higher values of resulting base isolated period resemble higher seismic mitigation efficiency of the base isolation system.

Fundamental periods of the BI-system were determined by performing fast Fourier transform (FFT) on the roof horizontal accelerations during each shake table test run. Additionally, Fourier transform of the transverse horizontal and the vertical accelerations were also studied. These two acceleration components were recorded simultaneously at the front and back of the base floor of the BI-structure.

Figures 5.15a to 5.15c show the Fourier amplitude of horizontal roof accelerations (parallel to the shake table motions), which is plotted on the FFT of the vertical accelerations at the front of the base floor during the M-level loading of each earthquake. As shown in these figures, within the frequency range of 0 to 15 Hz, two peak Fourier amplitudes corresponding to the 1st and 2nd vibration modes of the BI-structure were visible. However, the influence of vertical accelerations at this frequency range was negligible. Since the lateral load-displacement response of the bearings was highly nonlinear, the secant lateral stiffness, and in turn, the resulting vibration frequency of the bearings varied with

amplitude of lateral displacements. Accordingly, different modal frequencies at different test runs were observed. Furthermore, even during individual test runs, modal frequencies were not necessarily characterized with a single sharp peak in the Fourier amplitude of the response. Figures 5.15a to 5.15c show that, for each mode, the vibration frequencies fluctuated around the frequency at which the peak Fourier amplitude occurred. For instance in Fig. 5.15c, during the M-level of Tabas-s earthquake, two comparable peak values were obtained in the vicinity of the first vibration mode of the structure.

Fundamental base isolated frequencies corresponding to each test run were listed in column 7 of Table 5.3. It is worth noting that, as the intensity of input earthquake increased from "S" to "M" level, the resulting BI-frequency decreased which resulted in increased seismic isolation efficiency. The highest base isolation efficiency, with respect to the corresponding fixed base response, was obtained for the Tabas-s earthquake (see Table 5.3). Additionally, duplicating the maximum Tabas-s test (Test 10 in Table 5.3) resulted in comparable base isolated frequency and response attenuation. The same correlation was observed between Tests 3, 11, and 12, for the maximum El Centro-s earthquake. This is an indication of the robustness of the base isolation system.

From Figs. 5.15a to 5.15c, it was found that the frequency of the 2nd base isolated mode was approximately 12 Hz. During the El Centro-s and Tabas-s earthquakes, the 2nd mode had little contribution in the total response (See Figs. 5.15a and 5.15c). However, for the Saguenay-s earthquake, the 2nd mode had significant participation in the total response (see Fig. 5.15b). The Saguenay-s earthquake was characterized by a high energy content at high frequencies of excitation (see Fig. 5.4b). This intensified the 2nd mode effects in the response of the structure.

FFT of recorded horizontal accelerations perpendicular to the shake table motions contained negligible Fourier amplitudes compared to the longitudinal motions of the structure. Accordingly, the horizontal transverse component of motions at both front and rear of the structure were insignificant. This confirmed that, as was expected, torsional vibration modes did not influence the longitudinal response.

FFT of the vertical accelerations showed that at the M-level of the input earthquakes, the peak amplitude of FFT occurred within a frequency range of 43 to 46 Hz. At this frequency range, the Fourier amplitudes of the roof longitudinal horizontal accelerations were negligible (see Figs. 5.15a to 5.15c). Therefore, these frequencies were attributed to the rocking mode of the BI-structure. It was found that the frequency of the rocking mode was significantly larger than that of the fundamental base isolated mode. As such, the contribution of the rocking mode to the total response was deemed to be negligible. This was verified by noting the minor Fourier amplitudes of vertical accelerations over a frequency range of 43 to 46 Hz compared to the corresponding Fourier amplitudes of roof horizontal acceleration at 1st and 2nd base isolated modes of the BI-structure (see Figs. 5.15a to 15c). Vertical compression tests at zero lateral displacement on the prototype bearings showed that the bearing's vertical frequency under 1.6 MPa vertical pressure, ranged between 47 to 55 Hz (Toopchinezhad et al. 2008c). The observed frequencies for the rocking mode of the BI-structure were slightly lower than these anticipated values. This reduction was likely due to a decrease in vertical stiffness of the bearings with increased lateral displacement amplitude. Despite this reduction, the contribution of the rocking mode in all test runs was negligible as its frequency was still significantly higher than the base isolated frequency of the test-structure.

5.8.6. Damage Status in the Bearings

After completing the tests for each of the El Centro-s, Saguenay-s, and Tabas-s earthquakes, the bearings were visually inspected for external damage. No damage was observed in the bearings after each test or after the completion of all testing. This demonstrated the reliability of the bearing and their ability to withstand and survive multiple severe earthquakes. Robust BI-response for Tests 9 and 10 during the maximum Tabas-s earthquake, and Tests 3, 11, and 12 during the maximum El Centro-s earthquake suggested that any internal damage was negligible. It appears that rollover deformation (see deformed bearings in Figs. 5.5a, 5.5b, and 5.7b) beneficially put lower demand on the internal bonding between the reinforcement and elastomer layers. As a result, no observable delamination occurred in the bearings.

5.9. Concluding Remarks

A ¼ scale 2-story moment resisting steel frame was seismically isolated with an innovative base isolation system consisting of 4 square SU-FREI bearings. Unlike conventional bearings, the SU-FREI bearings were not bonded to any thick steel end plates. They were simply placed between the shake table and test-structure with no bonding at the bearings' top or bottom contact surfaces. Shake table tests, using 3 different input earthquakes, were carried out on the base isolated (BI) structure. Each earthquake was applied at 3 different levels with increasing intensity from run to run. Test results for the BI-structure were compared to analytical results for a corresponding 5%-damped linear fixed base (FB) structure in order to demonstrate the seismic mitigation efficiency of the proposed base isolation system.

From the test results (Table 5.3 and Figs. 5.12a to 5.12c), it was found that at maximum (M) level of the input earthquakes, measured roof accelerations in the BI-structure were as low as 24% to 32% of roof accelerations of the FB-structure. Base shear and base moment were found to be 30% to 35% and 23% to 33%, respectively, of those for the FB-structure. Total drift of the BI-structure was 28% to 42% of the corresponding value in the FB-structure. These values clearly indicate that the proposed BI system was able to significantly mitigate the seismic response of the structure. Test results also revealed that bearings oriented at 45° were as efficient as bearings oriented at 0° or 90° to the input motions.

For all tests, the bearings exhibited stable rollover behavior and effectively mitigated the seismic response. It was found that the SU-FREI bearings were also able to re-center the BI-structure when test was completed. No damage was visible in the bearings after completion of the entire test program. Additionally, consistent response of the BI-structure during duplicated test runs (Tests 9 and 10 also 11 and 12 in Table 5.3) indicated that any internal damage in the bearings was negligible. The expected performance from a base isolation system is to resist a severe earthquake without experiencing any type of failure mode (ASCE 2005). It is not common for a structure to be subjected to several severe earthquakes corresponding to the M-level of seismic hazard in the given region. Nevertheless, effective and consistent response of the proposed base isolation system to repeated test runs revealed the reliability of the bearings and suggested that in actual application there may be

no need to exchange the bearings for subsequent aftershocks or future additional major seismic events.

This study clearly demonstrated that the use of SU-FREI bearings in seismic mitigation of low-rise buildings can be highly effective. Lower weight, lower cost as a result of employing a mass production manufacturing technique, and superior damping properties are significant advantages of FREIs over traditional SREIs. The merit of the unbonded application is that it allows stable rollover deformation to occur in SU-FREI bearings. This phenomenon results in reduced secant lateral stiffness of the bearings and enhances their seismic mitigation efficiency. Since no vertical tension is introduced in SU-FREIs, tensile stresses between the elastomer and reinforcement layers are lower compared with the same bearing in a bonded application. Additionally, SU-FREIs exhibit relatively larger lateral displacement capacity. Considering the above mentioned advantages, there is a significant opportunity for economical use of SU-FREIs for isolation application of low-rise buildings of ordinary importance in high intensity seismic regions.

5.10. References

ASCE. (2005). "Minimum Design Loads for Buildings and other Structures." *ASCE/SEI 7-05*, American Society of Civil Engineers, New York.

Clough R. W. and Penzien J. (2003). *Dynamics of Structures*, 3rd Edition, *Computers and Structures Inc.*, Berkeley, CA.

Dehghani Ashkezari G., Aghakouchak A. A., Mehrdad K. (2008). "Design, Manufacturing and Evaluation of the Performance of Steel like Fiber-Reinforced Elastomeric Seismic Isolators." *Journal of Materials Processing Technology*, Vol. 197, No. 1-3, Pages 140-150.

Kelly J. M. (1999). "Analysis of Fiber-Reinforced Elastomeric Isolators." *Journal of Seismology and Earthquake Engineering (JSEE)*, Vol. 2, No. 1, Pages 19-34.

Kelly J. M. (2002). "Seismic Isolation Systems for Developing Countries." *Earthquake Spectra*, Vol. 18, No. 3, Pages 385-406.

May P. J. (2002). "Barriers to Adoption and Implementation of PBEE Innovations", PEER Report 2002/20, Pacific Earthquake Engineering Research Center, College of Engineering, University of California, Berkeley.

Moon B. Y., Kang G. J., Kang B. S., Kelly J. M. (2002). "Design and Manufacturing of Fiber-Reinforced Elastomeric Isolator for Seismic Isolation." *Journal of Materials Processing Technology*, Vol. 130–131, Pages 145–150.

Naeim F., and Kelly J. M. (1999). "Design of Seismic Isolated Structures." *John Wiley*, New York.

NBCC. (2005). "National Building Code of Canada" *Institute for Research in Construction, National Research Council of Canada*, Ottawa, Ontario.

Harris H. G. and Sabnis G. M. (1999). *Structural Modeling and Experimental Techniques, CRC Press*, New York.

Taylor A. W., Lin A. N., and Martin J. W. (1992). "Performance of Elastomers in Isolation Bearings: A Literature Review." *Earthquake Spectra*, Vol. 8, NO. 2, Pages 279-303.

Toopchinezhad H., Tait M. J., and Drysdale R. G. (2008a). "Testing and Modeling of Square Carbon Fiber-Reinforced Elastomeric Seismic Isolators." *Structural Control and Health Monitoring*, Vol. 15, No. 6, Pages 876–900, DOI: 10.1002/stc.225 (*Chapter 2 of this thesis*).

Toopchinezhad H., Tait M. J., and Drysdale R. G. (2008b). "Lateral Response Evaluation of Fiber-Reinforced Neoprene Seismic Isolators Utilized in an Unbonded Application." *Journal of Structural Engineering, ASCE*, Vol. 134, No. 10, Pages 1627-1638 (*Chapter 3 of this thesis*).

Toopchinezhad H., Drysdale R. G., and Tait M. J. (2008c). "Parametric Study on the Response of Stable Unbonded Fiber-Reinforced Elastomeric Isolators (SU-FREIs)." *Submitted on November 2008 (Chapter 4 of this thesis).*

Table 5.1. Tests carried out on the base isolated test structure

Bearing Orientation	0°			90°			90°				0°		45°		
Simulated Earthquake	El Centro			Saguenay			Tabas				El Centro		El Centro		
Test Run	1	2	3	1	2	3	1	2	3	4	1	2	1	2	3
Representative Earthquake Level	S	D	M	S	D	M	S	D	M	M	M	M	S	D	M
Test	1	2	3	4	5	6	7	8	9	10	11	12	13	14	15

Note: Representative earthquake levels are service (S), design (D), and maximum (M)

Table 5.2. Ground motion specifications

Ground Motion	Direction	Station	Epic. Dist. (km)	Station Site Class*	Original Earthquake (Full Scale)			Scaled Earthquake (Max. Level) (1/4 Scale)			
					PGA (g)	PGV (mm/s)	PGD (mm)	PGA (g)	PGV (mm/s)	PGD (mm)	Housner Intensity** (mm)
El Centro	LN (S00E)	117 (USGS)	8	Stiff Soil (D)	0.348	337.5	108.0	0.53	25.8	38.4	462
Saguenay	TR (N90)	DCKY	195	Hard Rock (A)	0.124	46.5	4.1	0.58	27.6	4.3	117
Tabas	LN (N74E)	Tabas	28	N/A	0.836	977.6	386.6	0.52	25.3	47.9	391

* Site classification based on ASCE (2005) and NBCC (2005) standards

** Housner Intensity for a 1/4 scale model defined as area under 5%-damped pseudo-velocity spectrum over the period range of 0.05 to 1.25 s (modified limits for 0.1 to 2.5 s used for full scale models)

Table 5.3. Measured response maxima and fundamental frequency of the base isolated (BI) structure and estimated response maxima of the corresponding 5%-damped fixed base (FB) structure

Test	Earthquake	Level	PGD (mm)	PGA (g)	x_0 (%t_r)	a_0 (g)	f_{BI} (Hz)	a_2 (g)		V_b/W		Min. FS_{ove}		Δ (%)	
					BI			FB	BI	FB	BI	FB	BI	FB	BI
1	El Centro-s	S	12.8	0.21	47.5	0.22	2.35	0.62	0.24	0.45	0.14	1.21	4.15	0.159	0.083
2		D	25.6	0.33	107.0	0.30	1.90	1.15	0.31	0.82	0.19	0.66	3.05	0.294	0.122
3		M	38.4	0.53	160.7	0.40	1.70	1.64	0.44	1.19	0.25	0.46	2.30	0.422	0.164
4	Saguenay-s	S	1.4	0.23	14.2	0.14	2.96	0.42	0.14	0.28	0.06	1.93	8.54	0.101	0.043
5		D	2.9	0.42	29.0	0.23	2.51	0.75	0.25	0.52	0.12	1.02	4.59	0.190	0.071
6		M	4.3	0.58	41.0	0.26	2.38	1.05	0.30	0.72	0.15	0.74	3.75	0.264	0.086
7	Tabas-s	S	15.9	0.18	36.1	0.15	2.64	0.57	0.18	0.41	0.10	1.35	5.55	0.144	0.061
8		D	31.8	0.36	66.0	0.22	2.16	1.14	0.25	0.82	0.15	0.92	3.88	0.285	0.084
9		M1	47.5	0.52	114.1	0.30	1.87	1.65	0.32	1.17	0.19	0.46	3.07	0.418	0.103
10		M2	47.9	0.50	119.6	0.32	1.89	1.71	0.34	1.20	0.20	0.45	2.91	0.432	0.107
11	El Centro-s	M1	38.3	0.52	166.7	0.38	1.71	1.71	0.41	1.24	0.23	0.44	2.42	0.441	0.157
12		M2	38.2	0.50	164.6	0.34	1.72	1.65	0.38	1.20	0.22	0.45	2.55	0.426	0.141
13*		S	12.8	0.20	48.5	0.19	2.35	0.61	0.22	0.44	0.12	1.23	4.56	0.157	0.072
14*		D	25.4	0.32	107.2	0.26	1.89	1.13	0.33	0.82	0.18	0.66	3.05	0.291	0.117
15*		M	38.0	0.48	163.7	0.40	1.71	1.62	0.42	1.17	0.24	0.46	2.35	0.418	0.166

Notes:

1- S, D, and M indicate service, design and maximum earthquake levels, respectively; PGD = peak ground (table) displacement; PGA = peak ground (table) acceleration; X_0 = base floor lateral displacement expressed as a percentage of total rubber thickness of the bearings (t_r = 19 mm); a_0 = base floor acceleration; f_{BI} = fundamental base isolated frequency (fixed base frequency f_{FB} = 7.14 Hz); a_2 = roof acceleration; V_b = base shear; W = total weight of structure above foundation (BI = 31.1 kN, FB = 20.7 kN); FS_{ove}= factor of safety against overturning; Δ = total drift which is calculated by dividing the roof lateral displacement, relative to the base floor, to total height of structure (H = 1628 mm).

2- The unidirectional shake table utilized in this study was operated in displacement control. Accordingly, the peak table displacement (PTD) in Test Runs 1 and 2 were set to be 1/3 and 2/3, respectively of the PTD at maximum earthquake level (Test Run 3).

* In these tests, the FREI bearings were turned by 45° hence they were laterally loaded along one of their diagonals. As with other test sequences, shake table motions were parallel to longitudinal direction of the superstructure.

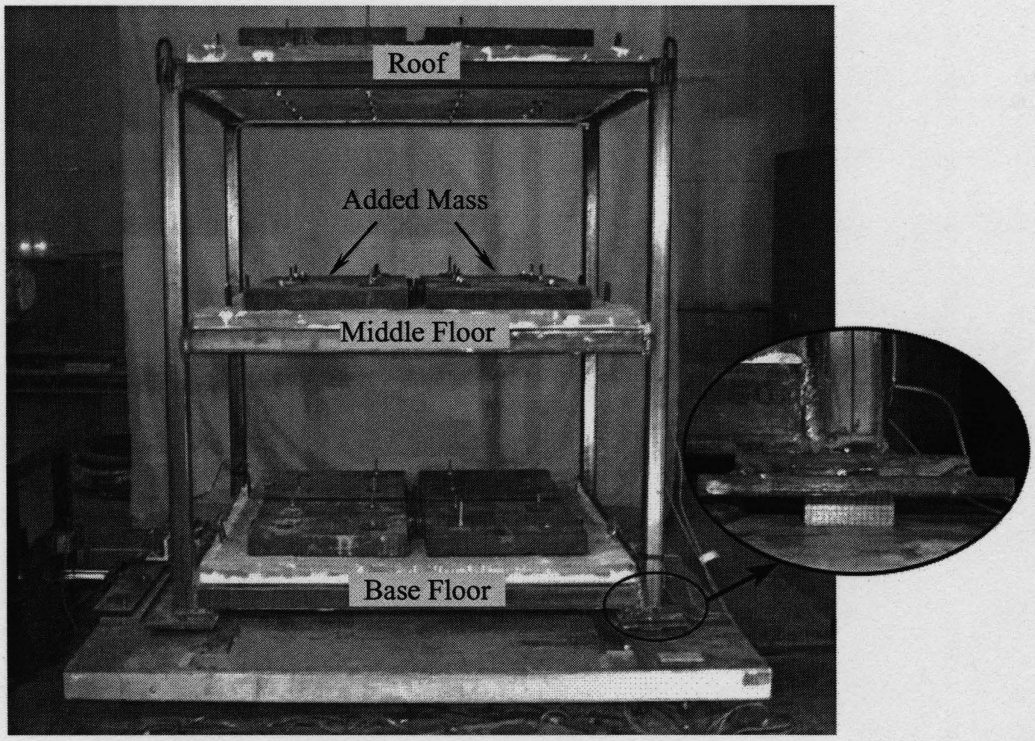

Figure 5.1. An overview of the BI-structure and a close-up view of one of the SU-FREI bearings located between the test-structure and shake table with no bonding at the contact surfaces of the bearing

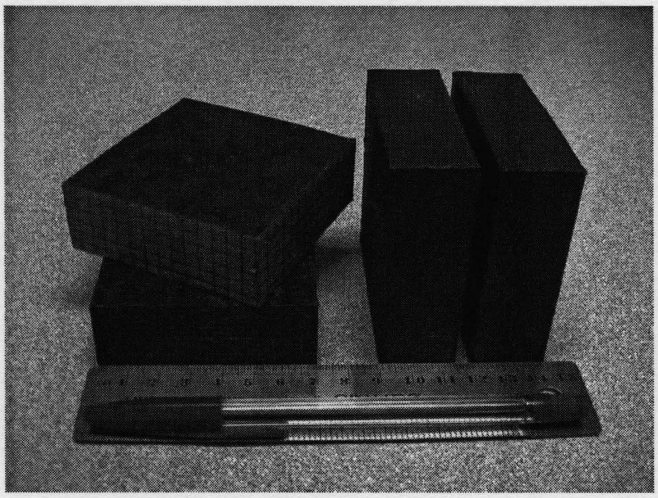

Figure 5.2. An overview of the FREI bearings used as seismic isolators

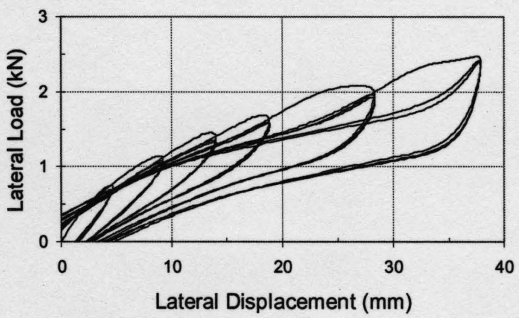

Figure 5.3. Lateral load-displacement hysteresis loops of the SU-FREI bearings under a set of cyclic lateral tests having an ascending pattern of displacement amplitudes ranging from 25% t_r to 200% t_r (where, t_r = 19 mm); Only half cycles are shown

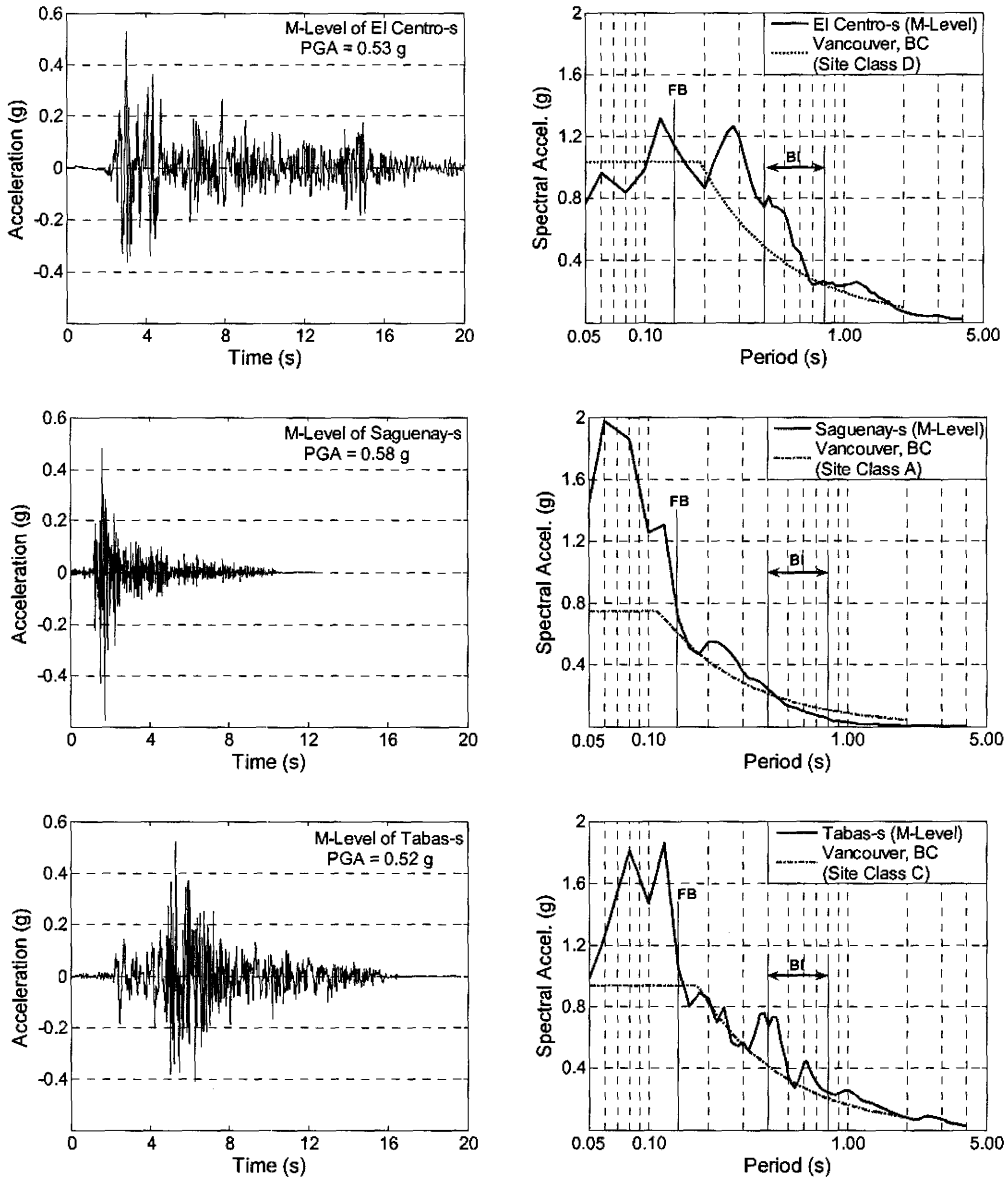

Figure 5.4. Maximum (M) level of the input earthquakes; (a) table acceleration time history; (b) comparison between 5%-damped spectral acceleration of the input earthquake and the maximum considered earthquake response spectrum for Vancouver, BC, Canada

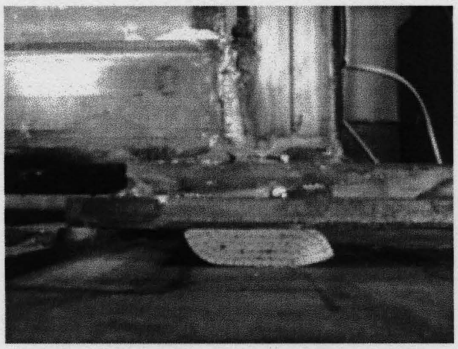

(a) El Centro-s (M-Level)

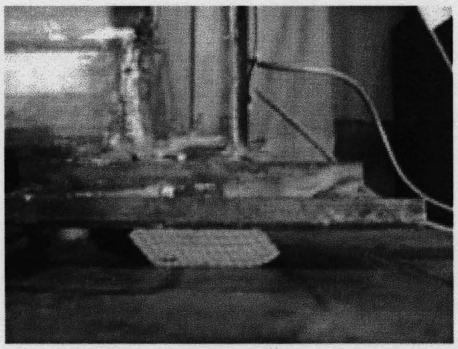

(b) Tabas-s (M-Level)

Figure 5.5. Photographs taken from one of the bearing isolators during shake table testing at the time instant of peak lateral displacement in the base isolation system

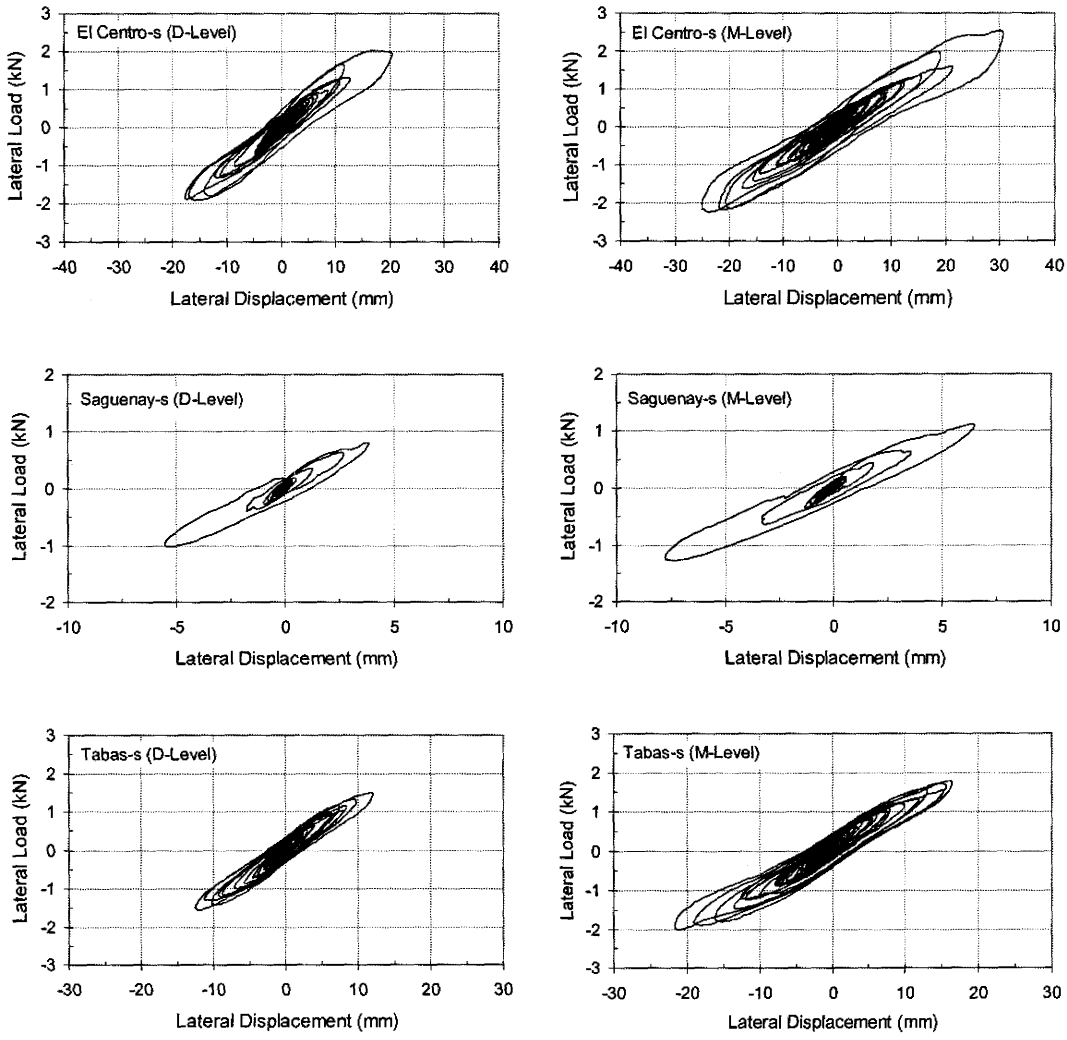

(a) Design (D) Level (b) Maximum (M) Level

Figure 5.6. Lateral load-displacement hysteresis loops of the SU-FREI bearings corresponding to the design and maximum level of different input earthquakes

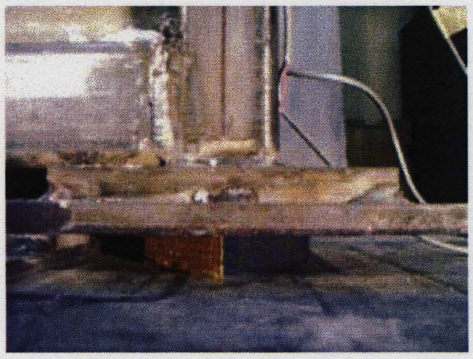

(a) Zero Lateral Displacement

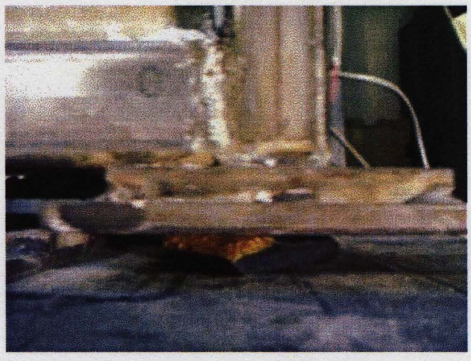

(b) Peak Lateral Displacement

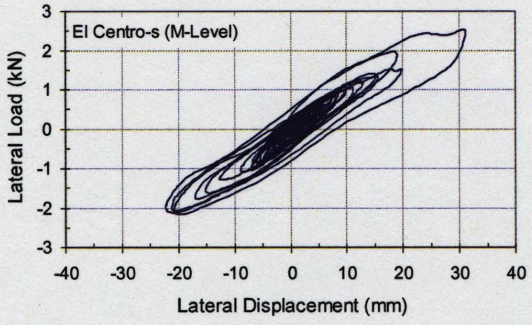

(c) Lateral Load-Displacement Hysteresis Loops

Figure 5.7. Lateral diagonal response of SU-FREI bearings at the maximum level of El Centro-s earthquake

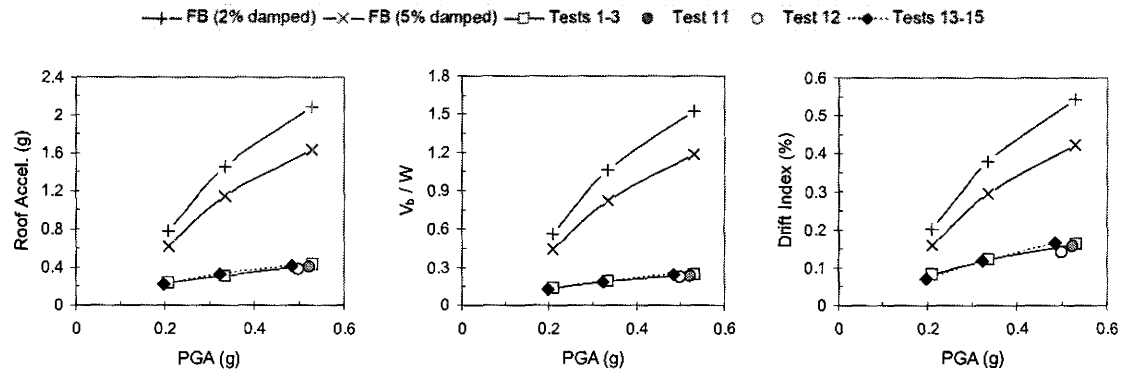

(a) Roof Accel. (b) Base Shear (c) Drift

Figure 5.8. Comparison between peak response values of the BI-structure and the corresponding 2% and 5% damped linear FB-structures to service, design, and maximum level of El Centro-s earthquake

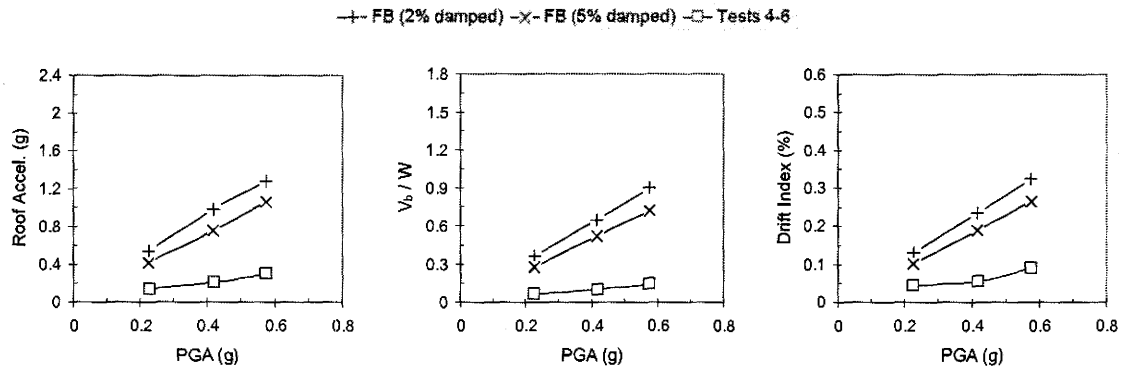

(a) Roof Accel. (b) Base Shear (c) Drift

Figure 5.9. Comparison between peak response values of the BI-structure and the corresponding 2% and 5% damped linear FB-structures to service, design, and maximum level of Saguenay-s

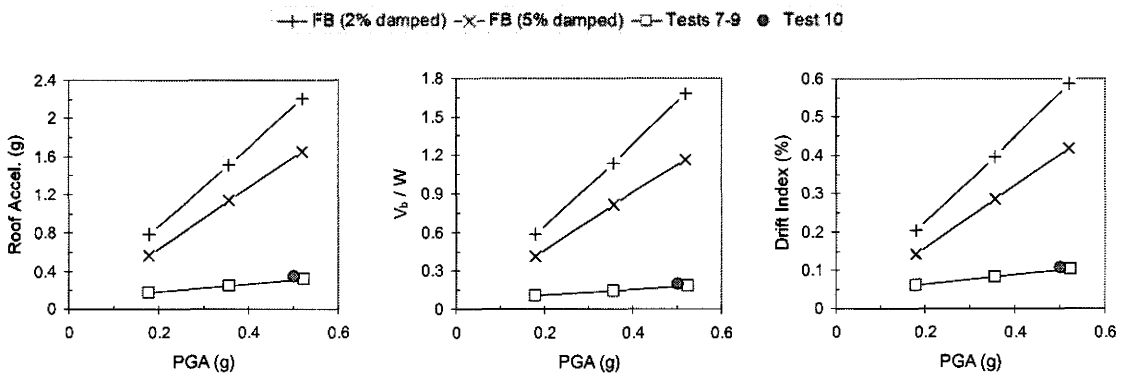

(a) Roof Accel. (b) Base Shear (c) Drift

Figure 5.10. Comparison between peak response values of the BI-structure and the corresponding 2% and 5% damped linear FB-structures with 2% and 5% damping to service, design, and maximum level of Tabas-s

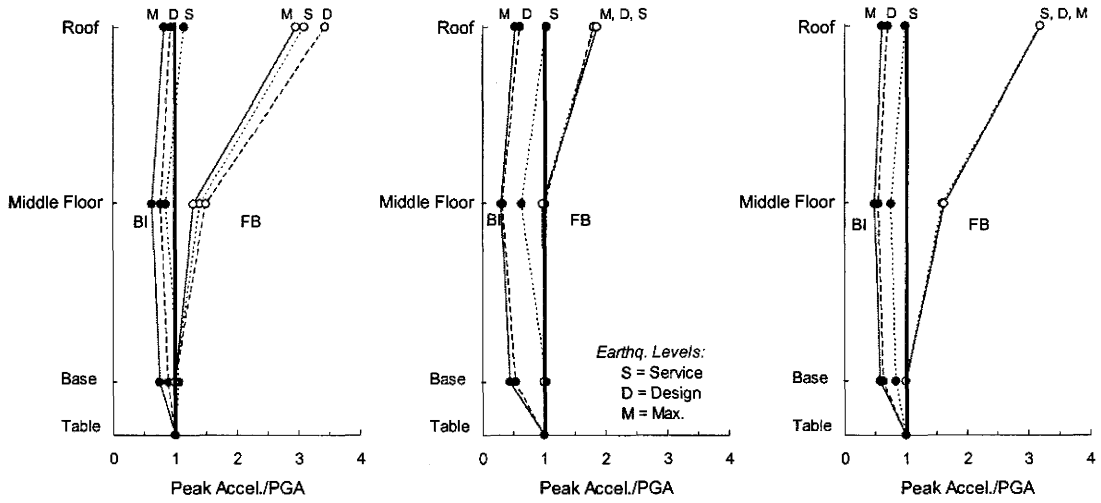

(a) El Centro-s (b) Saguenay-s (C) Tabas-s

Figure 5.11. Amplification envelopes in BI and the corresponding 5%-damped FB structures for different levels of the input earthquakes

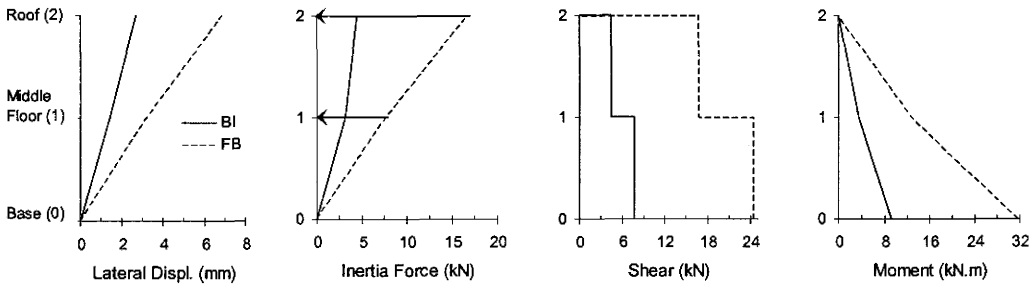

(a) El Centro-s (M-Level)

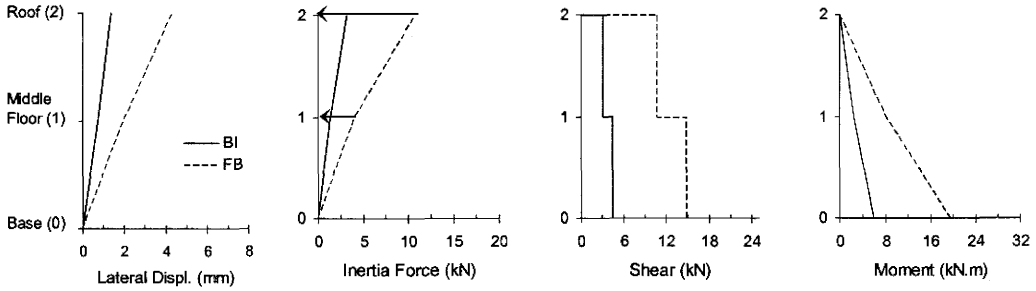

(b) Saguenay-s (M-Level)

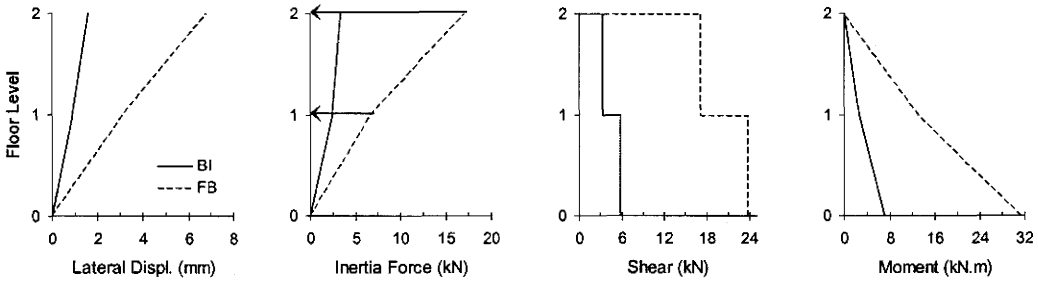

(c) Tabas-s (M-Level)

Figure 5.12. Comparison between response profiles of the BI-test-structure and the corresponding 5%-damped FB-structure under maximum (M) level of different input earthquakes. Response profiles are associated with the time instant of maximum drift

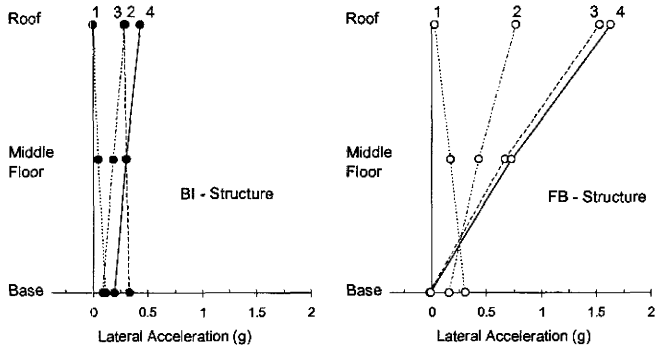

(a) El Centro-s (M-Level)

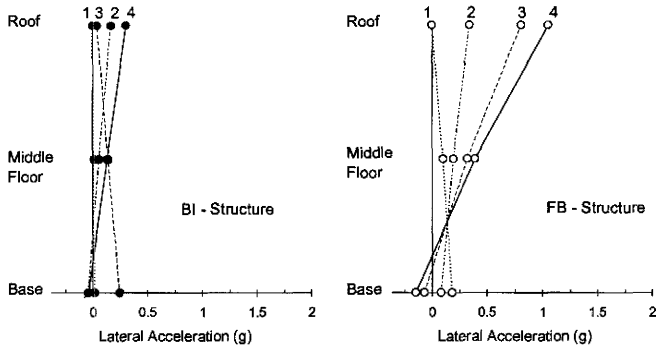

(b) Saguenay-s (M-Level)

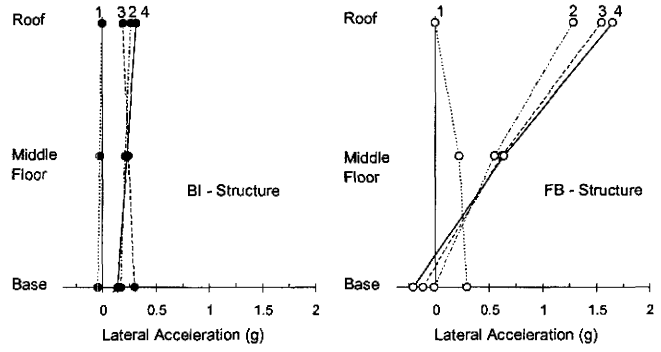

Tabas-s (M-Level)

Figure 5.13. Accelerations for the BI-structure versus the 5%-damped FB-structure; Evolution of the floor accelerations Profile within maximum amplitude half-cycle of response at four different time instants

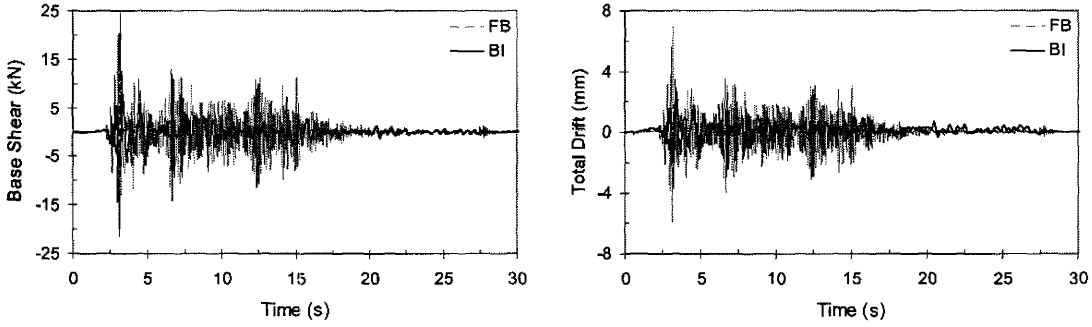

(a) El Centro-s (M-Level)

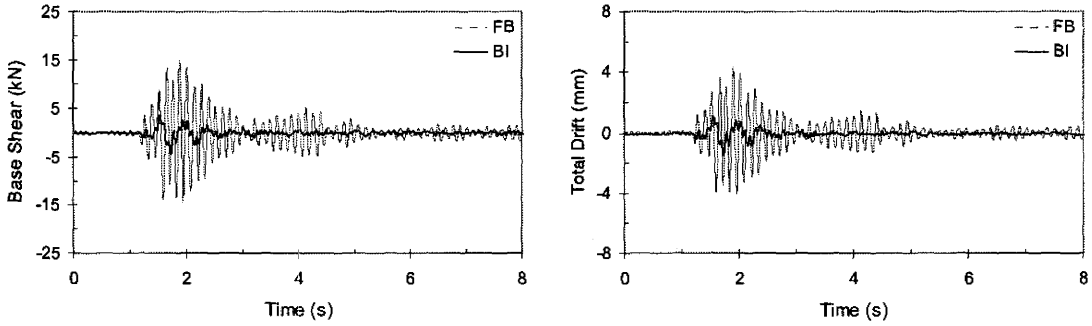

(b) Saguenay-s (M-Level)

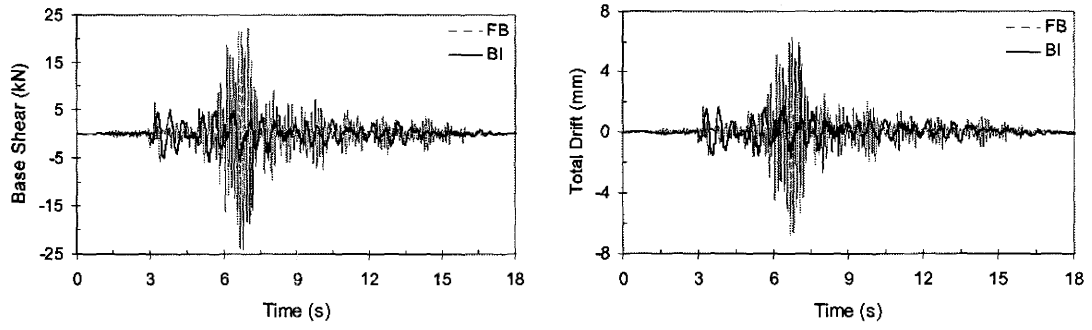

(c) Tabas-s (M-Level)

Figure 5.14. Time history of base shear and the roof lateral displacements relative to the base (total drift) in BI and corresponding 5%-damped FB structures during the maximum (M) level of different input earthquakes

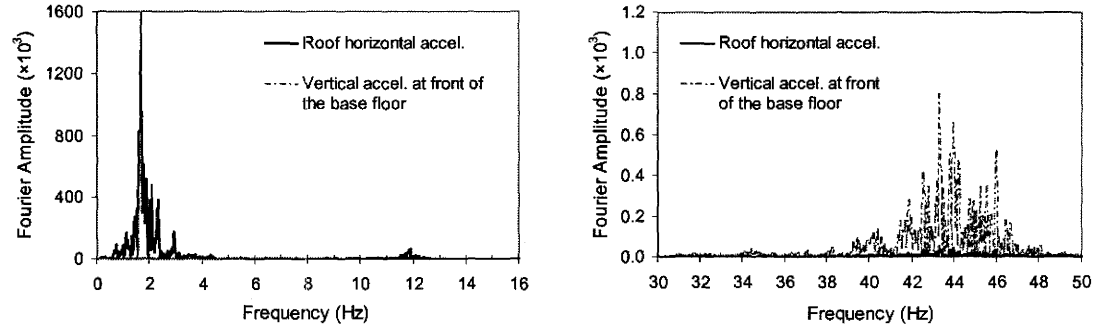

(a) El Centro-s

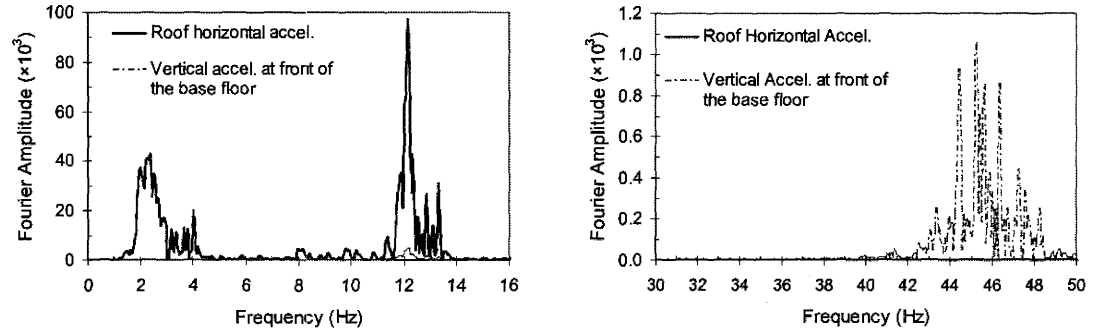

(b) Saguenay-s

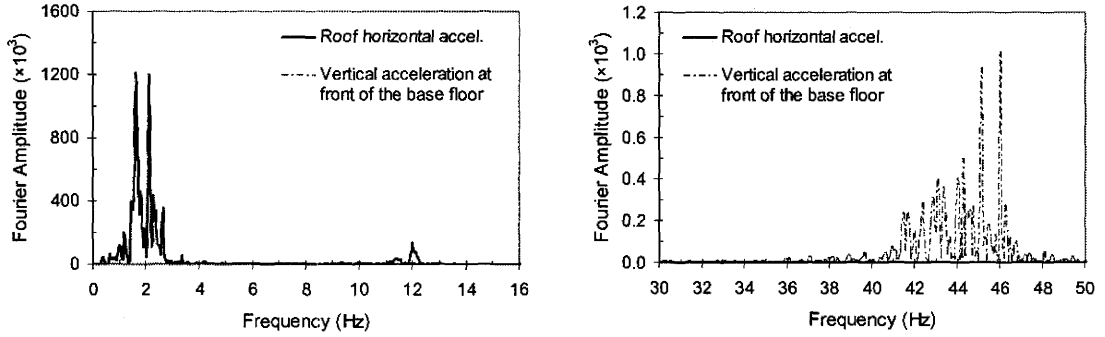

(c) Tabas-s

Figure 5.15. Fourier amplitude spectra of the BI-structure subjected to maximum level of different input earthquakes; comparison between Fourier amplitudes of the roof horizontal accelerations and the vertical accelerations at the front of base floor (all accelerations in terms of cm/s^2

Chapter 6: Simplified Analysis of a Low-Rise Building Seismically Isolated with SU-FREIs (Stable Unbonded Fiber-Reinforced Elastomeric Isolators)

6.1. Abstract

To evaluate the accuracy of simplified methods of analysis, the seismic responses of an ordinary low-rise base isolated (BI) structure to three different earthquakes are simulated and subsequently compared with results from a shake table study. The need for a simplified analysis arises from use of a base isolation system involving novel "stable unbonded fiber-reinforced elastomeric isolator" (SU-FREI) bearings. Two simplified analytical models are employed to simulate the nonlinear experimental lateral load-displacement hysteresis loops of these bearings. The experimental hysteresis loops were obtained from cyclic shear tests on prototype bearings under a constant compression load. In Model 1, the hysteresis loops are simulated based on both the rate and amplitude of lateral displacements experienced by the bearings. Model 2 uses a bilinear idealization to simulate the bearings hysteresis loops. As a novel application, due to the nonlinear lateral response behavior of the SU-FREIs, these models are employed in an iterative time history analysis approach. As a result of iterations, the model variables and the calculated peak lateral displacement of the bearings converge to their unique values. Analysis results show that the presented simplified models may be effectively used in response prediction of ordinary low-rise buildings that are seismically isolated by SU-FREI bearings.

6.2. Introduction

The objective of this paper is to present and evaluate two simplified models that can be used in response prediction of ordinary low-rise BI-buildings seismically isolated by SU-FREI bearings described below. The models simulate the experimental lateral load-displacement hysteresis loops obtained from cyclic lateral testing of prototype bearings. Both models were originally developed for response simulation of conventional steel-reinforced elastomeric bearings. However, due to the highly nonlinear lateral response

behavior of SU-FREIs, as a novel application, both models are modified to include an iterative time history analysis approach in order to select suitable model variables that match the experimental hysteresis loop corresponding to the calculated peak lateral displacement of the bearings.

Fiber-reinforced elastomeric isolator (FREI) bearings utilize fiber fabric as the reinforcement material instead of steel. A previous shake table study (Toopchinezhad et al. 2008d) showed that FREI bearings can be effectively employed in an unbonded application where they are simply placed between the superstructure and substructure with no bonding or fastening between the contact surfaces. Due to the unbonded application and lack of flexural rigidity in the fiber fabric reinforcement, FREI bearings exhibit "rollover deformation" during lateral loading where, at large lateral displacement, the originally vertical faces completely contact the horizontal upper and lower supports. Since the bearing is designed to maintain positive incremental load-resisting capacity throughout the load-displacement hysteresis loops (Toopchinezhad et al. 2008a, b), the rollover deformation is denoted as "stable rollover" (SR) and the bearing is called a "stable unbonded" (SU)-FREI bearing.

Compared to conventional steel-reinforced elastomeric bearings, some of the unique advantages of SU-FREIs are (Toopchinezhad et al. 2008a, b, c):

i) A significantly lower weight due to the use of fiber-reinforcement instead of internal steel plates, and elimination of the two thick mounting steel plates in SU-FREI bearings.

ii) An improved seismic mitigation efficiency due to the additional rotational degree of freedom at the contact surfaces of a SU-FREI bearing which results in a beneficial decrease in the bearings lateral stiffness compared to a similar bearing with bonded contact surfaces.

iii) A lower stress demand on the internal bonds between the elastomer and reinforcement layers as no vertical tension is introduced by the contact supports.

iv) Superior damping properties due to the interaction between fiber-reinforcement and elastomer.

v) Potentially more cost effectiveness, if the SU-FREIs are made as a long strip or a large sheet through a mass production manufacturing technique, and then cut to the required size.

Availability of a sufficiently accurate and easy to apply model is essential to the widespread use of SU-FREI bearings in ordinary low-rise buildings. The analysis and design costs of a BI-structure that employs SU-FREI bearings can be significantly reduced, if a simplified analysis can be employed effectively. It is also possible that the SU-FREI bearings could be supplied as catalogue products where the catalogue could include the design parameters that are required to model the lateral response of the supplied bearings to any input earthquake.

6.3. Base Isolated System

The base isolated structure (BI-structure), used in shake table tests (Toopchinezhad et al. 2008d) consisted of a single-span 2-story moment-resisting steel frame, as shown in Fig. 6.1, with dimensions of 1500 × 1400 mm and total height of 1628 mm. Square hollow steel sections (HSS 64×64×6.4 mm) were used for the columns and rectangular hollow steel sections (HSS 76×51×6.4 mm) were selected for the beams. The clear height from beam to beam of each story was 700 mm. Each floor consisted of a 105 mm thick precast concrete two-way floor slab. Four thick steel plates were firmly attached to each floor slab to provide the additional mass required to satisfy dynamic similitude (Sabnis and Harris, 1999). The BI-structure geometrically represented a ¼ scale model of a corresponding full scale prototype structure.

As shown in Fig. 6.1, the base isolation system comprised of 4 SU-FREI bearings. A single SU-FREI bearing was located at each column-line under a flat steel plate welded to the base of the column. The SU-FREI bearings were placed between the shake table and the superstructure with no bonding at their upper and lower contact surfaces. The bearings were constructed using an unfilled soft neoprene sheets and bi-directional (0°/90°) carbon

fiber fabric reinforcing material. The bearings were square with dimensions of 70 × 70 × 25 mm. The total thickness of the 12 neoprene layers in the bearings was t_r = 19 mm and the calculated matrix volume fraction, defined as the relative volume of matrix to the fibers in each fiber-reinforcement layer, was 54%. The shape factor (i.e., the ratio of vertically loaded area on one face of the elastomer layer to its perimeter load-free area) was approximately S = 11 and the aspect ratio (i.e., the ratio of length to total thickness of the bearing) was R = 2.8. Since the total weight of the superstructure was 31.1 kN, each bearing was subjected to approximately 1.6 MPa vertical pressure.

6.4. Lateral Response Properties of the SU-FREI Bearings

According to current code provisions such as in ASCE (2005), the deformation characteristics and damping values of any seismic isolator used in the design of seismically isolated structures should be determined based on cyclic tests on prototype samples of the isolators. The effective (secant) lateral stiffness and equivalent viscous damping ratio of the SU-FREI bearings were determined by conducting a set of cyclic shear tests on prototype bearings under constant 1.6 MPa vertical pressure (Toopchinezhad et al. 2008b). Lateral load-displacement hysteresis loops of the tested SU-FREI bearings were found to be highly nonlinear. In general, the hysteresis loops were influenced by rate, amplitude, and amplitude history of the lateral displacements. As the bearings were subjected to a relatively light vertical pressure, the effect of ± 50% variations of vertical pressure on the lateral response was found to be negligible (Toopchinezhad et al. 2008c); Less than 50% variation in the vertical pressure occurred during shake table testing (Toopchinezhad et al. 2008d).

Results from cyclic tests, previously conducted on prototype bearings (Toopchinezhad et al. 2008b), were used to model the SU-FREI bearings employed in the BI-structure. Figure 6.2 shows the lateral displacements used to evaluate the bearing properties. The pattern of lateral displacements shown in Fig. 6.2 consisted of 3 sinusoidal cycles at each of 6 ascending amplitudes of 25%, 50%, 75%, 100%, 150%, and 200% t_r. In order to remain in the operating limits of the test apparatus, the average rate of sinusoidal lateral displacements was set at 76 mm/s for all amplitudes. This rate corresponded to an

excitation frequency of 1 Hz at a design displacement of 100% t_r, which was sufficiently close to the bearings' natural frequency (i.e., approximately 1.5 Hz) to eliminate any significant displacement rate effect (Toopchinezhad et al. 2008b).

Figure 6.3a shows the lateral load-displacement hysteresis loops of the SU-FREI bearings obtained from cyclic testing. As seen in this figure, the first cycle, out of the three cycles applied at each level of lateral displacement, corresponds to the unscragged response of the bearing with larger load-resisting capacity and damping ratio than in the two following cycles. The hysteresis loops corresponding to the unscragged response at each level of lateral displacement are referred to hereafter as the "unscragged loops". The unscragged loops corresponding to each displacement level are shown in Fig. 6.3b. The effective lateral stiffness values cited in Table 6.1 are relative to the unscragged loops of the bearings at each level of lateral displacement. Damping ratios in this table conservatively reflect the minimum scragged values achieved at each level of lateral displacement.

6.5. Modeling of the Base Isolated System

6.5.1. Governing Equations

Figure 6.4 illustrates a simple 3 DOF mass-spring-dashpot idealization used to model the prototype BI-structure shown in Fig. 6.1. The bearings in the base isolation system have nonlinear lateral load-displacement behavior (as shown in Fig. 6.3a) which can be modeled with a nonlinear stiffness (spring k_b) along with an energy dissipator (dashpot c_b), both of which are determined experimentally from cyclic testing on prototype isolators. Since in a BI-system the superstructure remains nearly rigid, it has been modeled as a linear elastic system in this study. The governing equations for the dynamic system shown in Fig. 6.4 are as follows (Naiem and Kelly 1999);

$$\mathbf{M}^*\ddot{\mathbf{V}}^* + \mathbf{C}^*\dot{\mathbf{V}}^* + \mathbf{K}^*\mathbf{V}^* = -\mathbf{M}^*\mathbf{r}^*\ddot{u}_g \tag{6.1}$$

The mass, damping and stiffness of the BI-structure are determined using

$$\mathbf{M}^* = \begin{bmatrix} m+m_b & \mathbf{r}^T\mathbf{M} \\ \mathbf{M}\mathbf{r} & \mathbf{M} \end{bmatrix} \qquad \mathbf{C}^* = \begin{bmatrix} c_b & \mathbf{0} \\ \mathbf{0} & \mathbf{C} \end{bmatrix} \qquad \mathbf{K}^* = \begin{bmatrix} k_b & \mathbf{0} \\ \mathbf{0} & \mathbf{K} \end{bmatrix} \tag{6.2}$$

where, $\mathbf{M}$, $\mathbf{C}$ and $\mathbf{K}$ are mass, damping, and stiffness matrices of the 2-story superstructure, respectively, m represents total mass of the superstructure excluding the base floor ($m = m_1 + m_2$), m_b is the mass of base floor, and c_b and k_b are damping and stiffness of the base isolation system, respectively. Other terms in Eq. (6.3) are defined as follows;

$$\mathbf{r} = \begin{Bmatrix} 1 \\ 1 \end{Bmatrix} \qquad \mathbf{r}^* = \begin{Bmatrix} 1 \\ 0 \end{Bmatrix} \qquad \mathbf{V}^* = \begin{Bmatrix} v_b \\ \mathbf{v} \end{Bmatrix} \qquad \mathbf{v} = \begin{Bmatrix} v_1 \\ v_2 \end{Bmatrix} \tag{6.3}$$

It should be noted that the vertical component of ground motion has been ignored in this analysis.

6.5.2. Superstructure

Figure 6.5 shows a stick model of the superstructure. Neglecting the axial deformations in the structural elements, there are a total of eight DOFs. These are translational DOFs v_{t1} and v_{t2} at the middle floor and roof, respectively, as well as joint rotations $v_{\theta 1}$ to $v_{\theta 6}$. As a typical approach, a lumped mass idealization is utilized to construct the diagonal mass matrix of the superstructure and "static condensation" method (Chopra, 2007) is applied to eliminate the rotational DOFs from the dynamic analysis of the system. By separating the translational (dynamic) and rotational (static) DOFs, the undamped equations of motions for the superstructure can be written as follows;

$$\begin{bmatrix} \mathbf{m}_{tt} & \mathbf{0} \\ \mathbf{0} & \mathbf{0} \end{bmatrix} \begin{Bmatrix} \ddot{\mathbf{v}}_t \\ \ddot{\mathbf{v}}_\theta \end{Bmatrix} + \begin{bmatrix} \mathbf{k}_{tt} & \mathbf{k}_{t\theta} \\ \mathbf{k}_{\theta t} & \mathbf{k}_{\theta\theta} \end{bmatrix} \begin{Bmatrix} \mathbf{v}_t \\ \mathbf{v}_\theta \end{Bmatrix} = \begin{Bmatrix} \mathbf{p}_t(t) \\ \mathbf{0} \end{Bmatrix} \tag{6.4}$$

The condensed form of the stiffness matrix for the superstructure, to be used in Eq. (6.2), is given by

$$\mathbf{K} = \mathbf{k}_{tt} - \mathbf{k}_{\theta t}^{T} \mathbf{k}_{\theta\theta}^{-1} \mathbf{k}_{\theta t} \tag{6.5}$$

where,

$$\mathbf{k}_{tt} = 2\left(\frac{24EI_c}{L_c^3}\right)\begin{bmatrix} 2 & -1 \\ -1 & 1 \end{bmatrix} \tag{6.6}$$

$$\mathbf{k}_{\theta t}^{T} = 2\left(\frac{6EI_c}{L_c^2}\right)\begin{bmatrix} 1 & 1 & 0 & 0 & -1 & -1 \\ 0 & 0 & 1 & 1 & 1 & 1 \end{bmatrix} \tag{6.7}$$

$$\mathbf{k}_{\theta\theta} = 2(2E)\begin{bmatrix} 2I_c/L_c+2I_b/L_b & I_b/L_b & I_c/L_c & 0 & 0 & 0 \\ & 2I_c/L_c+2I_b/L_b & 0 & I_c/L_c & 0 & 0 \\ & & 4I_c/L_c+2I_b/L_b & I_b/L_b & I_c/L_c & 0 \\ & Sym. & & 4I_c/L_c+2I_b/L_b & 0 & I_c/L_c \\ & & & & 2I_c/L_c+2I_b/L_b & I_b/L_b \\ & & & & & 2I_c/L_c+2I_b/L_b \end{bmatrix} \tag{6.8}$$

The coefficient 2 in Eqs. (6) to (8) accounts for the two parallel planar frames in the superstructure. The mass matrix of the superstructure is defined as

$$\mathbf{M} = \mathbf{m}_{tt} = \begin{bmatrix} m_1 & 0 \\ 0 & m_2 \end{bmatrix} \tag{6.9}$$

From free vibration tests conducted on the fixed base superstructure (Toopchinezhad et al. 2008d), the modal frequencies were found to be 7.4 Hz and 25.4 Hz (0.14 s and 0.04 s periods). The fixed base model of the superstructure involves restraining the two rotational DOFs $v_{\theta 1}$ and $v_{\theta 2}$ in Fig. 6.5, and their corresponding rows and columns in Eqs. (6.7) and (6.8) were eliminated. The two modal frequencies of the fixed base superstructure, using $\mathbf{K}$ and $\mathbf{M}$ from Eqs. (6.5) and (6.9), respectively, were calculated to be 7.6 Hz and 26.0 Hz (0.13 s and 0.04 s), which is in very good agreement with the free vibration test results.

The damping matrix was taken as a linear combination of mass and stiffness matrices of the superstructure (Rayleigh damping). From the free vibration tests, the equivalent viscous

damping ratios of the first and second vibration modes were found to be approximately ξ = 0.6%. Accordingly, the damping matrix **C** was constructed using

$$\mathbf{C} = \alpha \mathbf{M} + \beta \mathbf{K} \tag{6.10}$$

where α and β were evaluated based on equivalent viscous damping ratio ξ, and modal natural frequencies ω_1 and ω_2 of the superstructure as follows (Chopra, 2007);

$$\alpha = \frac{2\xi\omega_1\omega_2}{\omega_1 + \omega_2}, \text{ and } \beta = \frac{2\xi}{\omega_1 + \omega_2} \tag{6.11}$$

6.5.3. SU-FREI Bearings

The lateral load $f_b(t)$ that is experienced by the base isolation system can be attributed to sum of the restoring and damping forces as follows;

$$f_b(t) = k_b(t)v_b(t) + c_b(t)\dot{v}_b(t) \tag{6.12}$$

Considering n identical bearing isolators in the base isolation system, the lateral stiffness and damping coefficient to be used in Eq. (6.2), are calculated by

$$k_b(t) = n k_{bi}(t) \tag{6.13}$$

$$c_b(t) = n c_{bi}(t) \tag{6.14}$$

where, $k_{bi}(t)$ and $c_{bi}(t)$ are the effective (secant) lateral stiffness and damping coefficient of an individual bearing "*i*" in the base isolation system at time instant *t*. For the given BI-structure, the total number of bearings in the base isolation system is n = 4. The two analytical models discussed here use different methods to simulate the effective lateral stiffness and damping coefficient of the SU-FREI bearings. Results obtained from a previous

study (Toopchinezhad et al. 2008d) indicated that the average 50 Hz vertical frequency of the SU-FREI bearings under 1.6 MPa vertical pressure was sufficiently large to prevent any significant contribution of the rocking modes in the total earthquake response of the BI-structure. Accordingly, in the models, the SU-FREI bearings are assumed to be rigid in the vertical direction.

6.5.4. Model 1: Rate and Amplitude Dependent Stiffness and Damping

Hwang et al. (2002) developed Eqs. (6.15) and (6.16) to simulate the stiffness and damping coefficients of conventional steel-reinforced elastomeric bearing in terms of lateral displacement amplitude (v_b), displacement rate ($\dot{v}_b$), and the energy dissipated by the bearing during cyclic loading reversals ($\int_0^t f_{bi}(t)\dot{v}_b(t)\,dt$).

$$k_{bi}(t) = a_1 + a_2 v_b^2(t) + a_3 v_b^4(t) + \frac{a_4 e^{a_9 \int_0^t f_{bi}(t)\dot{v}_b(t)dt}}{\cosh^2(a_5 \dot{v}_b(t))} \tag{6.15}$$

$$c_{bi}(t) = \frac{a_6 + a_7 v_b^2(t)}{\sqrt{a_8^2 + \dot{v}_b^2(t)}}\left(1 + e^{a_{10} \int_0^t f_{bi}(t)\dot{v}_b(t)dt}\right) \tag{6.16}$$

The 10 parameters, a_1 to a_{10}, in the above equations are constants which are evaluated by a least squares fit to the lateral load-displacement hysteresis loops obtained from cyclic shear tests on prototype bearings. However, it should be noted that none of these 10 parameters independently describe any particular elastomer behavior. The complex nonlinear response of the bearing is described as a whole by the combination of these 10 parameters.

The a-parameter values evaluated to predict the lateral response of the SU-FREI bearings and the comparison between the measured and predicted hysteresis loops are shown in Fig. 6.6. Although all cycles of the test were included in the evaluation of the a-parameter values, the predicted lateral response was unable to trace the unscragged loops attributed to the first cycles of the test at each increased displacement amplitude. As shown in Fig. 6.6, the

model showed better agreement with the scragged loops (i.e., response to Cycles 2 and 3 at each displacement level.). The peak response values are usually of most interest. To account for the unscragged stiffness at the peak bearing lateral displacement, a lower stiffness limit, $k_{bi,min}$, was imposed on Eq. (6.15) during the time history analysis. This limit ensures that the unscragged stiffness is used at the peak lateral displacement of the bearings, $v_{b,max}$. The procedure used in this analysis was as follows;

i) The initial $k_{bi,min}$ was set to be the effective lateral stiffness at 200% t_r displacement as cited in Table 6.1.

ii) A time history analysis on the BI-structure was carried out and the peak lateral displacement amplitude of the bearings ($v_{b,max}$) was obtained.

iii) The new value of $k_{bi,min}$ was calculated from Table 6.1 through linear interpolation between the unscragged stiffness values corresponding to the lateral displacement levels that bracketed the current $v_{b,max}$.

iv) By imposing the $k_{bi,min}$ calculated from the previous step, the value of $v_{b,max}$ was updated through repeating the time history analysis on the BI-structure.

v) The iterations were continued until $v_{b,max}$ converged to its unique value with 1% t_r accuracy.

The convergence, depending on the input earthquake, was typically achieved after 2 or 3 iterations.

For a scaled version of Saguenay earthquake where the peak lateral displacement amplitudes of the bearings are small, using the a-parameters given in Fig. 6.6 did not result in an accurate response prediction. An inspection of Fig. 6.6 indicates that, at 25% t_r (4.75 mm) the discrepancy between the simulated and the measured hysteresis loops increases. In order to improve the model, the a_1 to a_{10} parameters in Eqs. (15) and (16) were evaluated by curve fitting to the measured lateral load-displacement hysteresis loops up to 50% t_r as indicated in Fig. 6.7. This set of a-parameters was used in the time history analysis of the BI-structure to a scaled version of Saguenay earthquake.

6.5.5. Model 2: Bilinear Idealization

The unscragged load-displacement hysteresis loops shown in Fig. 6.3b can be idealized with a bilinear model based on parameters k_1, k_2, and q as shown in Fig. 6.8a, for a typical example of a bearing at 150% t_r lateral displacement. As shown in Fig. 6.8b, the characteristic strength q can be accurately calculated by taking the average values of q_1 and q_2 and post-yield stiffness k_2 can be reasonably selected to be the tangent stiffness at zero displacement (Naiem and Kelly 1999). The evaluation of elastic stiffness k_1 is discussed later in this section.

The effective (secant) lateral stiffness of each bearing i in the base isolation system is given by

$$k_{b,i}(t) = k_2 + \frac{q}{v_b(t)} \qquad for \;\; v_b \geq v_{b,y} \tag{6.17}$$

where the lateral yield displacement $v_{b,y}$ is defined by

$$v_{b,y} = \frac{q}{k_1 - k_2} \tag{6.18}$$

The effective equivalent viscous damping ratio $\xi_{eff}(t)$ of the bearings is defined by

$$\xi_{eff}(t) = \frac{4q\left(v_b(t) - v_{b,y}\right)}{2\pi k_{b,i}(t) v_b^2(t)} \tag{6.19}$$

where the numerator in Eq. (6.19) approximates the dissipated energy per cycle (the area within the hysteresis loop, W_d), and the denominator represents $4\pi W_s$ with restoring energy $W_s = \frac{1}{2} k_{b,i}(t) v_b^2(t)$. The damping ratio also can be expressed in terms of nondimensional parameters $y(t) = v_b(t)/v_{b,y}$ and $\alpha = q/(k_2 v_{b,y})$ as follows;

$$\xi_{eff}(t)=\frac{2\alpha}{\pi}\frac{y(t)-1}{(y(t)+\alpha)y(t)} \qquad for\ y(t)>1 \tag{6.20}$$

From Eq. (6.18), α also can be expressed as a function of k_1 and k_2 as follows;

$$\alpha=\frac{k_1-k_2}{k_2} \tag{6.21}$$

For a constant α, the maximum value of $\xi_{eff}(t)$, which occurs where $d\xi_{eff}(t)/dy(t)=0$, is given by (Naiem and Kelly 1999) as

$$\xi_{eff,\,max}=\frac{2\alpha}{\pi}\frac{1}{2(1+\alpha)^{\frac{1}{2}}+(2+\alpha)} \tag{6.22}$$

From Eqs. (6.20) and (6.22), it can be shown that the maximum damping ratio $\xi_{eff,\,max}$ occurs at $y_{\xi_{eff,max}}=1+(1+\alpha)^{\frac{1}{2}}$. Therefore, in the time history analysis for $y(t)\le y_{\xi_{eff,max}}$, the damping ratio of the bearings is taken as $\xi_{eff}(t)=\xi_{eff,\,max}$. For $y(t)>y_{\xi_{eff,max}}$, it is calculated from Eq. (6.20).

From Eq. (6.17), it is obvious that, unlike q and k_2, k_1 has no influence on the effective lateral stiffness. However, it significantly influences the damping ratio of the bearing. From Eqs. (6.21) and (6.22), it can be observed that the maximum damping ratio depends on the values of k_1 and k_2. From Table 6.1, a maximum calculated damping ratio of 12% was found from cyclic lateral tests on the prototype SU-FREI bearings. To achieve this damping ratio using Eq. (6.22), the corresponding value for α is found to be 1.136. Then, from Eq. (6.21), k_1 for the utilized SU-FREI bearings is calculated to be

$$k_1=2.136k_2 \tag{6.23}$$

The characteristic strength q and the post-yield stiffness k_2 for each of the unscragged hysteresis loops of the bearing shown in Fig. 6.3b are different. For example, Fig. 6.8 shows the aforementioned parameters for the unscragged hysteresis loop at 150% t_r lateral displacement. Table 6.2 contain the values of these parameters at different displacement amplitudes ranging from 25% to 200% t_r.

Since the peak response values are typically of most interest, appropriate values of k_1, k_2, and q that match the bearing peak lateral displacement amplitude ($v_{b,\max}$), calculated by time history analysis are used. This goal can be achieved through an iterative analysis procedure as follows;

i) The parameters k_1, k_2, and q at 200% t_r lateral displacement are initially used in the analysis.

ii) Time history analysis on the BI-structure is carried out and $v_{b,max}$ is calculated.

iii) The new values of parameters k_1, k_2, and q are calculated from Table 6.2 through linear interpolation between the values corresponding to the lateral displacement amplitudes that bracket the current $v_{b,max}$.

iv) The value of $v_{b,max}$ is updated through repeating the time history analysis on the BI-structure.

v) The iterations are continued until $v_{b,max}$ converges to a unique value.

In the time history analyses conducted in this paper, a convergence with ±1% t_r accuracy was typically achieved after 3 to 4 iterations.

6.6. Input Earthquakes

El Centro 1940 (longitudinal component), Saguenay, Quebec, Canada, 1988, (transverse component), and Tabas, Iran, 1978 (longitudinal component) were considered in this study. Given the geometric scale-factor of ¼ of the model building previously tested (Toopchinezhad er al. 2008d), the original ground motion records of these earthquakes were compressed in time by a factor of 2 in order to satisfy dynamic similitude requirements (Harris and Sabnis, 1999). Additionally, the accelerations of these

earthquakes were scaled so that their peak values met or exceeded the maximum expected PGA in Vancouver, BC as a typical region with high seismic risk in Canada (NBCC, 2005). The scaled earthquakes (also called input earthquakes) are hereafter denoted by El Centro-s, Saguenay-s, and Tabas-s. Figure 6.9 contains the time history plots of the input earthquakes.

6.7. Analytical Results and Discussion

In this section, the predicted lateral response of the BI-structure to different input earthquakes are compared with the measured lateral response during shake table tests (Toopchinezhad et al. 2008d). The objective is to assess the effectiveness of the presented models in dynamic response simulation of the BI-structure to different earthquakes. To achieve this, comparisons are made between the calculated peak response values of the BI-structure for lateral load and displacement at the level of bearing isolators. Also, the peak values of base shear, and total drift in the superstructure are compared as are the measured and predicted response histories of bearing lateral displacement and superstructure base shear are compared.

Table 6.3 contains the measured and predicted peak response values of the BI-structure to the three input earthquakes. The predicted peak response values in this table are normalized with respect to their corresponding measured values. In order to examine the improvement made as a result of implementing an iterative procedure, Table 6.3 includes the predicted peak response values attributed to both the first and last iterations made in the time history analysis. Additionally, for both analytical models, the predicted lateral load-displacement hysteresis loops corresponding to the first and last iterations are compared with the measured hysteresis loops. Time histories of the bearings lateral displacement (v_b) and the base shear in the superstructure (V_s) are examined to determine the effectiveness of the presented models in response-history prediction of the BI-structure. Unless otherwise stated, the analytical results discussed are attributed to the last iteration of the time history analysis.

Figures 6.10 and 6.11 contain the measured and predicted time histories of v_b and V_s during El Centro-s earthquake, using Models 1 and 2, respectively. Although both models are able

to reasonably simulate the response history of the BI-structure, they both underestimate the peak response values. As can be seen in Table 6.3, the peak response values calculated by Model 2 are in better agreement with the measured values. Model 1 is found to underestimate the peak value of base shear by 20%. However, the predicted base shear in Model 2 is within 3% of the measured value.

The maximum discrepancy between the measured and predicted responses using Model 2 is 11% for the peak lateral displacement of the bearings. Repeating the time history analysis (iterations) with updated design parameters of the bearings was found to have little influence on the results from Model 1 for the El Centro-s earthquake, except for the lateral bearing load, which shows a noticeable increase as a result of iterations. However, as shown in Table 6.3, iterating produced significant improvement in the accuracy of Model 2. Figure 6.12 contains the measured versus predicted lateral load-displacement hysteresis loops for one of the bearings in the base isolation system when subjected to the El Centro-s earthquake. As can be seen, iterations in the time history analysis significantly affect the peak lateral load and displacement of the bearings predicted by Model 2. Since all parameters involved in Model 2 are updated for each iteration, this model is more sensitive to iterations in the time history analysis.

The time history responses to the Saguenay-s earthquake are shown in Figs. 6.13 and 6.14. As seen in these figures, Model 2 is in better agreement with the measured response throughout the entire time history. According to Table 3, both models underestimate the peak responses to the Saguenay-s earthquake, except for the lateral load on the bearings which is overestimated by 4% in Model 2. The maximum discrepancy between the measured and predicted response is observed for the superstructure base shear where, Models 1 and 2 differ from the measured value by -16% and -23%, respectively. Iterations in the time history analysis are found to have negligible influence on results obtained by Model 1 for which $v_{b,max}$ converged to its unique value at the 2nd iteration. The measured versus predicted hysteresis loops for an individual bearing in the base isolation system are shown in Fig. 6.15. Unlike Model 1, iterations significantly improve the hysteresis loops predicted by Model 2.

Figures 6.16 and 6.17 contain the measured and predicted time histories of v_b and V_s during Tabas-s earthquake using Models 1 and 2, respectively. As shown, Model 2 is generally in better agreement with the measured responses throughout the entire time history plot. However, Model 1 estimates the peak response values more accurately than Model 2 (see Table 6.3). The peak bearing lateral displacement calculated by Model 1 overestimates the measured values by 10%, whereas, it is underestimated by 13% in Model 2. The maximum discrepancy occurs in prediction of the total drift index where differences of +16% and +24% for Models 1 and 2, respectively, are found. Figure 6.18 contains the measured versus predicted hysteresis loops during Tabas-s earthquake. As seen in this figure as well as in Table 6.3, iterations in the time history analysis are found to significantly influence the responses predicted by both models.

6.8. Summary and Conclusions

The accuracies of two different analytical techniques utilized to model the lateral load-displacement hysteresis loops of SU-FREI bearings subjected to different input earthquakes were investigated in this paper. Both of these models were constructed based on lateral load-displacement hysteresis loops of the prototype SU-FREI bearings obtained from cyclic lateral testing.

In Model 1, the lateral response of the bearings was simulated based on both the amplitude and rate of lateral displacements. A total of 10 unknown coefficients were determined through least squares curve fitting of the hysteresis loops of the bearing obtained from cyclic lateral testing. A lower stiffness limit was imposed to properly simulate the unscragged stiffness corresponding to the peak lateral displacement of the bearing during the time history analysis. Using an iterative procedure, only the imposed lower stiffness limit was updated based on the peak lateral displacement of the bearings, calculated by time history analysis. For each iteration, the 10 coefficients used in this model remained unchanged as they were evaluated based on all of the bearing's hysteresis loops at different displacement amplitudes. The imposed lower stiffness limit and the calculated peak lateral displacement converged to their unique values after 2 to 3 iterations, depending on the

input earthquake. Overall, this model showed good correlation with the measured response history of the BI-structure. However, the discrepancies between the measured and predicted response histories indicated that, in general, the model was not able to completely capture the influence of rate and amplitude of lateral displacements on effective stiffness and damping of the bearings.

In model 2, a bi-linear idealization was used to simulate the lateral load-displacement hysteresis loops of the bearings. The damping ratio in this model was calculated from the area within the hysteresis loops. Unlike Model 1, both effective stiffness and damping ratio were considered to be rate independent in Model 2. This model used characteristic strength (q), post-yield stiffness (k_2), and elastic stiffness (k_1) as the unknown parameters. The first two bearing parameters were determined from the shape of the unscragged hysteresis loops (i.e., first cycle of hysteresis loops at each increased displacement amplitude). The third parameter was evaluated so as to simulate the maximum bearing damping ratio that was achieved during cyclic testing. Considering the highly nonlinear nature of the bearing hysteresis loops, at each level of lateral displacement, different values were obtained for the 3 unknown parameters of this model. As the peak response values were of greatest interest, iterations were made in the time history analysis in order to utilize the appropriate set of k_1, k_2, and q parameters that was consistent with the calculated peak lateral displacement of the bearings. Since all 3 parameters of this model were updated, the results were more sensitive to iterations in the time history analysis. In general, regardless the input earthquake, the history of response predicted by this model was in better agreement, compared to Model 1, with the measured response.

The effective lateral stiffness and damping ratio of the SU-FREI bearings, which carried a relatively light vertical pressure, were found to be sensitive to the amplitude, amplitude history, and rate of lateral displacements experienced by the bearings (Toopchinezhad, et al. 2008c). As a result, the lateral load-displacement hysteresis loops of the bearings are highly influenced by characteristics of the input excitation. Additionally, the transition between unscragged and scragged responses of the elastomer used in the SU-FREI bearings adds to the complexity of the lateral response of the bearings.

Considering the restrictions and simplifying assumptions involved, neither model is able to fully capture the influence of all of the above mentioned effects. Accordingly, the accuracy of these models in response prediction was found to be dependent on the input earthquake. Nevertheless, for seismic isolation using SU-FREI bearings, it was found that both models may be used as effective simplified tools in analysis and design of low-rise BI-buildings of ordinary importance. For some special cases, due to the importance of the structure, where more accurate response prediction is required these models can be utilized in the preliminary design of the structure.

If the parameters required for the proposed models were evaluated by the bearing supplier and reported for different categories of bearings in their catalogues, this would significantly aid the designer. Using the design parameters cited in the catalogue, it would be possible to select an appropriate SU-FREI bearing and adjust the design of a base isolation system for a given structure.

6.9. References

ASCE. (2005). "Minimum Design Loads for Buildings and other Structures." *ASCE/SEI 7-05*, American Society of Civil Engineers, New York.

Chopra A. K. (2007). *Dynamics of Structures: Theory and Applications to Earthquake Engineering*, 3rd edition, Prentice Hall, Upper Saddle River, New Jersey.

FEMA. (2000). "Pre-Standard and Commentary for the Seismic Rehabilitation of Buildings." *FEMA 356*, Federal Emergency Management Agency, Washington, D.C.

Harris H. G. and Sabnis G. M. (1999). *Structural Modeling and Experimental Techniques*, CRC Press, New York.

Hwang J. S., Wu J. D., Pan T. C., and Yang G. (2002). "A Mathematical Hysteretic Model for Elastomeric Isolation Bearings." *Earthquake Engineering & Structural Dynamics*, Vol. 31, No. 4, Pages 771–789.

Naeim, F., and Kelly, J.M. (1999). *Design of Seismic Isolated Structures*, John Wiley, New York.

NBCC. (2005). "National Building Code of Canada." *Institute for Research in Construction, National Research Council of Canada*, Ottawa, Ontario.

Toopchinezhad H., Tait M.J., and Drysdale R.G. (2008a). "Testing and Modeling of Square Carbon Fiber-Reinforced Elastomeric Seismic Isolators." *Structural Control and Health Monitoring*, Vol. 15, No. 6, Pages 876-900, DOI: 10.1002/stc.225 *(Chapter 2 of this thesis)*.

Toopchinezhad H., Tait M.J., and Drysdale R.G. (2008b). "Lateral Response Evaluation of Fiber-Reinforced Neoprene Seismic Isolators Utilized in an Unbonded Application."

Journal of Structural Engineering, ASCE, Vol. 134, No. 10, Pages 1627-1638 *(Chapter 3 of this thesis).*

Toopchinezhad H., Drysdale R. G., and Tait M. J. (2008c). "Parametric Study on the Response of Stable Unbonded Fiber-Reinforced Elastomeric Isolators (SU-FREIs)." *Submitted on November 2008 (Chapter 4 of this thesis).*

Toopchinezhad H., Tait M. J., and Drysdale R. G. (2008d). "Shake Table Study on an Ordinary Low-Rise Building Seismically Isolated with SU-FREIs (Stable Unbonded Fiber-Reinforced Elastomeric Isolators)." *Submitted on November 2008 (Chapter 5 of this thesis).*

Table 6.1. Mechanical properties of the SU-FREI bearings including the effective lateral stiffness (k) and damping ratio (ξ) attributed to different amplitudes of lateral displacements

Displacement Amplitude	k (N/mm)	ξ (%)
25% t_r (4.75 mm)	164	12
50% t_r (9.50 mm)	123	11
75% t_r (14.25mm)	103	9
100% t_r (19.00 mm)	89	9
150% t_r (28.50mm)	73	8
200% t_r (38.00 mm)	69	8

Table 6.2. Parameters to be used in Model 2 (bilinear idealization)

$v_{b,max}$	q (N)	k_2 (N/mm)	k_1* (N/mm)
25% t_r (4.75 mm)	220	157.5	336.4
50% t_r (9.50 mm)	240	116.0	247.8
75% t_r (14.25mm)	240	97.7	208.7
100% t_r (19.00 mm)	250	84.1	179.6
150% t_r (28.50mm)	310	71.4	152.5
200% t_r (38.00 mm)	350	58.0	123.9

* For all cases $k_1 = 2.136\ k_2$

Table 6.3. Peak response values; comparison between the measured (shake table test results) and the normalized predicted responses

Earthquake	Response Parameter	Measured Response	Predicted Response/Measured Response			
			Model 1		Model 2	
			1st Iteration	Last Iteration	1st Iteration	Last Iteration
El Centro-s	(Bearing Lateral Load)	2.55 kN	0.76	0.85	0.75	0.91
	(Bearing Lateral Displacement)	30.53 mm	0.83	0.84	0.86	0.89
	(Superstructure Base Shear)	7.67 kN	0.81	0.80	0.77	0.97
	(Total Drift)*	0.16%	0.81	0.79	0.74	0.91
Saguenay-s	(Bearing Lateral Load)	1.28 kN	0.85	0.86	0.70	1.04
	(Bearing Lateral Displacement)	7.79 mm	0.92	0.92	0.94	0.93
	(Superstructure Base Shear)	4.51 kN	0.83	0.84	0.62	0.77
	(Total Drift)*	0.09%	0.93	0.94	0.67	0.84
Tabas-s	(Bearing Lateral Load)	2.00 kN	0.99	1.07	0.87	0.94
	(Bearing Lateral Displacement)	21.68 mm	1.14	1.10	1.05	0.87
	(Superstructure Base Shear)	5.80 kN	0.97	1.04	1.00	1.09
	(Total Drift)*	0.10%	1.13	1.16	1.17	1.24

* The total drift has been normalized with respect to the total height of the superstructure namely, H=1628 mm

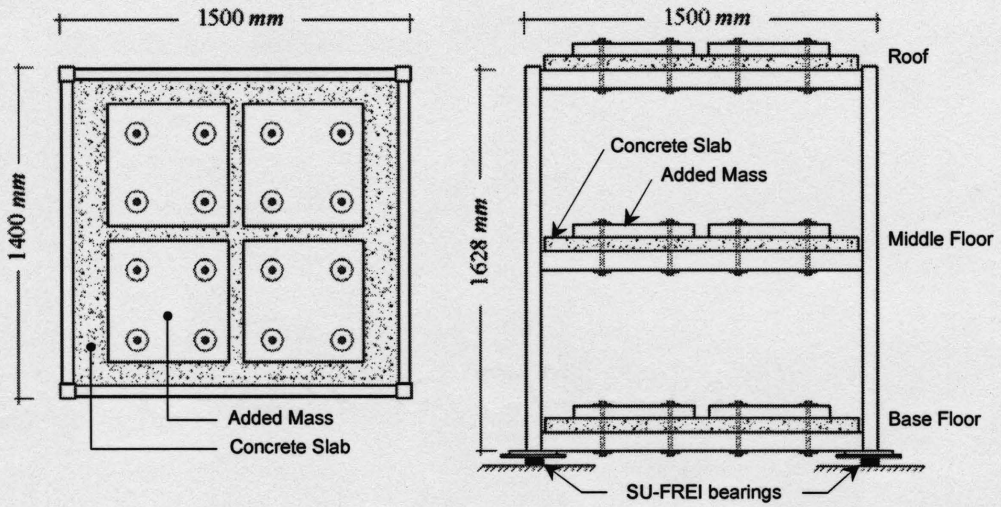

(a) Plan View (b) Elevation View

Figure 6.1. Sketch of the base isolated structure

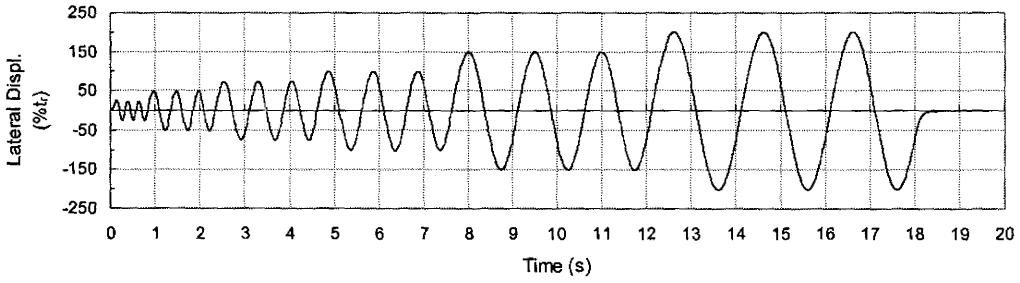

Figure 6.2. Time History of Input Lateral Displacements

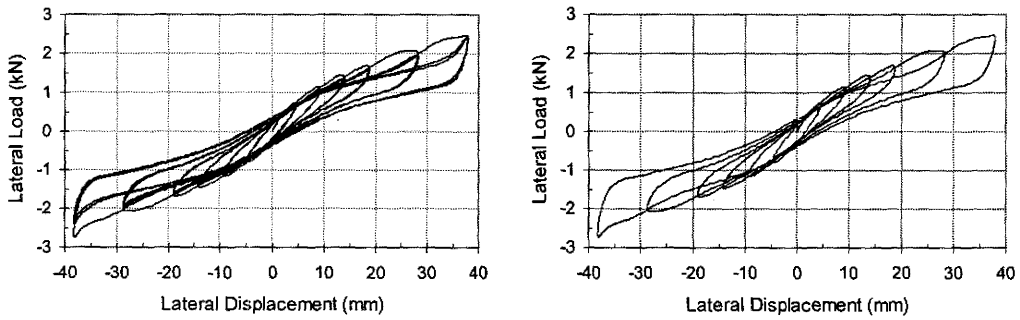

(a) Hysteresis Loops (All Cycles) (b) Unscragged Hysteresis Loops

Figure 6.3. Lateral response of the SU-FREI bearings (under 1.6 MPa constant vertical pressure)

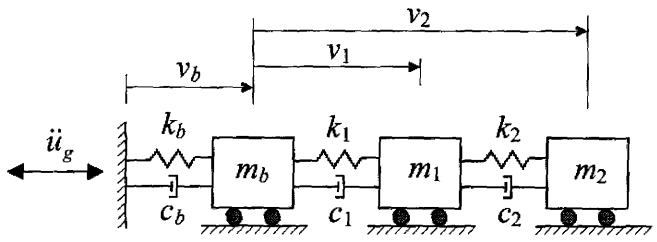

Figure 6.4. Mass-spring-dashpot idealization of the base isolated structure shown in Fig. 6.1

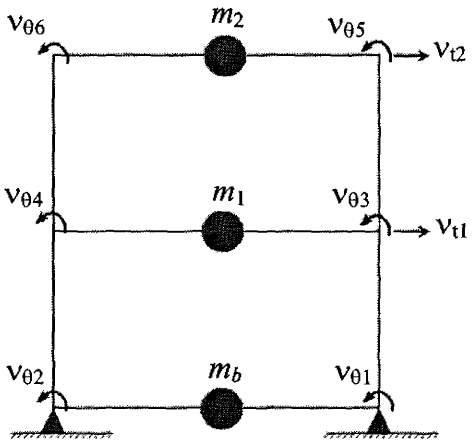

Figure 6.5. Translational (dynamic) and rotational (static) degrees of freedom in the superstructure

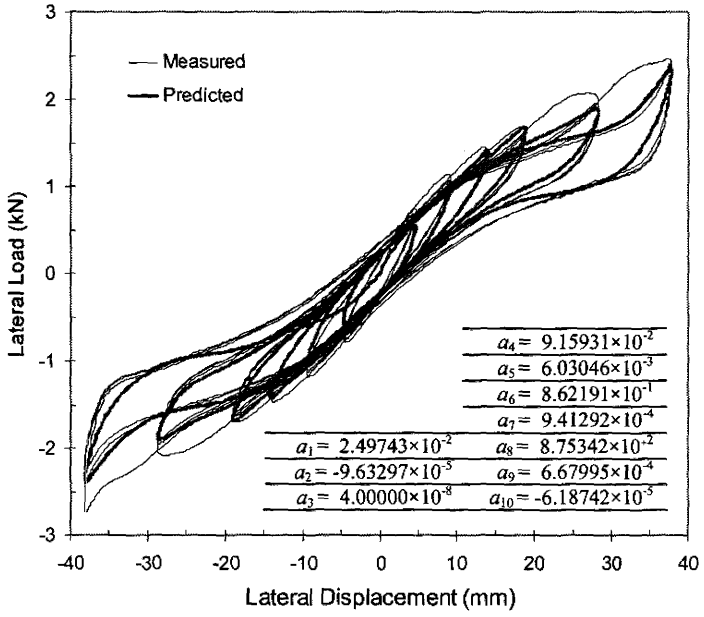

Figure 5.6. Comparison between the measured and predicted cyclic behavior of the SU-FREI bearings using Model 1

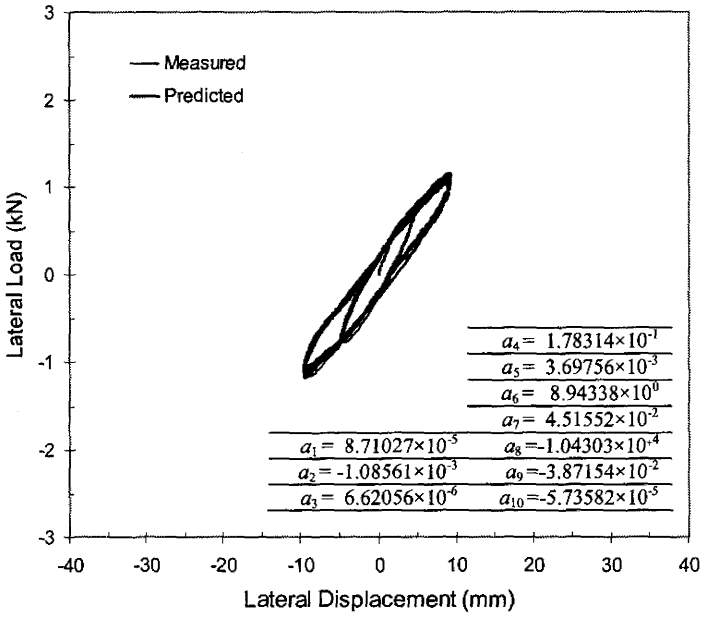

Figure 6.7. Comparison between the measured and Model 1 predicted cyclic behavior of the SU-FREI bearings, with the peak amplitude of bearing lateral displacement equal to or less than 50% t_r

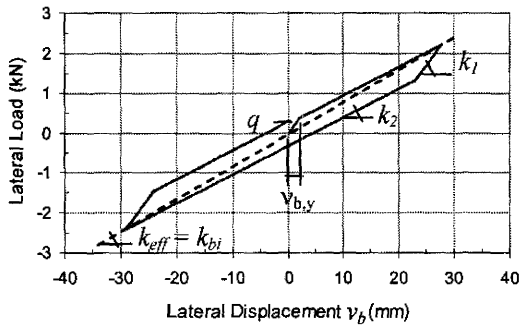

(a) Bilinear hysteresis loop attributed to lateral displacement amplitude of 150%t_r

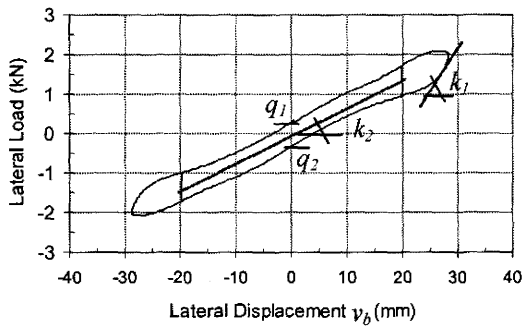

(b) Definition of the bilinear model-parameters on the unscragged hysteresis loop at 150% t_r, obtained from cyclic testing

Figure 6.8. Bilinear idealization (Model 2) of the SU-FREI Bearing lateral load-displacement hysteresis response

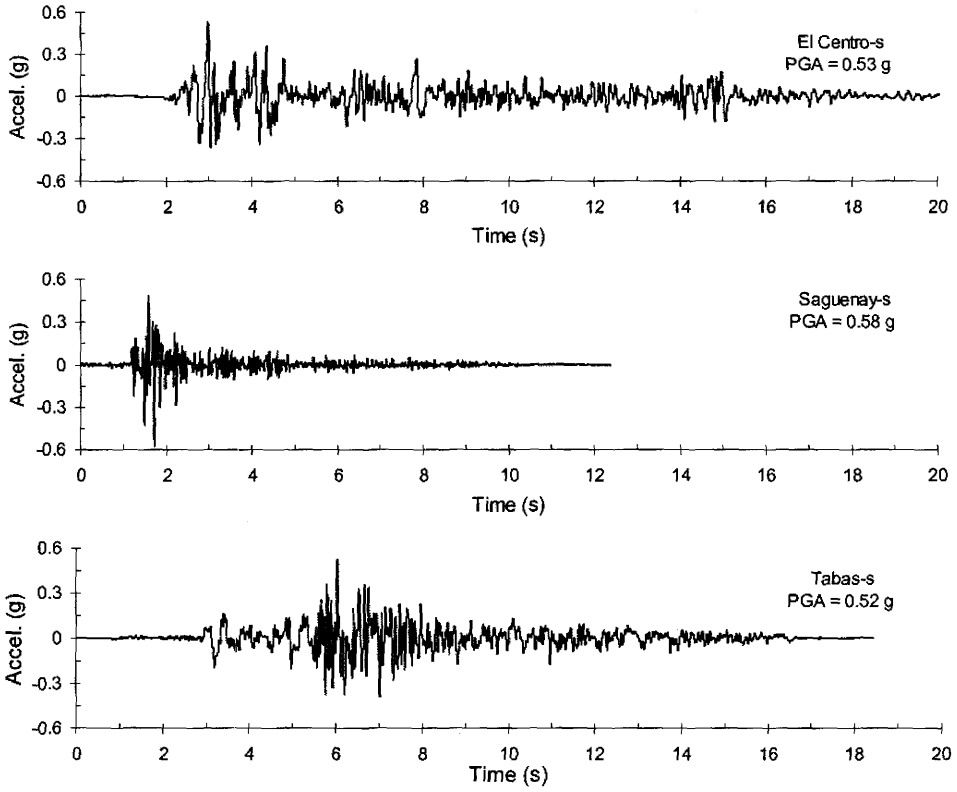

Figure 6.9. Ground acceleration time histories of the input earthquakes

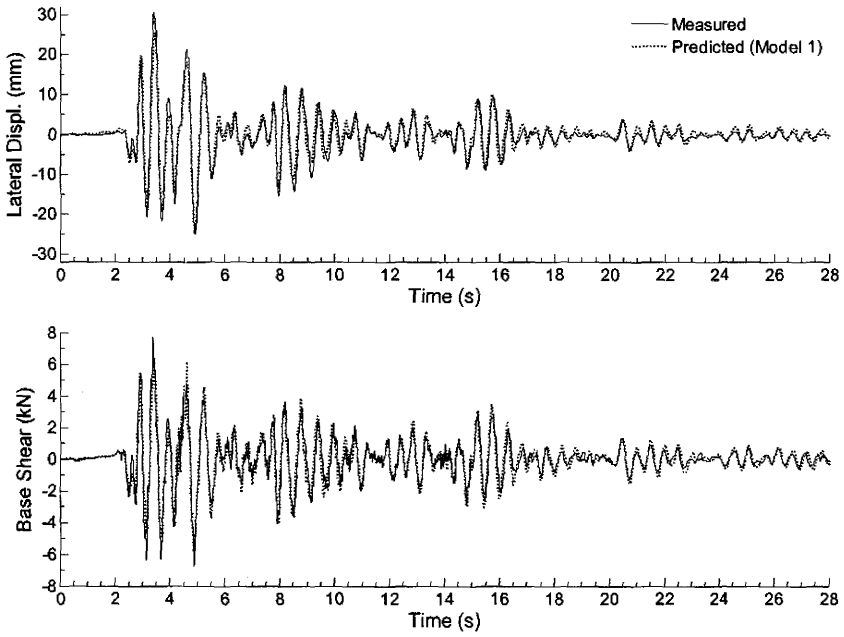

Figure 6.10. Measured versus predicted (Model 1) lateral bearing displacement (v_b) and superstructure base shear (V_s) for El Centro-s

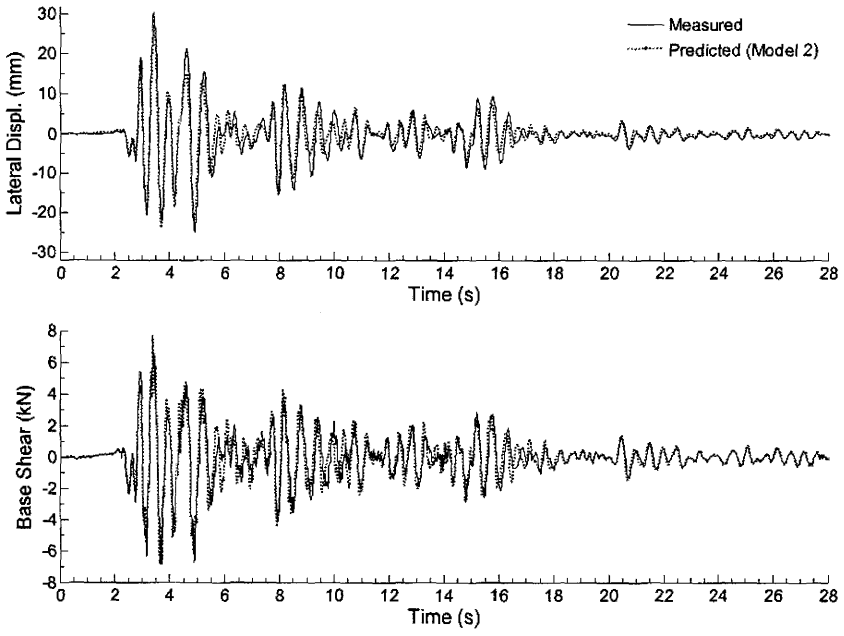

Figure 6.11. Measured versus predicted (Model 2) lateral bearing displacement (v_b) and superstructure base shear (V_s) for El Centro-s

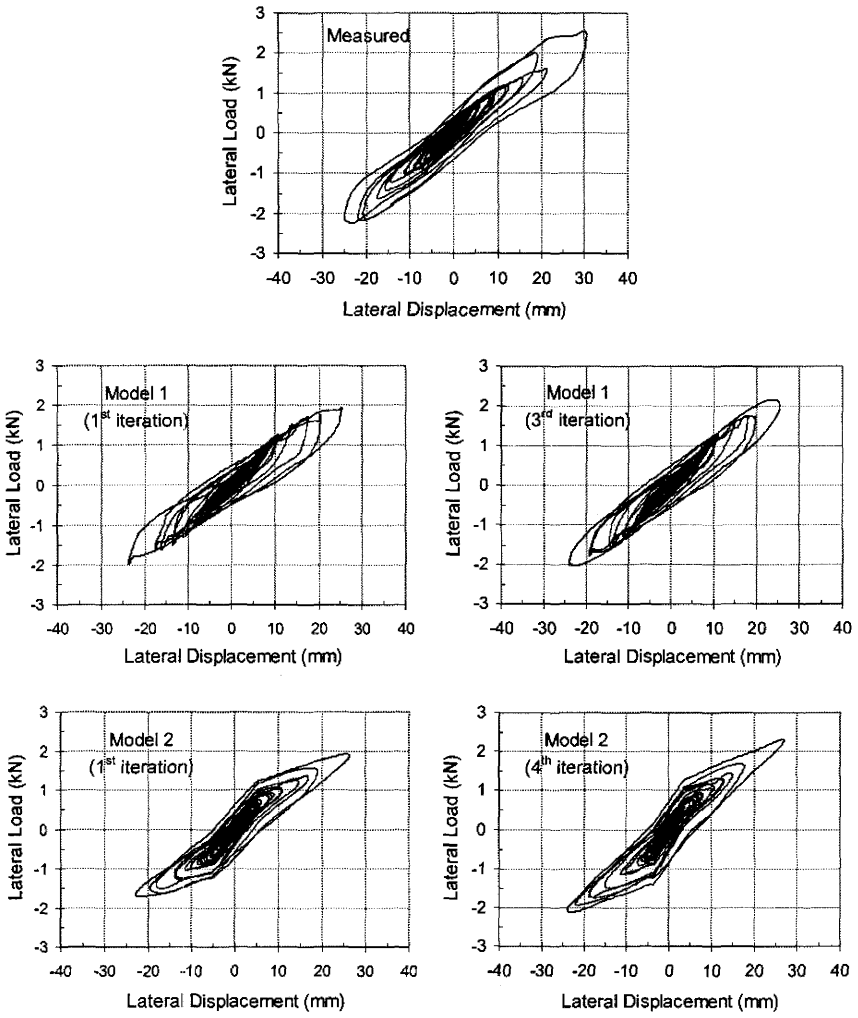

Figure 6.12. Measured versus predicted lateral load-displacement hysteresis loops for SU-FREI bearings subjected to El Centro-s earthquake

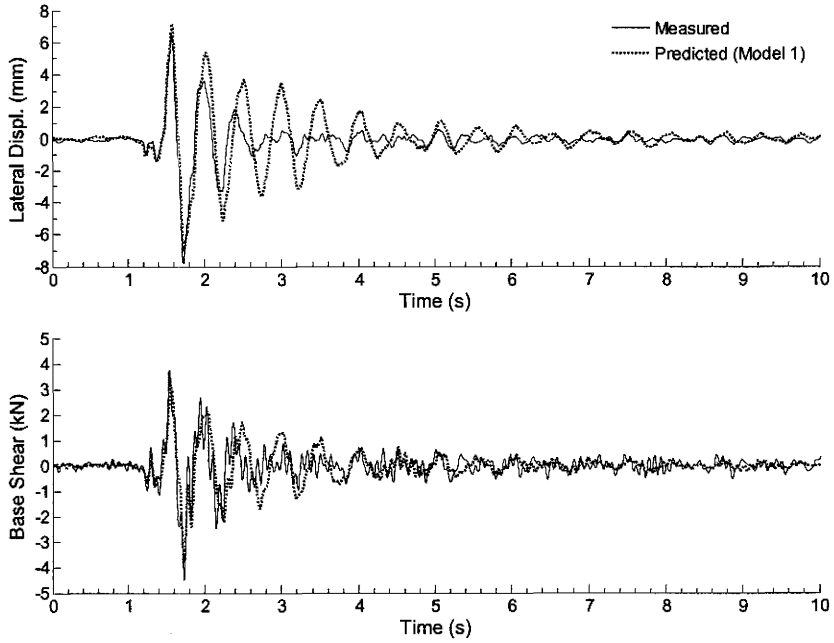

Figure 6.13. Measured versus predicted (Model 1) bearings' lateral displacement (v_b) and superstructure base shear (V_s) for Saguenay-s earthquake

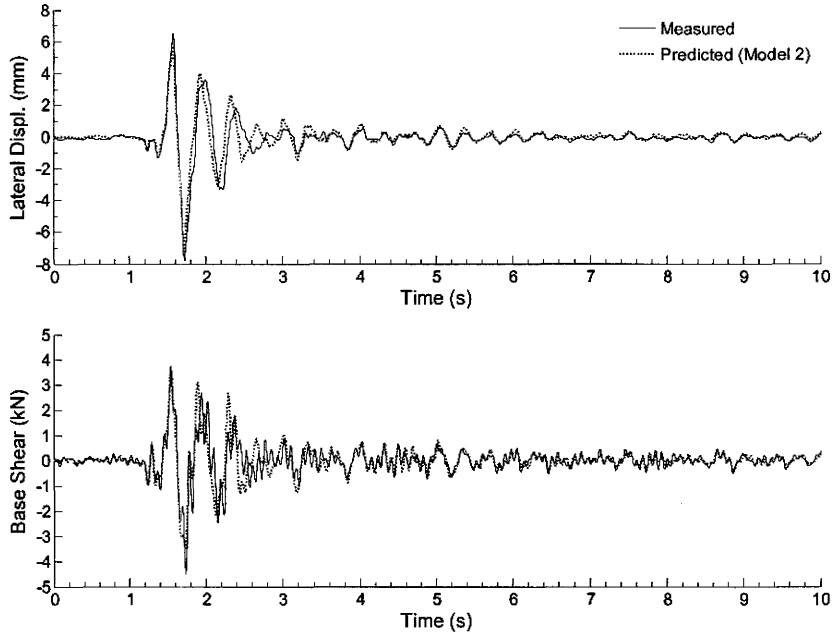

Figure 6.14. Measured versus predicted (Model 2) bearings' lateral displacement (v_b) and superstructure base shear (V_s) for Saguenay-s earthquake

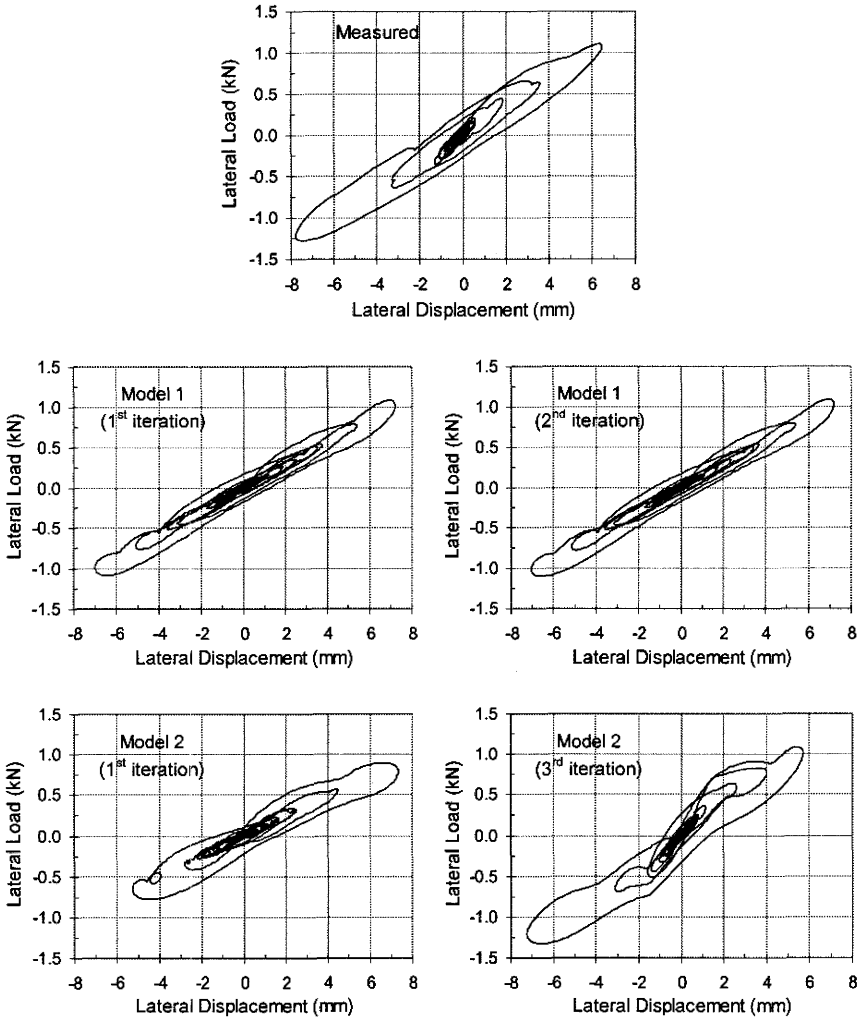

Figure 6.15. Measured versus predicted lateral load-displacement hysteresis loops for SU-FREI bearings subjected to Saguenay-s earthquake

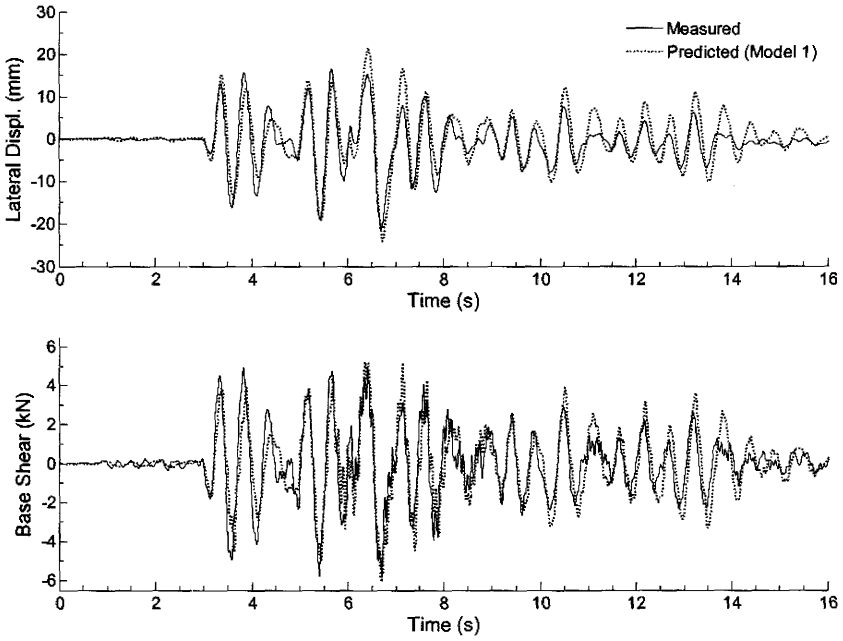

Figure 6.16. Measured versus predicted (Model 1) lateral bearing displacement (v_b) and superstructure base shear (V_s) to Tabas-s

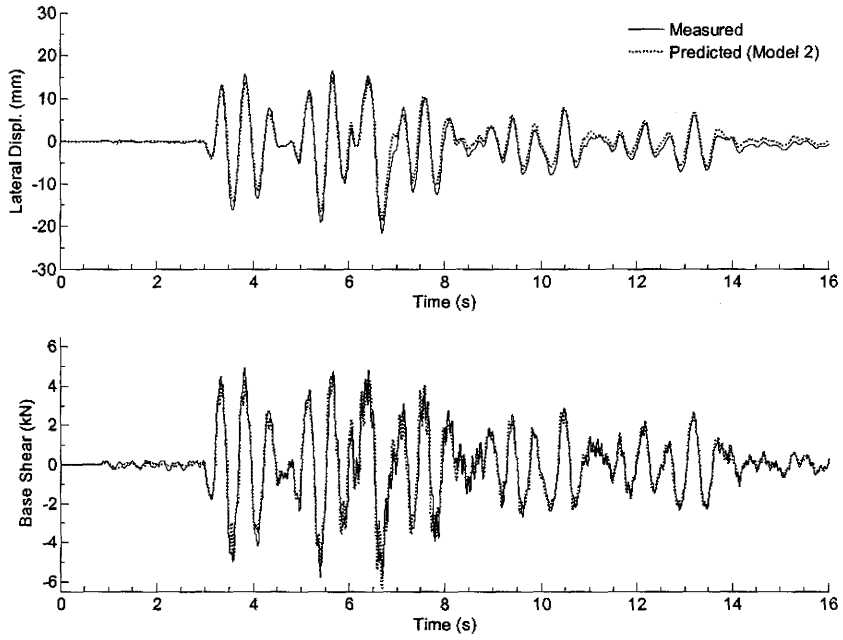

Figure 6.17. Measured versus predicted (Model 2) lateral bearing displacement (v_b) and superstructure base shear (V_s) to Tabas-s

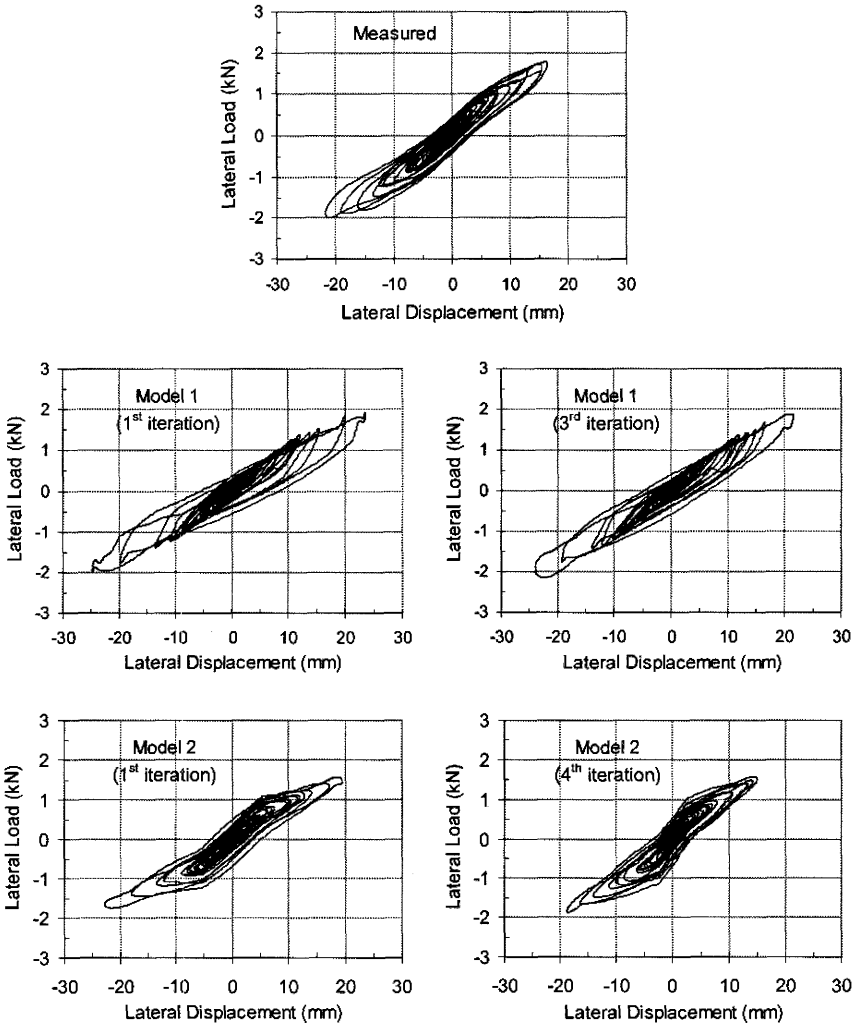

Figure 6.18. Measured versus predicted lateral load-displacement hysteresis loops for SU-FREI bearings subjected to Tabas-s earthquake

Chapter 7: Conclusions and Recommendations

7.1. Overview of the Research

The objective of this research was to investigate the performance of SU-FREIs (stable unbonded-fiber reinforced elastomeric isolators) as an effective seismic protection system for ordinary low-rise buildings. To achieve this objective, a set of comprehensive experimental and numerical studies were completed.

The experimental studies were conducted in three separate phases. In the first phase of experimental studies (Chapter 2) the full scale FREI bearings utilizing pure natural rubber as the elastomeric material were investigated. The main objective was to study the influence of bearing geometry on lateral response characteristics of the tested full scale bearings.

The mechanical properties of prototype ¼ scale SU-FREI bearings in both the vertical and lateral directions (Chapters 3 & 4) were investigated in Phase II of the experimental studies. In addition, the influences of parameters such as lateral displacement amplitude and rate, amplitude history, and variations in the vertical pressure on the lateral response of the bearings were studied. The ¼ scale bearings were fabricated using a soft compound of unfilled neoprene elastomer.

The feasibility of employing SU-FREI system for seismic mitigation of low-rise buildings was investigated through a comprehensive shake table study on a ¼ scale, 2 story test structure seismically isolated using ¼ scale SU-FREI bearings (Chapter 5).

Chapter 6 dealt with simulating the seismic response of the tested base isolated structure. Two simplified models to simulate the hysteretic response behavior of SU-FREI bearings during time history analysis were presented. These models were constructed based on the

lateral load displacement hysteresis loops of the prototype SU-FREI bearings obtained from cyclic lateral tests.

The main conclusions drawn from the aforementioned chapters are listed in the following section.

7.2. Conclusions

The experimental study on full-scale FREI bearings made from alternating bonded layers of a soft compound of pure natural rubber and carbon fiber fabric, as presented in Chapter 2, reveals the following conclusions:

1. Cyclic lateral tests reveal that, when an unbonded FREI is laterally deformed, its top and bottom faces roll off the upper and lower horizontal contact supports. This particular lateral deformation is denoted as "rollover deformation".
2. Rollover deformation occurs due to unbonded contact surfaces of the bearing as well as lack of appreciable flexural rigidity in the fiber-reinforcement sheets.
3. A properly designed unbonded FREI bearing can safely undergo large lateral displacements including extreme displacements of where its originally vertical faces fully contact the upper and lower horizontal supports. The bearing can maintain a positive incremental lateral load resisting-capacity throughout the hysteresis loops and remain stable. Such a permissible lateral deformation is denoted as "stable rollover" (SR)-deformation.
4. At the extreme lateral displacement when the originally vertical faces of an unbonded FREI bearing contact the horizontal contact supports, the lateral stiffness significantly increases. This phenomenon is advantageous as it puts a limit on the maximum deformations under unexpectedly large earthquakes and maintains the overall stability of the bearing.
5. SR-deformation in the unbonded condition significantly decreases the lateral stiffness of a FREI bearing compared to the same bearing with top and bottom faces bonded to the horizontal contact supports. This is due to the additional rotational degree of freedom at the contact surfaces of the unbonded bearing. The decreased stiffness results in increased seismic isolation efficiency.

6. Given the material properties, physical dimensions in plan, and the shape factor (i.e., the ratio of vertically loaded area on one face of the elastomer layer to its perimeter load-free area), the aspect ratio (i.e., the ratio of length to total thickness of the bearing, also called the second shape factor) was found to be an important parameter as it controls SR-deformation in an unbonded FREI. Bearings with low aspect ratios are more susceptible to exhibit unstable rollover deformation.
7. Although the bearings exhibit adequate lateral flexibility at 0° and 45° orientations, the damping values are found to be insufficient.
8. Vertical compression testing indicates that fiber-reinforcement can effectively increase the vertical stiffness of FREI bearings to a sufficiently large value.
9. The unbonded application is applicable when no separation occurs at the contact surfaces of the FREI bearing with its top and bottom supports as a result of overturning in the superstructure or strong vertical ground motion.

The experimental study conducted on ¼ scale FREI bearings made from alternating bonded layers of a soft compound of Neoprene rubber and carbon fiber fabric, presented in Chapter 3, indicates the following:

10. All tested bearings exhibit SR-deformation with adequate lateral flexibility and achieve the target base isolated period.
11. Damping values obtained are significantly larger than the supplier-specified inherent damping of the utilized elastomer. It is postulated that interaction between the elastomer and the fiber fabric results in a new source of energy dissipation in addition to the inherent damping of the elastomer.
12. In general, the tested SU-FREI bearings exhibit a highly nonlinear lateral response. The lateral response is characterized by higher effective stiffness and a higher damping ratio at lower amplitudes of lateral displacement and a lower stiffness and a lower damping ratio at higher displacement amplitudes.
13. The effective lateral stiffness and the damping ratio increase with an increase in the lateral displacement rate. However, the stiffness is generally found to be less sensitive than the damping ratio to variations in the rate of lateral displacement.

Chapter 4 contains the results of an experimental parametric study conducted on the ¼ scale FREI bearings. Since the bearings, with unbonded contact surfaces, exhibit SR-deformation, they are described as stable unbonded (SU)-FREI bearings. The main conclusions of this paper are:

14. When the SU-FREI bearings are subjected to an "ascending amplitude" (AA) pattern of cyclic sinusoidal lateral displacements, they exhibit unscragged response properties during the first cycle at each increased lateral displacement. The scragged response properties are obtained for the 2nd and 3rd cycles at this displacement as the hysteresis loops become stabilized. The unscragged lateral response values (stiffness and damping) are higher than the scragged response values.
15. The history of the input displacements significantly affects the lateral load-displacement hysteresis loops of the SU-FREI bearings. For instance, compared to AA-pattern, when the bearings are subjected to "descending amplitude" (DA) pattern of displacements, significantly different lateral response values are obtained. Additionally, under the DA-pattern, no appreciated unscragged response is observed (except for the very first cycle of the test at the largest displacement).
16. The effective lateral stiffness is less sensitive than damping to ±50% variations in the design vertical pressure on the bearings.
17. The lateral displacement capacity of the SU-FREI bearings is reached when the originally vertical faces of the bearings completely contact the top and bottom horizontal supports. The bearings can safely sustain this level of lateral displacement.
18. The SU-FREI bearings exhibit sufficient vertical stiffness under ±50% variations in the design vertical pressure. The vertical stiffness increases with increasing vertical pressure. Vertical frequencies are significantly larger than the base isolated lateral frequency of the bearings. As such, the rocking vibration modes in the base isolated response are not of concern.
19. Subsequent vertical tests after completing the lateral test program show only a small degradation in the vertical stiffness of the bearings. This indicates only minor internal damage in the bearings.

Chapter 5 contains the results of the shake table tests on a ¼ scale low-rise test structure seismically isolated with SU-FREI bearings. The major findings include:

20. SU-FREI bearings can be effectively used in seismic mitigation of low-rise buildings.
21. The SU-FREI bearings exhibit restoring capability to re-center the base isolated structure when test is completed.
22. Seismic response at 45° orientation of the bearings is comparable with the response at 0° orientation.
23. After completion of the entire test program, no visible damage was found in the bearings. In addition, consistent response of the base isolated structure during duplicated test runs indicated that internal damage in the bearings was negligible.
24. Since no externally applied vertical tension is introduced in a laterally deformed SU-FREI bearing, tensile stresses between the reinforcement and elastomer layers are lower than the same bearing with bonded contact surfaces. Therefore, a SU-FREI bearing, if deformed within its permissible range of lateral displacements, remains operational after the maximum level of the input earthquake.

In Chapter 6 the accuracies of two different simplified analytical models for prediction of seismic response of a base isolated low-rise building are investigated. In Model 1, the lateral response of the bearings is simulated based on a multi-parameter function of the amplitude and rate of lateral displacements. Model 2 employs a bi-linear idealization to simulate the bearings' lateral load-displacement hysteresis loops. Due to the highly nonlinear lateral response of the SU-FREI bearings, the models are employed in an iterative time history analysis approach. The primary conclusions are:

25. These simplified models are sufficiently accurate for design of most low-rise buildings seismically isolated with the proposed SU-FREI bearings. For especially important or seismically sensitive buildings, the simplified analysis may serve as the preliminary design followed by a more rigorous analysis.

26. The accuracy of Model 2 is significantly improved by applying an iterative procedure in the time history analysis. Model 1 is generally found to be less sensitive to the iterations.
27. Compared to Model 1, the response history predicted by Model 2 is generally in better agreement with the measured response.
28. To facilitate the design of a base isolation system for any given ordinary low-rise building, the parameters of the proposed models can be evaluated by the bearing supplier and cited for different categories of bearings in their catalogues.

Based on the results presented in this thesis, there is a significant potential for SU-FREI bearings to be considered as a practically viable solution to mitigation of seismic damage in ordinary low-rise buildings.

7.3. Recommendations for Future Studies

7.3.1. Experimental Studies

1. Investigation of the performance of the proposed SU-FREI bearings to wind-induced lateral loads was beyond the scope of this thesis. However, considering the anticipated low level wind loads on targeted low-rise buildings, and higher effective lateral stiffness and damping ratio of the bearings at low lateral displacements, the performance is generally expected to be satisfactory. This expectation can be documented by evaluating the load-displacement hysteresis loops at a lateral load corresponding to the wind design load, and investigating the dynamic effects of the wind on the base isolated structure.
2. An experimental study on corresponding full-scale prototype of the tested ¼ scale bearings would be useful to verify the expected relationship between the model and prototype in conformance to dynamic similitude law.
3. Cyclic testing under a real time earthquake loading would help to further refine the influence of loading history on the lateral response of SU-FREIs.
4. Comparison between responses of SREI and SU-FREI bearings having identical elastomer material, total thickness of elastomer layers, and shape factor would

provide a more complete understanding of the advantages/disadvantages of these two different types of elastomeric bearings.

5. It is postulated that a supplementary source of energy dissipation is due to interfacial relative slippage of fibers in the reinforcement sheets in SU-FREI bearings. The relative volume of carbon fiber to elastomer in an unbonded FREI bearing may affect this supplementary damping. This relative volume for the ¼ scale SU-FREI bearings studied in this thesis was approximately 14.5%. The supplementary damping in the full scale bearings considered in Paper I was not significant. The volume of carbon fiber-reinforcement in those bearings was approximately 5% of the total volume of elastomer. Comparisons between lateral responses of similar SU-FREI bearings having different fiber to rubber volume fraction would help to refine the role of fiber-reinforcement as supplementary damping in the SU-FREIs.
6. In an attempt to reduce the cost of SU-FREI bearings, use of cheaper fiber-reinforcement materials such as glass fiber instead of carbon fiber could be studied.
7. Bi-directional or three-directional shake table testing on a test-structure seismically isolated with SU-FREI bearings would provide a more complete understanding of the seismic response in more representative cases.
8. A study on the long-term performance including creep and longevity of SU-FREI bearings would be beneficial to assess the response deterioration of the bearings over a long period of time.

7.3.2. Analytical Studies

In contrast to the steel-reinforcement in a SREI, which is assumed to be rigid in both extension and flexure, the fiber-reinforcement used in a FREI is flexible in extension and has virtually no flexural rigidity. The fiber-reinforcement is composed of many individual fibers grouped in strands, and woven into a fabric. The fabric is more flexible in tension than the individual fibers, and may stretch when the bearing is loaded in the vertical direction. Since the flexibility of the fiber significantly

influences the mechanical properties of the isolator, it cannot be ignored in modeling and design of a FREI bearing.

Analytical solutions for estimating the compression and bending stiffnesses of infinitely-long (Kelly 1999, 2002, Kelly and Takhirov 2001, 2002, Tsai and Kelly 2001, Tsai 2004, Pinarbasi and Mengi 2008), rectangular with finite length (Tsai 2002, Tsai and Kelly 2001, 2002a), and circular (Tsai and Kelly 2001, 2002b, Tsai 2006) FREIs can be found in the literature. Also lateral stiffness and buckling load of infinitely-long FREI bearings have been investigated (Kelly 1999, Tsai and Kelly 2004, 2005a, b) assuming the upper and lower faces of the FREI bearings are constrained against rotation and warping (i.e., bonded application). Developing analytical closed-form equations to predict the lateral response of the SU-FREI bearings, based on material properties and physical dimensions, would be useful for simplified design of this type of bearing. In addition, use of finite element modeling (Mordini and Strauss 2008) would be beneficial to more completely study the influence of various design variables on both the vertical and lateral response of SU-FREI bearings.

7.3.3. References

Kelly, J. M. (1999). "Analysis of Fiber-Reinforced Elastomeric Isolators." *Journal of Seismology and Earthquake Engineering (JSEE)*, Vol. 2, No. 1, Pages 19-34.

Kelly, J. M. (2002). "Seismic Isolation Systems for Developing Countries." *Earthquake Spectra*, Vol. 18, No. 3, Pages 385-406.

Kelly J. M., and Takhirov S. M. (2001). "Analytical and Experimental Study of Fiber-Reinforced Elastomeric Isolators." *PEER Report 2001/11*, Pacific Earthquake Engineering Research Center, University of California, Berkeley.

Kelly J. M., and Takhirov S. M. (2002). "Analytical and Experimental Study of Fiber-Reinforced Strip Isolators." *PEER Report 2002/11*, Pacific Earthquake Engineering Research Center, University of California, Berkeley.

Mordini A., and Strauss A. (2008). "An Innovative Earthquake Isolation System using Fiber-Reinforced Rubber Bearings." *Engineering Structures*, (In Press) doi:10.1016/j.engstruct.2008.03.010

Pinarbasi S., and Mengi Y. (2008). "Elastic Layers Bonded to Flexible Reinforcements" *International Journal of Solids and Structures*, Vol. 45, No. 3-4, Pages 794–820.

Tsai, H. C. (2004). "Compression Stiffness of Infinite-Strip Bearings of Laminated Elastic Material interleaving with Flexible Reinforcements." *International Journal of Solids and Structures*, Vol. 41, No. 24-25, Pages 6647-6660.

Tsai, H. C. (2006). "Compression Stiffness of Circular Bearings of Laminated Elastic Material interleaving with Flexible Reinforcements." *International Journal of Solids and Structures*, Vol. 43, No. 11-12, Pages 3484–3497.

Tsai H. C., and Kelly J. M. (2001). "Stiffness Analysis of Fiber-Reinforced Elastomeric Isolators." *PEER Report 2001/05*, Pacific Earthquake Engineering Research Center, University of California, Berkeley.

Tsai, H. C., and Kelly, J. M. (2002a). "Stiffness Analysis of Fiber-Reinforced Rectangular Seismic Isolators." *Journal of Engineering Mechanics*, Vol. 128, No. 4, Pages 462- 470.

Tsai, H. C., and Kelly, J. M. (2002b). "Bending Stiffness of Fiber-Reinforced Circular Seismic Isolators." *Journal of Engineering Mechanics*, Vol. 128, No. 11, Pages 1150-1157.

Tsai, H. C., and Kelly, J. M. (2005a). "Buckling of Short Beams with Warping Effect Included." *International Journal of Solids and Structures*, Vol. 42, No. 1, Pages 239–253.

Tsai, H. C., and Kelly, J. M. (2005b). "Buckling Load of Seismic Isolators Affected by Flexibility of Reinforcement." *International Journal of Solids and Structures*, Vol. 42, No. 1, Pages 255–269.